

# Therapeutically important enzymes with polar substrates or products: characterization by capillary electrophoresis and identification of inhibitors

## **Dissertation**

zur

Erlangung des Doktorgrades (Dr. rer. nat.)

der

Mathematisch-Naturwissenschaftlichen Fakultät

der

Rheinischen Friedrich-Wilhelms-Universität Bonn

vorgelegt von

**Wenjin Li**

aus

Shanxi, China

Bonn 2014



Angefertigt mit Genehmigung der Mathematisch-Naturwissenschaftlichen Fakultät  
der Rheinischen Friedrich-Wilhelms-Universität Bonn

1. Referent: Prof. Dr. Christa E. Müller
2. Referent: Priv. Doz. Dr. Anke Schiedel

Tag der Promotion: 14. 11. 2014

Erscheinungsjahr: 2015



Die vorliegende Arbeit wurde in der Zeit von July 2009 bis February 2014 am Pharmazeutischen Institut unter der Leitung von Frau Prof. Dr. Christa E. Müller durchgeführt.

Mein besonderer Dank gilt Frau Prof. Dr. Christa E. Müller für ihre Unterstützung, ihre Diskussionsbereitschaft und ihre Anregungen, die zum Gelingen dieser Arbeit beigetragen haben.



*To My Parents*





## ABSTRACT

Enzymes are important drug targets, since they participate in many disease processes and can be inhibited by small drug molecules. In our research projects, a group of therapeutically important enzymes with polar substrates or products has been investigated by means of capillary electrophoresis (CE).

The first enzyme we investigated was ecto-5'-nucleotidase (*eN*), which can catalyze the hydrolysis of the phosphoric acid ester bond of AMP yielding the corresponding nucleoside adenosine and inorganic phosphate. Treatment with *eN* inhibitors may be a promising novel strategy for cancer therapy, because *eN* has been found to be overexpressed on many cancer cells, and *eN*-generated adenosine prevents tumor destruction by inhibiting antitumor immunity. We investigated nucleotide mimetics which consisted of a nucleoside scaffold substituted in the 5'-position with a dipeptide moiety. The compounds were investigated at rat *eN* using a capillary electrophoresis (CE)-based assay, and potent inhibitors were further investigated at human *eN*. The test results showed that the inhibitory potency of the compounds appeared to be pH-dependent: when the buffer pH was decreased, the potency of the compounds increased. Since tumor tissues typically show low extracellular pH values, the new inhibitors might act as tumor-selective *eN* inhibitors without affecting physiologically important functions of *eN*, such as the production of adenosine in blood vessels, which shows vasodilatory effects.

The second enzyme that we investigated was cerebroside sulfotransferase (CST), which catalyzes the transfer of a sulfate group from the co-substrate 3'-phosphoadenosine-5'-phosphosulfate (PAPS) to cerebroside yielding cerebroside sulphate and adenosine-3',5'-diphosphate (PAP). CST is a promising new therapeutic target for the treatment of metachromatic leukodystrophy (MLD), a devastating genetic disease. In the absence of an effective therapy, MLD leads to early death of the young patients. In the present study we developed a CE-based assay for monitoring the catalytic activity of CST. A low nanomolar limit of detection (LOD = 66.6 nM) was achieved for the enzymatic product PAP by using dynamic pH junction stacking. Our CE method was sensitive, robust and suitable for CST inhibitor screening,  $K_i$  value determination, and enzyme kinetic studies. Several reference compounds were tested including cerebroside, psychosine and Congo Red in order to validate our method. We investigated analogues of the CST substrate cerebroside with this newly developed CE method, in order to study structure-activity relationship (SAR) and to identify and develop novel CST inhibitors. A substrate analogue  $\alpha$ -galactosylceramide was identified to

be a novel inhibitor, which will be used as a lead structure for developing more potent competitive inhibitors, which are urgently needed for the treatment of MLD. Moreover, SAR information for the CST cerebroside binding site would be highly useful especially since a crystal structure of the CST cerebroside binding site is not available yet.

A further group of investigated enzymes were capsule biosynthesis enzymes from *Staphylococcus aureus*. We characterized the enzymes CapD and CapE of the *Staphylococcus aureus* serotype 5 biosynthesis cluster, which catalyze the first steps in the synthesis of the soluble capsule precursors UDP-D-FucNAc and UDP-L-FucNAc, respectively. A capillary CE-based method applying micellar electrokinetic chromatography (MEKC) was developed for the functional characterization of the enzymes using dynamic coating of the capillary with polybrene at pH 12.4. The limits of detection for the CapD and CapE products UDP-2-acetamido-2,6-dideoxy- $\alpha$ -D-xylo-hex-4-ulose and UDP-2-acetamido-2,6-dideoxy- $\beta$ -L-arabino-hex-4-ulose, respectively, were below 1  $\mu$ M. Using this new, robust and sensitive method we performed kinetic studies for CapD and CapE, and screened a compound library in search for enzyme inhibitors. Several active compounds were identified and characterized. Our studies contribute to a profound understanding of the capsule biosynthesis in pathogenic bacteria. This approach may lead to the identification of novel anti-virulence and antibiotic drugs.

# Table of contents

<b>1</b>	<b>Introduction.....</b>	<b>5</b>
1.1	Enzymes .....	5
1.1.1	Enzymes as drug targets.....	5
1.1.2	Enzyme kinetic mechanisms.....	8
1.1.3	Enzyme inhibitors .....	9
1.1.4	Inhibitor screening, $K_i$ value determination .....	12
1.2	Capillary electrophoresis.....	14
1.2.1	Introduction of capillary electrophoresis .....	14
1.2.2	Stacking methods for capillary electrophoresis .....	19
<b>2</b>	<b>Investigation of ecto-5'-nucleotidase - a novel anti-cancer drug target ....</b>	<b>23</b>
2.1	Introduction.....	23
2.2	Method development and validation.....	25
2.2.1	Optimization and validation of capillary electrophoresis method .....	25
2.3	Results .....	27
2.3.1	Kinetic characterization of ecto-5'-nucleotidase-catalyzed reactions .....	27
2.3.2	Inhibitors of ecto-5'-nucleotidase .....	28
2.3.3	Activators of ecto-5'-nucleotidase .....	35
2.4	Conclusions and discussion .....	36
<b>3</b>	<b>Investigation of cerebroside sulfotransferase as therapy target for metachromatic leukodystrophy .....</b>	<b>39</b>
3.1	Introduction.....	39
3.2	Method development and validation.....	43
3.2.1	Development and optimization of the capillary electrophoresis method.....	43
3.2.2	Calibration and validation of the capillary electrophoresis method .....	49
3.3	Results .....	50
3.3.1	Kinetic characterization and inhibition assays for cerebroside sulfotransferase with reference compounds .....	50
3.3.2	Kinetic characterization of cerebroside sulfotransferase-catalyzed reactions with artificial substrates .....	53
3.3.3	Inhibitors of cerebroside sulfotransferase .....	56
3.3.4	Structure-activity relationship study of the cerebroside sulfotransferase cerebroside binding site.....	57

3.4	Conclusions and discussion .....	58
<b>4</b>	<b>Analysis of the <i>Staphylococcus aureus</i> capsule biosynthesis pathway.....</b>	<b>61</b>
4.1	Introduction.....	61
4.2	Method development and validation.....	63
4.2.1	Development and optimization of capillary electrophoresis method .....	63
4.2.2	Calibration and validation of the capillary electrophoresis method .....	67
4.3	Results and discussion .....	70
4.3.1	Kinetic characterization of CapD- and CapE-catalyzed reactions.....	70
4.3.2	Inhibitors of CapD and CapE.....	71
4.3.3	CapAB kinase complex regulates capsule biosynthesis .....	74
4.3.4	<i>In vitro</i> reconstitution of UDP-D-FucNAc biosynthesis .....	75
4.4	Conclusions and discussion .....	77
<b>5</b>	<b>Summary and outlook.....</b>	<b>81</b>
5.1	Investigation of ecto-5'-nucleotidase as anti-cancer drug target.....	81
5.2	Investigation of cerebroside sulfotransferase as a target for metachromatic leukodystrophy .....	83
5.3	Analysis of the <i>Staphylococcus aureus</i> capsule biosynthesis pathway.....	85
<b>6</b>	<b>Experiments.....</b>	<b>87</b>
6.1	General.....	87
6.1.1	Chemicals.....	87
6.1.2	Material and instruments.....	88
6.1.3	Enzymes preparations .....	88
6.2	Operation for capillary electrophoresis.....	92
6.2.1	Strategy for establishing capillary electrophoresis methods.....	92
6.2.2	Capillary electrophoresis working process .....	94
6.2.3	Maintenance Procedures .....	108
6.2.4	Solutions for some problems .....	122
6.2.5	Important practical aspects .....	126
6.3	Investigation of ecto-5'-nucleotidase as anti-cancer drug target.....	128
6.3.1	Capillary electrophoresis set up .....	128
6.3.2	Assay description .....	129
6.3.3	Compound preparation and selection.....	131
6.4	Investigation of cerebroside sulfotransferase as therapy target for metachromatic leukodystrophy .....	136

6.4.1	Capillary electrophoresis set up .....	136
6.4.2	Assay description .....	138
6.4.3	Compound preparation and selection.....	141
<b>6.5</b>	<b>Analysis of the <i>staphylococcus aureus</i> capsule biosynthesis pathway .....</b>	<b>143</b>
6.5.1	Capillary electrophoresis set up .....	143
6.5.2	Assay description .....	144
6.5.3	Compound preparation and selection.....	150
<b>7</b>	<b>Abbreviations .....</b>	<b>165</b>
<b>8</b>	<b>Curriculum Vitae .....</b>	<b>169</b>
<b>9</b>	<b>References.....</b>	<b>175</b>
<b>10</b>	<b>Acknowledgements .....</b>	<b>189</b>



# 1 Introduction

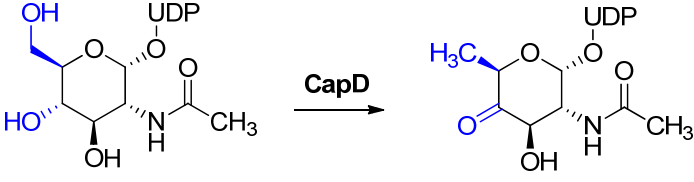
## 1.1 Enzymes

### 1.1.1 Enzymes as drug targets

Enzymes are attractive drug targets for pharmaceutical industry. Therefore nearly half of the drugs in clinical use today are enzyme inhibitors.<sup>1</sup> There are two main reasons for enzymes to be attractive targets for pharmacological research: one is the essential participation of enzymes in many disease processes, another reason is that enzymes can be inhibited by small drug molecules.<sup>1</sup> Enzyme catalysis is necessary for life. A classification of enzymes according to their catalytic ability is shown in Table 1.1.<sup>2</sup>

Table 1.1. Classification of enzymes

Classification	Related enzymes used in the current research project
Oxidoreductases	
Oxidoreductases are enzymes that catalyze oxidations and reductions	-
Transferases	Cerebroside sulfotransferase (CST) can catalyze the transfer of a sulfate group from PAPS to cerebrosidies
Transferases are enzymes that transfer a group from one molecule to another	<p style="text-align: center;"> <chem>C13H27</chem>              Cerebroside         </p> <p style="text-align: center;"> <math>\xrightarrow{\text{CST}}</math>              PAPS → PAP              Sulfatide         </p>
Hydrolases	Ecto-5'-nucleotidase (eN, CD73) can catalyze the hydrolysis of the phosphoric ester bond of AMP to the corresponding nucleoside adenosine and inorganic phosphate
Hydrolases are enzymes that hydrolyze compounds containing an ester or amide group	<p style="text-align: center;">             AMP         </p> <p style="text-align: center;"> <math>\xrightarrow{\text{eN}}</math>              Adenosine         </p>

<p>Lyases</p> <p>Lyases are enzymes that catalyze the cleavage of C-C, C-O, C-N, and other bonds by other means than by hydrolysis or oxidation</p>	<p>CapD can catalyze UDP-D-GlcNAc to UDP-2-acetamido-2,6-dideoxy-<math>\alpha</math>-D-xylo-hex-4-ulose</p> <div style="text-align: center;">  </div> <p style="text-align: center;">UDP-D-GlcNAc                      UDP-2-acetamido-2,6-dideoxy-<math>\alpha</math>-D-xylo-hex-4-ulose</p>
<p>Isomerases</p> <p>Isomerases are enzymes that catalyze the interconversion of all types of isomers</p>	-
<p>Ligases (synthases)</p> <p>Ligases are enzymes that catalyze the formation of a bond between two substrate molecules</p>	-

The arrangement in the enzymes' active site must change (including spatial orientation, bond strength and bond angle), in order to catalyze the transformation of substrate into product. To achieve this goal, the overall conformation of the enzyme must adjust, which will cause changes in both active site and potential allosteric sites. Some features of the active site structure that relate to enzyme catalysis and ligand interactions are described below:<sup>1</sup>

1. The active site of an enzyme is small compared to the whole enzyme.
2. The amino acids and cofactors in the active site are held in precise arrangement with respect to the substrate.
3. Usually the initial interactions between the enzyme and the substrate are noncovalent. For example, H-bond, electrostatic, hydrophobic, and van der Waals (VDW) interactions are observed.
4. The active site of enzymes usually is located in the clefts of the protein, which can exclude bulk solvent. The substrate molecule is desolvated upon binding, and it is shielded from bulk



solvent in the enzymes' active site, where the solvation is replaced by specific interactions within the protein.

5. The specificity of substrate utilization depends on the arrangement of atoms in the enzymes' active site.

The main features of enzyme's allosteric sites were initially presented by Monod, Wyman, and Changeux (known as MWC theory), which is shown in Figure 1.1:<sup>3</sup>

1. The proteins may have a quaternary structure with more than one identical subunits (e.g. human ecto-5'-nucleotidase exists as a dimer<sup>4</sup>).
2. A relaxed state and a tensed state both exist, and the transitions between these two conformations are reversible.<sup>3</sup> For example, the tensed and relaxed states coexist in ecto-5'-nucleotidase crystals.<sup>4</sup> Ligands would facilitate the transitions between two confirmations: activators would let the enzyme transit preferably to the relaxed state, while allosteric inhibitors would let the enzyme transit preferably to the tensed state.

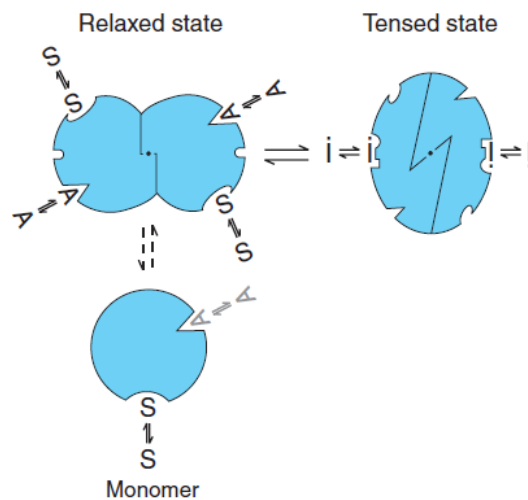
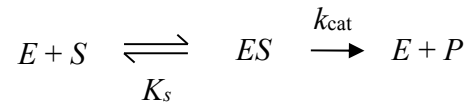


Figure 1.1. MWC model of allosteric sites and allosteric transitions.<sup>3</sup> Three class of molecules can bind to the enzyme: A (activator), I (inhibitor), and S (substrate). Transition between two states: relaxed state, tensed state, and the hypothetical monomer are shown.

### 1.1.2 Enzyme kinetic mechanisms

A simple enzyme-catalyzed reaction, which converts only one substrate into product can be described as below:<sup>1</sup>



In a rapid equilibrium, an initial loose association complex is formed between enzyme  $E$  and substrate  $S$ . Subsequently, the enzyme shifts to its active form and then converts substrate  $S$  into product  $P$ . Then the enzyme changes back to its inactive state, and meanwhile the product  $P$  dissociates from the enzyme. This process is time-dependent, and the time-dependent changes of the reactants of an enzyme-catalyzed reaction can be divided into three phases (Figure 1.2):<sup>5</sup>

1. Pre-steady-state phase: in the very beginning of this process, the complex  $ES$  is formed, meanwhile the free enzyme  $E$  decreases. The turnover rate  $v$  is low in this phase.
2. Steady-state phase: in this phase the turnover rate  $v$  reaches its maximum. The concentration of complex  $ES$  remains the same.
3. Substrate depletion: since more and more substrate  $S$  is converted to product  $P$ , the depletion of the substrate  $S$  will cause the decay of complex  $ES$ , which decreases the turnover rate  $v$ .

The mathematical description of enzyme kinetics is shown in equation 1, where the term  $V_{\max}$  refers to the maximum velocity obtained at infinite substrate concentration.<sup>1</sup>  $V_{\max}$  is mathematically equivalent to the product of  $k_{cat}$  and the enzyme concentration (equation 2).<sup>1</sup> The steady state enzyme velocity as a saturable function of substrate concentration could be described as equation 3, which is called the Michaelis-Menten equation, and is only valid in the steady-state.<sup>1</sup>

$$v = \frac{V_{\max} [S]}{K_s + [S]} \quad (1)$$

$$V_{\max} = k_{cat} [E] \quad (2)$$

$$v = \frac{V_{\max} [S]}{K_m + [S]} \quad (3)$$

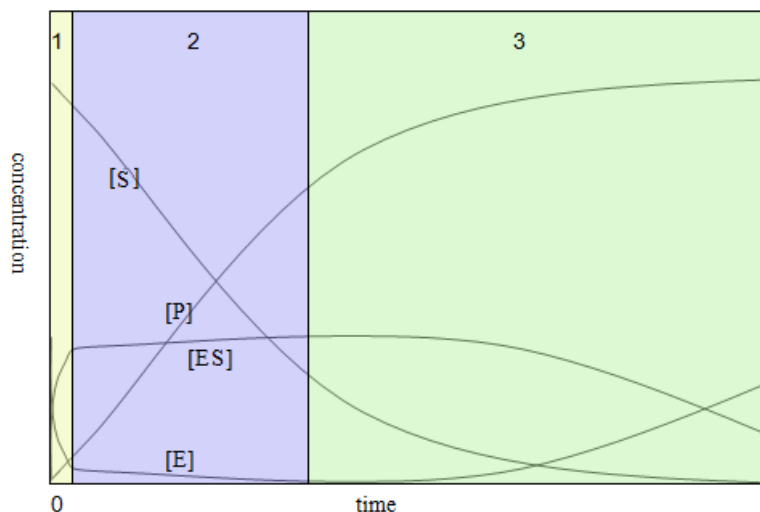


Figure 1.2. Time-related changes of the reactants in an enzyme-catalyzed reaction<sup>5</sup>. Where E stands for the enzyme, S stands for the substrate, ES stands for the enzyme-substrate complex.

Briefly, the relationship between steady state kinetic constants  $k_{cat}$ ,  $K_m$ , and  $k_{cat}/K_m$  and enzyme reaction pathway could be describe as below:<sup>1</sup>

- $K_m$  relates to  $ES$  dissociation:  $ES \rightarrow E + S$
- $1/K_m$  relates to  $ES$  formation:  $E + S \rightarrow ES$
- $k_{cat}$  relates to transition from  $ES$  to product:  $ES \rightarrow E + P$
- $k_{cat}/K_m$  relates to transition from the reactant state to product:  $E + S \rightarrow E + P$

### 1.1.3 Enzyme inhibitors

Enzyme inhibition is defined as the negative effect on enzyme activity by inhibitors specifically binding to defined catalytic or regulatory centers.<sup>1</sup> Some inhibitors bind so strongly to the enzyme that they cannot be detached, but most inhibitors bind reversibly and can be released or displaced from the enzyme. The former is irreversible inhibition, and the latter is reversible inhibition. Most drugs bind to their enzyme target through reversible interaction, as shown in Figure 1.3. There are three major forms of reversible enzyme inhibitor reactions.<sup>1</sup> Competitive inhibitors only bind to the same binding site as the substrate, uncompetitive inhibitors only bind to the enzyme's allosteric site, and noncompetitive inhibitors bind to both, substrate binding site and enzyme allosteric site. The ligand binding event can stabilize a particular microstate of the enzyme. This can shift the distribution of the enzyme states, because there is an energy barrier to

interconvert from one microstate to another microstate. The highest affinity inhibitor binding microstate can occur anywhere along the reaction pathway of the enzyme.<sup>1</sup>

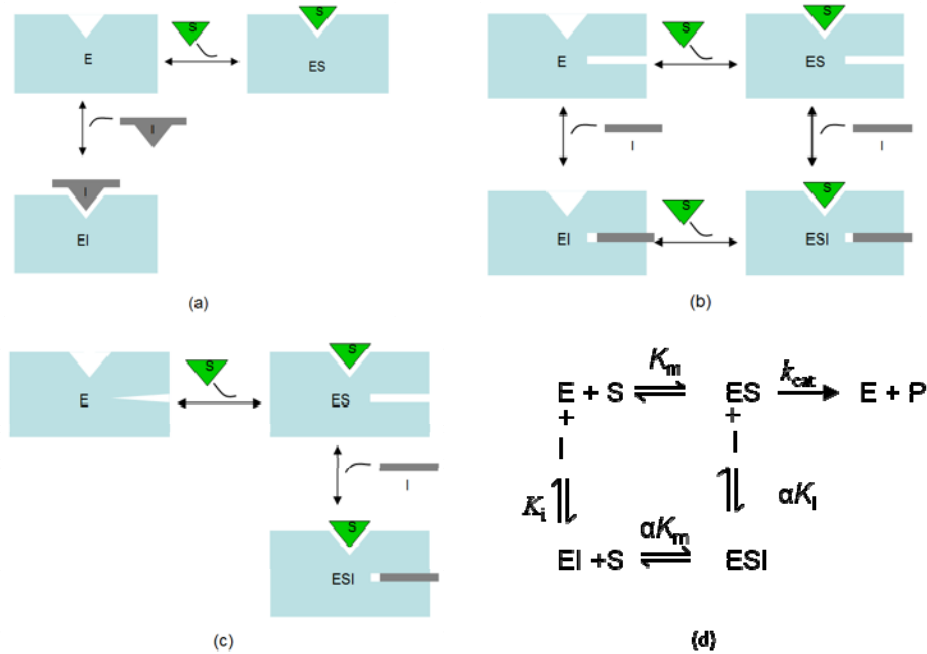
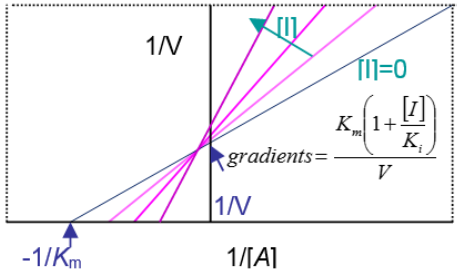
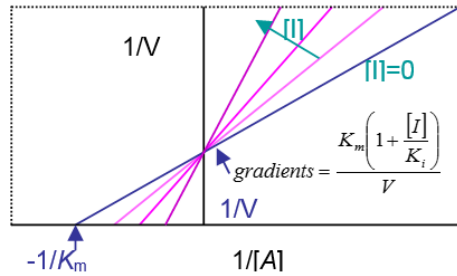


Figure 1.3. Three major forms of reversible inhibitor interactions with enzymes:<sup>1</sup> (a) competitive inhibition; (b) noncompetitive inhibition; (c) uncompetitive inhibition; (d) enzyme turnover equilibrium. *E* stands for enzyme, *S* stands for substrate, *I* stands for inhibitor, *EI* stands for enzyme-inhibitor complex, *ES* stands for enzyme-substrate complex, and *ESI* stands for enzyme-inhibitor-substrate complex.

There are several ways to determine the inhibition type of reversible inhibitors. One popular way is to use the Lineweaver-Burk plot. A summary of the Lineweaver-Burk equation and plot for non-competitive inhibition, competitive inhibition and uncompetitive inhibition, and effects of inhibitions with different modalities are described in Table 1.2.<sup>1</sup>

Table 1.2. Lineweaver-Burk equation and plot for non-competitive inhibition, competitive inhibition and uncompetitive inhibition, and effects of inhibition with different modalities <sup>1</sup>

Inhibition type	Effects of inhibitions with different modalities		Lineweaver-Burk equation and plot	
	$K_m$	$V_{max}$		
Non-Competitive	$\alpha > 1$	Increases curvilinearly with increasing [I]	Decreases curvilinearly with increasing [I]	$\frac{1}{v} = \frac{1 + \frac{[I]}{\alpha K_i}}{V} + \frac{K_m \left(1 + \frac{[I]}{K_i}\right)}{V[A]}$ 
	$\alpha = 1$	No effect	Decreases curvilinearly with increasing [I]	
	$\alpha < 1$	Decreases curvilinearly with increasing [I]	Decreases curvilinearly with increasing [I]	
Competitive	Increases linearly with increasing [I]	No effect	Decreases linearly with increasing [I]	$\frac{1}{v} = \frac{1}{V} + \frac{K_m \left(1 + \frac{[I]}{K_i}\right)}{V[A]}$ 

There are two important parameters for describing inhibition potency: IC<sub>50</sub> value and K<sub>i</sub> value. The IC<sub>50</sub> value is dependent on substrate concentration, but it is easier to be evaluated than the K<sub>i</sub> value. The K<sub>i</sub> value is more comparable to inhibition potency than the IC<sub>50</sub> value, because it is independent from the substrate amount, but the determination of the K<sub>i</sub> value is more complicated than that of the IC<sub>50</sub> value. Therefore we usually determine the IC<sub>50</sub> value first, in order to have an overview of the screening hits, and then we carry out K<sub>i</sub> value determination for the most potent compounds to make the inhibition potency comparable between different test methods or between different laboratories. As shown in equation 4, the IC<sub>50</sub> value is the concentration of inhibitor that results in inhibiting half of the maximal enzyme activity (Top - Bottom):

$$Y = Bottom + \frac{(Top - Bottom)}{1 + 10^{x - \log IC_{50}}} \quad (4)$$

There are two popular ways for K<sub>i</sub> value determination: by using the mixed-model inhibition equation<sup>6</sup> (it is also implemented in the software package Prism5), or by using the Dixon plot.<sup>7,8</sup>

#### 1.1.4 Inhibitor screening, K<sub>i</sub> value determination

Inhibitor screening, and K<sub>i</sub> value determination are the essential investigations of therapeutically important enzymes. The goal of inhibitor screening is to identify new enzyme inhibitors from compound libraries. Usually we use % *Inhibition* at a certain inhibitor concentration [I] to present the screening result, and the equation of % *Inhibition* is shown in equation 5, where v<sub>i</sub> and v<sub>0</sub> are the reaction velocity in the presence and absence of inhibitor at concentration [I], respectively, and S<sub>b</sub> is the background signal.

$$\%Inhibition = 100\left(1 - \frac{v_i - S_b}{v_0 - S_b}\right) \quad (5)$$

The goal of inhibitor K<sub>i</sub> value determination is to further characterize the property of potent inhibitors. Inhibition type determination is required before inhibitor K<sub>i</sub> value calculation, and enzyme kinetic studies with Michaelis-Menten curves are needed. Moreover, measuring initial velocity is an important experimental aspect for enzyme inhibitor investigation. Since only

during the initial velocity phase (up to about 10-20% substrate depletion) can the % *Inhibition* be relatively constant and close to the true value,<sup>1</sup> the substrate conversion rate in all enzyme inhibition assays should be strictly kept below 20%. The last but not least important point is that, a proper enzyme amount within the linear portion of enzyme titration on the observed reaction velocity is needed, in order to avoid an additional influence of the enzyme concentration factor.<sup>1</sup>

## 1.2 Capillary electrophoresis

### 1.2.1 Introduction of capillary electrophoresis

Capillary electrophoresis (CE) is a separation method, which is based on differences of analyte velocities in an electric field. The CE separation is performed in narrow-bore capillaries. Separation is an important method in analytical chemistry. A separation process means transforming a mixture of analytes into several pure distinct analytes.

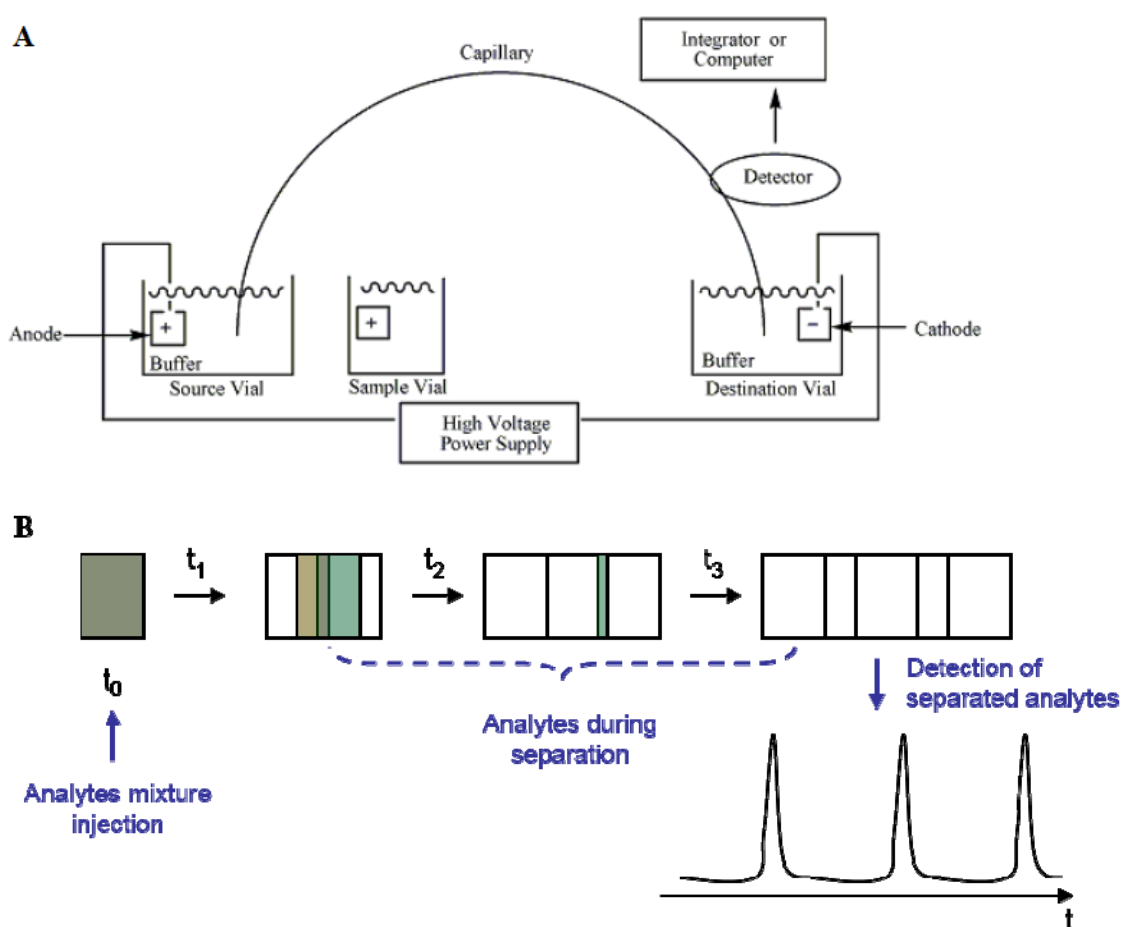


Figure 1.4. CE working process. **A.** Presentation of the CE system. **B.** Separation of analytes within the capillary according to time.

Figure 1.4 shows the CE working process. At time  $t_0$ , a mixture which contains three analytes is injected into the capillary. The three analytes have different velocities, therefore some of them move faster inside the capillary, while some of them move slower. After time  $t_3$  the separation is



completed. Since these solutes have certain spectra, an optical detector is used for the signal detection.

The velocity ( $v$ ) of an ion in an electric field can be described by equation 6, where  $\mu_e$  is mobility, and  $E$  is the applied electric field:<sup>9</sup>

$$v = \mu_e E \quad (6)$$

When an ion moves in an electric field, there are two forces applied on it. One is the electric force  $F_E$  (equation 7, where  $q$  is ion charge); another one is frictional drag through the medium  $F_f$  (equation 8, where  $\eta$  is solution viscosity,  $r$  is ion radius). After a short time, the two forces will create an equilibrium:  $F_E = F_f$ , leading to equation 9:<sup>9</sup>

$$F_E = q E \quad (7)$$

$$F_f = 6\pi\eta r v = 6\pi\eta r \mu_e E \quad (8)$$

$$\mu_e = \frac{q}{6\pi\eta r} \quad (9)$$

Additionally, electro-osmotic flow (EOF) is a fundamental constituent of CE separation, which is the bulk flow of liquid in the capillary. It is a consequence of the surface charge on the silica capillary inner wall. The EOF is controlled by the numerous silanol groups (SiOH) that can exist in anionic form (SiO<sup>-</sup>). When the silanol groups are deprotonated in the solution (at pH > 4), cations from the running buffer will build up near the surface to maintain a charge balance (Figure 1.5). When the voltage is applied across the capillary, cations near the capillary surface will move towards the cathode and drag the bulk solution together with them. The magnitude of the EOF mobility is described in equation 10, where  $\epsilon$  is the dielectric constant, and  $\zeta$  is the zeta potential:<sup>9</sup>

$$\mu_{os} = (\epsilon \zeta / \eta) \quad (10)$$

So the mobility of an ion that moves inside the capillary can be described as in equation 11:<sup>9</sup>

$$\mu = \mu_e + \mu_{os} \quad (11)$$

Usually the magnitude of  $\mu_{os}$  is much bigger than that of  $\mu_e$ , therefore all the solutes will move towards the cathode. EOF mobility ( $\mu_{os}$ ) can be adjusted through many ways; for example, by increasing buffer concentration one can decrease the zeta potential and EOF mobility; lowering of the electric field can decrease the EOF mobility; by using coated capillary walls one can increase, decrease or reverse the surface charge and the EOF mobility.

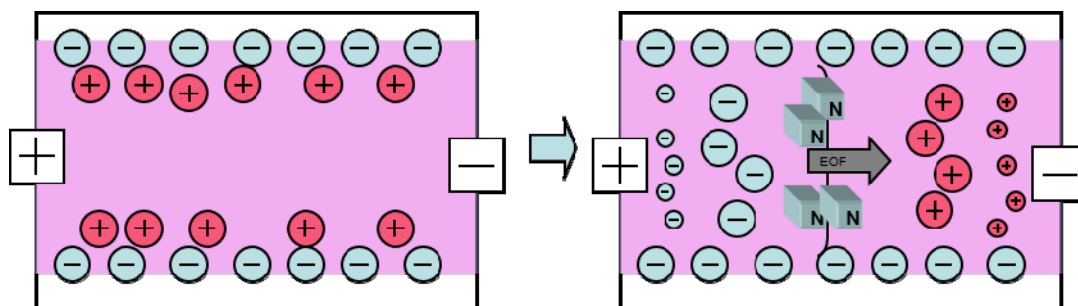


Figure 1.5. EOF in fused-silica capillary

Resolution is an important evaluation parameter for CE separation quality. It is defined in equation 10, where  $w$  is baseline peak width (in time),  $\sigma$  is the temporal standard deviation,  $t$  is migration time,  $w$  is peak width, and subscripts 1 and 2 refer to the two solutes:<sup>9</sup>

$$R = \frac{2(t_2 - t_1)}{w_1 + w_2} = \frac{t_2 - t_1}{4\sigma} \quad (12)$$

From equation 12 we can deduce that a better resolution ( $R$ ) will be achieved when the peak width ( $w$ ) is smaller. In other words, a good resolution needs sharp analyte peaks. In order to make analyte peaks sharp, usually the injection plug length should be less than 1 mm, and a stacking approach is required when a large volume of analyte is injected. Figure 1.6 shows: as the injection amount is increased, the peak size is increased, and resolution  $R$  is decreased, and finally peak distortion occurs (at -10 kV for 60 seconds).

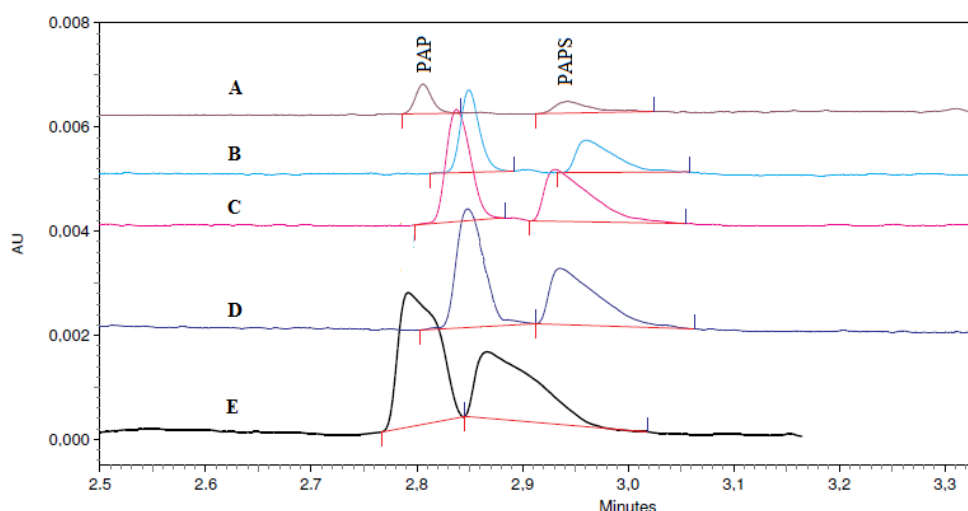


Figure 1.6. An example to show how the injection influences resolution. Separation of PAP and PAPS in a dynamically coated capillary. Separation buffers: phosphate 75 mM, with 0.002% polybrene, pH 8 (adjusted by phosphoric acid), separation voltage -25 kV, capillary temperature 15°C, and capillary length (50 cm \* 75 μM). **A**: injection -6 kV for 10 seconds,  $R=1.6$ ; **B**:

injection -6 kV for 30 seconds, R=1.05; C: injection -10 kV for 30 seconds, R=0.82; D: injection -6 kV for 60 seconds, R=0.67; E: injection -10 kV for 60 seconds, R=0.60.

There are two kinds of injection methods: hydrodynamic injection and electrokinetic injection. Electrokinetic injection is dependent on the EOF, sample concentration, and sample mobility in the electric field. The quantity injected, Q (g or moles), can be calculated by equation 13, where r is the capillary radius,  $c_0$  is the analyte concentration,  $\tau$  is the injection duration:<sup>9</sup>

$$Q_{in} = \pi r^2 c_0 (\mu_e + \mu_{os}) E \tau \quad (13)$$

One important feature of electrokinetic injection is the injection difference between different ions, which is caused by different mobility of different ions in the same electric field. The hydrodynamic injection volume V can be calculated by equation 14, where  $\Delta P$  is injection pressure difference across the capillary:<sup>9</sup>

$$V = \frac{\pi r^4}{8L\eta} (\Delta P) \tau \quad (14)$$

Usually  $\Delta P$  is around 0.5 psi,  $\tau$  is around 1-5 s. Equation 14 shows that the hydrodynamic injection volume will decrease when the total length of the capillary increases. There is no injection selection between different ions within the same sample solution, but both, analytes and background substances, will be injected into the capillary by using hydrodynamic injection.

There are three kinds of detectors for CE: ultraviolet (UV) detector, diode array detector (DAD) detector, and laser-induced fluorescence (LIF) detector. The UV detector and DAD detector are suitable for compounds that absorb light in the ultraviolet (UV) range, 200-400 nm. Absorption of light occurs when electrons of irradiated absorbing molecules are promoted to a higher energy level, because the frequency of the electronic oscillation in the molecule coincides with the frequency of the irradiating light. The wavelength corresponding to this frequency ( $\lambda_{max}$ ) is that at which the compound absorbs most light. It is determined by the structure of the absorbing molecule. Instruments designed to measure absorbance invariably make their measurements by determining the amount of light that is not absorbed, that is, the light which is transmitted by the solution. Naturally, the light transmitted by a solution of a chromophore decreases as the concentration of the chromophore increases. Any instrument that measures absorbance must

make a comparison of  $I_0$  (the light transmitted by a solution not containing the chromophore), with  $I$  (the light transmitted by a solution that does contain the chromophore), and the absorbance can be calculated with the Lambert-Beer equation (equation 15):<sup>9</sup>

$$A = -\log_{10}(I/I_0) \quad (15)$$

The UV detector (fixed wavelength detector) utilizes lamps that emit light at discrete wavelengths. The DAD detector (variable wavelength detector) uses light sources that give a continuous emission spectrum in a large range. A continuously adjustable monochromator is used for wavelength selection. The LIF detector (fluorescence detector) is suitable for fluorescent compounds. The phenomenon of fluorescence is, like that of absorption, the result of an electronic transition which converts the absorbing molecule to an excited state. The difference between fluorescent and non-fluorescent compounds is determined by what happens when the excited state returns to the ground state. The non-fluorescent molecules lose their energy as heat, while the fluorescent molecules emit part of the energy as light. During the period between absorption and emission, the molecule loses some of its energy by vibrational relaxation so that the emitted light is of lower energy and consequently higher wavelength than the exciting light. The LIF detector possesses high sensitivity, because the intensity of emitted light is directly proportional to the power of the exciting radiation. This method can be used to detect compounds that have intrinsic fluorescence or can be derivatized by reacting with a fluorescent compound, e.g. fluorescamine or dansyl chloride.

Compared to other separation methods (such as high performance liquid chromatography (HPLC), or thin-layer chromatography), CE has several advantages:

1. CE is applicable to a wider selection of analytes (small molecules and proteins).
2. CE requires minute amounts of sample.
3. CE consumes limited quantities of reagents (organic solvents are expensive to purchase, to store and to dispose)

To establish a good CE method, we aim to achieve good separation, good detection (low concentration of analyte), good reproducibility, and minimum amount of analytical steps. It is easier to detect analytes in pure standard solutions than in biological matrices, because biological samples contain high salt and high protein amounts. For high salt-containing samples, one can

use high concentration separation buffers. There are three ways to prepare high protein-containing samples before injection:

1. We can perform deproteinization before the CE separation with acetonitrile. When the protein size is smaller than 5000 Da, acetonitrile (2 volumes acetonitrile: 1 volume protein serum) is a good means to remove the protein, while acetonitrile can also provide sample stacking.
2. Micellar electrokinetic chromatography (MEKC) is a way to prevent protein adsorption to the capillary wall, because the MEKC surfactants solubilize proteins.
3. For analysis of small analytes, simple deproteinization can be performed by taking the analyte from the supernatant.

There is a group of important parameters for bioanalytical method validation according to the guidelines published by the International Conference on Harmonisation (ICH) of Technical Requirements for Registration of Pharmaceuticals for Human Use, and the US Food and Drug Administration (FDA), respectively,<sup>10,11</sup> including limitation of quantification (LOQ), limitation of detection (LOD), precision and accuracy. LOQ presents the lowest concentration of an analyte in a sample that can be quantitatively determined with a certain method, and LOD presents the lowest concentration that the bioanalytical procedure can reliably differentiate from background noise. LOQ and LOD can be obtained from equation 14 and equation 15, respectively.

$$\text{LOQ} = (S_{y,x}/\text{slope}) * 10 \quad (14)$$

$$\text{LOD} = (S_{y,x}/\text{slope}) * 3.3 \quad (15)$$

Where  $S_{y,x}$  and slope can be obtained from linear regression of the calibration curve.

Precision is the closeness of a series of measurements obtained from multiple sampling of the same homogenous sample under the described conditions, which can be presented with relative standard deviation (RSD) in an acceptable range of 20%.<sup>10,11</sup> Accuracy is the degree of closeness of the determined value to the true value, which has an acceptable range of 80-120%.<sup>10,11</sup>

### **1.2.2 Stacking methods for capillary electrophoresis**

Micellar electrokinetic chromatography (MEKC) is a popular technology for increasing detection sensitivity of CE, which introduces micelles or surfactants into the CE running buffer.<sup>12</sup> The

addition of cationic surfactants to the running buffer causes a reversal of the EOF, because the capillary is positively charged by adsorption of cationic surfactants.<sup>13,14</sup>

As shown in Figure 1.7, by using polybrene dynamic coating, both EOF and negatively charged analytes move towards the positive electrode. The more the analytes are negatively charged, the faster they migrate towards the detection window. Moreover, by electrokinetic injection, more negatively charged analytes can be selectively injected into the capillary.

Another simple CE sample pre-concentration method is field amplified sample stacking (FASS), which means to use a low concentration of sample matrix and a high concentration separation buffer.<sup>12</sup> The mechanism can be described as follows: sample ions have an enhanced electrophoretic mobility in a lower conductivity environment. When voltage is applied to the capillary, ions in the sample plug accelerate towards the adjacent separation buffer zone. On the boundary, the ions slow down because of the higher conductivity environment, so that the sample components are stacked within a smaller zone.

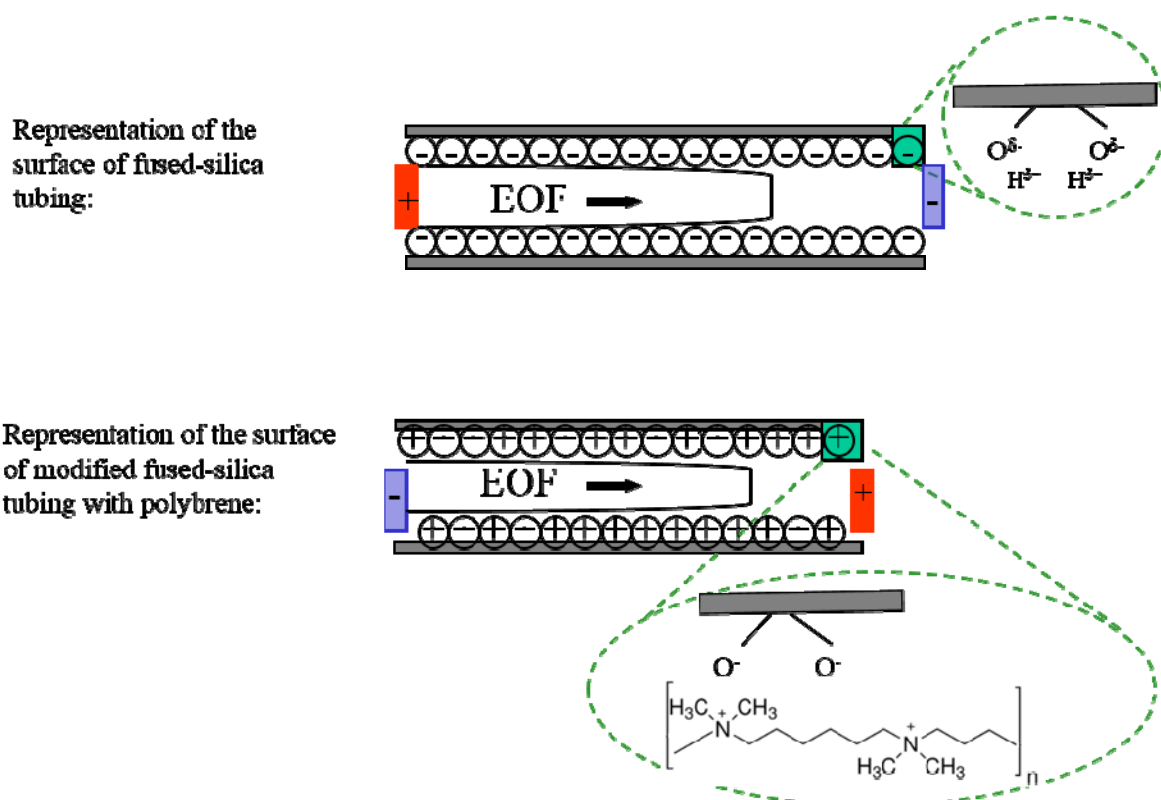


Figure 1.7. Differences between normal fused-silica and polybrene coated fused-silica capillary

A further CE sample stacking method, which was applied in our research project, is the dynamic pH junction method, which means to fill in buffers of different pH values into the capillary in order to achieve stacking effects on the boundary of the different buffers.<sup>12</sup> The detailed mechanism of the dynamic pH junction stacking method is described in Chapter 4.





## 2 Investigation of ecto-5'-nucleotidase - a novel anti-cancer drug target

### 2.1 Introduction

Ecto-5'-nucleotidase (*eN*), a  $Zn^{2+}$ -binding glycosylphosphatidylinositol-(GPI)-linked membrane-bound hydrolytic enzyme, plays a crucial role in switching on adenosine signaling via the P1 receptors ( $A_1$ ,  $A_{2A}$ ,  $A_{2B}$ ,  $A_3$ ).<sup>15,16</sup> Since P1 receptors have a very broad tissue distribution and are involved in multiple physiological functions, *eN* became a therapeutically interesting target for the treatment of inflammation, chronic pain, hepatic fibrosis, cancer and neurological disorders.<sup>17-27</sup> More interestingly, *eN* has been found to be overexpressed on many cancer cells, which enhances tumor growth and metastasis,<sup>20,28-30</sup> and deletion of *eN* on tumor cells significantly improved anti-tumor T cell immunity. Moreover, both, local and systemic production of adenosine by *eN*, might modulate anti-tumor responses *in vivo* (see Figure 2.8).<sup>28</sup> Therefore, treatment with *eN* inhibitors might be a promising novel strategy for cancer therapy.

*eN* belongs to the ecto-nucleotidase family, which consists of four main groups or families of ecto-nucleotidases: the E-NTPDase family (ecto-nucleoside triphosphate diphosphohydrolase family), the E-NPP family (ecto-nucleotide pyrophosphatase/phosphodiesterase family), ecto-5'-nucleotidase (*eN*), and alkaline phosphatases (AP).<sup>31,32</sup> Extracellular nucleotides, which act as signaling molecules, can be inactivated by hydrolysis via ecto-nucleotidases (Figure 2.1). *eN* hydrolyzes extracellular nucleoside monophosphate (AMP) to adenosine.<sup>33</sup> In mammals, the cytosolic 5'-nucleotidase and the ecto-5'-nucleotidase (*eN*) are structurally unrelated.<sup>34</sup> Determination of the primary structures of *eN* (from human placenta, rat liver and the electric ray fish) showed that in all three cases the mature enzymes consist of 548 amino acids with a molecular mass of about 61 kDa, and a metal content of two zinc ions per dimer was determined.<sup>34,35</sup> The primary structures of *eN* which were determined from rat liver and human placenta display nearly 90% amino acid identity.<sup>36</sup> The crystal structures of *eN* showed that the mammalian *eN* forms dimers, and the C-terminal domain contains the dimerization interface (Figure 2.2).<sup>4,37,38</sup>

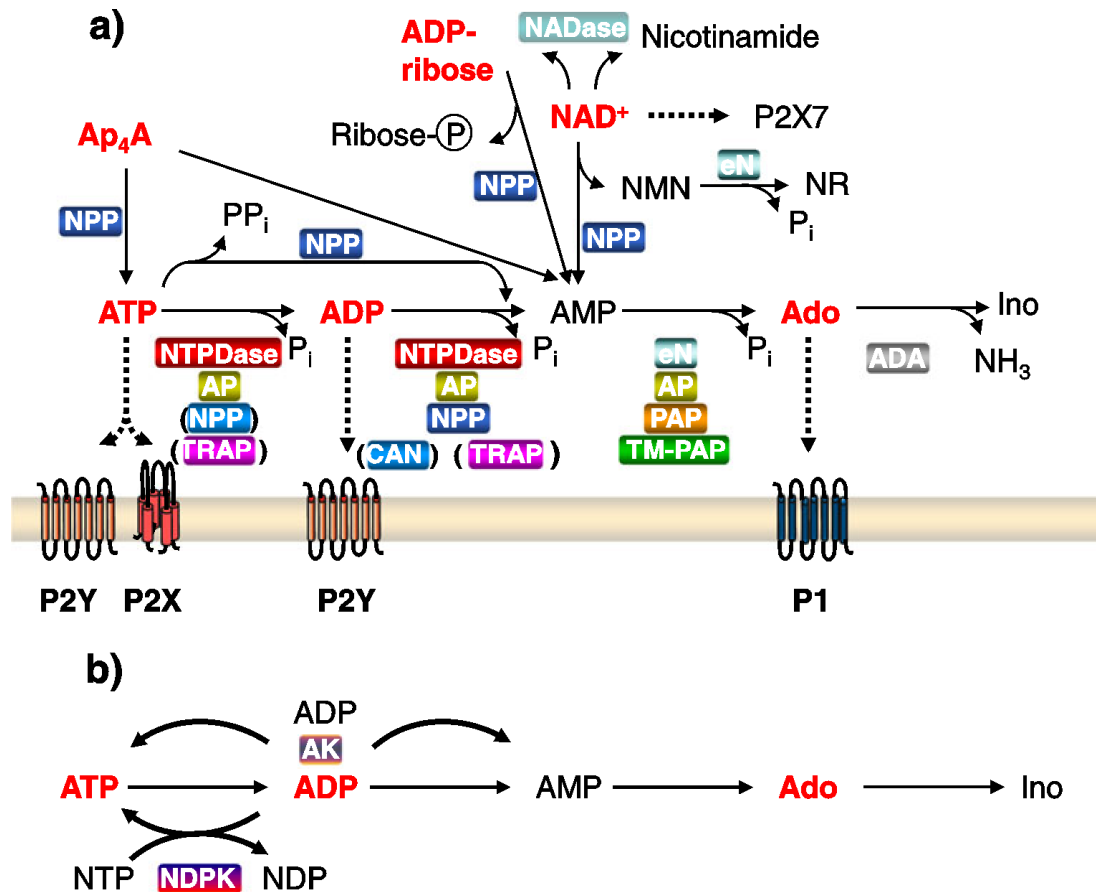


Figure 2.1. Overview of extracellular nucleotide metabolism pathway.<sup>15</sup> (a) Degradation of extracellular nucleotides and purinergic receptor activation. (b) Ecto-anabolism of nucleotides.

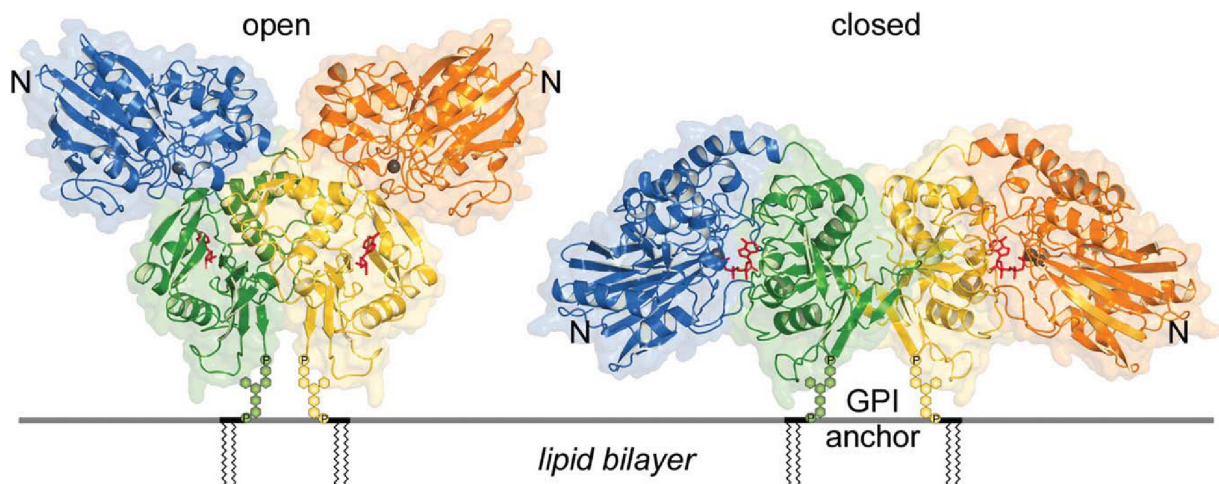


Figure 2.2. Crystal structure of human eN in an open conformation, and a closed conformation.<sup>4</sup> The N- and C-terminal domains of one subunit of the dimer are shown in blue and green, respectively. The N- and C-terminal domains of the adjacent subunit are shown in orange and yellow, respectively. Ligands (adenosine and AOPCP in the open and closed forms respectively) are shown as red sticks while the metal ions are shown as gray spheres.

It has been well known that nucleoside analogues are cornerstones of treatment for patients with cancer, and have been in clinical use for almost 50 years.<sup>39</sup> Novel nucleoside analogues still possess great potential, due to their increased selectivity and reduced side-effects in comparison with previously developed compounds.

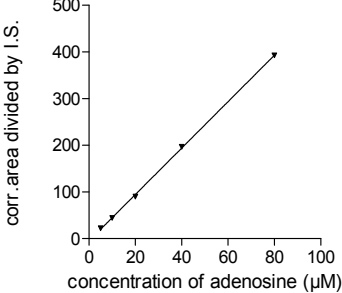
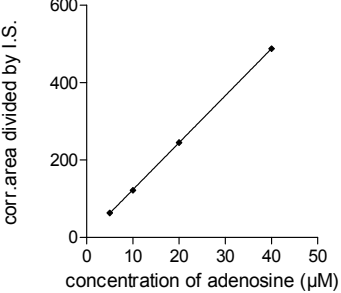
We investigated nucleotide mimetics which consisted of a nucleoside scaffold substituted in the 5'-position with a dipeptide moiety. The compounds were investigated at rat *eN* using a capillary electrophoresis-based assay. Potent inhibitors were further investigated at human *eN*.<sup>40</sup> The test results showed that the inhibitory potency of the compounds appeared to be pH-dependent: when the buffer pH was decreased, the potency of the compounds increased. Since low extracellular pH values are a hallmark of cancer (the extracellular pH value in normal tissue is around 7.5, and in many tumor tissue is more acidic and can be as low as 5.8),<sup>41–45</sup> the new inhibitors might act as tumor-selective *eN* inhibitors without affecting physiologically important functions of *eN*, such as the production of adenosine in blood vessels, which shows vasodilatory effects.<sup>46</sup>

## **2.2 Method development and validation**

### **2.2.1 Optimization and validation of capillary electrophoresis method**

A sensitive method for *eN* testing has been previously published,<sup>40</sup> and we further optimized this method by introducing an internal standard (I.S.) into the sample preparation step. An internal standard was not used in the published method, however, by using I.S., both, systematic errors and random errors can be avoided.<sup>47</sup> We tried different internal standards with various concentrations. Uridine 6.25  $\mu\text{M}$  has been found to be most suitable. A typical electropherogram of the *eN* reaction is shown in Figure 2.3. The limit of quantification (LOQ) was improved from 4.07  $\mu\text{M}$  to 2.70  $\mu\text{M}$ , while the accuracy and precision values were within a well acceptable range for the measurement of low concentrations of analytes.<sup>10,11</sup>

Table 2.1. Quantification of eN reaction product with different I.S.: method validation

Parameters	I.S. UMP, 25 $\mu$ M	I.S. Uridine, 6.25 $\mu$ M			
Regression equation (n=6)	$y = 4.974 x - 4.882$	$y = 12.16 x - 1.654$			
					
R <sup>2</sup>	0.9988	0.9996			
LOD ( $\mu$ M)	3.14	0.89			
LOQ ( $\mu$ M)	9.51	2.70			
Calibration range ( $\mu$ M)	5 - 80	5 - 40			
	Concentration ( $\mu$ M)	Accuracy (n=6, % recovery)	Accuracy acceptable range <sup>a</sup>	Precision (n=6, RSD <sup>b</sup> %)	Precision acceptable range <sup>a</sup>
I.S. UMP product	40	109.6	80-120%	4.1	20%
	20	99.3	80-120%	5.9	20%
	10	95.5	80-120%	4.5	20%
	5	101.4	80-120%	2.1	20%
I.S. Uridine product	40	106.7	80-120%	4.3	20%
	20	101.7	80-120%	2.7	20%
	10	101.5	80-120%	1.3	20%
	5	100.6	80-120%	0.8	20%

<sup>a</sup> According to guidelines of the International Conference on Harmonisation of Technical Requirements for Registration of Pharmaceuticals for Human Use <sup>10</sup>

<sup>b</sup> Relative standard deviation

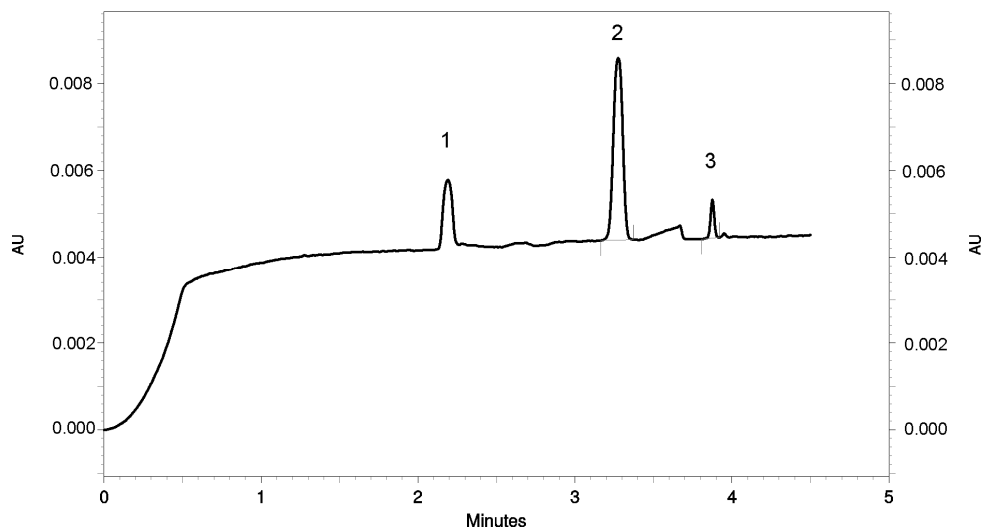


Figure 2.3. Representative electropherogram of *eN*. Borax buffer (40 mM), pH 9.1, hydrodynamic injection 0.5 psi, 5 sec),  $\lambda_{\max} = 260$  nm, separation voltage = 20 kV. Uncoated fused-silica capillaries of 40 cm total length (30 cm effective length)  $\times$  75.5  $\mu\text{m}$  (inner diameter)  $\times$  363.7  $\mu\text{m}$  (outer diameter). Peaks: **1**, buffer; **2**, adenosine; **3**, I.S. uridine.

## 2.3 Results

### 2.3.1 Kinetic characterization of ecto-5'-nucleotidase-catalyzed reactions

Reported  $K_m$  values for the *eN* substrate AMP range between 1 and 50  $\mu\text{M}$ .<sup>15,48–51</sup> We used reaction buffers with different pH values to determine the  $K_m$  value of AMP. As shown in Figure 2.4, *eN* (rat enzymes) displayed a  $K_m$  value of  $50.4 \pm 10.2$   $\mu\text{M}$  and a  $V_{\max}$  value of  $0.281 \pm 0.013$   $\mu\text{mol}/\text{min}/\text{mg}$  in pH 4.9 buffer; a  $K_m$  value of  $45.9 \pm 5.28$   $\mu\text{M}$  and a  $V_{\max}$  value of  $0.738 \pm 0.096$   $\mu\text{mol}/\text{min}/\text{mg}$  was obtained in pH 5.6 buffer; and a  $K_m$  value of  $45.2 \pm 3.2$   $\mu\text{M}$  and a  $V_{\max}$  value of  $1.31 \pm 0.10$   $\mu\text{mol}/\text{min}/\text{mg}$  was determined in pH 7.4 buffer. The three enzyme kinetic curves at different pH values were determined at the same time with the same enzyme aliquot. Therefore data are well comparable. The stability of the enzyme was tested, and the result showed that the enzyme was stable during the incubation time. The buffer pH stability during the enzyme reaction was tested, and the result showed that the buffer kept the same pH range during the enzymatic reaction. The enzyme is more active at higher pH value, indicated by decrease in the  $V_{\max}$  values with decreasing pH value, while the  $K_m$  values stayed around 45  $\mu\text{M}$ .

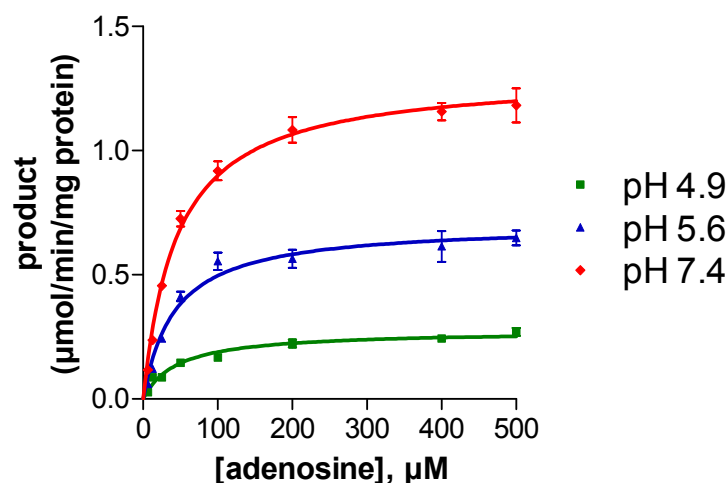


Figure 2.4. Enzyme kinetics of *eN*. Michaelis-Menten plot for *eN* in reaction buffers with different pH values, each curve was carried out in three independent assays. At pH 4.9,  $K_m$   $50.4 \pm 10.2 \mu\text{M}$ ,  $V_{\text{max}}$   $0.281 \pm 0.013 \mu\text{mol}/\text{min}/\text{mg}$ ; at pH 5.6,  $K_m$   $45.9 \pm 5.28 \mu\text{M}$ ,  $V_{\text{max}}$   $0.738 \pm 0.096 \mu\text{mol}/\text{min}/\text{mg}$ ; at pH 7.4,  $K_m$   $45.2 \pm 3.2 \mu\text{M}$ ,  $V_{\text{max}}$   $1.31 \pm 0.10 \mu\text{mol}/\text{min}/\text{mg}$ .

### 2.3.2 Inhibitors of ecto-5'-nucleotidase

We tested a series of novel nucleotide mimetics which consisted of a nucleoside scaffold substituted in the 5'-position with a dipeptide moiety (Table 2.2). The compounds were investigated at rat *eN*, and several compounds have been found out to be pH-dependent inhibitors: when the buffer pH values decreased, the potency of the compounds increased. The most potent pH-selective compound AMB552.3a was further investigated at human *eN*, and its pH-dependent inhibition manner was found to be retained at human *eN*. Furthermore, the inhibition mechanism for ATP, AOPCP and AMB552.3a in pH 5.6 buffer was investigated (Figure 2.5). AMB552.3a was found to act as a non-competitive inhibitor, while ATP and AOPCP appeared to be competitive inhibitors.

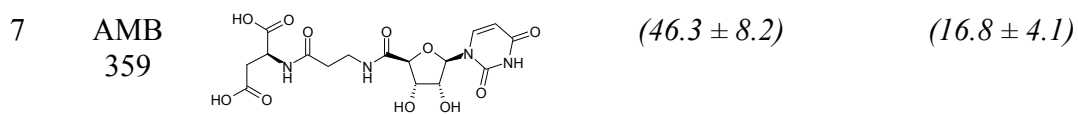
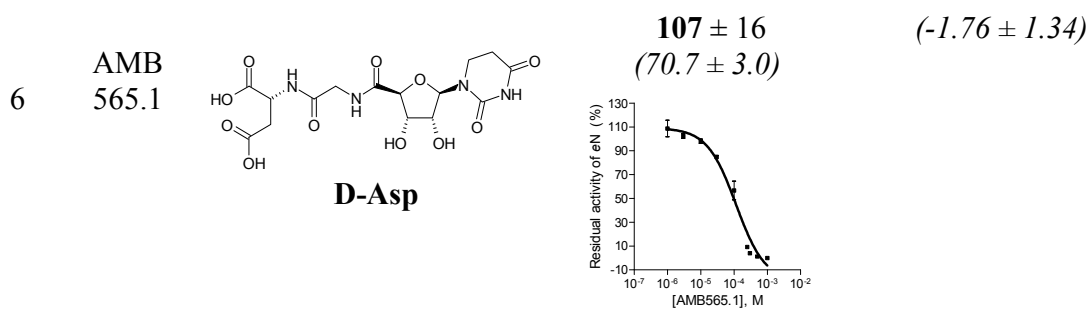
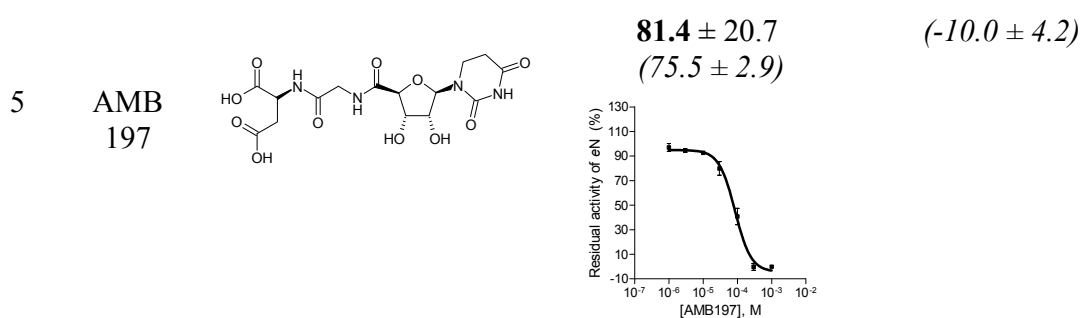
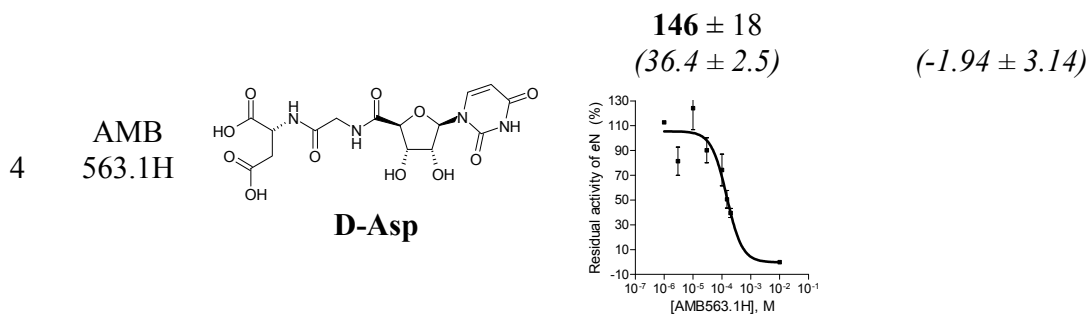
Table 2.2. Test result of pH-dependent inhibitors and reference compounds

No.	Code name	Structure	rat eN <b>IC<sub>50</sub> ± SEM (μM)</b> <i>(or % inhib. at 100 μM)</i> at pH 5.6	rat eN <b>IC<sub>50</sub> ± SEM (μM)</b> <i>(or % inhib. at 100 μM)</i> at pH 7.4
<b>Nucleotide standard inhibitors</b>				
1	ATP		competitive <b>136 ± 51</b> <i>(53.6 ± 4.5)</i> <b>(K<sub>i</sub> = 10.6 ± 4.0)</b>	competitive <b>934 ± 115</b> <i>(14.1 ± 4.0)</i> <b>(K<sub>i</sub> = 70.8 ± 8.7)</b>
2	ADP		<b>6.65 ± 0.63</b> <i>(90.5 ± 2.4)</i>	<b>15.4 ± 4.3</b> <i>(84.4 ± 1.5)</i>
3	AOPCP		competitive <b>0.950 ± 0.018</b> <i>(97.3 ± 0.1)</i> <b>(K<sub>i</sub> = 0.0736 ± 0.0014)</b>	competitive <b>0.379 ± 0.075</b> <i>(90.0 ± 3.0)</i> <b>(K<sub>i</sub> = 0.0287 ± 0.0057)</b>

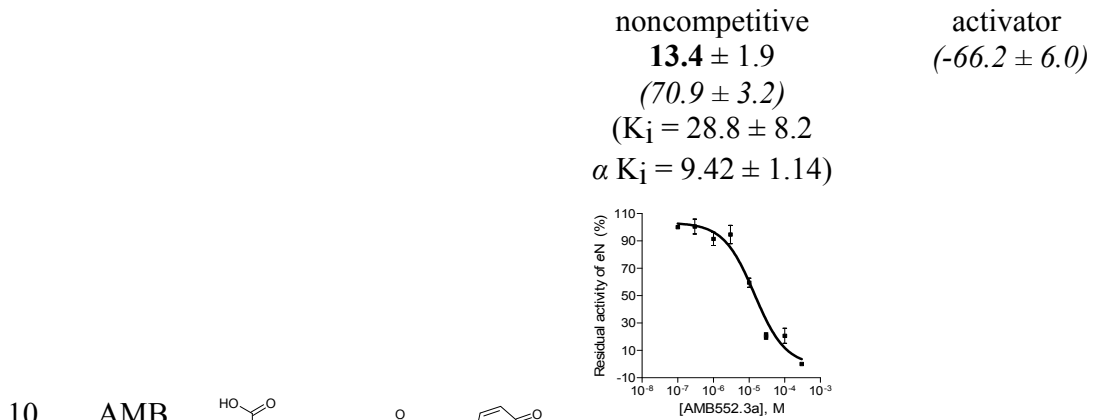
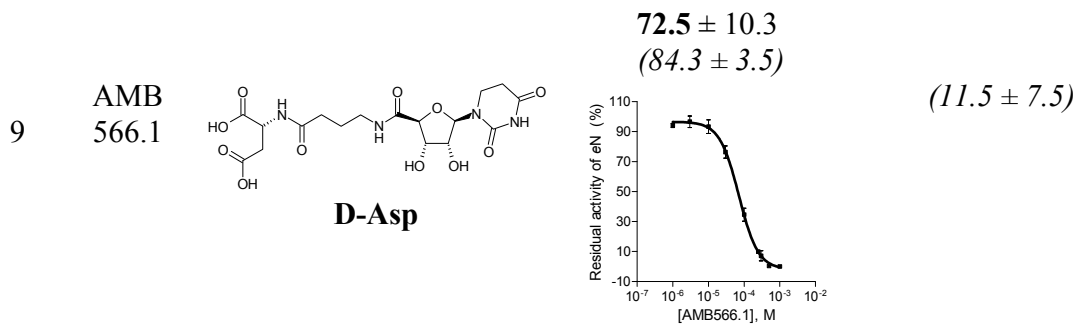
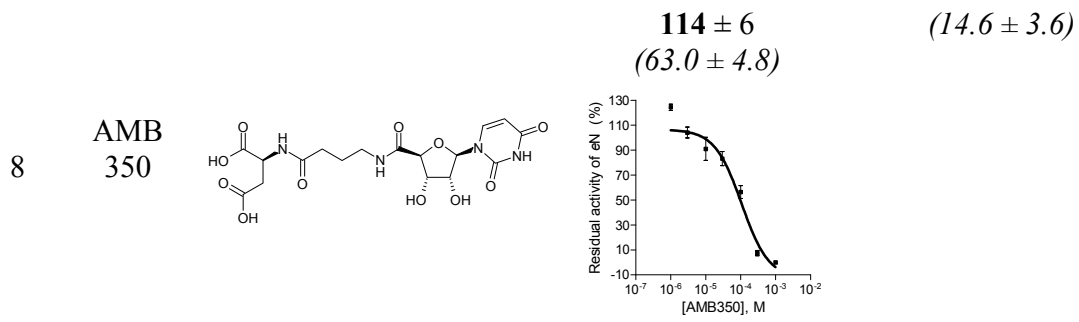
---

## Nucleotide mimetics

---

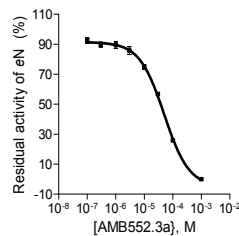






human eN  
 $50.3 \pm 3.6$   
 $(81)$

human eN  
 $(14)$



11

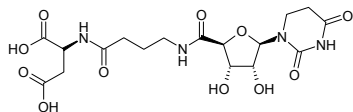
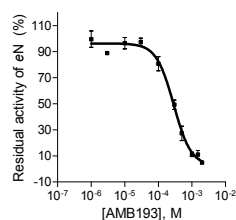
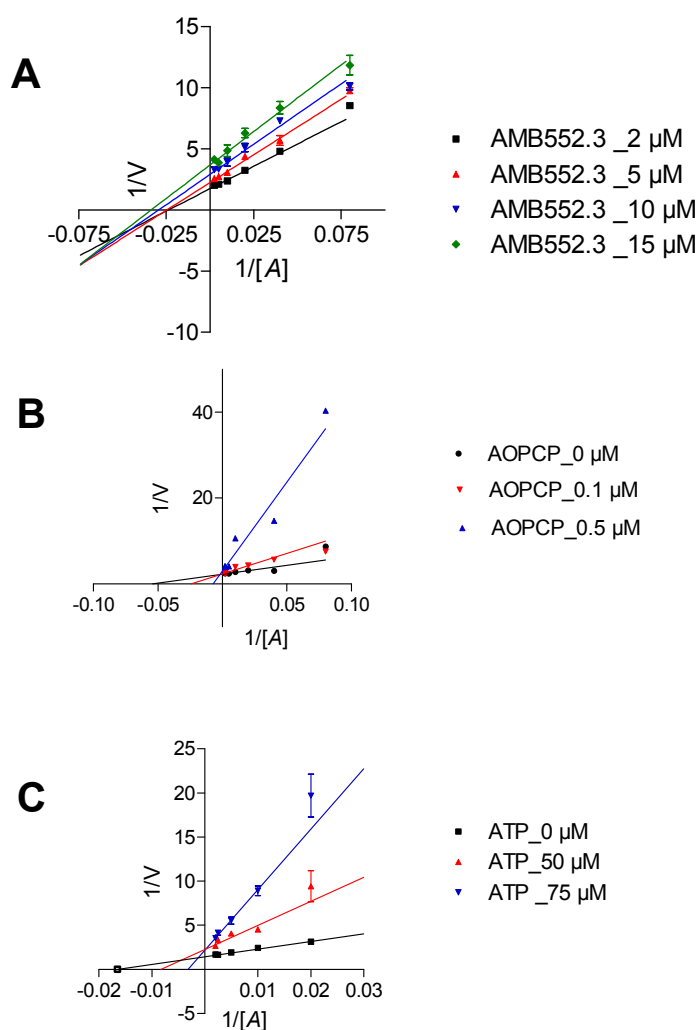
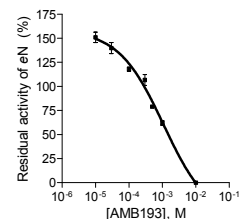
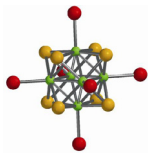
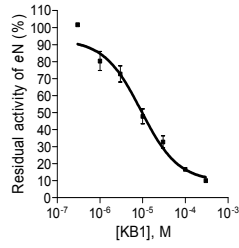
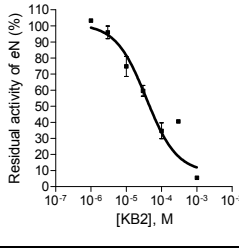
AMB  
193
 $345 \pm 73$   
 $(46.9 \pm 4.0)$ 

 $960 \pm 84$   
 $(12.0 \pm 1.5)$ 


Figure 2.5. Determination of enzyme inhibition mechanism of AMB552.3a and reference compounds at buffer pH 5.6. (A) *eN* inhibition by AMB552.3a is non-competitive (AMB552.3a concentrations for determination were 2  $\mu\text{M}$ , 5  $\mu\text{M}$ , 10  $\mu\text{M}$  and 15  $\mu\text{M}$ ); (B) *eN* inhibition by AOPCP is competitive (AOPCP concentrations for determination were 0  $\mu\text{M}$ , 0.1  $\mu\text{M}$  and 0.5

$\mu\text{M}$ ); (C) *eN* inhibition by ATP is competitive (ATP concentrations for determination were 0  $\mu\text{M}$ , 50  $\mu\text{M}$  and 75  $\mu\text{M}$ ).

Additionally, a series of polyoxometalates (POMs), which contain early transitional metal ions such as tungsten (W), molybdenum (Mo), niobium (Nb), antimony (Sb) or vanadium (V) surrounded by oxygen atoms, has been tested at rat *eN* (see Table 2.3). Polyoxometalates (POMs) are inorganic cluster metal complexes that have been shown to possess a variety of biological activities such as antibacterial, anticancer, antidiabetic, and antiviral effects.<sup>52–54</sup> Several inhibitors of *eN* have been identified (Table 2.3), and the inhibition mechanisms were investigated (Figure 2.6). These inhibitors are KB1, KB2 and KB4, which are all non-competitive, with  $\text{IC}_{50}$  values  $11.4 \pm 1.8$ ,  $52.3 \pm 27.2$ , and  $4.57 \pm 1.28 \mu\text{M}$ , respectively. The aqueous solubility of KB4 and KB1 was good, whereas the solubility of KB2 was poor.

Table 2.3. Test result of POMs

Code name	Structure	rat <i>eN</i> $\text{IC}_{50} \pm \text{SEM} (\mu\text{M})$ ( $K_i \pm \text{SEM} \mu\text{M}$ )	Inhibition curves
			
KB1	$[(\text{Re}_6\text{S}_8)(\text{OH})_6]^{4-}$	$11.4 \pm 1.8$ ( $K_i = 12.9 \pm 5.5$ $\alpha K_i = 12.6 \pm 7.0$ )	
KB2	$[(\text{Re}_6\text{Se}_8)(\text{OH})_6]^{4-}$	$52.3 \pm 27.2$ ( $K_i = 25.6 \pm 13.7$ $\alpha K_i = 19.4 \pm 1.6$ )	

KB4  $[(\text{Re}_6\text{S}_8)(\text{HCOO})_6]^{5-}$   $4.57 \pm 1.28$   
 $(K_i = 2.89 \pm 0.32)$   
 $\alpha K_i = 2.54 \pm 0.24)$

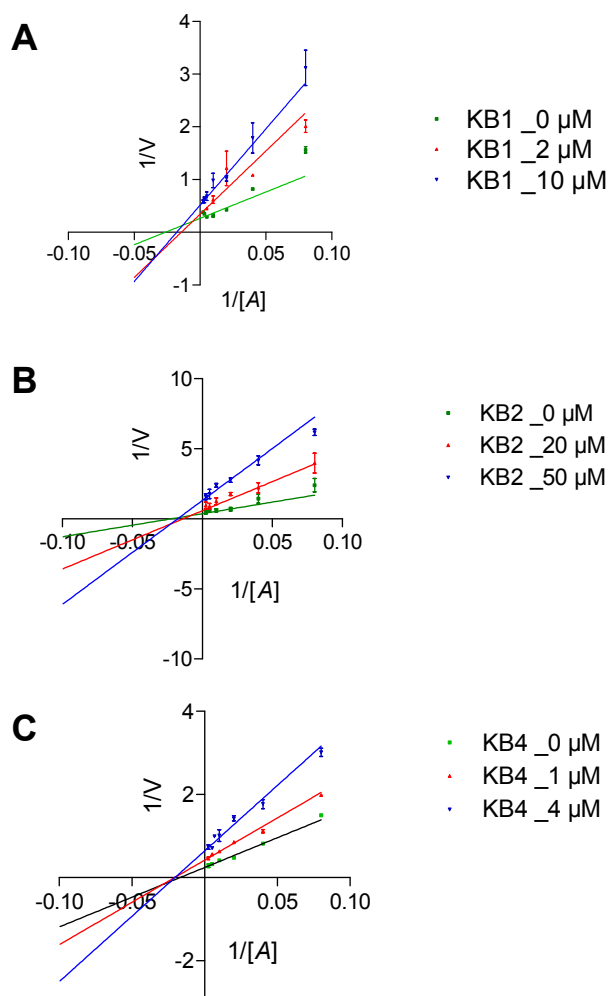
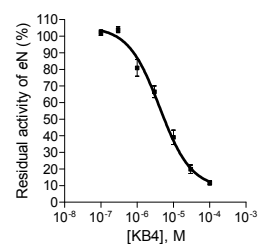


Figure 2.6. Determination of enzyme inhibition mechanism. (A) *eN* inhibition by KB1 is non-competitive (KB1 concentrations for determination were 0  $\mu\text{M}$ , 2  $\mu\text{M}$  and 10  $\mu\text{M}$ ); (B) *eN* inhibition by KB2 is non-competitive (KB2 concentrations for determination were 0  $\mu\text{M}$ , 20  $\mu\text{M}$  and 50  $\mu\text{M}$ ); (C) *eN* inhibition by KB4 is non-competitive (KB4 concentrations for determination were 0  $\mu\text{M}$ , 1  $\mu\text{M}$  and 4  $\mu\text{M}$ ).

### 2.3.3 Activators of ecto-5'-nucleotidase

Previous reports showed that *eN* can be activated by thyroid hormones and protein kinase C.<sup>55-57</sup> In the present study we have found two new activators of rat *eN* at pH 7.4 (Figure 2.7), NaCP<sub>8</sub>W<sub>12</sub> and AMB552.3a activated *eN* with EC<sub>50</sub> values of 11.4 ± 1.3 μM, and 3.05 ± 0.57 μM, respectively.

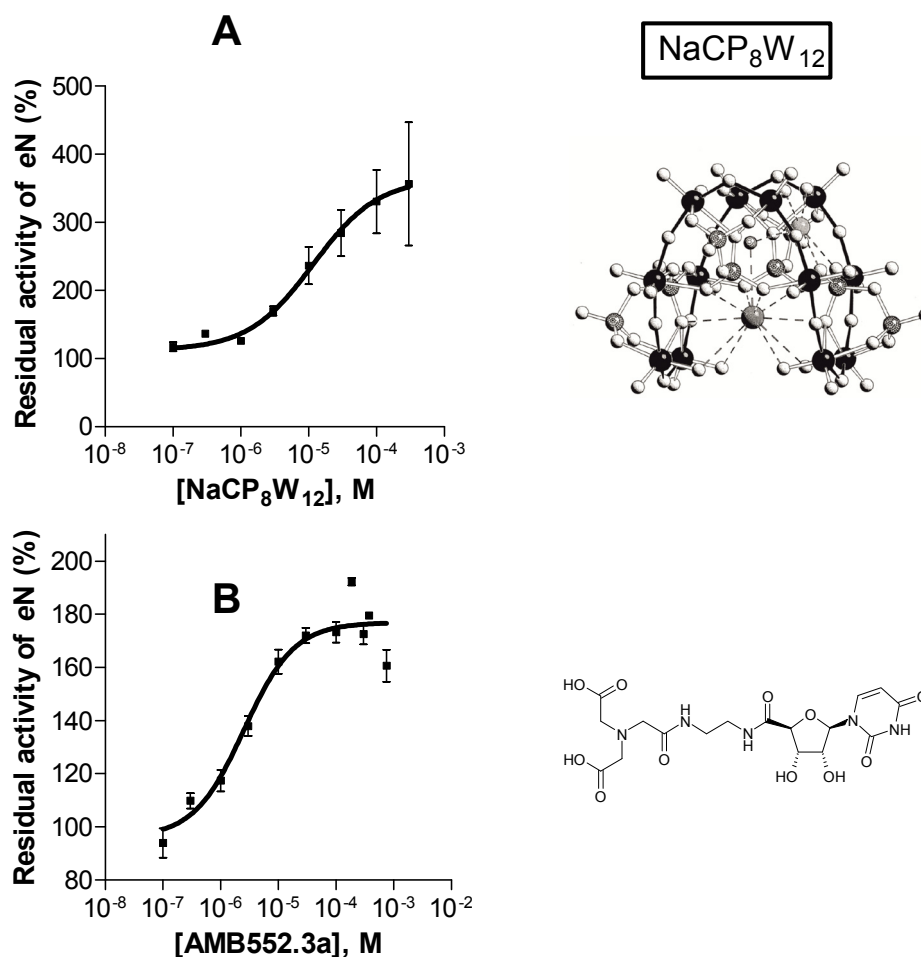


Figure 2.7. Activators of *eN* at pH 7.4 in HEPES buffer. The concentration of *eN* substrate AMP was 500 μM ( $K_m$  45 μM) (A) Activation of *eN* by NaCP<sub>8</sub>W<sub>12</sub> was up to 400%, the EC<sub>50</sub> value was 11.4 ± 1.3 μM (B) Activation of *eN* by AMB552.3 was up to 200%, the EC<sub>50</sub> value was 3.05 ± 0.57 μM.

## 2.4 Conclusions and discussion

Several novel nucleotide mimetics have been found as pH-dependent *eN* inhibitors in our study. *eN* is upregulated in tumors (Figure 2.8<sup>28,58</sup>). Tumor tissues are hypoxic and have an acidic environment.<sup>20,28,29,44</sup> The new pH-dependent inhibitors, which can be envisaged as small molecules targeting *eN* in a tumor-selective manner, might be a novel strategy for selective tumor therapy.

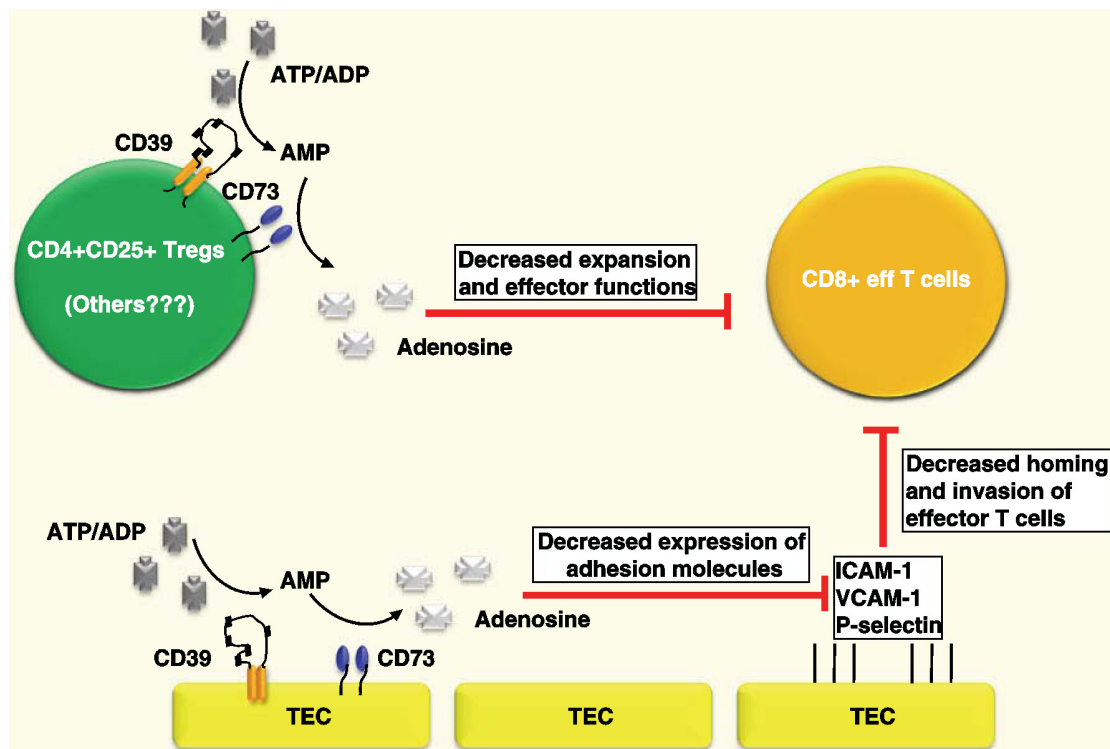


Figure 2.8. Scheme of purinergic signaling pathways in cancer.<sup>28,58</sup> Production of adenosine by *eN* on both local tumor resident cells (TEC) and systemic bone marrow-derived cells (CD4+CD25+ regulatory T cells (Tregs)) might modulate anti-tumor responses: on tumor resident cells, adenosine decreases expression of adhesion molecule (intercellular adhesion molecule-1(ICAM-1), vascular cell adhesion molecule-1(VCAM-1), P-selectin), which results in decreasing homing and invasion of effector T cells; and on bone marrow derived cells, adenosine decreases expansion and effector functions of T cells.

The most potent pH-dependent inhibitor AMB552.3a was further examined by crystal structure analysis. Cocrystal structures of human *eN* with AOPCP and AMB552.3a are shown in Figure 2.9.<sup>4</sup> The N-terminal domain contains the metal ion binding site and the C-terminal domain contains the substrate binding site, whereby the active site is located at the interface between the

N- and C-terminal domains. AOPCP was crystallized with the closed conformation of *eN*, therefore we can see its interaction with the whole active site, whereas AMB552.3a was crystallized with the open conformation of *eN* and we can only see the C-terminal domain interaction. The nucleobase of AMB552.3a was tightly sandwiched via  $\pi$ -stacking interactions between the side chain of F417 and F500 (adenine clamp), and the uracil base and the ribose moieties form hydrogen bonds with the side chains of N390, R395, and D506. Other compounds except for AOPCP have not been co-crystallized in the closed conformation of *eN*,<sup>4</sup> in other words, we could not examine the interaction of our inhibitors with the N-terminal domain of *eN*. According to our result, both ATP and AMB552.3a, are pH-dependent inhibitors, whereas AOPCP is not pH-dependent. Thus we presume that the pH-dependent interaction moiety is located in the N-terminal domain. The crystal structure of AMB552.3a probably only reflects part of the inhibition mode, because the tail of AMB552.3a is less ordered and sticks out into the solvent.

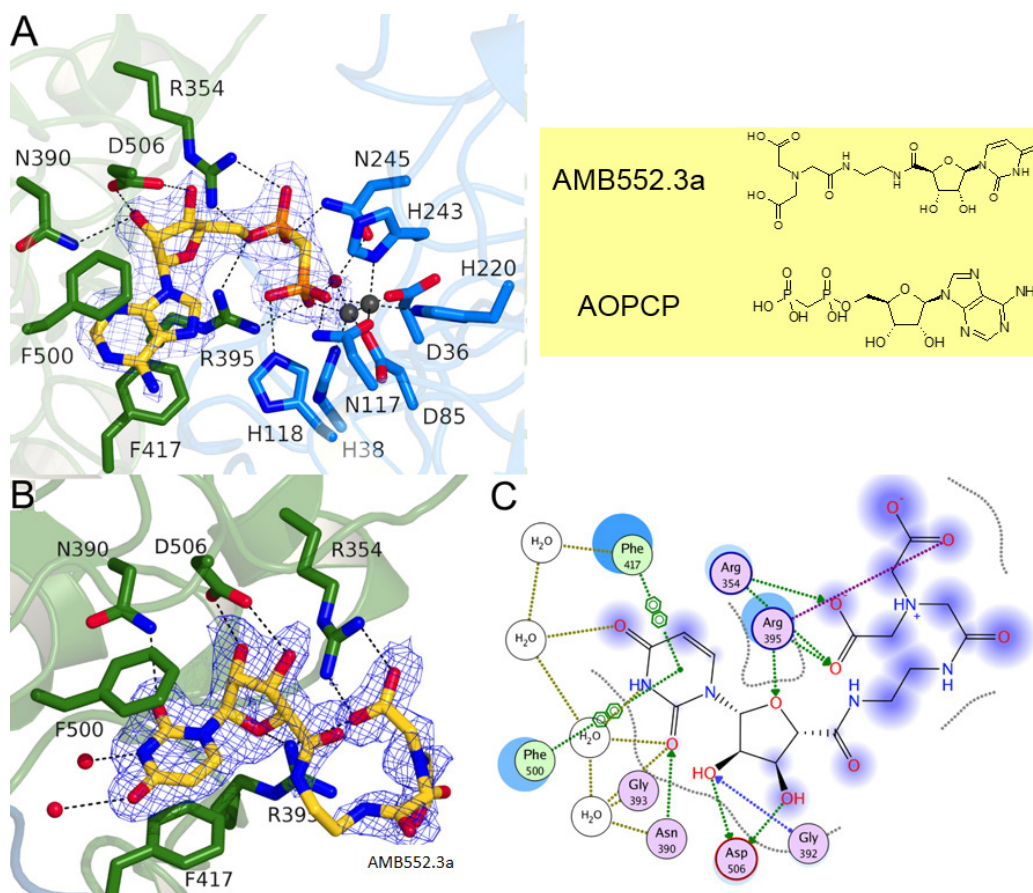


Figure 2.9. Binding mode of AOPCP and AMB552.3a.<sup>4</sup> (A) Stereo-view of AOPCP bound to the human *eN* active site of the closed conformation. The two zinc ions are shown as gray spheres. The protein residues of the C-terminal domain forming the substrate binding site are shown in

green whereas the amino acids of the N-terminal domain are shown in blue. A water molecule, which coordinates on metal ions, is shown in red. The AOPCP omit-electron density map is shown in blue. (B) Stereo-view of AMB552.3a bound at the human eN C-terminal domain of the open conformation. The AMB552.3a omit-electron density map is shown in blue. (C) Schematic representation of the interaction of AMB552.3a with the human eN C-terminal domain.

We predicted the  $pK_a$  values of our pH-dependent inhibitors with the software MarvinSketch (Table 6.1), in order to find out the influence of the compounds'  $pK_a$  values on their pH-dependent behaviour. The prediction showed that some inhibitors display changes in microspecies distribution in the pH range of 5.0 - 7.4 (e.g. ATP), while some inhibitors have stable microspecies distribution in the same pH range (e.g. AMB552.3a), which may lead to the conclusion that the different performances of the compounds are not exclusively caused by changes in microspecies distribution under different pH conditions. We further confirmed the microspecies distribution of AMB552.3a by a potentiometric  $pK_a$  determination method (Figure 2.10). The test result was similar to our predicted  $pK_a$  value.

Position	1	2	3	4
	$pK_a$	$pK_a$	$pK_b$	$pK_a$
mean	2.2	2.81	8.84	9.8
SD	0.1	0.04	0.01	0.2

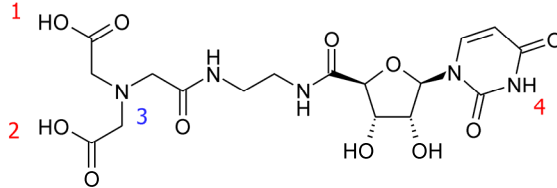


Figure 2.10. Results of potentiometrical  $pK_a$  determination of AMB552.3a ( $n=3$ ). The results show that in the pH range of 5.0 - 7.4 the ionic charge of compound AMB552.3a is -1. At positions 1 and 2, the two carboxylic groups are deprotonated, while at position 3 the tertiary amine is protonated.



## 3 Investigation of cerebroside sulfotransferase as therapy target for metachromatic leukodystrophy

### 3.1 Introduction

The enzyme cerebroside sulfotransferase (CST) is a promising target for metachromatic leukodystrophy (MLD), a rare and severe genetic disease. CST catalyzes the last step in the synthesis of cerebroside sulfate (sulfatide), namely the transfer of a sulfate group from 3'-phosphoadenosine-5'-phosphosulfate (PAPS) to cerebroside (Fig. 3.1).<sup>59</sup> MLD is characterized by an accumulation of sulfatide in cells, and this accumulation causes progressive destruction of white matter throughout the nervous system.<sup>60,61</sup> About 50-60% of MLD patients are of the late-infantile form with age onset before 3 years; affected children lose speech, become weak, and typically do not survive past childhood. Around 20-30% of MLD patients are of the juvenile form with age onset before 16 years of age; affected individuals may survive for about 20 years after diagnosis. The remaining 15-20% of MLD patients are of the adult form; these patients may survive for 20-30 years after diagnosis.<sup>60,62</sup> Therapeutic options for MLD include enzyme replacement, substrate reduction, stem cell transplantation, and gene therapy.<sup>60,63</sup> The only conceivable approach allowing the development of small molecules as drugs for MLD would be substrate reduction therapy. Therefore we are aiming at developing CST inhibitors to reduce the biosynthesis of sulfatide and as a consequence to prevent sulfatide aggregation in the central and peripheral nervous system.<sup>59</sup>

There are three kinds of published assays for the monitoring of sulfotransferase activity: (i) a radioisotopic assay, which monitors the transfer of radioactive sulfate from [<sup>35</sup>S]-labelled 3'-phosphoadenosine-5'-phosphosulfate ([<sup>35</sup>S]PAPS) to cerebroside sulfate (sulfatide), the product of CST; [<sup>35</sup>S]cerebroside sulfate is measured by end-point methods via thin-layer or paper chromatography.<sup>64-72</sup> (ii) In another assay sphingolipids are quantified by HPLC-MS/MS or LC-ESI MS/MS.<sup>73-76</sup> (iii) Furthermore, a coupled enzymatic assay was developed, in which the auxiliary enzyme aryl sulfotransferase IV (AST-IV) further catalyzes the sulphating of PAP with *p*-nitrophenyl sulfate to form PAPS, and the product *p*-nitrophenol is monitored.<sup>77</sup> The drawback of the radioisotopic assay includes the high price of [<sup>35</sup>S]PAPS and the lengthy

procedure associated with thin-layer chromatography, which is not compatible with high-throughput screening. The main challenge of monitoring sphingolipids is the quantification of all sphingolipid species, since they typically consist of a mixture of lipids of different alkyl chain lengths, which may additionally contain double bonds and/or hydroxyl groups. Although the development of a coupled enzyme assay procedure solved most of the shortcomings of previously applied methods, it is still not ideal since inhibitors of the auxiliary enzyme might be identified as false-positive hits in CST inhibitor screening. Therefore, a suitable method which would allow the direct measurement and quantification of one of the enzymatic reaction products would be highly desirable.

We have now developed a simple, economic, powerful and highly sensitive capillary electrophoresis (CE) method for the monitoring of CST activity via quantification of the enzymatic product adenosine-3',5'-diphosphate (PAP) (Fig. 3.1). This is the first validated CE method for monitoring of the catalytic activity of the enzyme CST. In order to enhance detection sensitivity of PAP, we applied micellar electrokinetic chromatography (MEKC) with polybrene as an additive to the running buffer, combined with dynamic pH junction stacking (Figure 3.2). Our new CE method enables an efficient separation of the components in the enzyme reaction mixture and allows for enzyme kinetic studies, compound library screening, and inhibitor characterization.

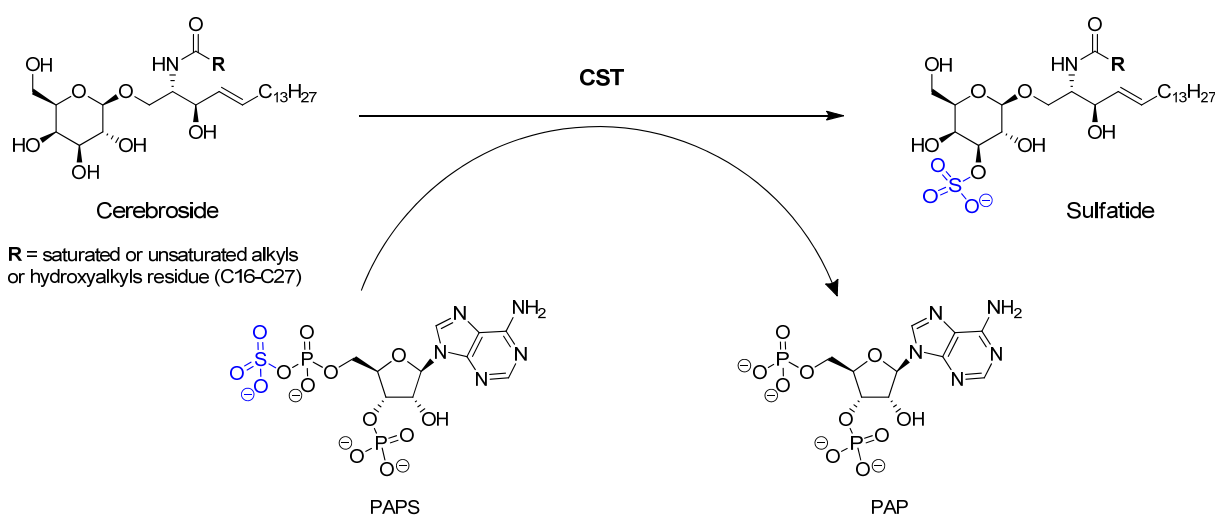


Figure 3.1. Proposed pathway for CST biosynthesis<sup>59</sup>. CST can catalyze the conversion of cerebroside to sulfatide, and PAPS is sulfate donor, therefore the enzymatic products of CST are sulfatide and PAP.

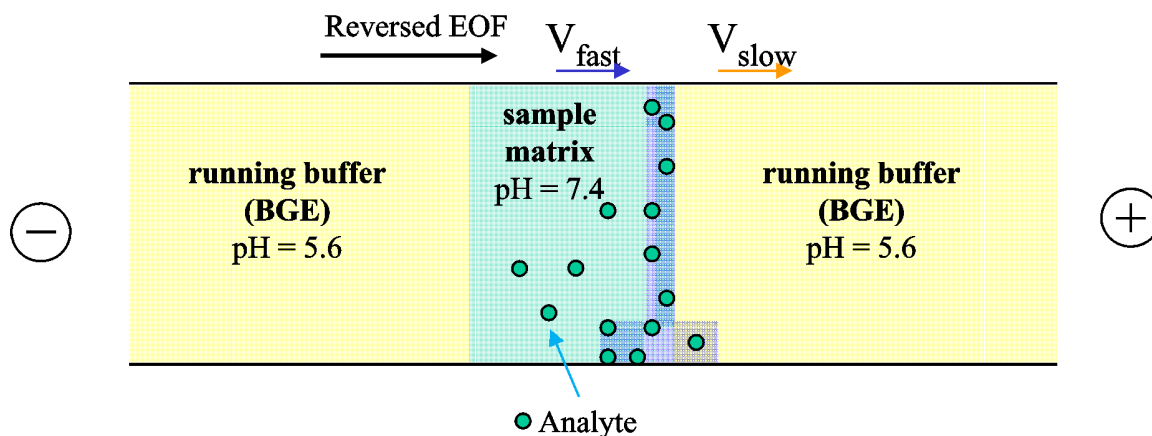


Figure 3.2. The dynamic pH junction model based on the results of experiments. The capillary was conditioned with BGE buffer (pH 5.6), and then the sample matrix (pH 7.4) was electrokinetic injected. The analytes are negatively charged and migrated to detection window faster in pH 7.4 buffer than pH 5.6 buffer, therefore a stacking effect occurred on the boundary of these two buffers.

Sulfation is a widely observed biological reaction conserved from bacterium to human that plays a key role in various biological processes such as growth, development and defense against adversities.<sup>78,79</sup> Deficiencies due to the lack of the ubiquitous sulfate donor PAPS are lethal in humans.<sup>78-80</sup> A large group of enzymes called sulfotransferases catalyze the transfer reaction of the sulfate group of PAPS to the acceptor group of numerous biochemical and xenochemical substrates<sup>75,81</sup>. Structure-based sequence alignments based on an X-ray crystal structures indicate that the PAPS-binding site is conserved.<sup>78,79,82</sup> Therefore, the development of competitive inhibitors for the CST substrate cerebroside rather than for the co-substrate PAPS may reduce side effects that can be expected from competitive inhibitors of the CST co-substrate PAPS. A mimic of the transition state-like intermediate state in the cerebroside binding site might efficiently inhibit CST catalytic reaction.<sup>1</sup> A proposed reaction mechanism between the enzyme, the PAPS, and the substrate based on a crystal structure is shown in Figure 3.3,<sup>83-85</sup> which might give us new ideas about how to design a transition state mimic of a lipid inhibitor.

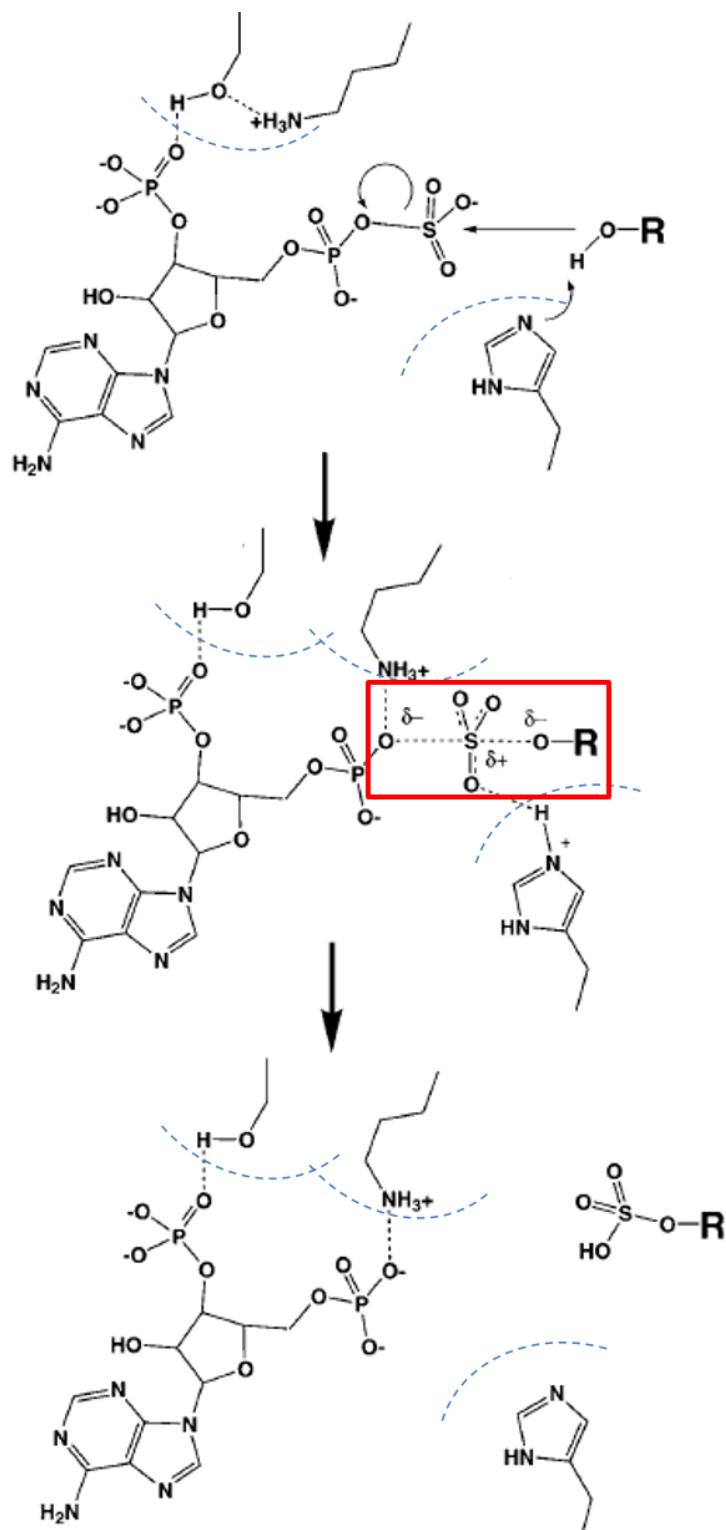


Figure 3.3. Proposed transition state of the substrate according to crystal structures from the sulfotransferase family.<sup>83–85</sup> The proposed reaction mechanism could be described in two steps: 1. The hydroxyl group of the substrate acts as a nucleophile, which when deprotonated by a conserved histidine in the active center of the enzyme attacks the sulfur atom of PAPS. 2. The formed transition state is subsequently converted to the final product.

## 3.2 Method development and validation

### 3.2.1 Development and optimization of the capillary electrophoresis method

Our goal was to develop a sensitive CE method for monitoring CST reactions. Our group has long-standing experience in the quantification of nucleotides by CE, and especially in enzyme assays involving the formation or transformation of nucleotides.<sup>40,86–92</sup> Thus we decided to quantify the nucleotide PAP which is formed from the co-substrate PAPS during the CST reaction. This was found to be easier than detecting the lipid sulfatide, which constitutes a mixture of compounds with different alkyl chains of different lengths that may additionally contain double bonds or hydroxyl groups (see Fig. 3.1).

As a starting point, a CZE method with borax buffer in fused-silica (FS) capillary was applied. However, the CST reaction matrix was high protein-containing and high lipid-containing, we had to use centricon to do additional sample preparation step (Figure 3.4): the reaction was stopped by filtering the 50  $\mu$ l reaction solution with 3 kD centricon for 30 min (14,000g). The < 3 kD part (around 25  $\mu$ l) was collected and be measured by CE.

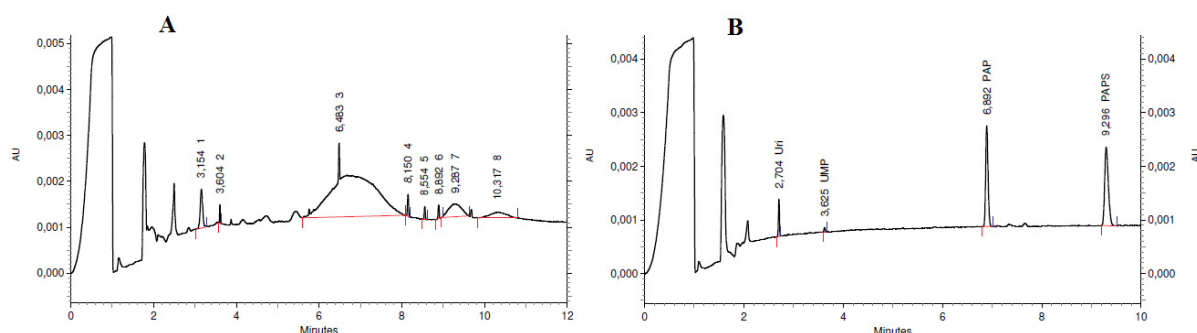


Figure 3.4. The electropherogram results for centricon sample preparation. FS Capillary with 40 cm (30 cm) length and 75  $\mu$ m internal diameter, 25°C, acquisition rate is 4 Hz, 260 nm detection window, running buffer borax 40 mM with pH value 9.1, separation voltage 20 kV, injection 0.5 psi for 5 sec. **A.** Without centricon filtration, the peaks of product cannot be detected. **B.** With centricon filtration, the product PAP (retention time 7 min) can be detected.

Since the sample preparation step with centricon was not the optimal way for high throughput screening (HTS), we used dynamic coating of the capillary by adding polybrene to running buffer, because cationic surfactants can reduce the attachment of proteins and lipids onto the fused-silica capillary inner wall, and thereby can support a sweeping effect of negatively charged

analytes when a reverse electroosmotic flow (EOF) is applied.<sup>87,90,93</sup> This type of MEKC mode represents a powerful CE technique,<sup>13,93-97</sup> which is especially suitable for charged analytes.<sup>87,89,90,92,93</sup> In previous studies, the buffers used in combination with polybrene dynamic coating of the capillary had a pH range between 2-11, and the most widely used buffers for dynamic polybrene coating were borax/boric acid, phosphate, and folic acid, respectively.<sup>98-103</sup> According to the prediction of net charges of PAP and PAPS (Figure 3.5), a pH 8 running buffer has firstly been selected. Because at pH 8 there is no net charge difference between PAP and PAPS, they can be separated due to the difference in size. We have optimized other parameters, e.g. capillary length, in order to achieve good separation (Figure 3.6). The LOD of PAP was 3.09  $\mu\text{M}$ .

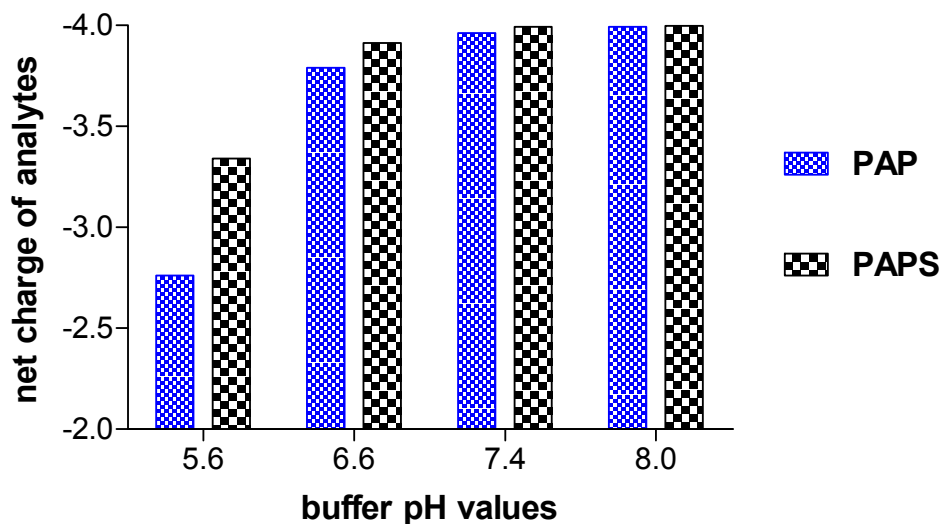


Figure 3.5. Prediction of net charges of PAP and PAPS under different buffer pH values determined by the software program Marvin Sketch. The prediction showed that that at pH 8, there is no net charge differences between PAP and PAPS; whereas at pH 5.6, the net charge differences between PAP and PAPS are maximal. Moreover, When PAP migrates from the pH 7.4 buffer to the pH 5.6 buffer, its net charge is decreased, which will slow down its moving velocity and result in a stacking effect at the boundary between these two buffers.

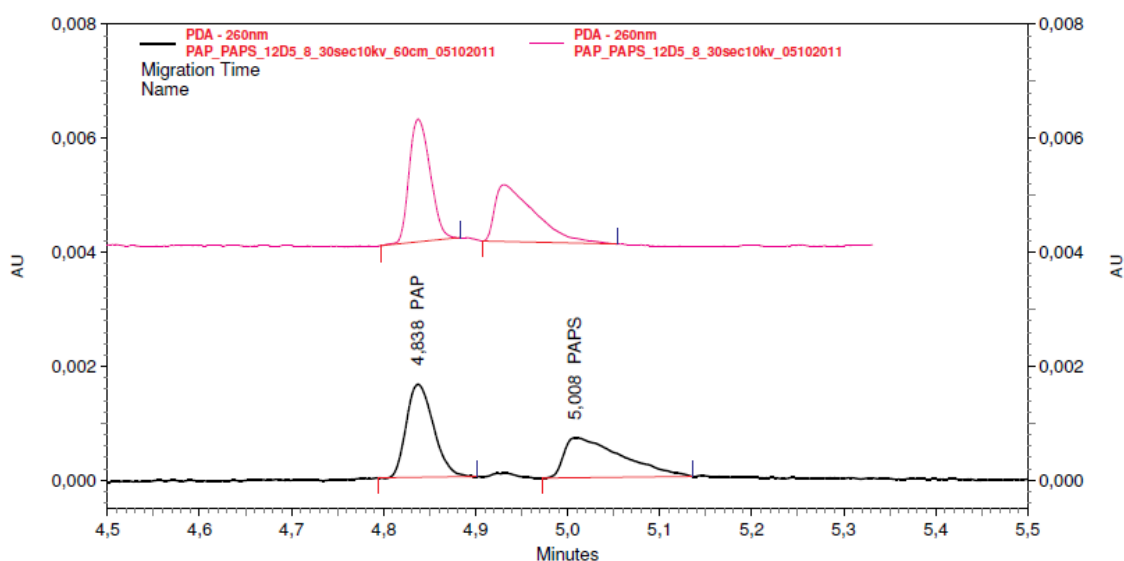


Figure 3.6. The electropherogram results with different capillary lengths. 25°C, acquisition rate is 4 Hz, 260 nm detection window, running buffer phosphate 75 mM, with 0.002% polybrene, pH 8, separation voltage -25 kV, injection -10 kV for 30 sec, PAP and PAPS final concentrations were 6.25  $\mu$ M. Upper curve (in red) was with FS capillary with 50 cm (40 cm); lower curve (in black) was with FS capillary with 60 cm (50 cm).

However, we needed a much more sensitive method for the detection of PAP. Therefore we further applied dynamic pH junction stacking (see Fig. 3.2). In this method, the stacking is based on differences in the analyte's ionization due to different buffer pH values in the sample matrix as compared to the background electrolyte (BGE).<sup>12,104</sup> This results in a velocity difference of the analytes in the sample matrix as compared to the BGE thereby causing a stacking effect at the boundary of these two buffers.<sup>105–113</sup> Both, the coenzyme PAPS and its enzymatic product adenosine-3',5'-diphosphate (PAP) are expected to be negatively charged in buffers of pH values ranging between 2-10, and the maximum charge difference between PAPS and PAP was predicted to occur at pH 5.6. We further combined dynamic pH junction stacking with MEKC, in order to selectively maximize the signal of the enzymatic product PAP. Therefore, a 75 mM phosphate buffer of pH 5.6 containing 0.002% polybrene was chosen as the running buffer. Electrokinetic injection was used since negatively charged analytes will be selectively injected into the capillary by this injection mode.<sup>12</sup> Since the more negatively charged analytes will migrate faster toward the detection window than the less charged analytes (due to the addition of the cationic surfactant polybrene causing a reversal of the electroosmotic flow (EOF)), the

velocity of PAP will be faster at pH 7.4 (where it has a higher negative charge) than at pH 5.6 buffer. Therefore PAP will stack at the boundary of these two buffers, when it migrates from the pH 7.4 buffer to the pH 5.6 buffer zone. We achieved this pH junction stacking effect simply by an additional sample preparation step: the CST reaction samples were dissolved in 5 mM phosphate buffer, pH 7.4, containing 0.0001% polybrene, before transferring them into the CE sample vials and subsequently eluted with the running buffer of pH 5.6 (75 mM phosphate buffer). An additional benefit of this procedure is the field amplifying sample stacking (FASS) effect due to significant differences in buffer concentration (ionic strength of sample matrix as compared to BGE (see Figure 3.10)).<sup>12,95,96,106,114</sup>

In the next step, several parameters of the CE measurements were further optimized. We investigated different separation voltages (15-25 kV), injection volumes (6-10 kV, 10-60 s), and capillary lengths (40 cm and 50 cm effective length). A voltage of -15 kV yielded the best compromise in terms of migration time, current generated, and separation efficiency. In order to improve resolution and at the same time maximizing the injection amount, an electrokinetic injection at -10 kV for 30 s was chosen. The longer capillary which enabled a better separation of the analytes, was preferred. Finally, we achieved a clear separation between the coenzyme PAPS and the enzymatic product PAP through pH-stacking (Fig. 3.7-3.9). The identity of each peak was confirmed by spiking with reference compounds.



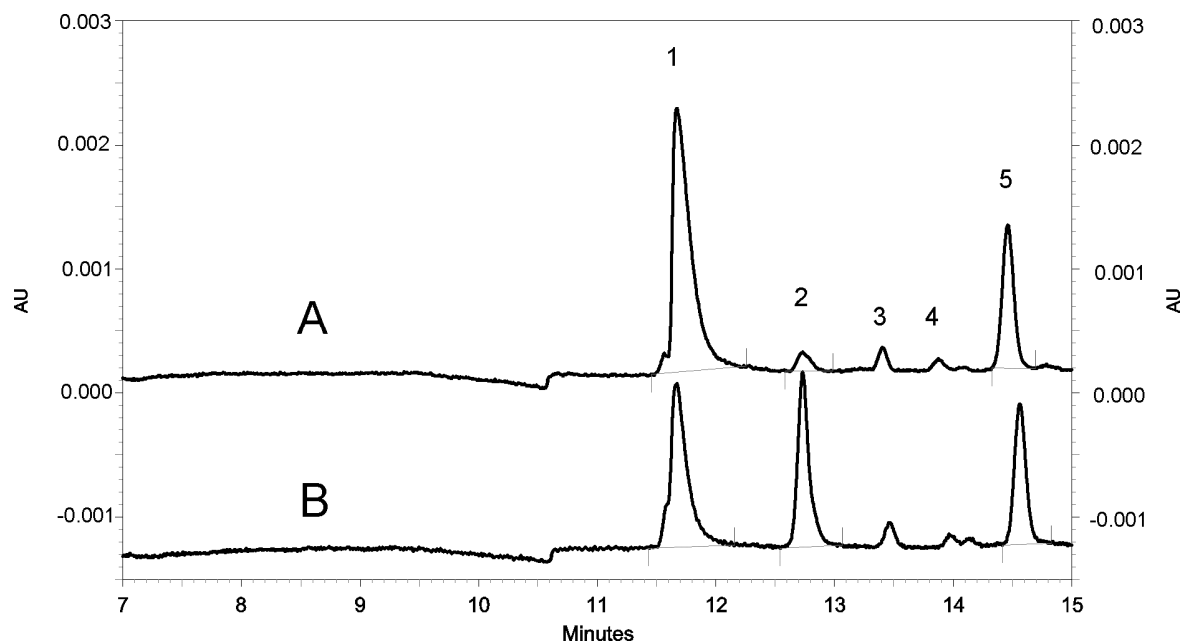


Figure 3.7. Representative electropherogram of cerebroside sulfotransferase (CST) reactions. (A) The CST reaction in the presence of the CST inhibitor Congo Red ( $600 \mu\text{M}$ ). (B) CST reaction without inhibitor. Peaks: 1, PAPS; 2, PAP; 5, I.S. GDP; 3 and 4, impurities of PAPS.

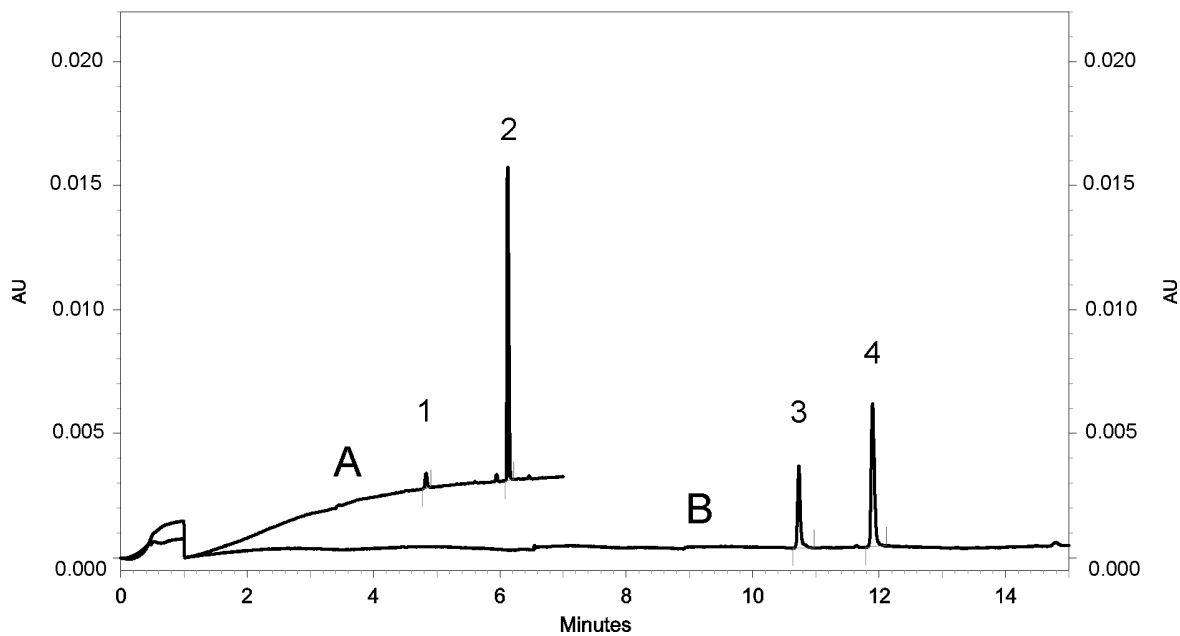


Figure 3.8. PAP  $1 \mu\text{M}$  peak with pH-stacking (B, in pH 5.6 BGE) and without pH-stacking (A, in pH 8 BGE). peak 1 and 3: PAP; peak 2 and 4: I.S.

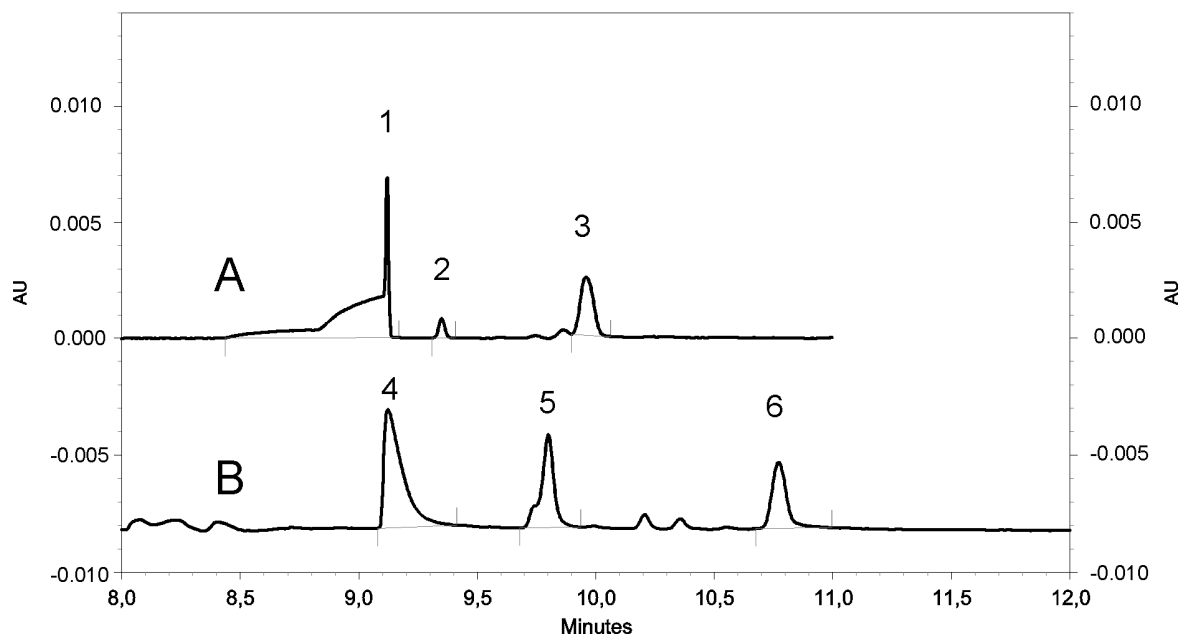


Figure 3.9. The pH stacking effect compared between pH 6.5 BGE (A) and pH 5.6 BGE (B). peak 1 and 4: PAPS; peak 2 and 5: PAP, peak 3 and 6: I.S.

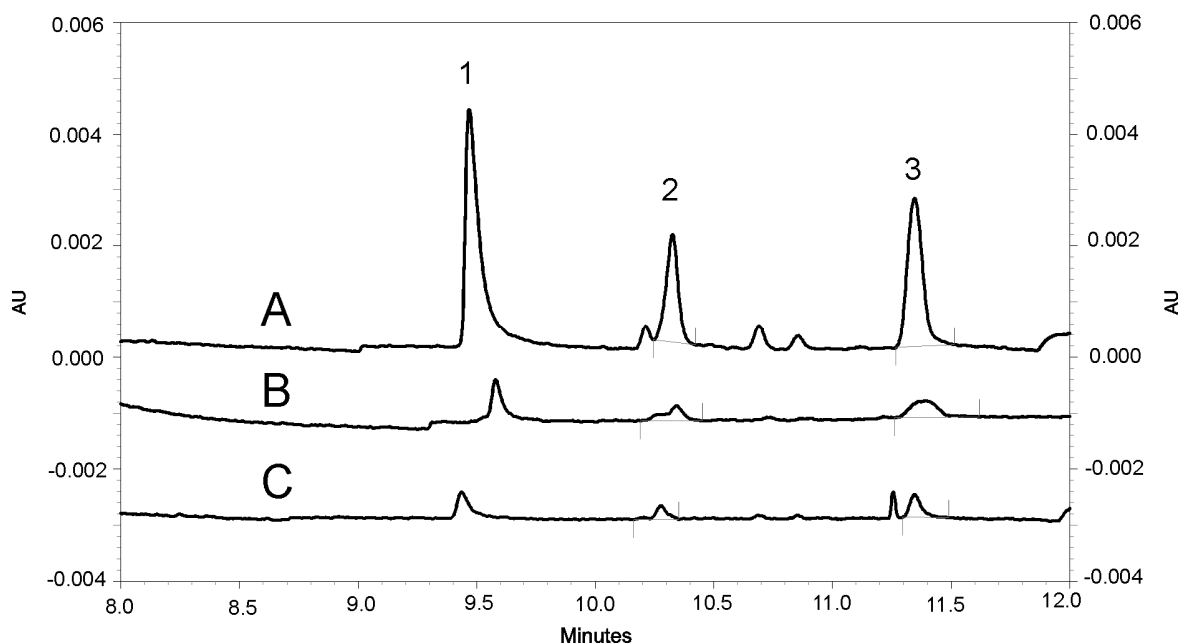


Figure 3.10. Field amplifying stacking effect due to significant differences in buffer concentration. BGE: 75 mM phosphate buffer of pH 5.6 containing 0.002% polybrene. **A.** Stacking buffer 5 mM phosphate buffer of pH 7.4 containing 0.0001% polybrene; **B.** Stacking buffer 75 mM phosphate buffer of pH 7.4 containing 0.002% polybrene; **C.** 10 mM HEPES with 16 mM MgCl<sub>2</sub>, pH 7.1. The result showed that only when the stacking buffer and BGE buffer were both phosphate buffers containing polybrene, and the stacking buffer concentration was

lower than that of the BGE buffer (in this case, 15 folds lower), a field amplifying stacking effect could be achieved. With HEPES buffer (C) a field amplifying stacking effect could not be observed. peak 1: PAPS; peak 2: PAP, peak 3: I.S.

### 3.2.2 Calibration and validation of the capillary electrophoresis method

The newly developed CE method was validated according to the guidelines published by the International Conference on Harmonisation (ICH) of Technical Requirements for Registration of Pharmaceuticals for Human Use, and the US Food and Drug Administration (FDA), respectively.<sup>10,11</sup> A summary of the parameters of method validation is provided in Table 3.1. A strictly linear correlation between analyte concentration and peak-area ratio of analyte to I.S. was observed from 0.0625  $\mu$ M to 1.25  $\mu$ M for PAP. LOD and LOQ for PAP were 66.6 nM (LOD) and 202 nM (LOQ), which demonstrating good sensitivity of the new method. Accuracy and precision were within an acceptable range for the measurement of low concentrations of analytes.<sup>10,11</sup> The validation of the CE method demonstrated its suitability for the analysis of enzyme kinetics and for inhibitor testing. To the best of our knowledge, our CE method is the first validated testing system for morning CST catalytic activity.

Table 3.1. Quantification and method validation of CST reaction product

Parameters	Regression equation (n=5)	R <sup>2</sup>	LOD (nM) (S <sub>y,x</sub> /slope)*3.3	LOQ (nM) (S <sub>y,x</sub> /slope)*10
Adenosine - 3',5'- diphosphate (PAP)	y = 45.63 x - 0.61 (Calibration range: 0.0625 - 1.25 $\mu$ M)	0.998	66.6	202
<b>Validation of PAP</b>				
PAP Conc ( $\mu$ M)	Accuracy (n = 5, % recovery)	Accuracy acceptable range <sup>a</sup>	Precision (n = 5, RSD <sup>b</sup> %)	Precision acceptable range <sup>a</sup>
0.0625	112.4	80-120%	12.4	20%
0.125	96.5	80-120%	3.1	20%
0.25	97.2	80-120%	6.8	20%
0.625	100.6	80-120%	5.9	20%
1.25	99.9	80-120%	1.9	20%

<sup>a</sup> According to guidelines of the International Conference on Harmonisation of Technical Requirements for Registration of Pharmaceuticals for Human Use <sup>10</sup>

<sup>b</sup> Relative standard deviation

### 3.3 Results

#### 3.3.1 Kinetic characterization and inhibition assays for cerebroside sulfotransferase with reference compounds

The linear range of the CST reaction with cerebroside was determined under different conditions (Figure 3.11).

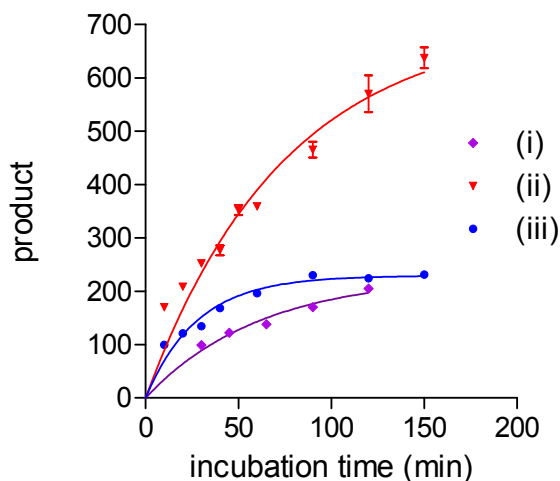


Figure 3.11. Determination of CST-catalyzed reaction. The concentration of cerebroside was kept at 100  $\mu\text{M}$ , and a linear range was found to be under the following conditions: (i) the linear range was 60 min, when the PAPS concentration was 30  $\mu\text{M}$ , with 6.25  $\mu\text{l}$  CST (per 50  $\mu\text{l}$  reaction vial); (ii) the linear range was 60 min, when the PAPS concentration was 100  $\mu\text{M}$ , with 3.125  $\mu\text{l}$  CST (per 50  $\mu\text{l}$  reaction vial); (iii) the linear range was 30 min, when the PAPS concentration was 30  $\mu\text{M}$ , with 3.125  $\mu\text{l}$  CST (per 50  $\mu\text{l}$  reaction vial). The result indicates that, the linear range increased when the enzyme amount was higher or when the substrates concentrations were higher.

Apparent enzyme kinetics parameters (Michaelis-Menten constant and maximal velocity) were determined for the reference substrates cerebroside and psychosine (Fig. 3.8).<sup>64,66,69,115,116</sup> Cerebroside displayed a  $K_m$  value of 60.3  $\mu\text{M}$  and a  $V_{\text{max}}$  value of 0.0738  $\mu\text{mol}/\text{min}/\text{mg}$ , which is well in agreement with reported results ( $K_m$  values of 26-52  $\mu\text{M}$  <sup>64,66,69,115,116</sup>). For psychosine a  $K_m$  value of 103  $\mu\text{M}$  and a  $V_{\text{max}}$  value of 0.105  $\mu\text{mol}/\text{min}/\text{mg}$  was determined, in the same range as that for cerebroside. To our knowledge, this is the first determination of a  $K_m$  value for psychosine.

Next we used the new CE method to characterize the reported CST inhibitor Congo Red,<sup>65</sup> and an  $IC_{50}$  value of 38.1  $\mu\text{M}$  was determined (Fig. 3.9). Moreover, we analyzed the inhibition mechanism with respect to the substrate cerebroside. Congo Red had previously been reported to be a competitive inhibitor with respect to the CST co-substrate PAPS.<sup>65</sup> In our studies we showed that it acted as an uncompetitive inhibitor with respect to the CST substrate cerebroside displaying an  $\alpha K_i$  value of 29.6  $\mu\text{M}$ . Our results are well in agreement with the published data ( $K_i = 41 \mu\text{M}$ , competitive versus PAPS<sup>65</sup>). Our study represents the first determination of the inhibition type of a CST inhibitor versus the substrate cerebroside.

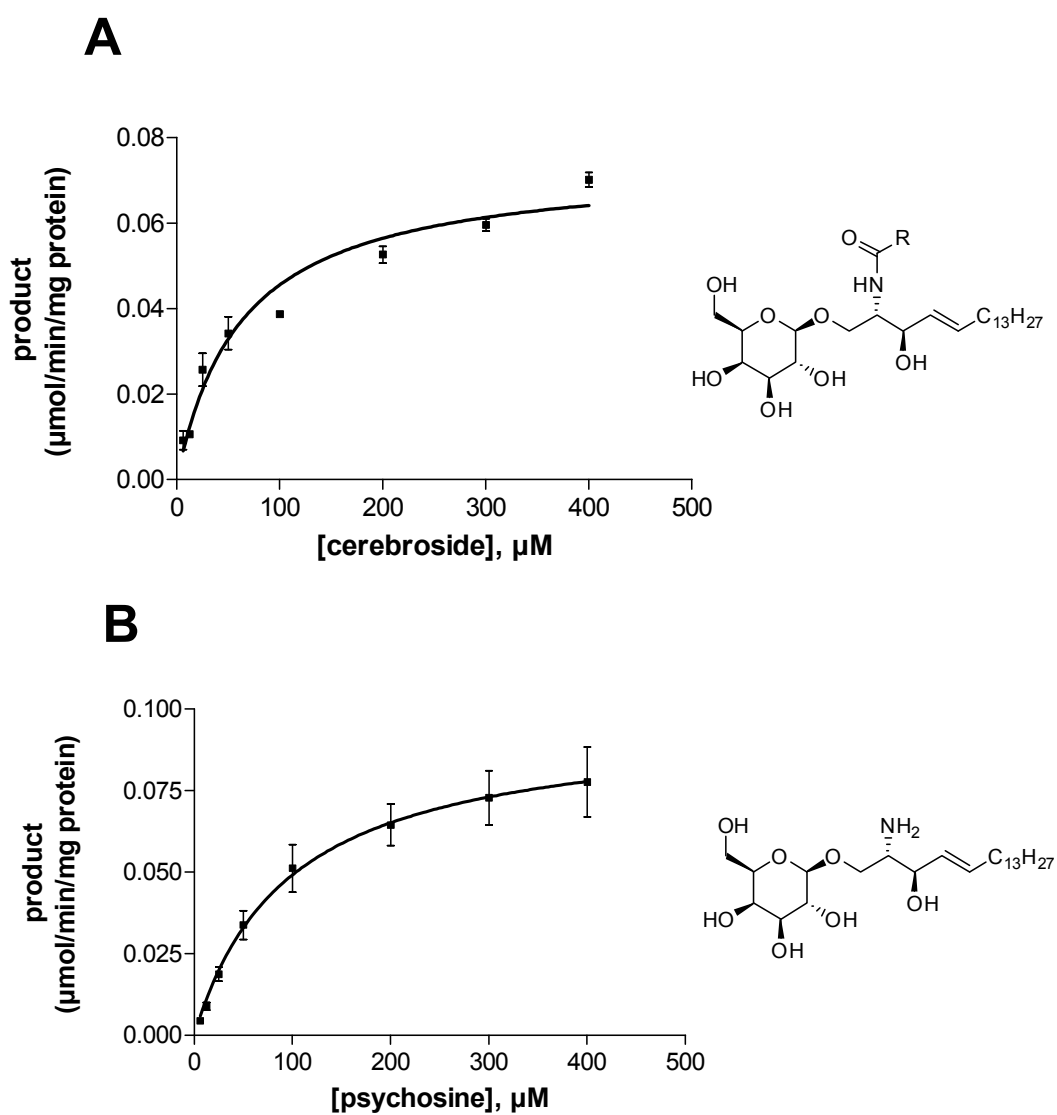


Figure 3.12. Enzyme kinetics of CST with cerebroside and psychosine. (A) Michaelis-Menten plot for cerebroside,  $K_m = 60.3 \pm 21.7 \mu\text{M}$ ,  $V_{\text{max}} = 0.0738 \pm 0.0039 \mu\text{mol}/\text{min}/\text{mg}$ ; (D) Michaelis-Menten plot for psychosine,  $K_m = 103 \pm 11 \mu\text{M}$ ,  $V_{\text{max}} = 0.105 \pm 0.018 \mu\text{mol}/\text{min}/\text{mg}$ .

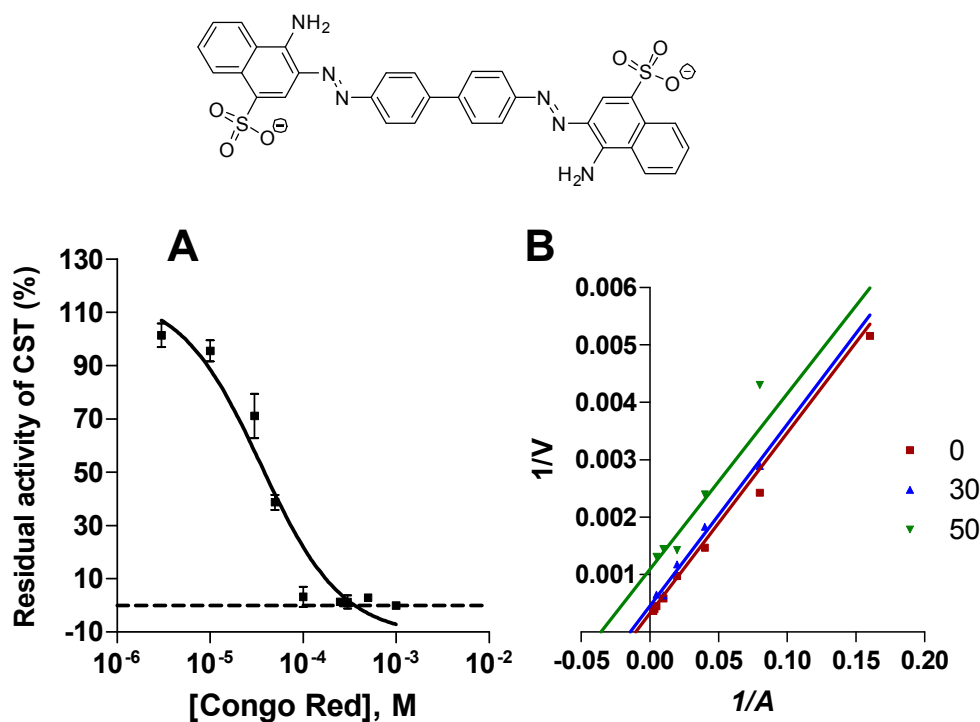
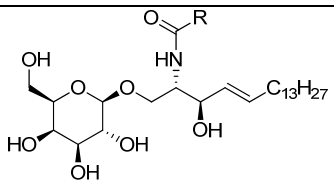
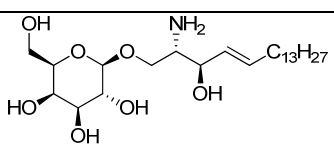
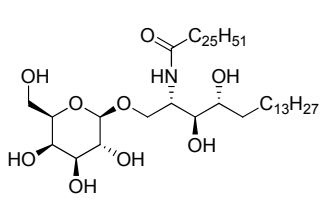
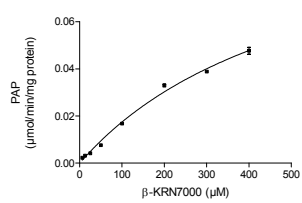
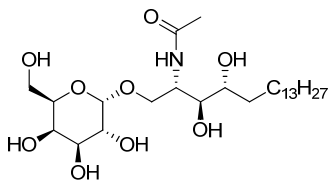
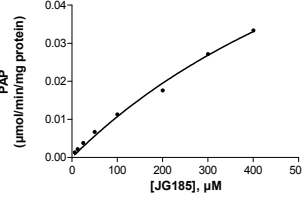
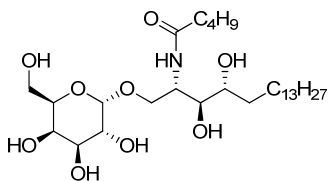
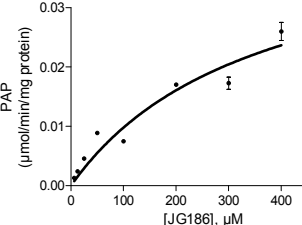


Figure 3.13. Characterization of the cerebroside sulfotransferase (CST) inhibitor Congo Red. (A) Concentration-inhibition curve of Congo Red ( $IC_{50} 38.1 \pm 6.5 \mu\text{M}$ ); (B) Lineweaver-Burk plot for Congo Red versus the CST substrate cerebroside. Congo Red showed an uncompetitive mechanism of inhibition versus cerebroside with a  $K_i$  value of  $29.6 \mu\text{M}$ .

### 3.3.2 Kinetic characterization of cerebroside sulfotransferase-catalyzed reactions with artificial substrates

We tested a group of carefully selected analogues of the natural CST substrate galactocerebroside. Altogether, 14 compounds were investigated as potential artificial substrate of CST (see Table 6.4). Enzyme kinetic parameters (Michaelis-Menten constant and maximal velocity) were determined for all identified artificial substrates (Table 3.2).

Table 3.2. Testing of galactocerebroside analogues as potential substrate of CST

Compound	Structure	$K_m$ ( $\mu\text{M}$ )	$V_{\text{max}}$ ( $\mu\text{mol}/\text{ml}/\text{min}$ )	$k_{\text{cat}}/K_m$
<b><math>\beta</math>-glycolipids</b>				
cerebroside (reference)		<b>60</b>	<b>0.0738</b>	123
psychosine (reference)		<b>103</b>	<b>0.105</b>	102
$\beta$ -KRN7000 (C26)	 	<b>550</b>	<b>0.113</b>	20.5
<b><math>\alpha</math>-glycolipids</b>				
JG185 (C2)	 	<b>907</b>	<b>0.1080</b>	11.9
JG186 (C5)	 	<b>358</b>	<b>0.0449</b>	12.5

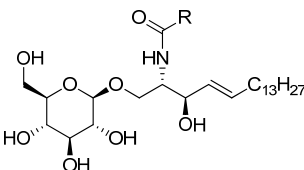
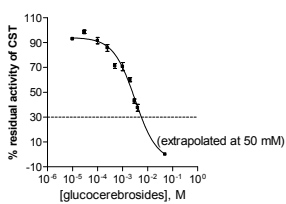
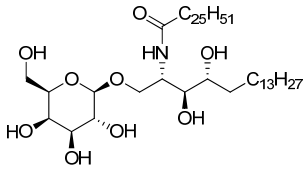
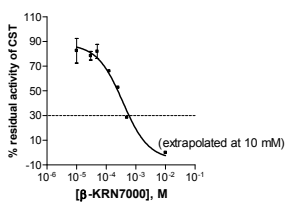
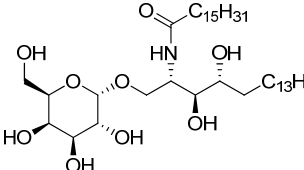
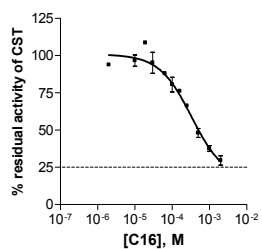
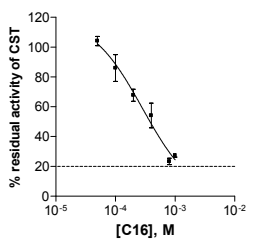
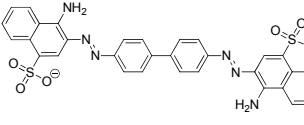
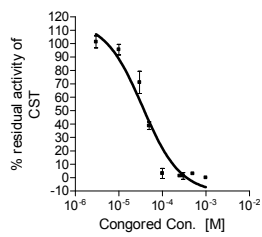
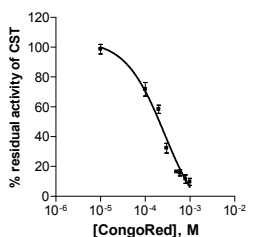


PBS25 (C8)		<b>390</b>	<b>0.0584</b>	15.0
JG189 (C11)		<b>493</b>	<b>0.0590</b>	12.0
JG187 (C19)		<b>521</b>	<b>0.0519</b>	9.96
KRN7000 (C26) (commercial)		<b>438</b>	<b>0.0758</b>	17.3
JG188		<b>751</b>	<b>0.0834</b>	11.1

### 3.3.3 Inhibitors of cerebroside sulfotransferase

13 compounds were investigated for searching competitive inhibitor versus cerebroside and KRN7000 (see Table 6.4), IC<sub>50</sub> values versus the natural substrate cerebroside and the artificial substrate KRN7000 are shown in Table 3.3.

Table 3.3. Inhibition testing of CST

Compound	Structure	IC <sub>50</sub> ± SEM (μM) <sup>a</sup> (to cerebroside) (inhi% at 100 μM)	IC <sub>50</sub> ± SEM (μM) (to KRN7000) (inhi% at 100 μM)
glucocerebroside (commercial β-glycolipids mixture)		<b>3780 ± 762</b> (9%)	(-5%)
			
β-KRN7000 (C26)		<b>363</b> (38%)	(-42%)
			
C16 (α-glycolipids)		<b>340 ± 33</b> (12%)	<b>328 ± 114<sup>a</sup></b> (14%)
			
Congo Red (reference)		<b>43.76</b> (67%)	<b>278 ± 40<sup>b</sup></b> (29%)
			

<sup>a</sup>The substrate concentration for inhibition testing was 100  $\mu\text{M}$ , the concentration of the cofactor PAPS was 30  $\mu\text{M}$ .

<sup>b</sup>The substrate concentration for inhibition testing was 466  $\mu\text{M}$ , the concentration of the cofactor PAPS was 30  $\mu\text{M}$ .

### 3.3.4 Structure-activity relationship study of the cerebroside sulfotransferase cerebroside binding site

Regarding the structure-activity relationship study of the CST cerebroside binding site, two critical points were discovered: The stereochemistry at the 1-, 4-, and 5-positions of galactocerebroside dramatically influences the activity of CST, and the lipid moiety can also have an effect on the CST activity. Details are shown as below:

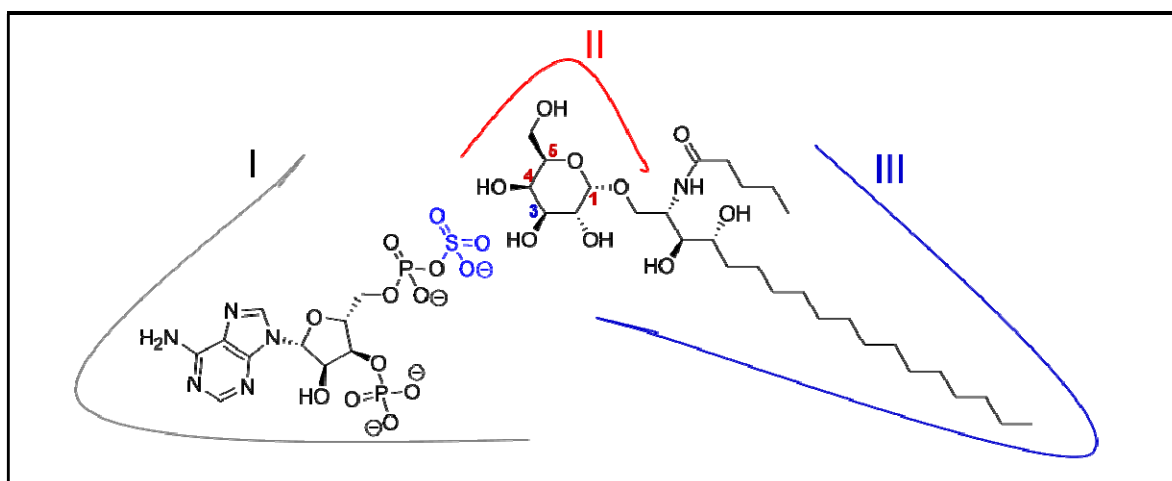


Figure 3.14. Interaction sites of substrate and co-substrate in the catalytic site of CST

1. Domain I was reported to bind PAPS (see Figure 3.3).<sup>83–85</sup>
2. Domain II around the sugar head should be highly specific.
  - Position 1:  $\beta$ -glycosides can fit into the enzyme active site better than  $\alpha$ -glycosides ( $\beta$ -glycosides have smaller  $K_m$  values, see Table 3.2); and  $\beta$ -glycosides could be better catalyzed in the CST active site ( $\beta$ -glycosides have larger  $k_{cat}/K_m$  values, see Table 3.2), which is in agreement with the previous study (The previous study showed that CST prefers  $\beta$ -glycosides<sup>64</sup>).

- Position 4: glucocerebrosides can inhibit cerebrosides (see Table 3.2), which shows that the position 4 is crucial in the active site, which is in agreement with the previous study (The previous study showed that glucocerebrosides, Gg4Cer, Gb4Cer and nLc4Cer are not substrates<sup>64</sup>).
  - Position 5: NP230 is neither substrate, nor inhibitor, which shows that in position 5 there is a space limitation (see Table 6.4).
3. Domain III around the lipid tail appears to be specific, because lipids with different chain lengths showed diverse activities (see Table 3.2).

### 3.4 Conclusions and discussion

We developed and validated a sensitive and robust test system for the enzyme cerebrosidase sulfotransferase (CST), which constitutes a potential target for the treatment of metachromatic leukodystrophy (MLD). The new CE-based method was shown to be suitable for performing enzyme kinetic studies, for inhibitor screening and  $K_i$  value determination. The CE method utilizes a sample matrix consisting of 5 mM phosphate buffer with 0.0001 % polybrene at pH 7.4 and a BGE consisting of a 75 mM phosphate buffer with 0.002 % polybrene at pH 5.6, to induce a dynamic pH junction-sweeping stacking effect for the enzymatic product PAP leading to a low detection limit (LOD = 66.6 nM). Several reference compounds were tested including the substrates cerebrosidase and psychosine and the inhibitor Congo Red in order to further validate the method.

We tested a group of carefully selected analogues of CST nature substrate galactocerebrosidase. We obtained detailed SAR information for the CST cerebrosidase binding site by analyzing numeral artificial substrates, and novel competitive CST inhibitor versus galactocerebrosidase has been found. Inhibitory effects on CST was observed with several compounds, and concentration-inhibition curves were determined for the most potent inhibitor C16 (Table 3.3). C16 was found to be the first competitive inhibitor versus galactocerebrosidase, with an  $IC_{50}$  340  $\mu$ M, and an  $IC_{50}$

328  $\mu\text{M}$  versus artificial CST substrate KRN7000, respectively. Moreover, glucocerebrosides and  $\beta$ -KRN7000 showed significant inhibition (70%) of CST activity at a test concentration of 1 mM (see Table 3.3). The new CST inhibitor C16 can be the lead structure and be further optimized for potent CST inhibitors, which are urgently needed for the treatment of MLD. Our ultimate goal is to develop CST inhibitors for substrate reduction therapy to help young MLD patients to survive this devastating genetic disease.



## 4 Analysis of the *Staphylococcus aureus* capsule biosynthesis pathway

### 4.1 Introduction

*Staphylococcus aureus* is an opportunistic bacterial pathogen responsible for a diverse spectrum of human and animal diseases, and it is also major cause of wound infections. Since capsules enhance microbial virulence by rendering the bacterium resistant to phagocytosis, many microorganisms that cause invasive disease produce extracellular capsular polysaccharides. Inhibitors targeting capsule biosynthesis may have the potential for use in combination therapeutics.<sup>117,118</sup> Inhibition of capsule formation would also unmask patterns on the bacterial cell surface, which are important for pathogen recognition and clearance by the innate immune system. *S. aureus* strains are classified into 11 capsular serotypes, and most clinical isolates of *S. aureus* correspond either to type 5 (CP5) or type 8 (CP8).<sup>119</sup> CP5 has the structure  $(\rightarrow 4)\text{-}3\text{-O-Ac-}\beta\text{-D-ManNAcA-(1}\rightarrow 4)\text{-}\alpha\text{-L-FucNAc-(1}\rightarrow 3)\text{-}\beta\text{-D-FucNAc-(1}\rightarrow n$ ; CP8 only differs in the glycosidic linkages between the sugars and the sites of O-acetylation.<sup>119,120</sup> The biosynthesis of *S. aureus* CP5 is facilitated by several highly conserved enzymes, including enzymes CapD and CapE which catalyze the conversion of UDP-D-GlcNAc to UDP-2-acetamido-2,6-dideoxy-D-xylo-4-hexulose and UDP-2-acetamido-2,6-dideoxy-L-lyxo-4-hexulose, respectively.<sup>120</sup> The biosynthesis of *S. aureus* CP5 is shown as below:

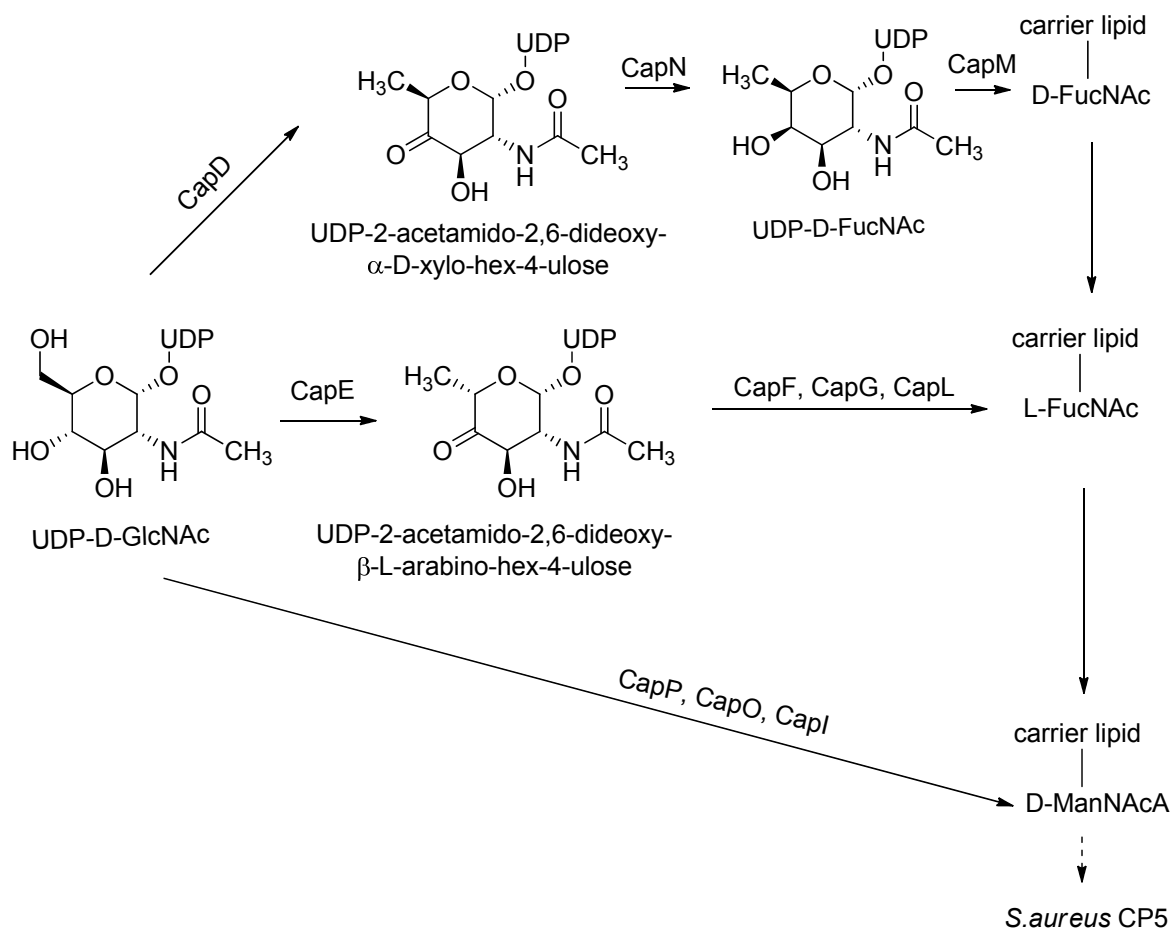


Figure 4.1. Proposed pathway for *S. aureus* CP5 biosynthesis (adapted from O’Riordan & Lee, 2004<sup>121</sup>). CapD and CapE catalyze the conversion of UDP-D-GlcNAc to UDP-2-acetamido-2,6-dideoxy- $\alpha$ -D-xylo-4-hexulose, and UDP-2-acetamido-2,6-dideoxy- $\beta$ -L-arabino-hex-4-ulose, respectively.

In order to study the catalytic activities of CapD and CapE at the molecular level, we developed and optimized a capillary electrophoresis (CE)-based detection method. CE is a simple, economic and powerful method for monitoring enzyme reactions, especially those that are generating charged products.<sup>87,89,90,92</sup> A CE method for studying CapE activity has been described using borax buffer pH 9 as a running buffer, and hydrodynamic injection.<sup>120,122</sup> We have now developed a considerably improved method, which is faster, more sensitive and robust, enabling efficient separation of the components in the enzyme reaction mixture and allowing for enzyme kinetic studies, compound library screening, and inhibitor testing. The new CE method is based on micellar electrokinetic chromatography (MEKC), in which surfactants are used as running buffer additives. Recently, CE approaches using cationic surfactant as dynamic coatings



on silica-fused capillaries have gained considerable interest, because they allow a significant improvement in detection sensitivity.<sup>87,90</sup> The addition of cationic surfactants to the running buffer causes the reversal of the electroosmotic flow (EOF) due to adsorption of these surfactants to the capillary wall thereby creating a positively charged surface. With this setup, EOF and migration of negatively charged analytes are both directed towards the positive electrode. The use of the polycationic polymer polybrene (PB) for dynamic coating results in an effective stacking of sample zones due to its sweeping effect.<sup>90,123</sup> Because of the strong preconcentration effects of polycationic polymers, the detection limits of analytes may be strongly improved, down to the nanomolar range.<sup>87,90</sup> The newly developed method is much faster and significantly more sensitive compared to the previously reported procedure and allows for the screening of compound libraries in search of inhibitors.

## **4.2 Method development and validation**

### **4.2.1 Development and optimization of capillary electrophoresis method**

A sensitive analytical method for monitoring the catalytic activities of capsule biosynthetic enzymes was required, which would not only allow characterization of the enzymatic reactions, but also be suitable for the screening of inhibitors. Since both, substrate (UDP-D-GlcNAc) and products (UDP-2-acetamido-2,6-dideoxy- $\alpha$ -D-xylo-hex-4-ulose and UDP-2-acetamido-2,6-dideoxy- $\beta$ -L-arabino-hex-4-ulose), of CapD and CapE are negatively charged in alkaline buffer, we chose CE separation applying a micellar electrokinetic chromatography (MEKC) mode and reverse electroosmotic flow (EOF) for detection. The choice of the buffer is crucial for obtaining clear and narrow peaks without producing excessive Joule heating. The prediction of charge differences between substrate and products is helpful for choosing a suitable pH value for the running buffer, and this was accomplished by means of the Marvin Sketch software (ChemAxon, Hungary) (Figure 4.2).

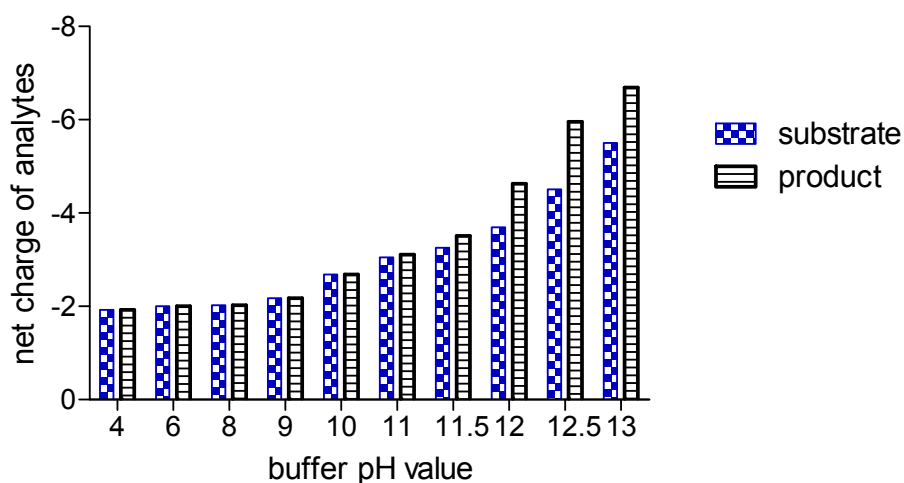


Figure 4.2. Prediction of net charges of analytes under different buffer pH values

As shown in Figure 4.2, a high pH value was predicted to be favourable for obtaining net charge differences between substrate and products. However, when the separation buffer pH value is too high, excessive Joule heating may destroy the capillary detection window after a few runs. To balance these two factors, a pH value of 12.4 was predicted to provide optimal conditions. Therefore, 3-(cyclohexylamino)-1-propane sulfonic acid (CAPS, 68 mM) buffer was chosen, which covers the high pH range. The combination of CAPS with the detergent polybrene (hexadimethrine bromide, 0.002%) represents a new combination in MEKC. To confirm that this CE method allows the separation of UDP-D-GlcNAc from the CapD enzymatic product, the recently described PglF reaction was analyzed.<sup>122</sup> PglF from *C. jejuni* had been demonstrated to catalyze the 4,6-dehydration of UDP-D-GlcNAc yielding UDP-2-acetamido-2,6-dideoxy- $\alpha$ -D-xylo-hex-4-ulose,<sup>122</sup> the same product as proposed for the CapD-mediated reaction. *In vitro* reconstitution of PglF catalytic activity was performed using a soluble derivative of the native *C. jejuni* membrane protein lacking transmembrane domains as originally described by Schoenhofen *et al.*<sup>122</sup> As predicted, the PglF-His<sub>6</sub> enzymatic product migrated faster in the capillary than UDP-D-GlcNAc as a result of a reduced net negative charge (Figure 4.3). The enzymatic activity of CapE can be analyzed using the same method, since its product<sup>120</sup> is a stereoisomer (diastereomer) of UDP-2-acetamido-2,6-dideoxy- $\alpha$ -D-xylo-4-hexulose and thus displays almost very similar CE migration behavior. To increase the sensitivity and to achieve faster separation of the analytes enabling high throughput screening, the CE method was further

optimized. To this end, we investigated different separation voltages (15-25 kV), injection volumes (1-5 kV, 5-30 s), and capillary lengths (30 cm and 50 cm effective length). A voltage of -15 kV yielded the best compromise in terms of migration time, current generated and separation efficiency. In order to improve peak shape and sensitivity, different injection times and injection voltages were applied. A small injection voltage was found to be beneficial for high accuracy and an electrokinetic injection at -1 kV for 20 s was chosen. Two different capillary lengths (30 cm or/and 50 cm effective length) were compared in terms of CE performance. The long capillary enabled better separation of analytes and was therefore preferred.

In recent years MEKC has been developed as a powerful CE technique.<sup>13,94-97</sup> In previous studies, the buffers used in combination with polybrene dynamic coating of the capillary had a pH range between pH 2 and pH 11, and the most widely used buffers for dynamic polybrene coating were borax, boric acid, phosphate, and folic acid.<sup>98-103</sup> A high pH CAPS buffer has not been previously used in combination with dynamic polybrene coating of the capillary. With CAPS/polybrene as a running buffer, analytes will migrate towards the detection window depending on their negative charge, with faster migration observed with higher negative charge. Moreover, by electrokinetic injection, a high quantity of negatively charged analytes can selectively be injected into the capillary,<sup>12</sup> leading to increased concentrations of anionic analytes.

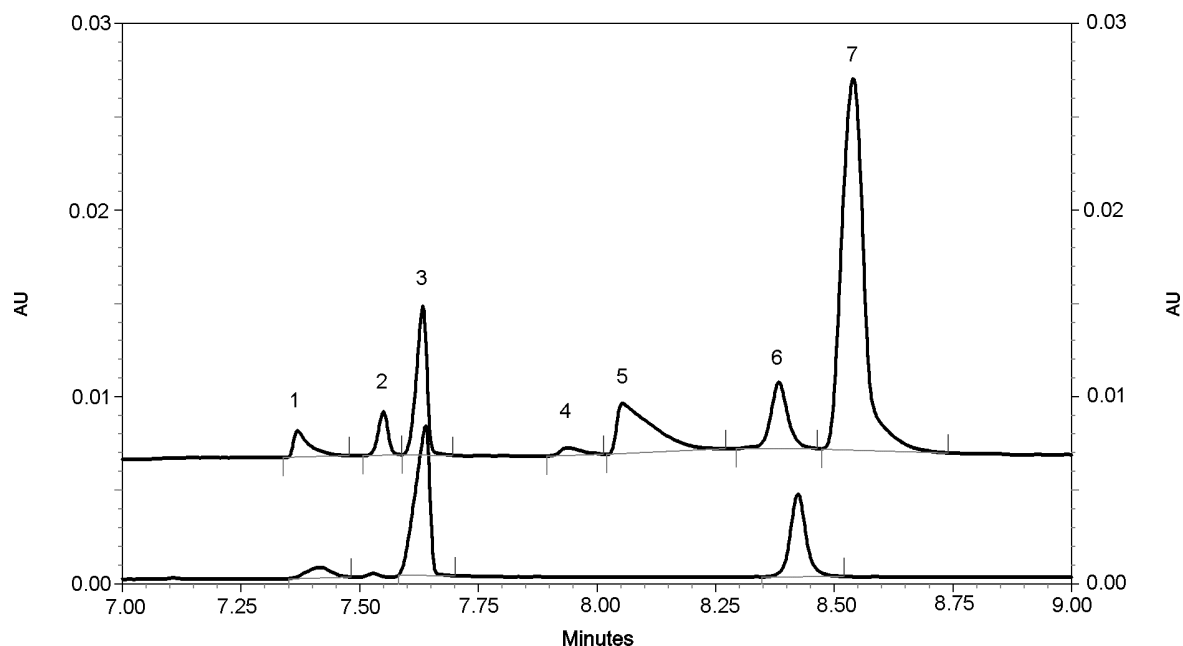


Figure 4.3. Representative electropherograms of CapD (A) and PglF (B) reactions. CAPS buffer (68 mM) containing polybrene (0.002%), pH 12.4, electrokinetic injection (-1 kV, 20sec),  $\lambda_{\text{max}} = 260$  nm, separation voltage = -15 kV. Uncoated fused-silica capillaries of 60 cm total length (50 cm effective length)  $\times$  75.5  $\mu\text{m}$  (inner diameter)  $\times$  363.7  $\mu\text{m}$  (outer diameter). Peaks: **1**, UDP; **2**, NADP impurity; **3**, I.S. PAP; **4** and **5**, NADP impurities; **6**, product UDP-2-acetamido-2,6-dideoxy- $\alpha$ -D-xylo-4-hexulose; **7**, substrate UDP-D-GlcNAc and cofactor NADP.

CE analysis of the quenched CapD reaction mixture revealed a peak with identical UV spectrum and retention time as observed for the PglF enzymatic product (Figure 4.3), which was further confirmed by MS: a molecular mass of 588.3 (negative mode;  $[M - H]^-$ ) was determined for the HPLC-purified CapD and PglF reaction products, consistent with the expected mass of 589.3 for UDP-2-acetamido-2,6-dideoxy- $\alpha$ -D-xylo-4-hexulose. The identity of each peak in CE electropherogram was confirmed by spiking with reference compounds. In contrast to CapE, which displayed full *in vitro* activity without externally added cofactors, CapD activity was dependent on the presence of detergent and NADP; addition of NAD or the absence of any cofactor resulted in less than 5% substrate conversion (Figure 4.4).

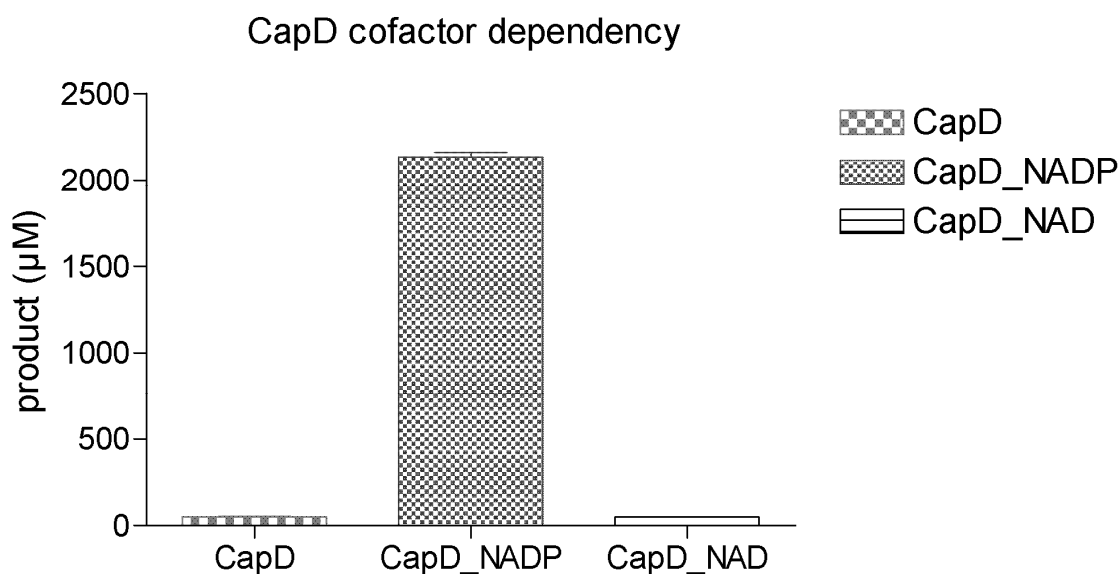


Figure 4.4. CapD cofactor dependency. CapD activity was dependent on the presence of NADP; addition of NAD or the absence of any cofactor resulted in less than 5% substrate conversion to product UDP-2-acetamido-2,6-dideoxy- $\alpha$ -D-xylo-hex-4-ulose. Enzyme reaction incubated at 30°C for 2 hours, containing 3 mM UDP-D-GlcNAc and 2 mM NAD/NADP or no cofactor.

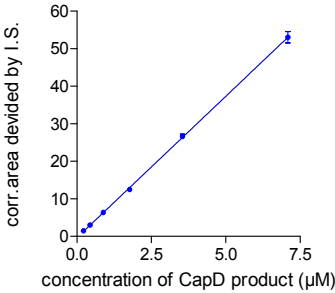
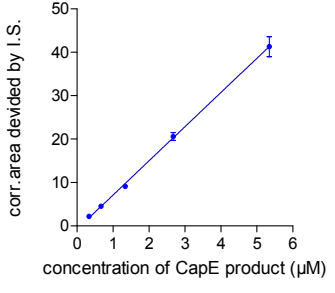
#### 4.2.2 Calibration and validation of the capillary electrophoresis method

Since UDP-2-acetamido-2,6-dideoxy- $\alpha$ -D-xylo-hex-4-ulose and UDP-2-acetamido-2,6-dideoxy- $\beta$ -L-arabino-hexos-4-ulose are not commercially available, we used enzymatic products for calibration to allow for product quantification. For CapD assays, the CE system was calibrated and validated with the PglF enzymatic product (100% substrate conversion). For CapE assays, the CE system was calibrated and validated with the CapE product UDP-2-acetamido-2,6-dideoxy- $\beta$ -L-arabino-hex-4-ulose (100% substrate conversion). Since the nucleotide-activated sugars in the reaction mixture were partially hydrolyzed, the degradation product UDP was quantified to determine the actual concentration of PglF and CapE enzymatic product (at 100% substrate conversion).

The newly developed CE method was validated according to the guidelines published by the International Conference on Harmonisation (ICH) of Technical Requirements for Registration of Pharmaceuticals for Human Use, and the US Food and Drug Administration (FDA), respectively.<sup>10,11</sup> A summary of the parameters of method validation is provided in Table 4.1. A

strictly linear correlation between product concentration and peak-area ratio of product to I.S. was observed from 0.22  $\mu\text{M}$  to 7.09  $\mu\text{M}$  for the CapD product and from 0.33  $\mu\text{M}$  to 5.34  $\mu\text{M}$  for the CapE product. LOD and LOQ for both products were nearly identical: 0.71  $\mu\text{M}$  (LOD) and 2.15  $\mu\text{M}$  (LOQ) for the CapD product, and 0.81  $\mu\text{M}$  (LOD) and 2.45  $\mu\text{M}$  (LOQ) for the CapE product thus demonstrating high sensitivity of the new method. Accuracy and precision were within an acceptable range for the measurement of low concentrations of analytes.<sup>10,11</sup> The validation of the CE method demonstrated its suitability for the analysis of enzyme kinetics and for inhibitor testing.

Table 4.1. Quantification of CapD and CapE reaction products: method validation

Parameters	CapD product UDP-2-acetamido-2,6-dideoxy- $\alpha$ -D-xylo-hex-4-ulose		CapE product UDP-2-acetamido-2,6-dideoxy- $\beta$ -L-arabino-hex-4-ulose		
	Regression equation (n=6)	$y = 7.533x - 0.35$ calibration with I.S. PAP 		$y = 7.873x - 0.767$ calibration with I.S. PAP 	
$R^2$	0.9927		0.9801		
LOD ( $\mu\text{M}$ )	0.71		0.81		
LOQ ( $\mu\text{M}$ )	2.15		2.45		
Calibration range ( $\mu\text{M}$ )	0.22 - 7.09		0.33 - 5.34		
	Concentration ( $\mu\text{M}$ )	Accuracy (n=6, % recovery)	Accuracy acceptable range <sup>a</sup>	Precision (n=6, RSD <sup>b</sup> %)	Precision acceptable range <sup>a</sup>
CapD product	0.44	100.9	80-120%	14.4	20%
	0.89	100.4	80-120%	2.3	20%
	3.55	101.0	80-120%	5.4	20%
	7.09	99.9	80-120%	7.0	20%
CapE product	0.67	100.9	80-120%	4.4	20%
	1.34	93.6	80-120%	7.0	20%
	2.67	101.5	80-120%	11	20%
	5.35	99.9	80-120%	11	20%

<sup>a</sup> According to guidelines of the International Conference on Harmonisation of Technical Requirements for Registration of Pharmaceuticals for Human Use<sup>10</sup>

<sup>b</sup> Relative standard deviation

Previously reported CE methods for the detection of UDP-2-acetamido-2,6-dideoxy- $\alpha$ -D-xylo-hex-4-ulose and UDP-2-acetamido-2,6-dideoxy- $\beta$ -L-arabino-hex-4-ulose used 25 mM borax buffer, pH 9.4 or 9.5, and hydrodynamic injection.<sup>121,122</sup> The LOD and LOQ values for UDP-2-acetamido-2,6-dideoxy- $\alpha$ -D-xylo-hex-4-ulose for the previously published method<sup>122</sup> were 7.3  $\mu$ M and 22.2  $\mu$ M, respectively. With our new method, the migration time of UDP-2-acetamido-2,6-dideoxy- $\alpha$ -D-xylo-hex-4-ulose was reduced by 50% (from 18 min to 9 min), while the LOD was improved by 10-fold from 7.3  $\mu$ M to 0.71  $\mu$ M (Figure 4. 5).

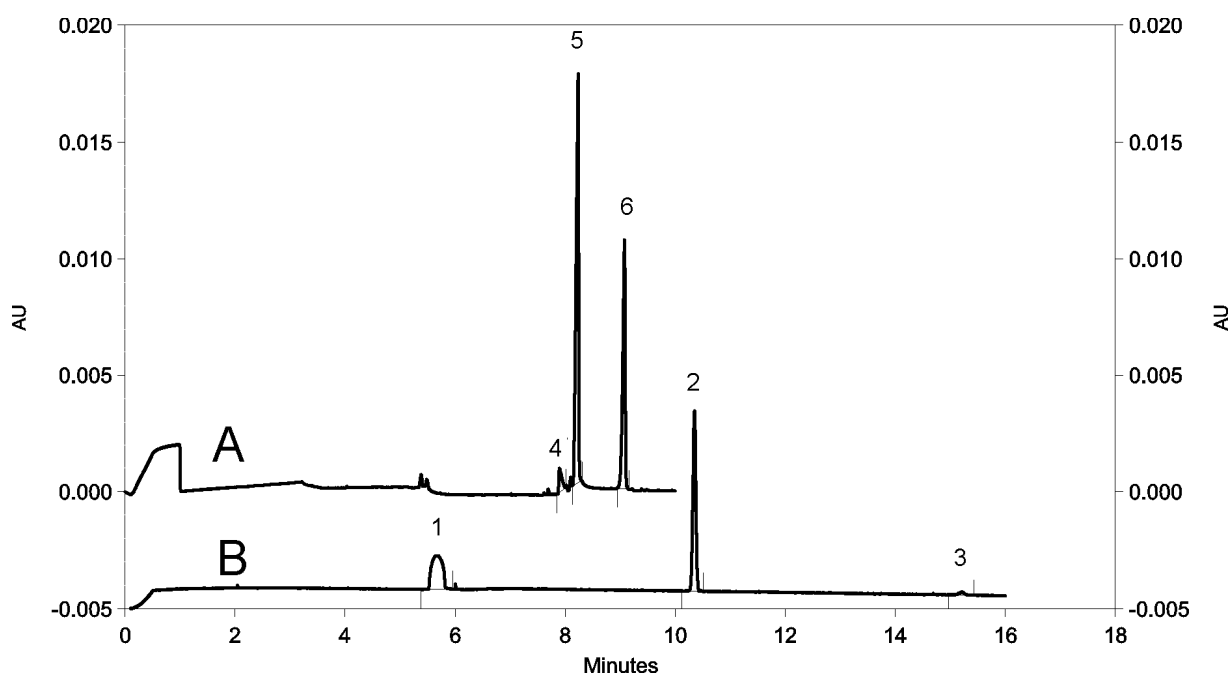


Figure 4.5. Electropherograms for methods comparison. Electropherograms obtained with the previously published method (A) and with the new method (B). (A) 68 mM CAPS buffer containing polybrene 0.002%, pH 12.4, electrokinetic injection (-1 kV, 20sec),  $\lambda_{\max}$  = 260 nm, separation voltage = -15 kV. Uncoated fused-silica capillaries of 60 cm total length (50 cm effective length)  $\times$  75.5  $\mu$ m (id)  $\times$  363.7  $\mu$ m (od). (B): 25 mM borax buffer, pH 9.4, hydrodynamic injection (0.5 psi, 10 sec),  $\lambda_{\max}$  = 260 nm, separation voltage = 18 kV. Uncoated fused-silica capillaries of 60 cm total length (50 cm effective length)  $\times$  75.5  $\mu$ m (id)  $\times$  363.7  $\mu$ m (od). A and B chromatograms are shown at the same scale. Peaks: **1**, buffer; **2**, I.S. Uridine; **3**, product of Pg1F by using the published method; **4**, UDP; **5**, I.S. PAP; **6**, product of Pg1F by using the new method.

## 4.3 Results and discussion

### 4.3.1 Kinetic characterization of CapD- and CapE-catalyzed reactions.

Enzyme kinetics (Michaelis-Menten constant and maximal velocity) were determined for both CapD and CapE (Figure 4.6). CapD displayed a  $K_m$  value of  $3650 \pm 270 \mu\text{M}$  and a  $V_{\text{max}}$  value of  $0.127 \pm 0.011 \mu\text{mol}/\text{min}/\text{mg}$ . For CapE, a  $K_m$  value of  $457 \pm 76 \mu\text{M}$  and a  $V_{\text{max}}$  value of  $0.071 \pm 0.004 \mu\text{mol}/\text{min}/\text{mg}$  were determined. The CapD *in vitro* reaction was in the linear range (steady-state phase) for up to 120 min, whereas CapE measurements were in the linear range for 60 min under the conditions applied.

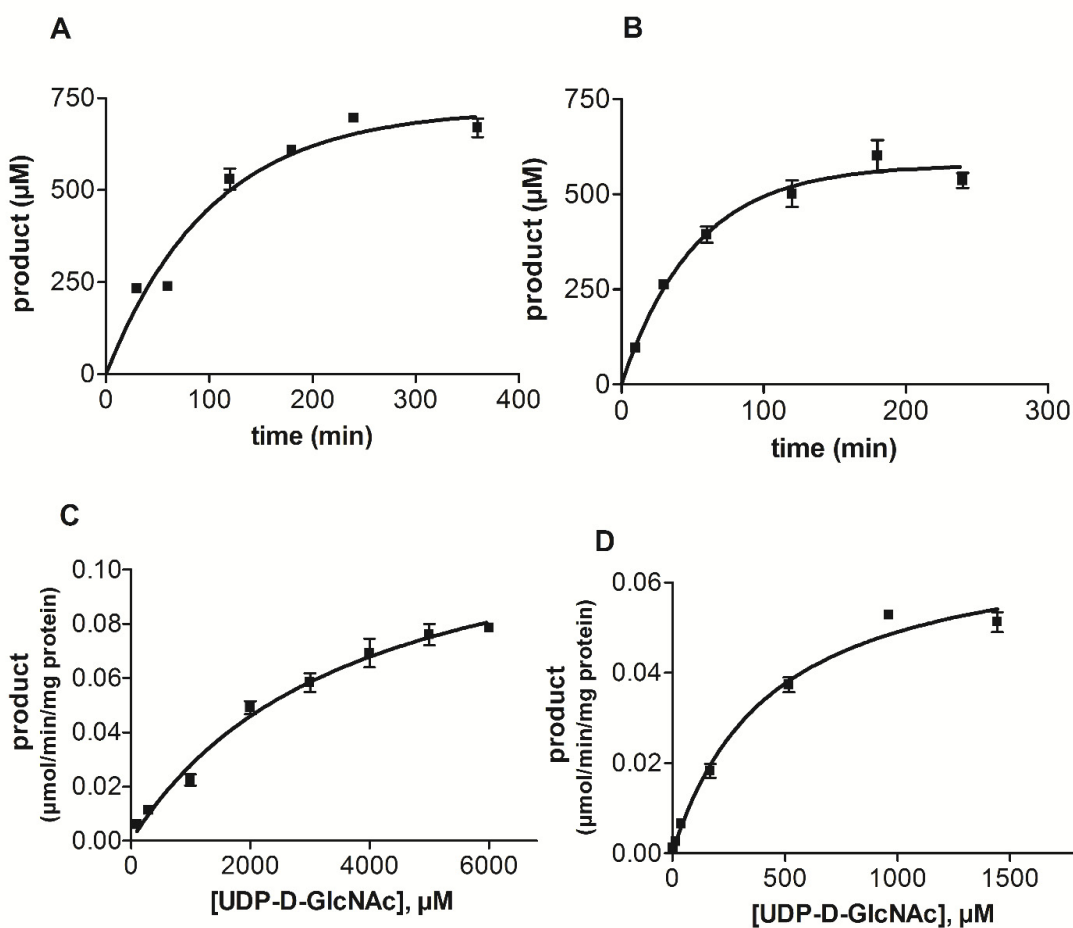


Figure 4.6. Enzyme kinetics of CapD and CapE. Time-dependent enzymatic reaction of CapD (A) and CapE (B). (C) Michaelis-Menten plot for CapD,  $K_m$   $3650 \pm 270 \mu\text{M}$ ,  $V_{\text{max}}$   $0.127 \pm 0.011 \mu\text{mol}/\text{min}/\text{mg}$ ; (D) Michaelis-Menten plot for CapE,  $K_m$   $457 \pm 76 \mu\text{M}$ ,  $V_{\text{max}}$   $0.071 \pm 0.004 \mu\text{mol}/\text{min}/\text{mg}$ .



### 4.3.2 Inhibitors of CapD and CapE

We tested a series of selected small molecules including uracil nucleotide derivatives,<sup>92,124</sup> compounds known to bind to nucleotide binding sites<sup>125</sup> and clinically applied antibiotics. Altogether, 73 compounds were investigated for CapD inhibition, and 46 compounds were screened for inhibition of CapE (Table 6.1 and Table 6.2). Inhibitory effects on CapD or CapE were observed with several compounds, and concentration-inhibition curves were determined for the most potent inhibitors (Figure 4.7). Suramin<sup>126</sup> was found to be a potent CapE inhibitor with an  $IC_{50}$  value of  $1.82 \pm 0.40 \mu\text{M}$ , whereas CapD was not inhibited at a test concentration of  $10 \mu\text{M}$ . Intriguingly, the  $\beta$ -lactam antibiotic ampicillin efficiently inhibited CapD enzymatic activity ( $IC_{50}$   $40.1 \pm 14.9 \mu\text{M}$ ). Beta-lactam antibiotics interfere with bacterial peptidoglycan (PG) biosynthesis by inhibiting penicillin-binding proteins (PBPs) and thus the transpeptidation of cell wall building blocks.<sup>127</sup> The  $\beta$ -lactam ring structurally mimics the D-Ala-D-Ala terminus of the pentapeptide side chain that is attached to the MurNAc moiety of the central PG precursor lipid II. Because of this structural analogy, we investigated the effects of different cell wall precursor molecules on CapD enzymatic activity. The pentapeptide L-Ala-D-Glu-L-Lys-D-Ala-D-Ala was found to inhibit CapD enzymatic activity with an  $IC_{50}$  value of  $73.9 \pm 12.8 \mu\text{M}$ . Moreover, lipid II showed significant inhibition (67%) of CapD activity at a test concentration of  $100 \mu\text{M}$ . Both, ampicillin and lipid II, were found to be selective inhibitors of CapD. Concentration inhibition curves for suramin at CapE, and the pentapeptide (side chain) and ampicillin at CapD are shown in Figure 4.7. Furthermore, the inhibition mechanisms for suramin, ampicillin and the pentapeptide L-Ala-D-Glu-L-Lys-D-Ala-D-Ala were investigated (Figure 4.8). Suramin was found to act as a non-competitive inhibitor at CapE. Ampicillin appeared to be a non-competitive inhibitor at CapD while the pentapeptide L-Ala-D-Glu-L-Lys-D-Ala-D-Ala showed a competitive inhibition mechanism at CapD.

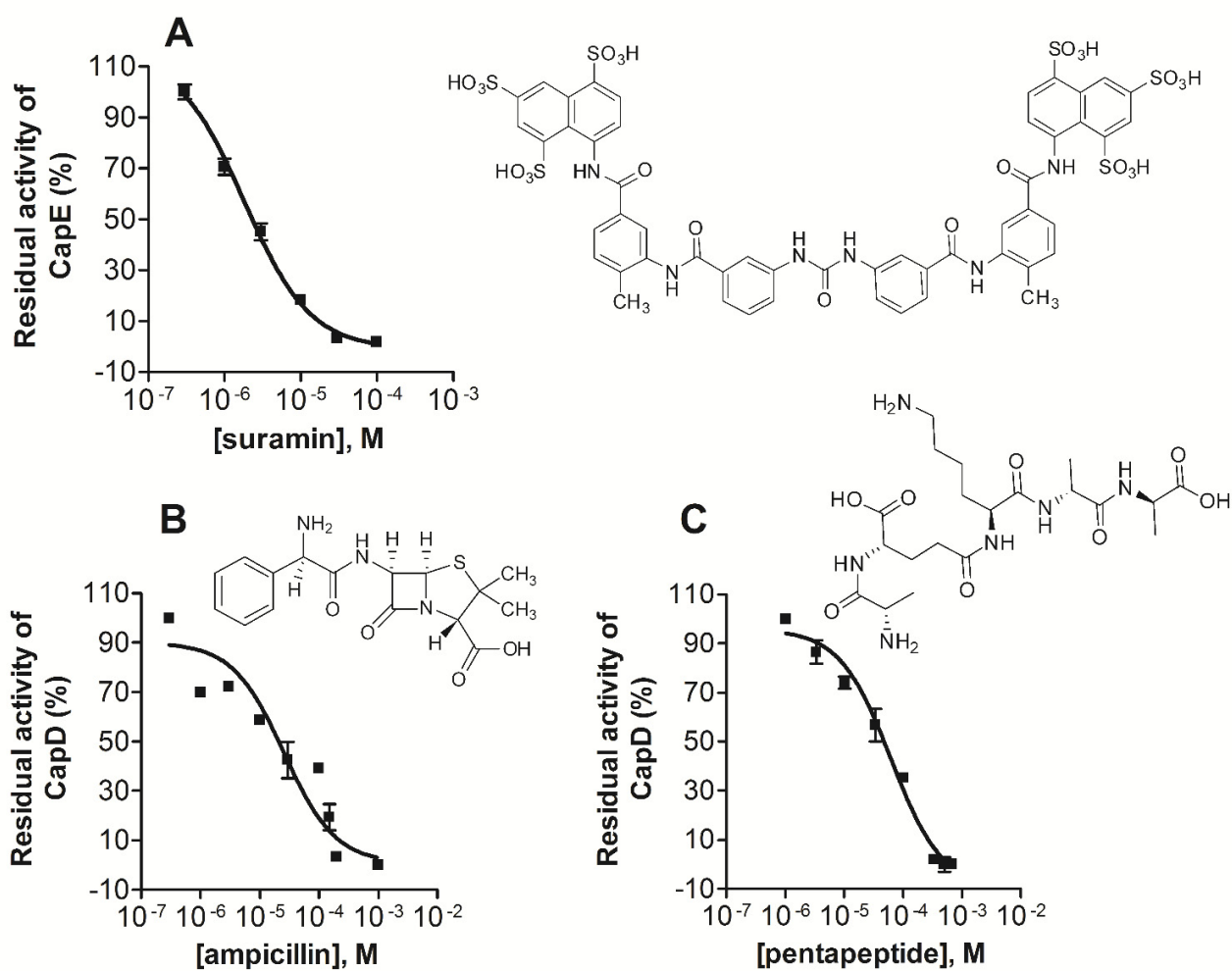


Figure 4.7. Concentration-dependent inhibition of CapD and CapE. (A) CapE inhibition by suramin ( $IC_{50} 1.82 \pm 0.40 \mu\text{M}$ ); (B) CapD inhibition by ampicillin ( $IC_{50} 40.1 \pm 14.9 \mu\text{M}$ ); (C) CapD inhibition by the pentapeptide L-Ala-D-Glu-L-Lys-D-Ala-D-Ala ( $IC_{50} 73.9 \pm 12.8 \mu\text{M}$ ). Substrate concentration was 1 mM.

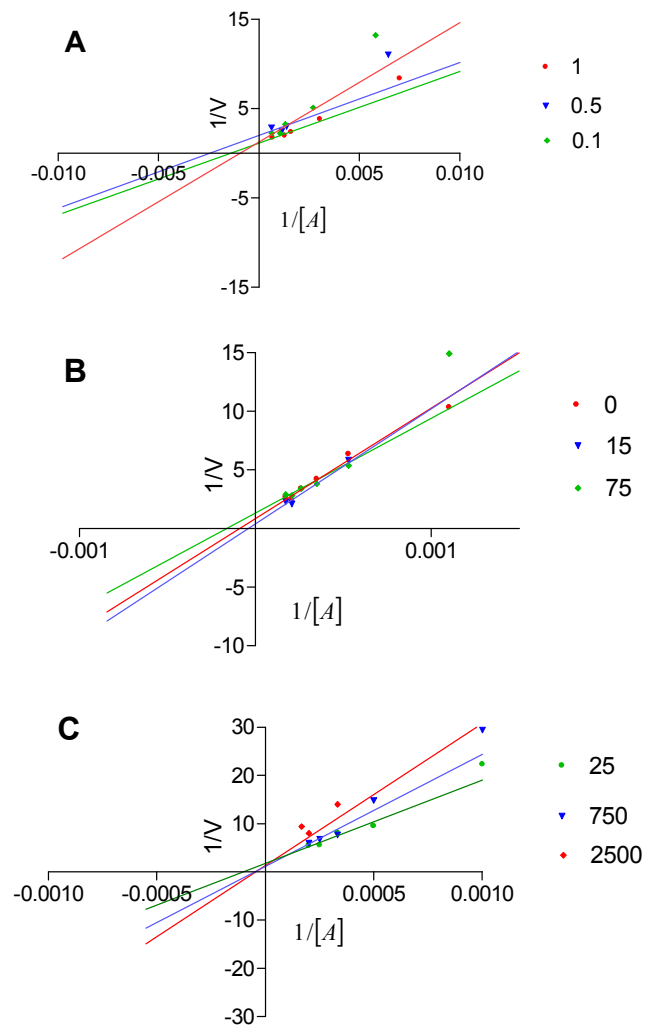


Figure 4.8. Determination of enzyme inhibition mechanism. (A) CapE inhibition by suramin is non-competitive (suramin concentrations for determination were 0.1  $\mu\text{M}$ , 0.5  $\mu\text{M}$  and 1  $\mu\text{M}$ ); (B) CapD inhibition by ampicillin is non-competitive (ampicillin concentrations for determination were 0  $\mu\text{M}$ , 15  $\mu\text{M}$  and 75  $\mu\text{M}$ ); (C) CapD inhibition by the pentapeptide L-Ala-D-Glu-L-Lys-D-Ala-D-Ala is competitive (pentapeptide concentrations for determination were 25  $\mu\text{M}$ , 750  $\mu\text{M}$  and 2500  $\mu\text{M}$ ).

To determine whether the inhibitory effects of ampicillin on CapD would translate into an effect on CP5 production, a testing *in vivo* was followed up.<sup>93</sup> The *S. aureus* strains Reynolds were grown in the presence and absence of ampicillin. CP5 products by the *S. aureus* strain Reynolds were evaluated at ampicillin concentrations ranging from 67 – 270  $\mu\text{M}$ . Concentrations up to 270  $\mu\text{M}$  (100  $\mu\text{g/ml}$ ) ampicillin can be achieved *in vivo*<sup>128</sup>. Like the majority of *S. aureus* strains, Reynolds is resistant to ampicillin and penicillin, and the minimum inhibitory concentration of ampicillin for Reynolds is >128  $\mu\text{g/ml}$ . After overnight incubation, the treated and untreated staphylococci were washed and treated with trypsin to remove protein A. Serial dilutions of the

bacterial suspensions were incubated overnight with CP5-specific rabbit serum. The absorbed sera were then tested on a microtiter plate coated with purified *S. aureus* CP5. The CFU/ml that resulted in 50% binding compared to the unabsorbed serum was calculated. Growth in the presence of ampicillin inhibited CP5 production, as 3.6- to 5.9-fold higher bacterial concentrations were required to achieve an IC<sub>50</sub> value comparable to the culture cultivated in the absence of ampicillin (Figure 4.9). CP5 production by *S. aureus* grown in media containing 270 μM ampicillin (100 μg/ml) was evaluated six times, and these experiments indicated that a bacterial concentration of  $8.6 \pm 2.9$  (average  $\pm$  SEM) fold higher than that of the antibiotic-free culture were required to achieve 50% inhibition of antibody binding.

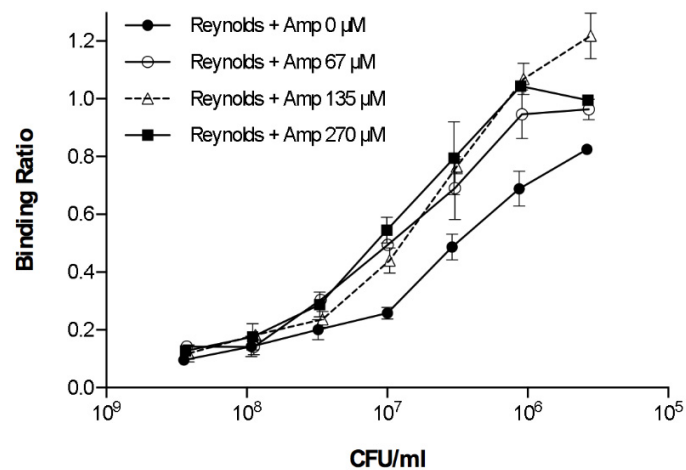


Figure 4.9. ELISA inhibition experiment showing that CP5 production by *S. aureus* Reynolds is inhibited when the culture is incubated in the presence of ampicillin (Amp). The binding ratio is calculated by comparing the OD<sub>405 nm</sub> of the serum samples incubated with different bacterial concentrations with that of the serum sample containing no bacteria. For quantitation, the 50% inhibitory bacterial concentration was compared between cultures grown in the presence or absence of ampicillin (CFU, colony-forming units).

### 4.3.3 CapAB kinase complex regulates capsule biosynthesis

We investigated the role of the tyrosine kinase complex CapAB in the regulation of CapD and CapE. We identified CapE as regulatory target of the CapAB kinase complex and show that tyrosine phosphorylation enhances its catalytic activity *in vitro*. To study the impact of CapAB mediated phosphorylation on CapE enzymatic activity, CapE assays were performed in the presence of either active or of heat-inactivated CapAB kinase complex, as shown in Figure 4.10.

The conversion of UDP-D-GlcNAc was increased in the presence of active CapAB, indicating that the CapE catalyzed reaction is positively modulated through phosphorylation. We tried different batches of CapE enzymes, CapAB activated CapE in a stable way (Figure 4.10). Further testing with CapE mutations have been carried out with the same method.

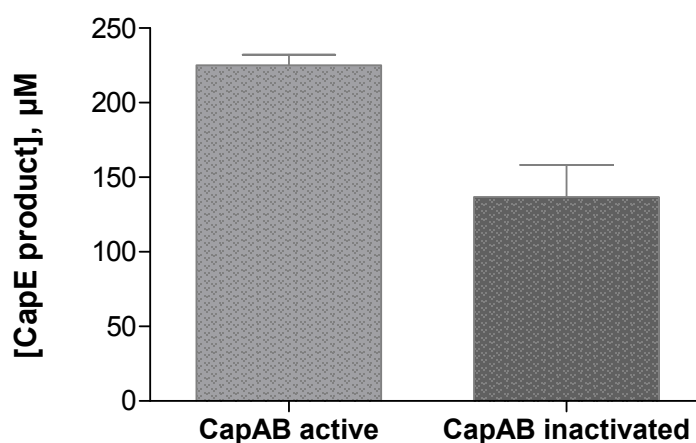


Figure 4.10. CapAB kinase complex regulates CapE. CapE was incubated in presence of either active CapAB (gray) or heat-inactivated CapAB (black) with UDP-D-GlcNAc for 30 min. Reactions were analyzed by CE.

#### 4.3.4 *In vitro* reconstitution of UDP-D-FucNAc biosynthesis

Homology searches with CapD and CapN suggested that both proteins are involved in the synthesis of the first soluble capsule precursor UDP-D-FucNAc.<sup>121</sup> More recently, CapD enzyme was characterized at the molecular level, and the enzymatic product was shown to be UDP-2-acetamido-2,6-dideoxy-D-xylo-4-hexulose (unpublished data). CapN is proposed to further convert the CapD reaction product to UDP-D-FucNAc by stereospecific reduction of the C-4 keto group.<sup>121</sup>

For analysis of the CapN reaction, a CE method described by Kneidinger *et al.*<sup>120</sup> was applied. As shown in Figure 4.11, purified recombinant CapN-His<sub>6</sub> was able to convert UDP-2-acetamido-2,6-dideoxy-D-xylo-4-hexulose (retention time 15.45 min) into a new carbohydrate species displaying altered CE migration behavior (retention time 14.53 min); no such peak was observed with the heat-inactivated negative controls (Figure 4.11). In good agreement with the studies of Kneidinger *et al.* on UDP-L-FucNAc biosynthesis, CapN enzymatic product migrated

faster in the capillary than PglF enzymatic product, but slower than UDP-D-GlcNAc (retention time 13.88 min). Analogous results were obtained using CapD enzymatic product as substrate for CapN reactions. CapN enzymatic activity was dependent on the addition of NADPH; no conversion was observed in the absence of externally added cofactors. Utilization of NADH as cofactor could not be tested as the NADH preparation produced some minor peaks in CE analysis, migrating at the height of the enzymatic product. The HPLC purified PglF and CapN enzymatic products were subjected to Maldi-TOF mass spectrometry and molecular masses of 588.1 and 590.4 (negative mode;  $[M - H]^-$ ) were determined, in accordance with the expected neutral masses of 589.3 and 591.4 for UDP-2-acetamido-2,6 dideoxy-D-xylo-4-hexulose and UDP-D-FucNAc, respectively. These results confirm that CapN functions as a reductase and, using NADPH as a cofactor, is able to convert the substrate UDP-2-acetamido-2,6-dideoxy-D-xylo-4-hexulose to form the first soluble capsule precursor UDP-D-FucNAc.

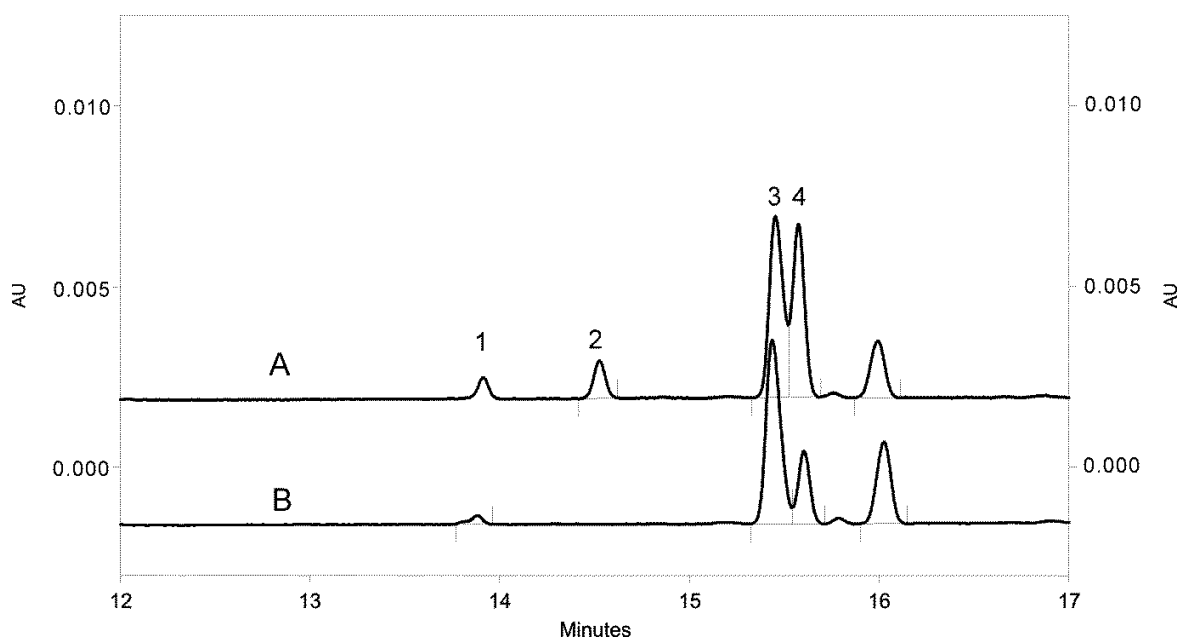


Figure 4.11. Capillary electrophoresis (CE) analysis of CapN *in vitro* activity. Purified CapN and PglF were incubated simultaneously in a combined assay in the presence of UDP-GlcNAc and NADPH. (A) PglF/CapN reaction. (B) Control reaction, CapN heat inactivated. 1; UDP-GlcNAc; 2, UDP-FucNAc (CapN product); 3, UDP-2-acetamido-2,6-dideoxy-D-xylo-4-hexulose (PglF product); 4, NADP.

## 4.4 Conclusions and discussion

The enzymatic reactions involved in the syntheses of the soluble capsule precursors UDP-L-FucNAc and UDP-D-ManNAcA have already been studied *in vitro*.<sup>120,129,130</sup> However, *in vitro* characterization of the biosynthesis of the first soluble capsule precursor (UDP-D-FucNAc) has long been hampered by the fact that CapD, the enzyme catalyzing the initiating step, is a protein with multiple transmembrane domains. We have now been able to reconstitute CapD enzymatic activity *in vitro* and characterize the full-length membrane protein at the molecular level with our new CE method, thus providing the basis for future reconstitution of the complete biosynthetic pathway.

Since established antibiotics are becoming increasingly inefficient, there is an urgent need to explore new treatment strategies to counteract drug-resistant pathogens.<sup>131</sup> Capsule biosynthesis is not essential for bacterial cell viability; however, inhibitors targeting this process may have the potential for use in combination therapeutics. Combining antibiotics with agents that are not microbicidal when administered alone has been proven to be a successful strategy for the treatment of multi-drug-resistant bacterial infections.<sup>117</sup> Inhibition of capsule formation may unmask patterns on the bacterial cell surface, which are important for pathogen recognition and clearance by the innate immune system. Establishment of a robust, validated test system allowed for inhibitor screening of compound libraries. To identify inhibitors with moderate affinity (e.g. fragment-based screening)<sup>132,133</sup> and/or moderate water-solubility, a sensitive assay was required. Therefore, we developed a method for the quantitation of the enzymatic reaction products with a low detection limit, in order to be able to employ low substrate concentrations around the  $K_m$  value of the enzymes. The developed assay allowed the fast screening of a library of selected small molecules as potential inhibitors of CapD and CapE, respectively. Suramin, a drug used for the treatment of trypanosome infections,<sup>126</sup> showed selective inhibition of CapE with an  $IC_{50}$  value of 1.82  $\mu$ M tested at a substrate concentration of 1 mM ( $K_m$  value of CapE 457  $\mu$ M). It acted as a non-competitive inhibitor with respect to the substrate UDP-D-GlcNAc. Due to its relatively high potency and selectivity versus CapE, suramin may be a useful tool for studying capsule biosynthetic enzymes. The evaluation of suramin derivatives may yield even more potent CapE inhibitors. Although suramin is still therapeutically used to treat tropical infectious

diseases, it is not an ideal drug. Its molecular size (1297 g/mol) and high negative charge at physiologic pH due to six sulfonate groups hamper peroral bioavailability. Suramin has been found to interact with a number of protein targets, including purine P2 receptors,<sup>134</sup> ectonucleotidases,<sup>54</sup> G proteins,<sup>135</sup> and ribosomes.<sup>136</sup> It has been shown to penetrate into cells by an active transport mechanism and can even cross the blood-brain barrier.<sup>137</sup> Therapeutic plasma concentrations of suramin are in the range of 10-50  $\mu\text{M}$ ,<sup>138</sup> and at the concentrations reached in clinical applications, bacterial CapE is likely to be completely inhibited.

In CapD inhibition studies, we identified the  $\beta$ -lactam antibiotic ampicillin as an inhibitor of CapD ( $\text{IC}_{50}$  40.1  $\mu\text{M}$ ) showing a non-competitive mechanism of enzyme inhibition. The related amoxicillin and the ampicillin prodrug pivampicillin were inactive at a test concentration of 10  $\mu\text{M}$ , while dicloxacillin was similarly potent as ampicillin in the screening assay (Table 6.1). All further investigated  $\beta$ -lactams (cefotaxime, cefuroxim, ceftazidime, ceftazidime sodium, ceftazidime sodium, oxacillin, phenoxymethylpenicillin, benzylpenicillin, flucloxacillin, piperacillin, sulbactam, ticarcillin, bacampicillin, cloxacillin, penicillin G, mecillinam, ertapenem, meropenem, aztreonam, and potassium clavulanate) did not show any significant inhibition at a test concentration of 10  $\mu\text{M}$ . Ampicillin is a perorally bioavailable drug, able to penetrate eukaryotic lipid bilayers. Ampicillin also appears to cross the staphylococcal cell membrane. The inhibitory concentration of ampicillin at CapD is not much higher than typically observed therapeutic drug levels.<sup>139</sup> CapD catalytic activity was also inhibited in the presence of the PG precursors UDP-D-MurNAc-pentapeptide and lipid II. The findings that ampicillin and the structurally analogous D-Ala-D-Ala dipeptide inhibit CapD activity (Table 6.1) suggest that the C-terminal end of the pentapeptide side chain may represent the minimal structure required for inhibition. Moreover it is conceivable that the inhibitory effect of ampicillin on capsule production observed in whole cells might be of clinical relevance and raises the possibility of additional target sites for  $\beta$ -lactam antibiotics.

A novel mechanism for regulation of CP biosynthesis has been approved. In *S. aureus*, CP biosynthesis occurs predominantly in the late-exponential and post-exponential growth phase.<sup>140</sup> Post-translational control of *S. aureus* capsule expression is exerted by the bacterial tyrosine kinase (BY kinase) complex CapAB.<sup>141</sup> As deduced from kinase assays, the dehydrogenase CapE is an endogenous substrate of CapAB, and phosphorylation of CapE results in enhanced



conversion of the precursor UDP-D-GlcNAc *in vitro*. It could be also demonstrated that the synthesis of UDP-D-ManNAcA is regulated by CapAB-mediated tyrosine phosphorylation of the dehydrogenase CapO.<sup>142</sup> In contrast, no regulatory target of the CapAB complex could be identified within the first reaction cascade; neither CapD nor CapN are phosphorylated by CapAB.



## 5 Summary and outlook

This PhD thesis consisted of three projects dealing with enzymes that are of considerable interest as novel drug targets.

### 5.1 Investigation of ecto-5'-nucleotidase as anti-cancer drug target

Ecto-5'-nucleotidase (*eN*, CD73) catalyzes the hydrolysis of nucleoside monophosphates (mainly AMP), yielding the corresponding nucleoside (mainly adenosine) and inorganic phosphate. The enzyme has been found to be overexpressed on many cancer cells, and *eN*-generated adenosine prevents tumour destruction by inhibiting antitumor immunity. Therefore treatment with *eN* inhibitors may be a promising novel strategy for cancer therapy. In the present study we studied nucleotide mimetics synthesized in our group which consist of a nucleoside scaffold substituted in the 5'-position with a dipeptide moiety. The compounds were investigated at rat *eN* using a capillary electrophoresis-based assay; identified inhibitors at rat *eN* were further investigated at human *eN*.

Several novel nucleotide mimetics have been found to act as pH-dependent *eN* inhibitors showing increased potency at acidic pH values. The most potent compound was AMB552.3a, showing a non-competitive mechanism of inhibition (see Figure 5.1). Since tumor tissues typically show low extracellular pH values, the new inhibitors might act as tumor-selective *eN* inhibitors without affecting physiologically important functions of *eN*, such as the production of adenosine in blood vessels mediating vasodilatory effects.

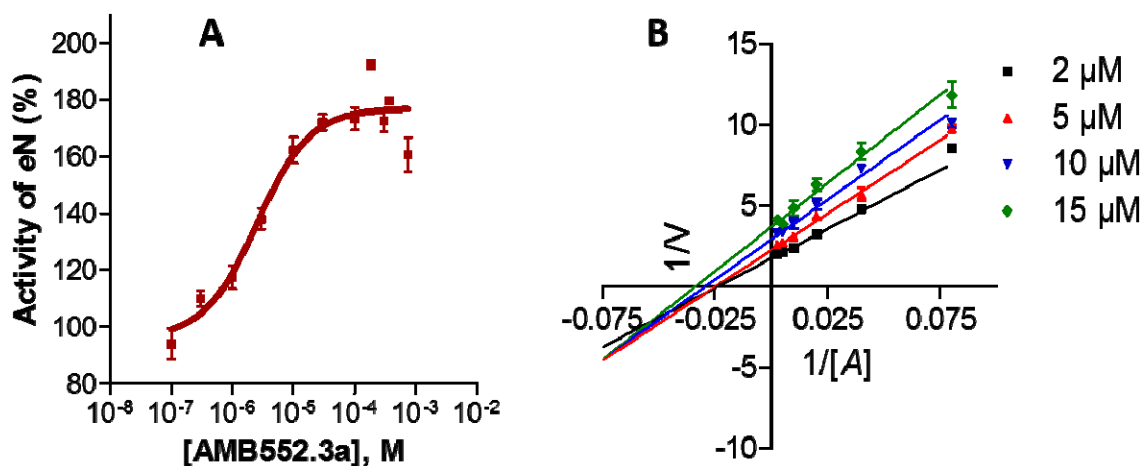


Figure 5.1. (A) Compound AMB552.3a was found to act as an allosteric enhancer of *eN* at physiologic pH of 7.4. Since low extracellular pH values are a hallmark of cancer,<sup>41–45</sup> AMB552.3a might act as tumor-selective *eN* inhibitors without affecting physiologically important functions of *eN*, such as the production of adenosine in blood vessels, which shows vasodilatory effects.<sup>46</sup> (B) Determination of enzyme inhibition mechanism for AMB552.3a at pH 5.6: AMB552.3a is a non-competitive inhibitor for *eN* at pH 5.6 (inhibitor concentrations for determination were 2  $\mu$ M, 5  $\mu$ M, 10  $\mu$ M and 15  $\mu$ M).

## 5.2 Investigation of cerebroside sulfotransferase as a target for metachromatic leukodystrophy

- Cerebroside sulfotransferase (CST) is a promising new therapeutic target for the treatment of metachromatic leukodystrophy (MLD), a devastating genetic disease. In the absence of an effective therapy, MLD leads to early death of the young patients. In the present study we developed and validated a test system for the monitoring of the catalytic activity of cerebroside sulfotransferase (CST) via quantification of adenosine-3',5'-diphosphate (PAP) by capillary electrophoresis (CE).
- The CE method is sensitive, robust and suitable for CST inhibitor screening,  $K_i$  value determination, and enzyme kinetic studies. The new assay will be useful for the identification and development of novel CST inhibitors which have great potential for the treatment of MLD.
- C16 (*N*-((2*R*,3*R*,4*S*)-3,4-dihydroxy-1-(((2*S*,3*R*,4*S*,5*R*,6*R*)-3,4,5-trihydroxy-6-(hydroxymethyl)tetrahydro-2*H*-pyran-2-yl)oxy)octadecan-2-yl)palmitamide) was found to be the first competitive inhibitor versus galactocerebroside of CST, with an  $IC_{50}$  value 340  $\mu$ M. The new CST inhibitor C16 can be used as a lead structure and be further optimized to obtain potent CST inhibitors, which are urgently needed for the treatment of MLD.

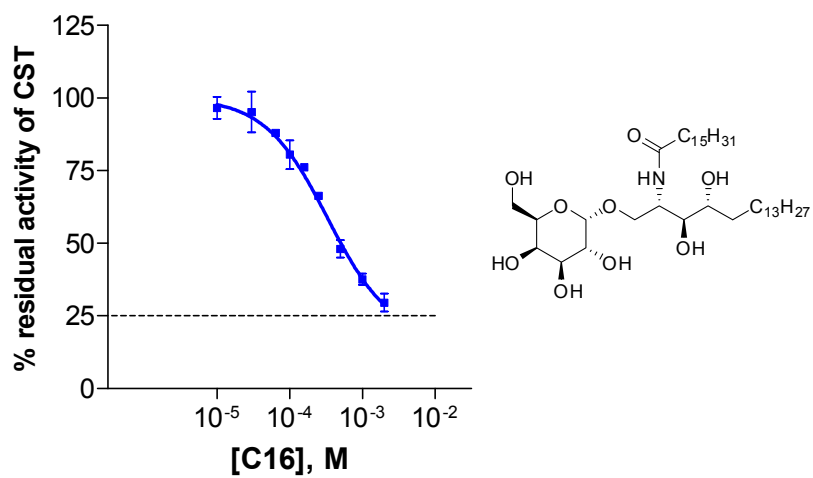


Figure 5.2. Concentration-inhibition curve of the cerebroside sulfotransferase (CST) inhibitor C16 (IC<sub>50</sub> = 340  $\mu$ M).

### **5.3 Analysis of the *Staphylococcus aureus* capsule biosynthesis pathway**

Bacterial polysaccharide capsules are of clinical relevance for most Gram-positive pathogens and the biochemistry of the synthesis of this important cell envelope constituent is not fully understood. For functional characterisation of the capsule biosynthesis enzymes CapD and CapE, a new and robust CE-based method applying micellar electrokinetic chromatography (MEKC) was developed. Especially for the purified integral membrane protein CapD, which catalyze the first step in the synthesis of the soluble capsule precursor UDP-D-FucNAc, is for the first time be functional characterized according to our knowledge. With this newly established method, kinetic studies for CapD and CapE enzymes were performed and a compound library was screened in search for inhibitors. Besides the identification of a numerous inhibitors, the finding that selected beta-lactam antibiotics as well as structurally similar peptidoglycan precursors inhibit CapD activity, suggests an integrated mechanism of regulation for cell envelope biosynthesis pathways. The inhibitory effect on capsule production observed in whole cells might further be of clinical relevance and raises the possibility of additional target sides for  $\beta$ -lactam antibiotics.

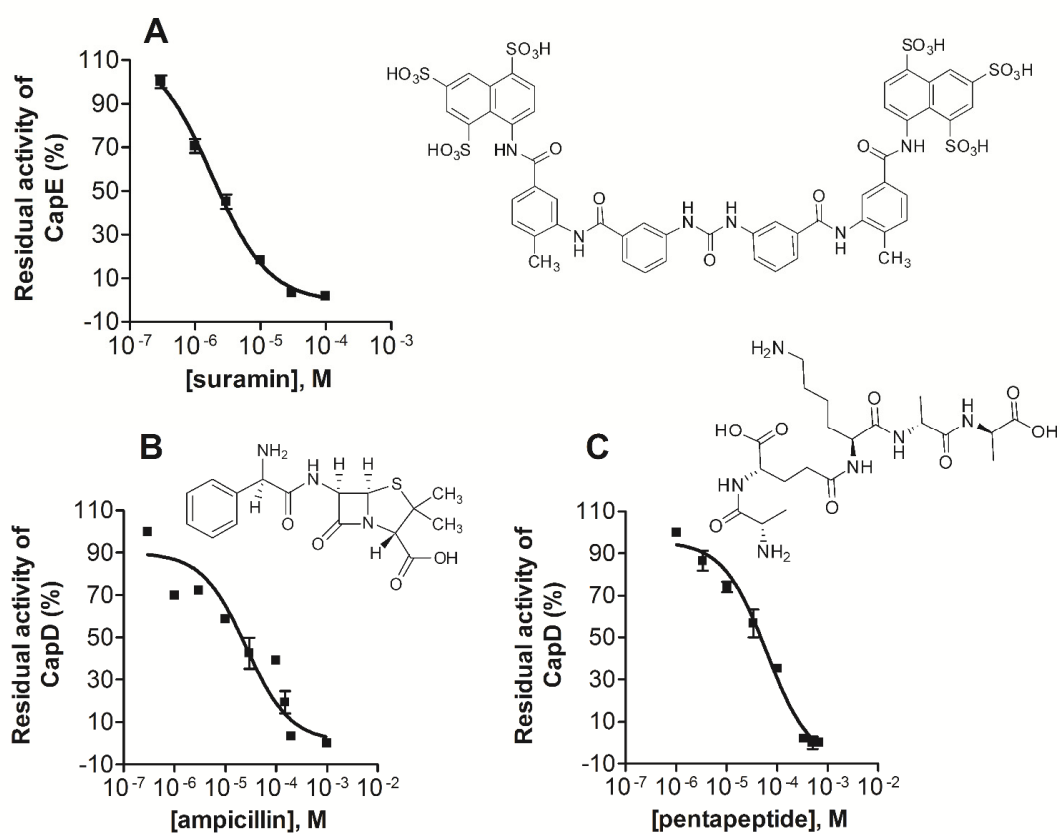


Figure 5.3. Concentration-dependent inhibition of CapD and CapE. (A) CapE inhibition by suramin ( $IC_{50} 1.82 \pm 0.40 \mu\text{M}$ ); (B) CapD inhibition by ampicillin ( $IC_{50} 40.1 \pm 14.9 \mu\text{M}$ ); (C) CapD inhibition by the pentapeptide L-Ala-D-Glu-L-Lys-D-Ala-D-Ala ( $IC_{50} 73.9 \pm 12.8 \mu\text{M}$ ). Substrate concentration was 1 mM.



## 6 Experiments

### 6.1 General

#### 6.1.1 Chemicals

3-(cyclohexylamino)-1-propanesulfonic acid (CAPS)	Sigma-Aldrich
3'-Phosphoadenosine-5'-phosphosulfate (PAPS, 850 $\mu$ M, 75 $\mu$ l per vial)	Bellbrook Labs, 2059
adenosine 3',5'-diphosphate sodium salt (PAP),	Sigma-Aldrich
adenosine 5'-monophosphate sodium salt (AMP)	Sigma-Aldrich
ATP disodium salt	AppliChem, A1348
boric acid	Merck
calcium chloride dihydrate	Fluka, 21097
calcium chloride, anhydrous	AppliChem, A3652
cerebrosides	Matreya LLC
di-natriumtetraborat 10 Hydrate (Borax)	Merck
disodium hydrogen phosphate, anhydrous	AppliChem, A1046
DMSO (cell culture)	AppliChem, A3672
glucocerebrosides	Matreya LLC
guanosine 5'-diphosphate (GDP)	Sigma-Aldrich
HEPES	Roth, 9105.4
hexadimethrine bromide (polybrene)	Sigma-Aldrich
hydrochloric acid 37%	Sigma-Aldrich, 30721
magnesium chloride	Sigma, M8266
potassium chloride	Fluka, 60128
sodium chloride	Roth, 9265.1
sodium hydroxide	Fluka, 71689
Triton™ X-100	Sigma-Aldrich
uridine	Sigma-Aldrich
uridine 5'-monophosphate disodium salt (UMP)	Sigma-Aldrich
$\alpha$ -Galactosyl Ceramide (KRN7000)	Avanti Polar Lipids, 867000P

## 6.1.2 Material and instruments

autoclave	VX-95, Systec 3850 ELV, Systec
balance, analytical	XA205DU Excellence, Mettler Toledo
balance, precision	SBC 42, SCALTEC 440-47N, KERN
centrifuges	Mikro 200, Hettich Allegra™ 21 R, Beckman Coulter Avanti™ J-201, Beckman Rotofix 32, Hettich
MilliQ	PURELAB flex, ELGA
pH-meter	691 pH Meter, Metrohm Seven Easy, Mettler Toledo
pipets	Eppendorf
vortex mixer	UNIMAG Zx <sup>3</sup> , UniEquip Vortex Genius 3, IKA MS2 Minishaker, IKA
centricon 50 kDa	Amicon Ultra, Ultracel – 50K UFC905024, Lot : R9MN42350
fused-silica capillary	Polymicro Technologies
P/ACE MDQ CE	Beckmann

## 6.1.3 Enzymes preparations

### 6.1.3.1 eN

Recombinant rat eN, which was obtained from Prof. Zimmermann's group, was expressed in insect cells and was purified by affinity chromatography using agarose-coupled GSH as

described previously.<sup>48</sup> The GPI-anchor was eliminated, and GST was attached to *eN* to obtain a fusion protein. The purity analysis is shown in Figure 6.1: the GST was around 25 kDa, GST-5NT was around 100 kDa, and BSA was around 70 kDa.

Recombinant Human *eN* was obtained from R&D Systems (5795-EN-010).

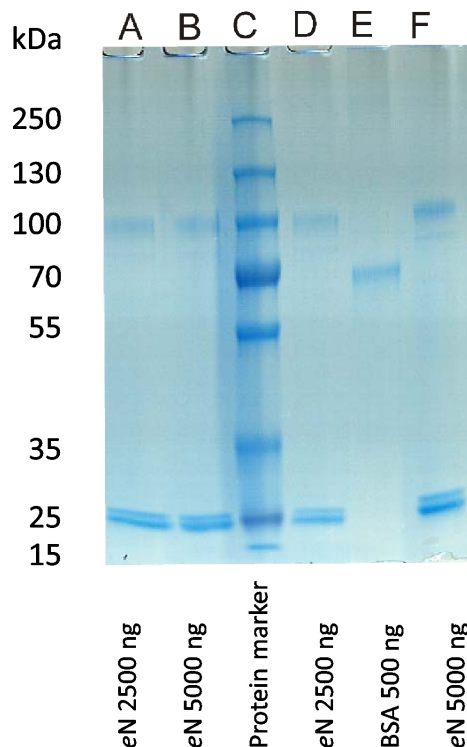


Figure 6.1. *eN* purity analysis. A: 2500 ng (0.26 mg/ml preparation). B: 5000 ng (0.26 mg/ml preparation). C: prestained protein ladder in Tris-glycine (15%). D: 2500 ng (0.49 mg/ml preparation). E: BSA 500 ng. F: 5000 ng (0.49 mg/ml preparation)

### 6.1.3.2 CST

The human CST enzyme, a Golgi type II membrane protein with maximum activity between pH 6.5 and 7.0<sup>17,64</sup>, was obtained from PD Dr. Matthias Eckhardt's group (AK Gieselmann), which was produced by Dr. Isabell Zech. The concentration for batch D1\_V244 was 0.3 mg/ml. For the production of soluble CST, they constructed a plasmid which encodes a fusion protein of the signal peptide of transin fused to the IgG-binding domain sequence from staphylococcal protein A and the luminal domain of human CST. The signal peptide of transin leads to the secretion of the fusion protein and the IgG-binding domain sequence (protein A Tag) enables the purification of the protein from the cell culture supernatant. They generated a stably transfected CHO cell

line and use the supernatant from the cells for the purification procedure. For the purification they use IgG Beads. The protein A-tag of the fusion protein binds to the beads and after washing steps the elution is done under acidic conditions.

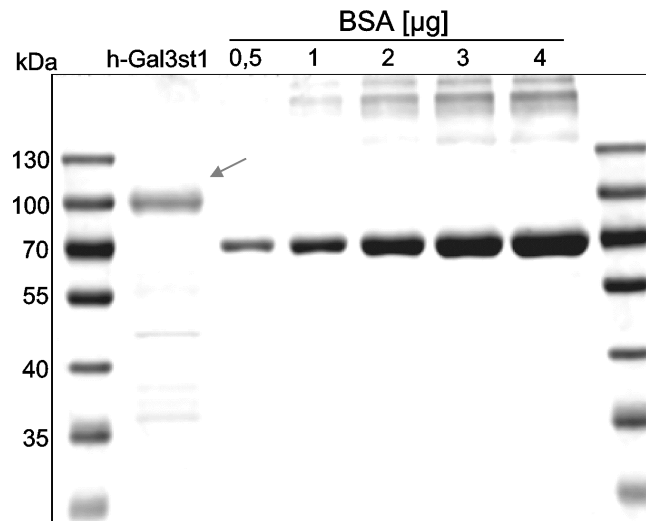


Figure 6.2. CST purity analysis. The determination of CST-concentration with a coomassie-stained gel by using BSA standards. The concentration of BSA as standard was 0,71 µg/18 µl; purified human CST amount was 18 µl.

### 6.1.3.3 CapD and CapE

CapD and CapE were obtained from Prof. Sahl's group, which were produced by Hannah Ulm and Marvin Rausch.

Oligonucleotide primers for amplification of genomic sequences encoding *capD* (*capD*\_for: 5'-TATACATATGGCTAGCTTATCTGTGAAATTG-3'; *capD*\_rv: 5'-TTTGTCTCGAGATAATTATCTCCCTTTTGC-3') and *pglF* (*pglF*\_for: 5'-GCGCGCATATGCTTGTGGATTTTAAACCTTC-3'; *pglF*\_rv 5'-GCGCGCTCGAGTTATACACCTTCTTTATTGTGTT-3') were purchased from Operon Technologies (Germany) PCR reactions were carried out using Phusion DNA polymerase (NEB). Genomic DNA of *S. aureus* Newman was used as a template for *capD* amplification. A truncated version of *pglF* gene (amino acids 130-590) was amplified using genomic DNA from a clinical isolate of *C. jejuni* as a template. PCR products were digested with type II restriction endonucleases (*NheI/XhoI* for *capD*; *NdeI/XhoI* for *pglF*; NEB) and ligated (T4 DNA ligase, Roche) with appropriately restricted expression vectors (Novagen). *CapD* was cloned into

pET24a. *PglF* was cloned into pET28a. The resulting plasmids were confirmed by DNA sequencing (Sequiseve, Germany) and used for recombinant expression of hexahistidine-tagged fusion proteins. Plasmid pKKBK50d used for overexpression of CapE-His<sub>6</sub>, has been described previously<sup>120</sup>. Recombinant hexahistidine-tagged fusion CapD (CapD-His<sub>6</sub>) was expressed in host strain *E. coli* C43 (DE3).<sup>93,143</sup> Recombinant hexahistidine-tagged fusion CapE (CapE-His<sub>6</sub>) was expressed in host strain *E. coli* BL21 (DE3). *PglF*, which has the same product (UDP-2-acetamido-2,6-dideoxy- $\alpha$ -D-xylo-hex-4-ulose) as CapD, was obtained as a recombinant truncated version of the enzyme from *C. jejuni*, as described by Schoenhofen et al<sup>122</sup>.

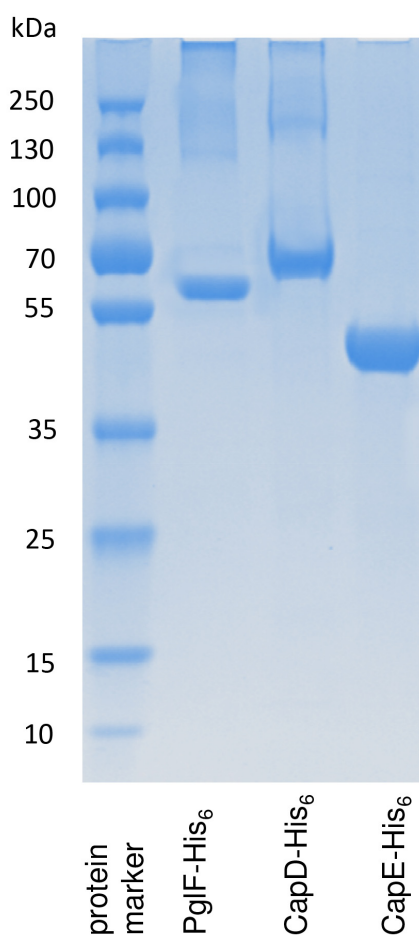


Figure 6.3. SDS-PAGE analysis of purified recombinant enzymes CapD, *PglF* and CapE. Protein marker: PageRuler Plus Pre-Stained Protein Ladder (10 - 250 kDa); Fermentas.

## 6.2 Operation for capillary electrophoresis

### 6.2.1 Strategy for establishing capillary electrophoresis methods

A simple workflow of CE method for small molecules detection is shown in Figure 6.4. The general strategy is summarized as below:

#### Step 1: Separation of analytes

The analytes that need to be separated are substrate and product of a certain enzyme (enzyme cofactors should be also considered). One can separate them based on their charge or size differences. Charge differences can be predicted by software Marvin (ChemAxon). When the analyte has a good chromophore (e.g. aromatic rings), DAD detector can be used. Usually the best separation will be achieved in a buffer pH nearby the pKa value of analytes. A basic capillary zone electrophoresis mode can be chosen as the starting point.

#### Step 2: Quantification of analytes – stacking

In order to maximize the sensitivity of detection for enzyme product, one can examine the product property and apply suitable stacking method.

#### Step 3: Internal standard (I.S.)

Internal standard is necessary for the method validation. A good internal stand should:

- Have no interaction with the other assay components.
- Have a good separation from the other analytes.
- Have a quick migration time.

#### Step 4: Method optimization – other parameters

All CE method parameters (including injection time, separation voltage, capillary length, etc.) can be further optimized, in order to achieve a fast and clean separation.

#### Step 5: Sample preparation

The sample must be homogenized and deproteinized before CE injection.

### Step 6: Validation

Before the inhibitor screening or the enzyme kinetic characterization, a validation step is required.

### Step 7: Application

After optimization and validation, the new CE method is ready for application. Usually a good CE analysis method should be simple, fast, cheap and sensitive:

- Simple: the analytes should be consumed as less as possible, and the sample preparation steps should be kept as simple as possible. For example, there are many ways to stop the enzyme reaction: by heating, by adding organic solvent, or by filtering. If the analytes are stable under heating, the heating method is usually preferred.
- Fast: the migration of analytes should be as quick as possible. For example, to reduce migration time by increasing the separation voltage, by using shorter capillary, or by changing the buffer pH value.
- Cheap: it would be good to find a cheaper way to carry out the assay. For example, a low LOQ method consumes less enzyme, and a good dynamic coating is cheaper than coated capillary.
- Sensitive (Low LOQ): sample stacking is the most useful way to achieve a lower LOQ.

### Step 8: To monitor new enzyme catalyze activity

First of all, we keep the enzyme incubation time within the steady-state. The next step is to make sure that the enzyme reaction can be stopped completely, and meanwhile to check the substrate degradation under the experimental condition (e.g. by 99°C heating). Last but not the least is to check other noises in this assay, because it is possible to observe an apparent reaction in the absence of enzyme substrate. (Because enzymatic activities may be contained in the water by the presence of bacteria, or additional substrate may come from the endogenous substrate in the crude tissue preparation, or chemical hydrolysis may occur). In order to detect noises, we need a blank control, which contains inactive enzyme, and the blank rate must be subtracted from the apparent rate.

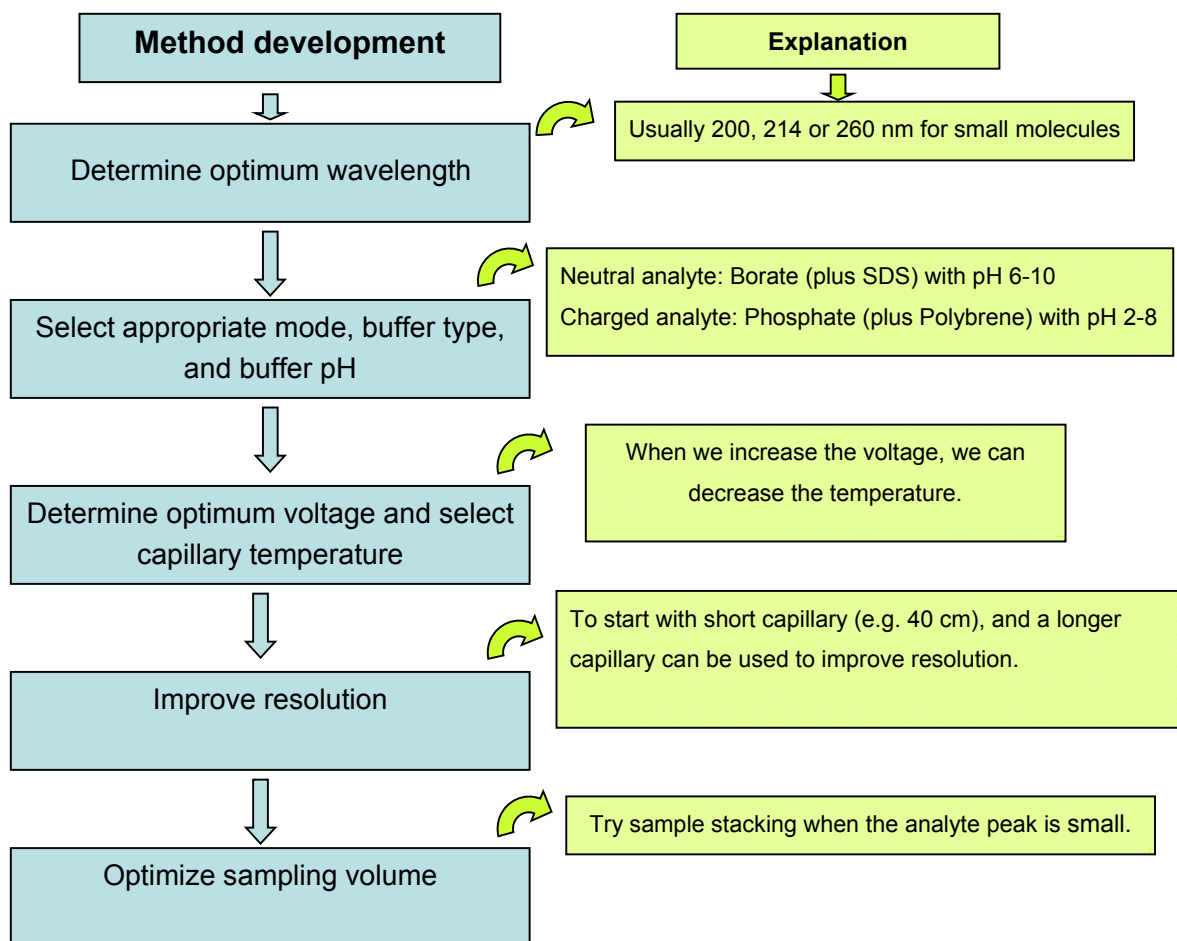


Figure 6.4. Simple workflow for CE method development

### 6.2.2 Capillary electrophoresis working process

#### 1. Prepare samples and buffers

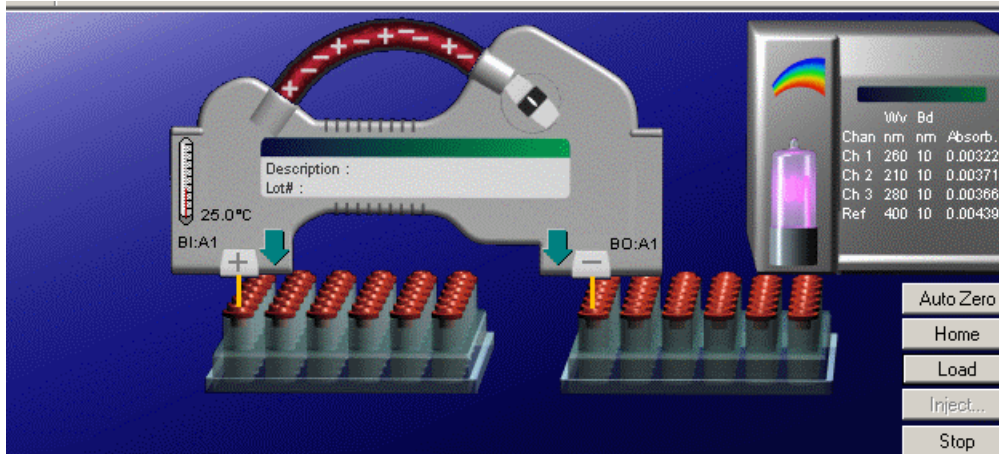
We use three trays inside the CE instrument: BI, BO, and SI.

- BI: buffer inlet tray for 2.0 ml vials
- BO: butter outlet tray for 2.0 ml vials
- SI: Sample inlet tray for 0.5 ml vials or PCR vials

The picture below shows that the capillary can stay in position BI: A1 and BO: A1

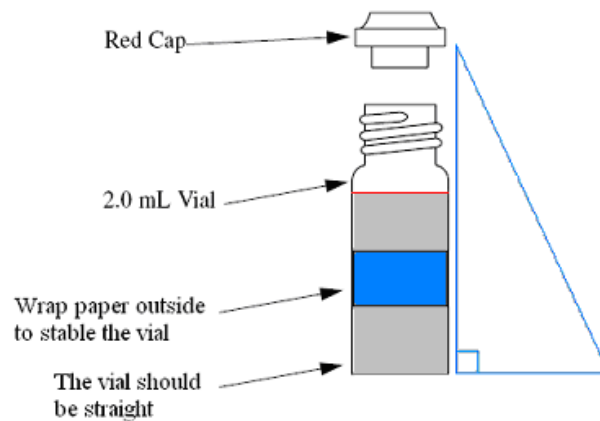


Every time when you turn on the instrument, it needs a few minutes for configuration. Don't open its cover until the light is ready and the capillary is in the home position (usually BI: A1 and BO: A1)



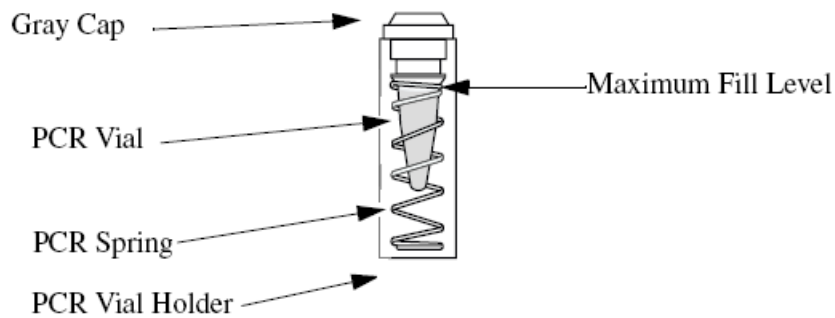
The 2.0 ml glass vial is for the buffer tray. As shown below:

- The vial should be straight. If it is not straight, don't use it.
- Wrap paper outside the vial to fix the vial in the buffer tray.
- Wash the vial with water after using and dry it before the next use.
- Fill the buffer to the red line.
- Before you load the vial, make sure the cap fits the bottle and no buffer is outside the bottle. If the cap is not fit or dirty, don't use it. If there is buffer outside, please dry it first.



The PCR vial is for sample tray. As shown below:

- Wash the vial only with Millipore water after using and dry it before the next use.
- Make sure there are no bubbles inside the sample.
- Before you load the vial, make sure the cap fits the bottle and no buffer outside the bottle.  
If the cap is not fit or dirty, don't use it. If there is buffer outside, please dry it first.

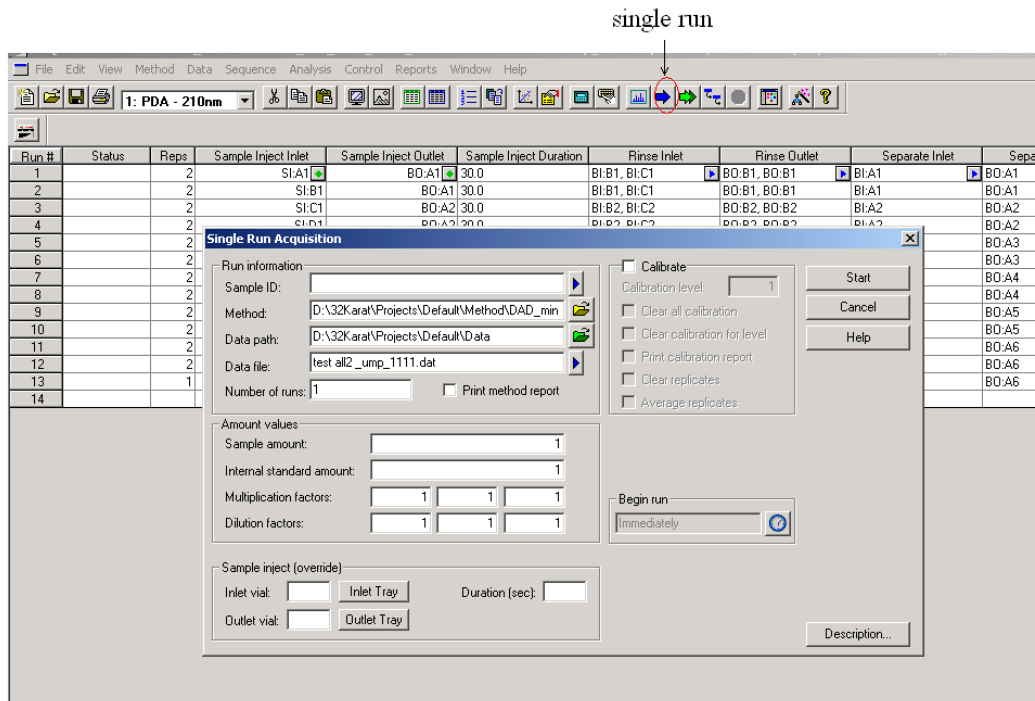


## 2. Run sequence or single run

### 2.1 single run

As shown below, when you click the single run button, you can open the dialog window and then set your run:

- Method path: where you load your method
- Data path: where you save your result
- File name: the name of your result
- Sample inject: the sample position
- Description: detail information about your assay
- Number of run: you can repeat your measurement



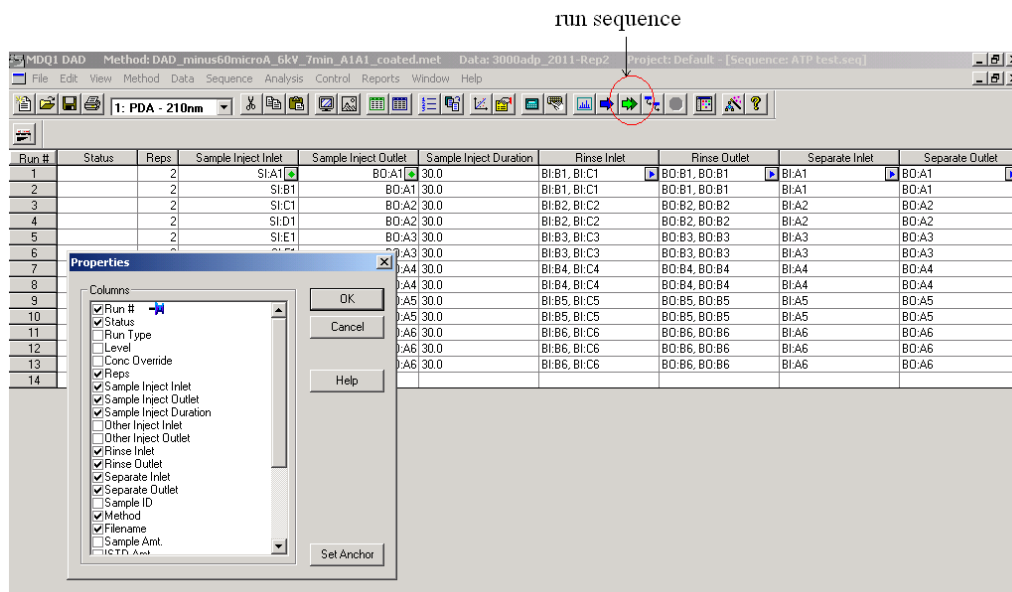
## 2.2 Sequence (multiple runs)

As shown below, you can open the sequence window and write your sequence:

- Method: load your method
- File name: the name of your result
- Sample inject inlet: the sample position
- Description: detail information about your assay
- Repts: you can repeat your measurement
- Sample Injection Duration: it can be overwrite, but usually you don't need to change it

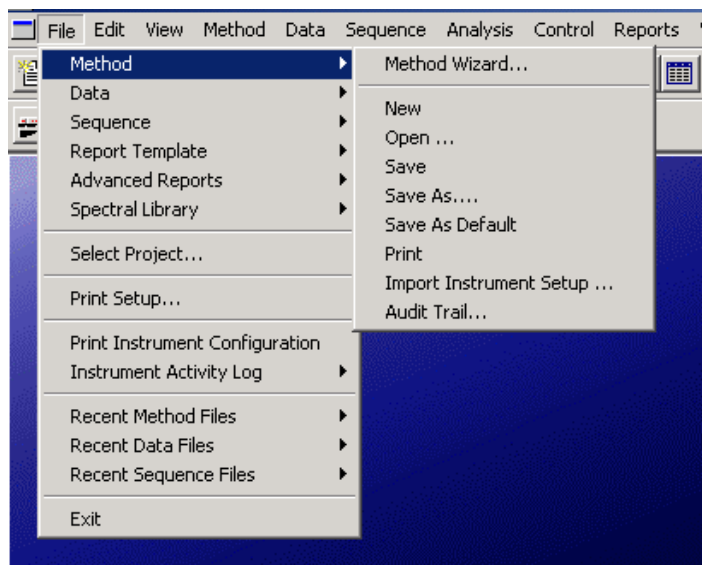
Then you save method and sequence, and click the run sequence button.

Notice: if you open a sequence from project A, then the data will be stored under project A too, no matter which project you log in with.



### 3. Writing methods

Method wizard -> New



#### 3.1 initial condition

As shown below: This window shows the initial condition. For the Auxiliary data channels, if you choose the Voltage or Current, you will have a window to monitor how it changes. Please save the method after your change.

Initial Conditions | PDA Detector Initial Conditions | Time Program

**Auxiliary data channels:**  
 Voltage max: 30.0 kV  
 Current max: 300.0  $\mu$ A  
 Power  
 Pressure

**Mobility channels:**  
 Mobility  
 Apparent Mobility  
 Plot trace after voltage ramp

**Analog output scaling:**  
 Factor: 1

**Temperature:**  
 Cartridge: 25.0  $^{\circ}$ C  
 Sample storage: 25.0  $^{\circ}$ C

**Peak detect parameters:**  
 Threshold: 2  
 Peak width: 9

**Trigger settings:**  
 Wait for external trigger  
 Wait until cartridge coolant temperature is reached  
 Wait until sample storage temperature is reached

**Inlet trays:**  
 Buffer: 36 vials  
 Sample: 48 vials

**Outlet trays:**  
 Buffer: 36 vials  
 Sample: No tray

### 3.2 PDA detector condition (For DAD detector)

Please pay attention to the Electropherogram channel data. Please choose the window with the wavelength that you want. Then save method.

Initial Conditions | PDA Detector Initial Conditions | Time Program

**Electropherogram scan data:**  
 Acquisition enabled  
 Data rate: 4 Hz  
 Scan range from 190 to 300 nm

**Electropherogram channel data:**

	Acquisition enabled	Reference channel	Wavelength (nm)	Bandwidth (nm)
Channel 1:	<input checked="" type="checkbox"/>	<input type="checkbox"/>	214	10
Channel 2:	<input type="checkbox"/>	<input type="checkbox"/>	254	10
Channel 3:	<input type="checkbox"/>	<input type="checkbox"/>	280	10
Peak detect:	<input type="checkbox"/>	<input type="checkbox"/>	250	120

**Filter:**  
 High sensitivity  
 Normal  
 High resolution  
 Peak width (points): 16-25

**Relay 1:**  
 Off  
 On

**Relay 2:**  
 Off  
 On

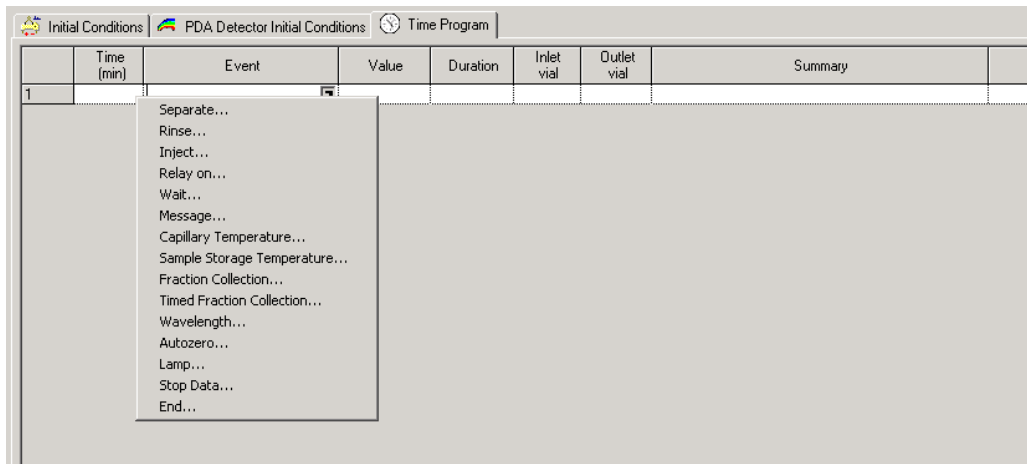
**Reference channel:**  
 Wavelength: 400 nm  
 Bandwidth: 10 nm

**Absorbance signal:**  
 Direct  
 Indirect

### 3.3 Time program

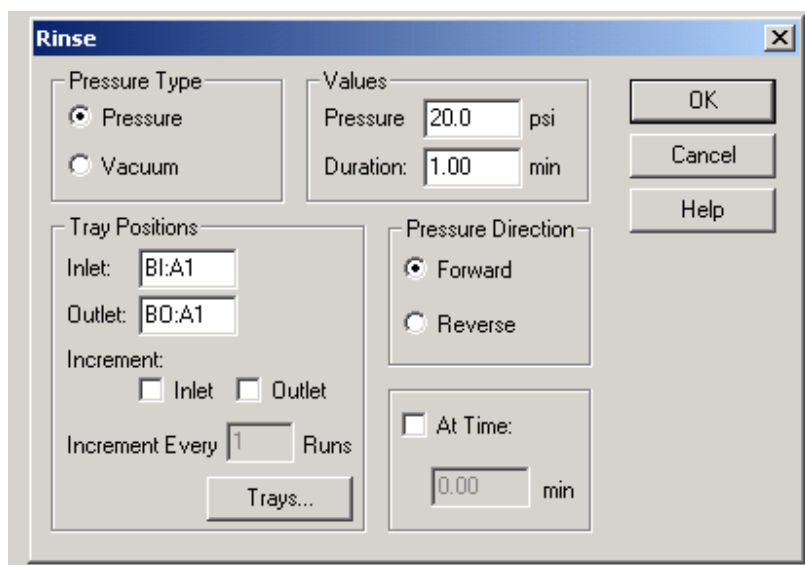
Click Event to write your method:

- Rinse
- Inject
- Separate
- End



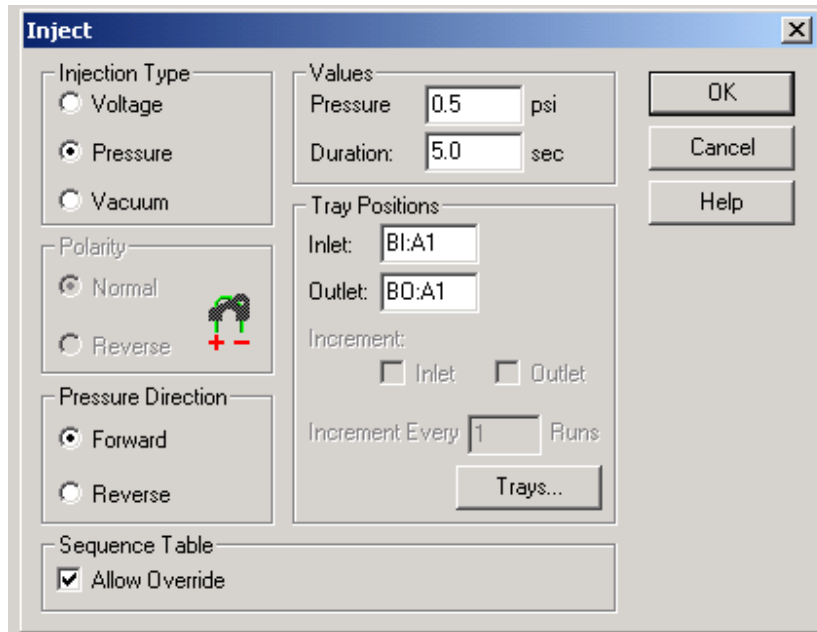
Rinse stage:

- Pressure Type: Pressure or Vacuum. Usually we use pressure. Then give pressure value and duration.
- Tray positions: Choose the inlet (rinse buffer) and outlet (waste)



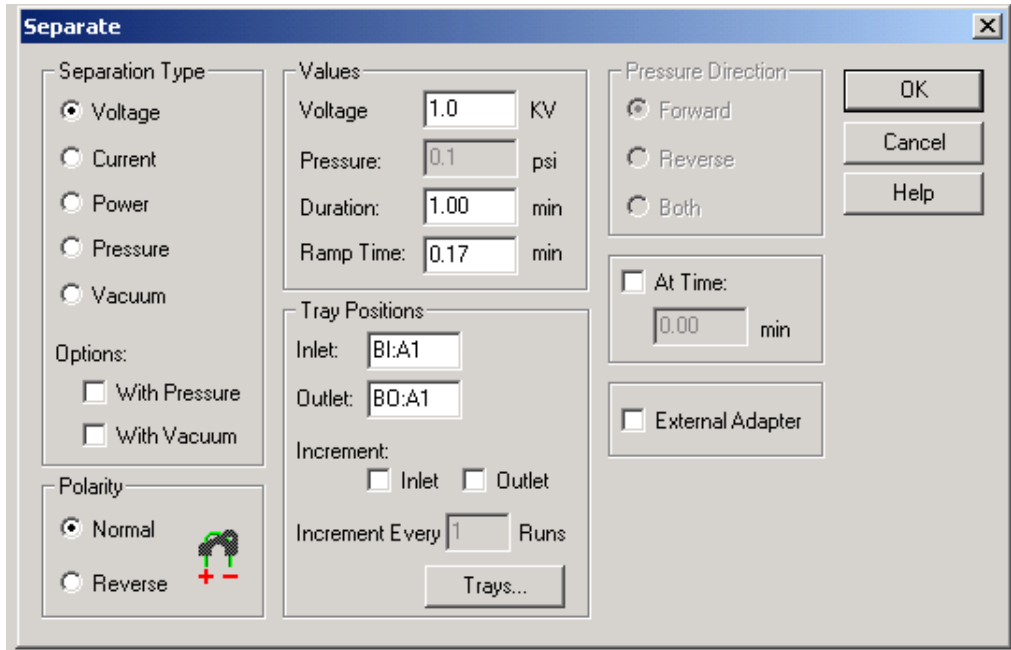
## Inject stage

- Injection Type: Voltage, Pressure or Vacuum. Usually we use pressure and voltage (not for neutral solute). Then give value and duration.
- Tray positions: Choose the inlet (sample) and outlet
- Allow override: Usually we allow this part to be overridden.



## Separation:

- Separation Type: Voltage, Current, Power, Pressure or Vacuum. Usually we use pressure, current and voltage. The one you choose will be a constant during the separation. Then give value and duration.
- Ramp time: usually it is 0.5 min
- Tray positions: Choose the inlet (separation buffer) and outlet (separation buffer)
- Polarity: When you use FS capillary, it is Normal. When you use coated capillary, it can be Normal or Reverse.
- At time: choose at time 0.00 min

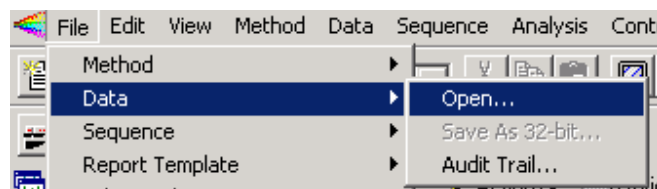


An example:

	Time (min)	Event	Value	Duration	Inlet vial	Outlet vial	Summary
1		Rinse - Pressure	50.0 psi	2.00 min	BI:B1	BO:B1	forward
2		Rinse - Pressure	50.0 psi	2.00 min	BI:C1	BO:B1	forward
3		Inject - Voltage	6.0 KV	30.0 sec	SI:A1	BO:A1	Override, reverse polarity
4		Inject - Pressure	0.5 psi	5.0 sec	BI:B1	BO:B1	No override, forward
5	0.00	Separate - Current	60.0 $\mu$ A	7.00 min	BI:A1	BO:A1	0.50 Min ramp, reverse polarity
6	1.00	Autozero					
7	7.00	End					

## 4. Data analysis

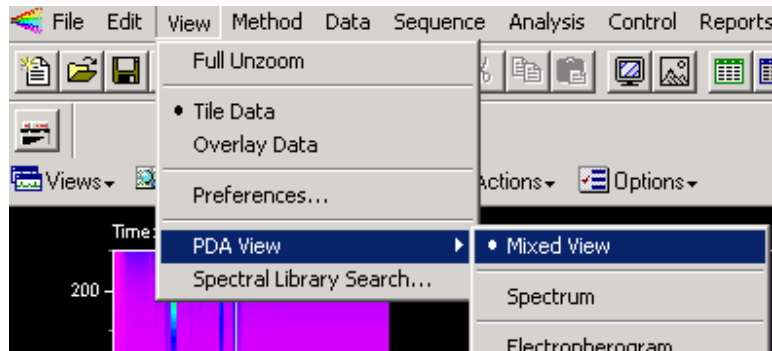
### 4.1 open data:



Method->From Results: In the Options section, if you choose From Result, you can check the method within this source data. You can choose it when you are in the offline mode. But if you analysis data by using online mode, better don't choose it.



#### 4.2 mixed view:



4.3 save standard spectrum in library: if you find a good spectrum you can save it and use it for identification in future.

Utilities->Save trace->click the spectrum and save it

4.4 Add trace from the library: you can use a standard spectrum in the library for comparison and identification with your own result.

Add Trace...->Open Spectrum File...

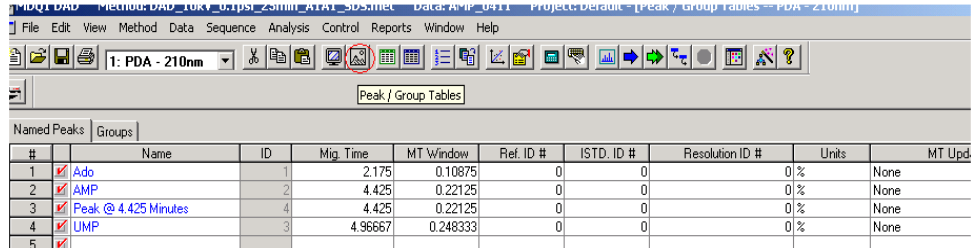
#### 4.5 Custom reports

##### 4.5.1 Define peaks

- Open the window with a certain wave length. For example: PDA-260nm.
- Select MAN PEAK and click before and after the peak you → ANALYSE
- If more peaks than you want are identified, select INT OFF and select the → ANALYSE
- DEFINE PEAK: select range → Replace existing peaks in table and click OK
- If you want to further change your defined peak range, just click modify button.

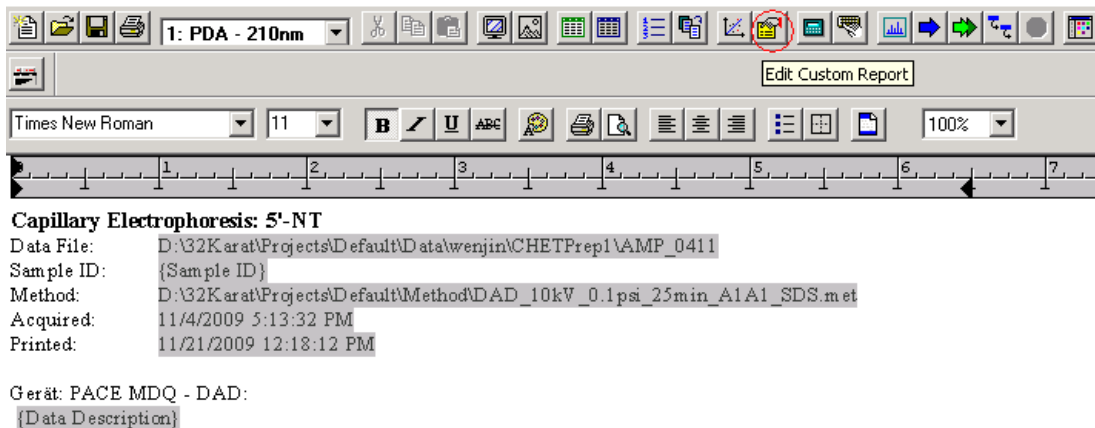
## 4.5.2 Generate report

Select PEAK/GROUP TABLES and rename each peak appropriately → ANALYSES



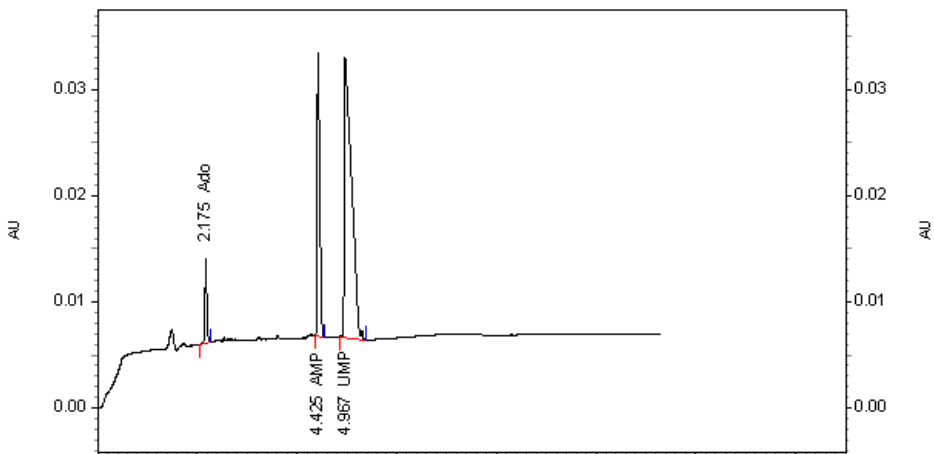
#	Name	ID	Mig. Time	MT Window	Ref. ID #	ISTD. ID #	Resolution ID #	Units	MT Upd
1	Ado	1	2.175	0.10875	0	0	0%	None	
2	AMP	2	4.425	0.22125	0	0	0%	None	
3	Peak @ 4.425 Minutes	4	4.425	0.22125	0	0	0%	None	
4	UMP	3	4.96667	0.248333	0	0	0%	None	
5									

Select EDIT CUSTOM REPORT, and then load your own template. You should choose the wave length that you analysis under the property option, for example: PDA-260nm. Otherwise you could not have the right result.



**Capillary Electrophoresis: 5'-NT**  
Data File: D:\32Karat\Projects\Default\DATA\wenjin\CHETPrep1\AMP\_0411  
Sample ID: {Sample ID}  
Method: D:\32Karat\Projects\Default\Method\DAD\_10kV\_0.1psi\_25min\_A1A1\_SDS.met  
Acquired: 11/4/2009 5:13:32 PM  
Printed: 11/21/2009 12:18:12 PM

Gerät: PACE MDQ - DAD:  
{Data Description}



Print it out with a printer or a PDF printer. Use corrected peak area for calculations. You may need Excel or Prism for further analysis.

## 5. Other aspects

### 5.1 Calibrating the PDA Detector

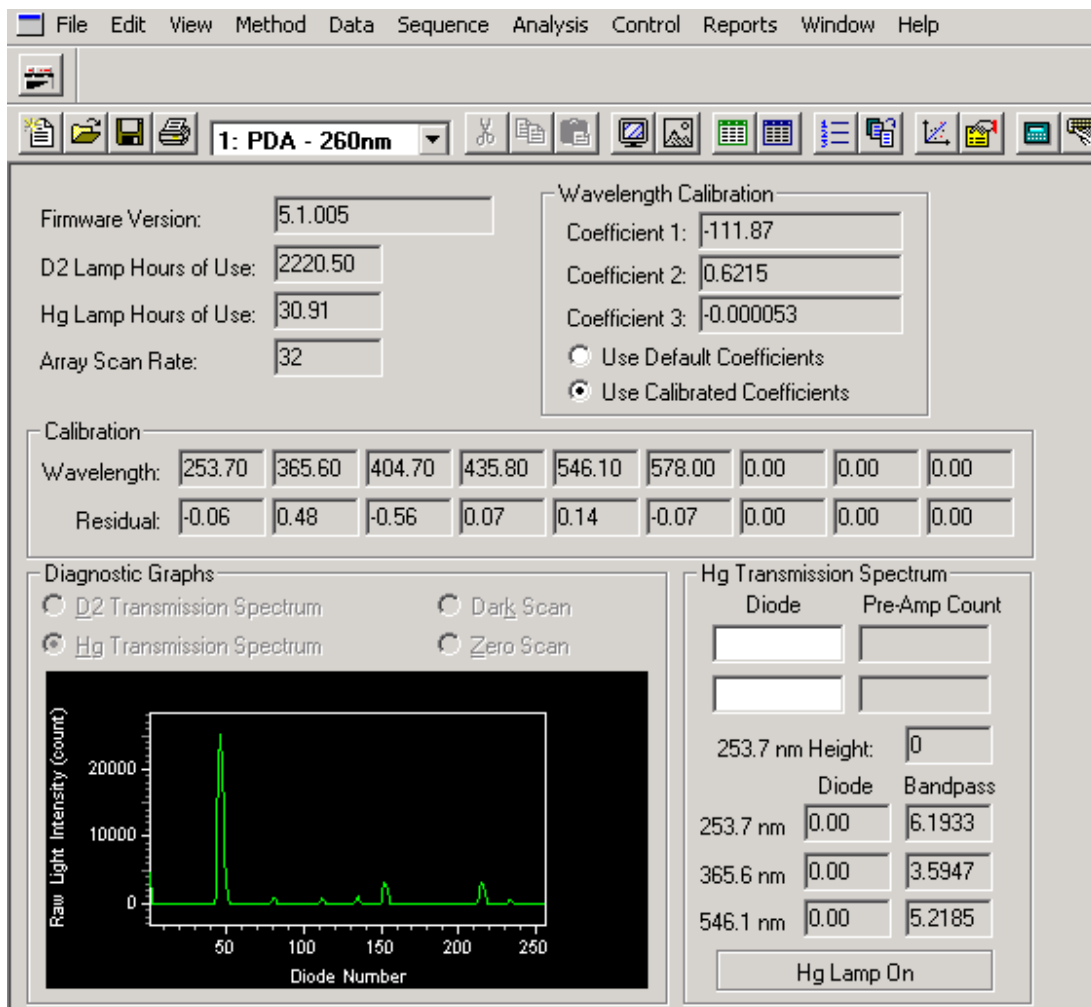
Calibration should be made again when the following experiment conditions changed:

- Internal standard (I.S.): if a new I.S. is purchased (e.g. different batch) or a new concentration is used, the calibration should be updated.
- Injection method (including capillary length): different injection way or amount will change the injected plug length or ion proportion, which can affect the resolution
- Capillary batch: the quality of different capillary batch can change, which will affect the resolution.
- D2 lamp is changed.

Calibrate the PDA detector as below:

To open calibration window by choosing: Control->Diagnostics->Calibrate

To turn on Hg light by choosing: Diagnostic Graphs->Hg Transmission Spectrum



After the Hg Lamp On (as shown above), click right mouse button and choose: Calibration

## 5.2 The corr. area calculation setting

Method->Advanced->Capillary/performance

To choose the right length parameters is important for the corr.area calculation.

The USP standard is OK.

File Edit View Method Data Sequence Analysis Control Reports Window Help

1: PDA - 214nm

Export Custom Parameters Capillary/Performance Files Advanced Reports

Capillary Information

Capillary length: 60  meters  cm

Capillary length to detector: 50  meters  cm

Capillary lot number:

Capillary installation date:

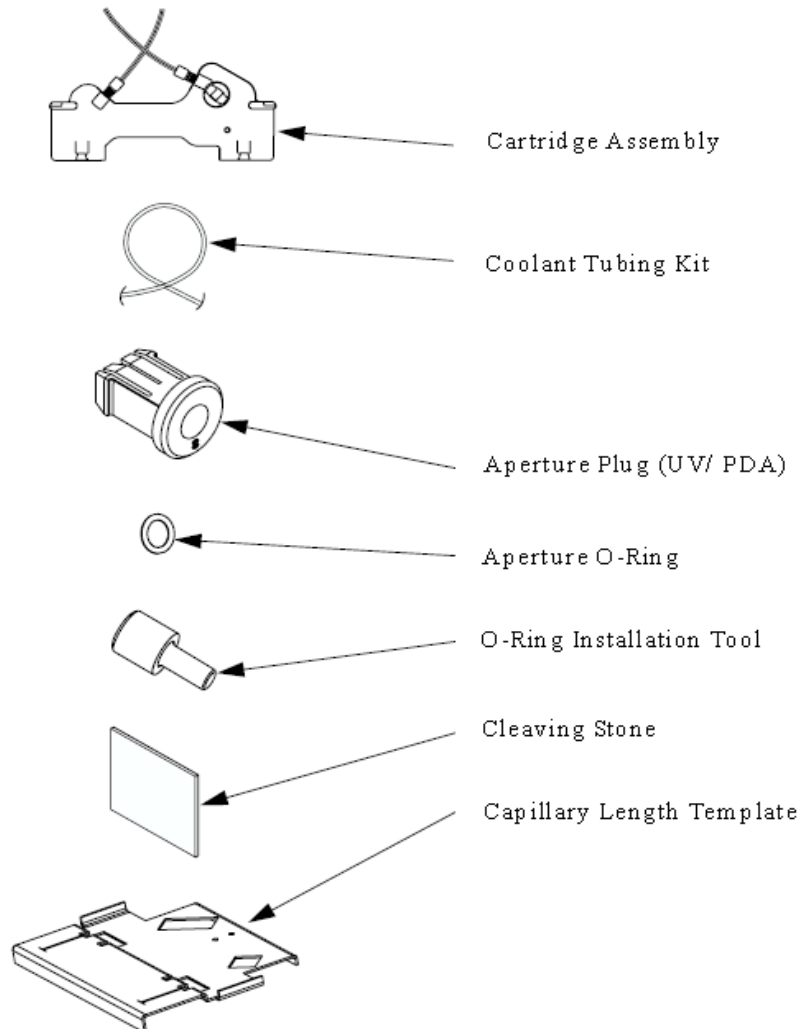
Capillary description:

Calculate performance parameters for this channel

Calculation method(s):  USP  EMG  DAB, BP, EP, ASTM  AOH  JP

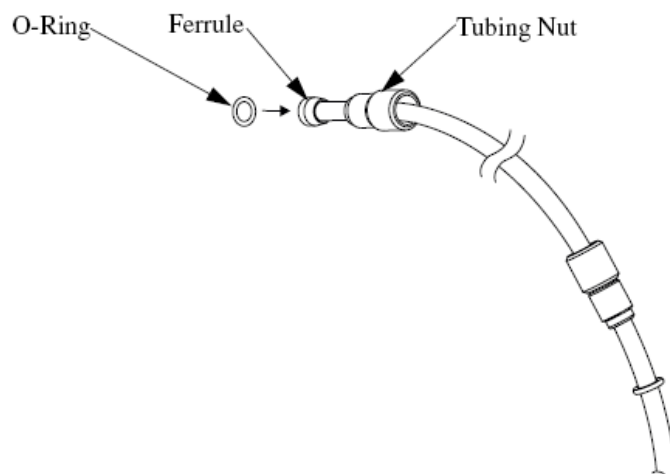
## 6.2.3 Maintenance Procedures

### 1. Capillary cartridge rebuilds



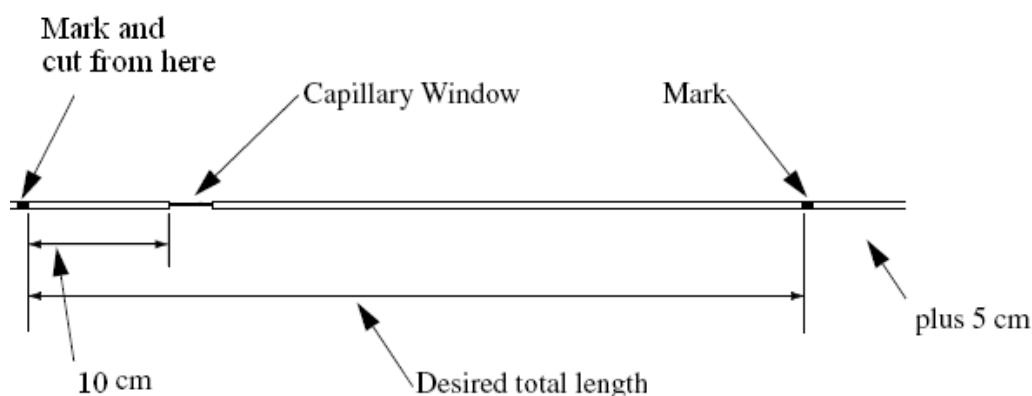
#### 1.1 Remove the old parts:

- Remove two of the seal-retainer clips from the capillary cartridge.
- Remove the aperture by pushing from the front of the cartridge and pulling out from the back. Make sure the O-ring is removed.
- Pull the capillary out of the cartridge.
- If the capillary length needs to be changed, the coolant tubing also needs to be changed. Loosen and remove the tubing nuts. Select the desired coolant tubing from the Cartridge Tubing Kit .Insert the coolant tubing in the cartridge inlet and press it firmly into the cartridge base.



### 1.2 Prepare a capillary:

- Mark the capillary window position.



- Using the capillary cleaving stone. Pull capillary straight off without bending. **Do not saw back and forth with the cleaving stone. Be sure to wear safety glasses when cleaving and breaking the capillary.** Use a fire to burn the window, but not that wide. Then clean the window with alcohol carefully.
- Carefully push and twist the capillary through the cartridge until it appears at the cartridge inlet. Continue by pulling the capillary through the cartridge until the capillary window appears in the cartridge window
- From the back side of the cartridge, place the aperture and from the front side of the cartridge, place the retainer O-ring by using the O-ring insertion tool.
- Carefully insert the capillary Seal Retainer Clips over the capillary at each end and press to snap in place.

- At the cartridge inlet, carefully push the capillary into the cartridge until the capillary stops against the wall of the coolant tubing.
- Holding the capillary against the template, cut off additional length.
- Insert the new cartridge. Then clean it before the first use: 15min, 20psi with NaOH, then 15min, 20psi with buffer, at last 15min separation with buffer (until the baseline is flat).  
For coated capillary, use Millipore water instead of NaOH, and increase pressure to 50psi.

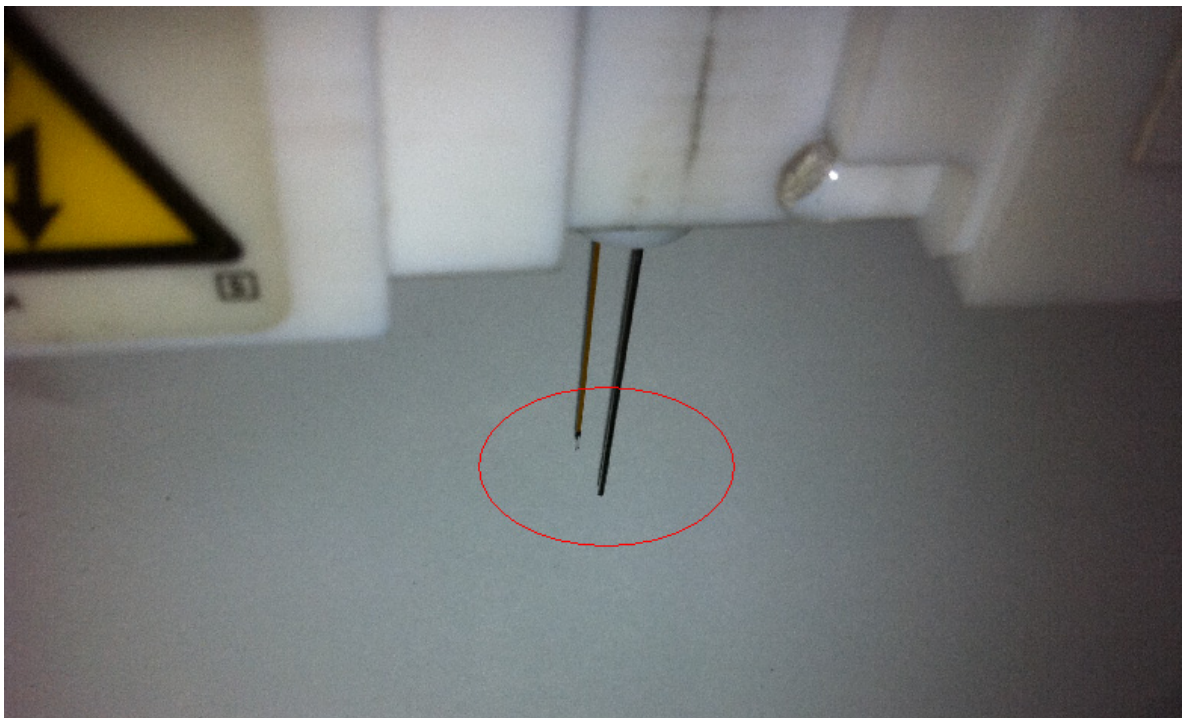
! Seal it, without coolant leakage.

! Do it carefully, to prevent capillary damage.

! There should be a cartridge inside the CE when you turn on the instrument, otherwise the coolant will go out.

The most important thing is: electrode should be longer than the capillary. The length difference between electrode and capillary depends on the injection way:

- Hydrodynamics injection: 1 mm
- Electrostatics injection: 2-3 mm





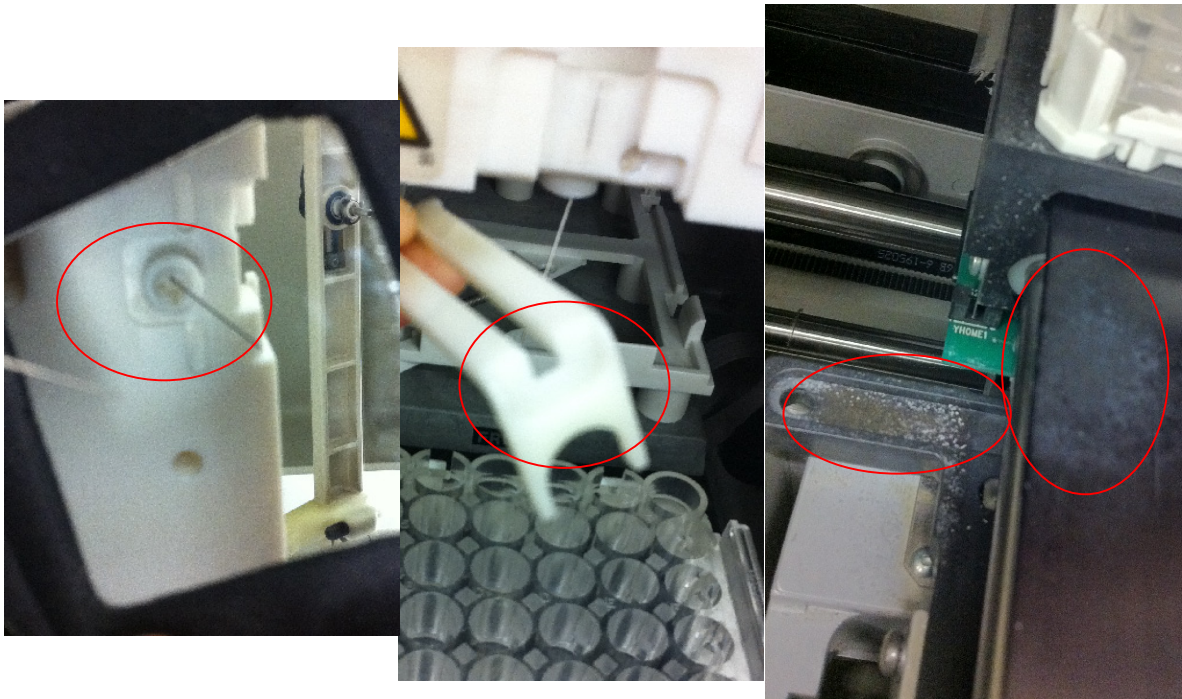
The way to break the capillary:

Pulling while breaking.

## 2. Instrument care

The most important thing for CE is to clean it! Especially for the interface block part, when you work with gel, cleaning is the first step for every day's work. To be CE expert is the second important thing for CE user.

The following 4 parts should be cleaned weekly with water and ethanol: electrodes, holders, area below sample track and sample track.



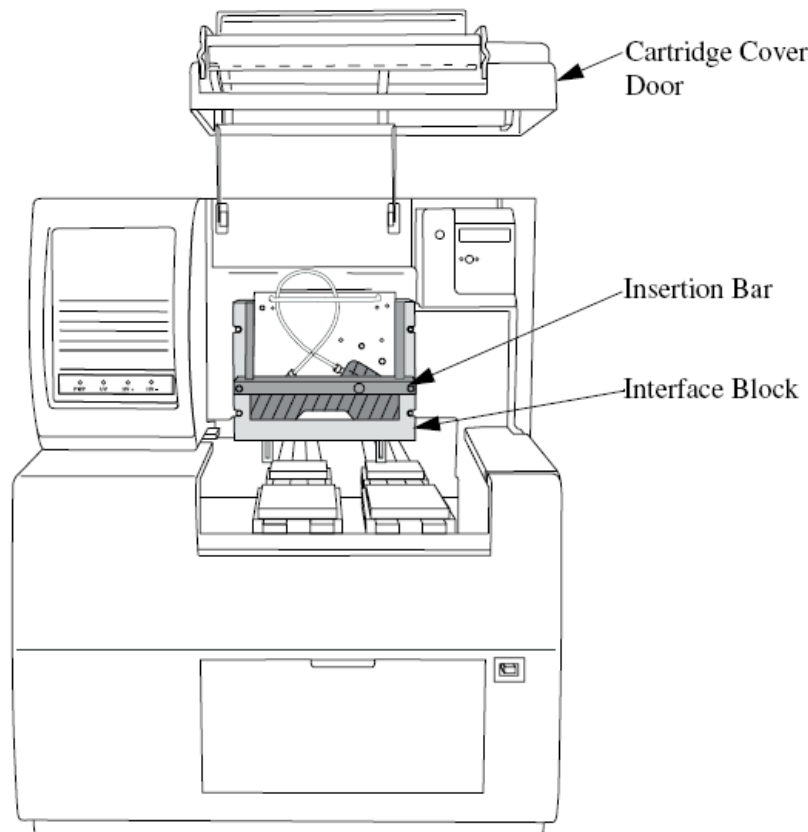
2.1 Before you begin, you will need:

- VE water
- Paper

2.2 All surfaces that come into contact with samples must be treated.

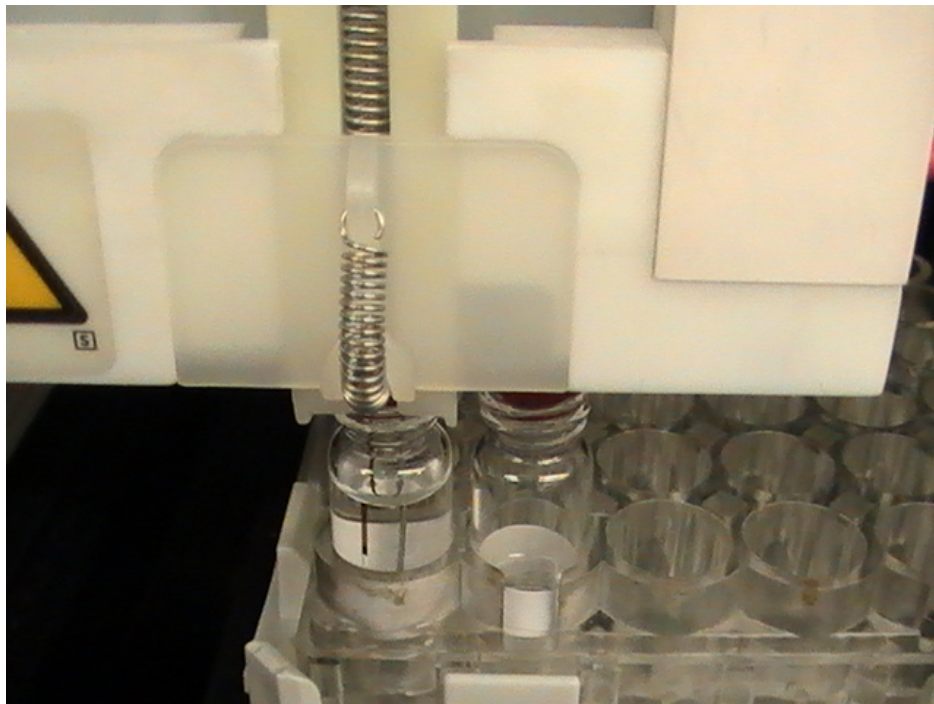
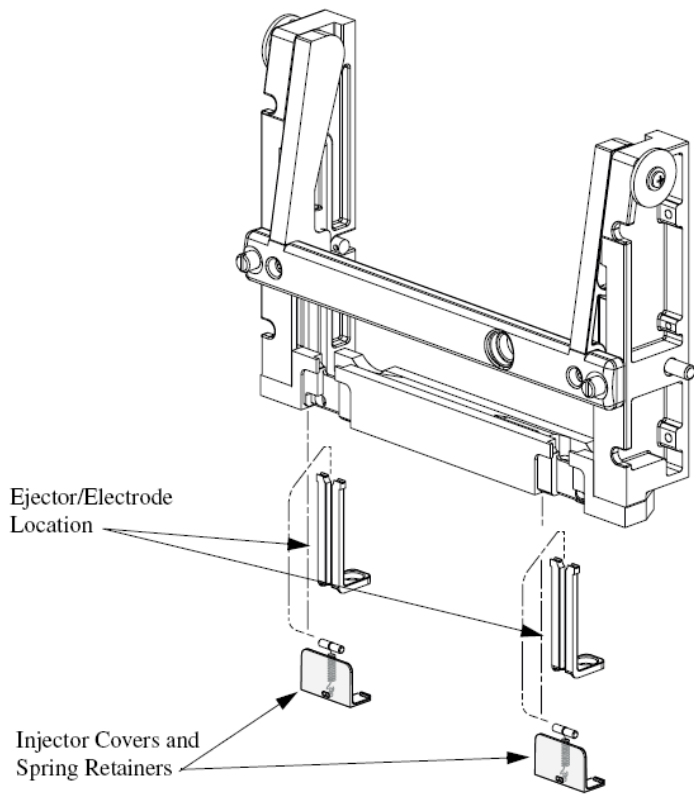
- Lift the cartridge cover door at the front of the P/ACE MDQ.
- Turn the system power off.

- Remove the capillary cartridge and buffer/sample trays as required to clean all internal surface areas. Clean each surface at least two times and allow the instrument to dry completely.
- Clean all external instrument surface areas thoroughly, at least two times and allow the instrument to dry completely.



### 2.3 Cleaning the Interface Block, Ejectors and Electrodes

- Lift the cartridge cover door.
- Loosen the two thumb screws and lift the insertion bar.
- Remove the capillary cartridge from the interface block.
- Remove the ejector covers and ejectors for cleaning
- Using cotton swabs, clean interface block, electrodes and ejector surfaces with VE water followed by methanol, and then let it dry.
- Reinstall the capillary cartridge in the interface block.
- Lower the insertion bar and tighten the two thumb screws.
- Close the cartridge cover door.



### 3. Change modular

#### UV or PDA Detector/Capillary Cartridge Installations:

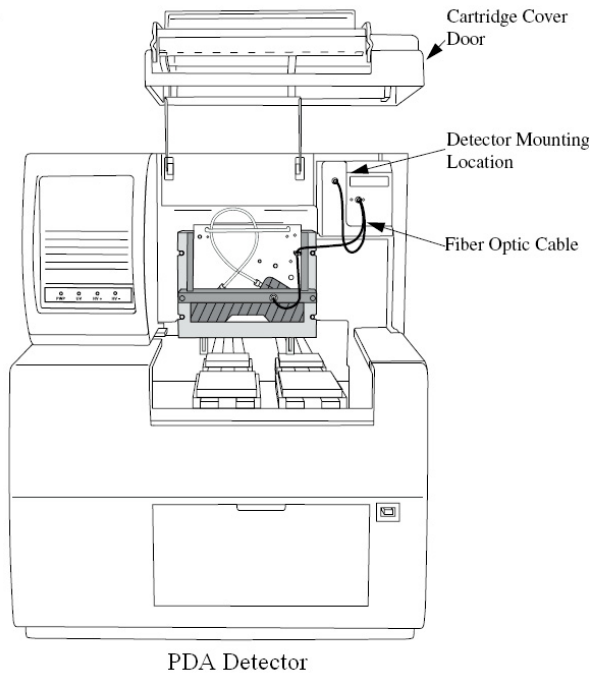
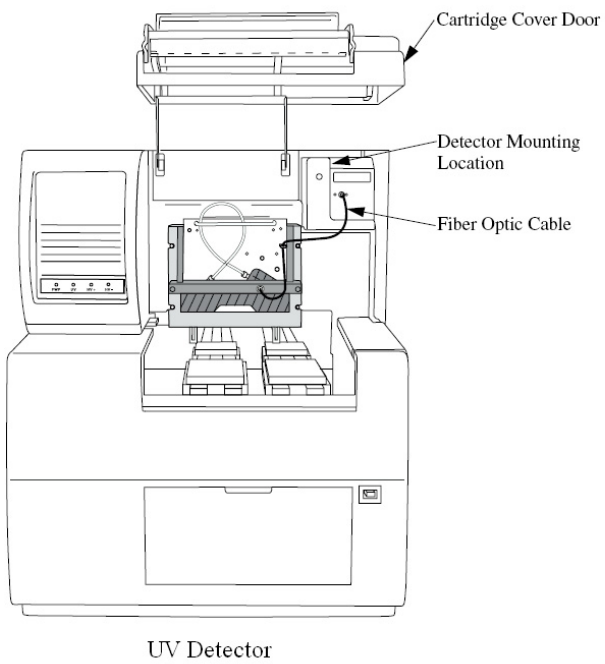
##### 3.1 Before you begin, you will need:

- • UV or PDA Detector
- • Fiber optic cable (UV cable is 2 ended and the PDA cable is 3 ended)

##### 3.2 Proceed as follows:

- Verify that power is off and no capillary cartridge is installed.
- Lift the cartridge cover door and find the detector mounting location as shown below: UV detector is the left one and PDA detector is the right one.
- Position the detector on the mounting location. Carefully slide the detector back to make contact with the back-plane receptacle.
- Tighten the thumb screw until snug.
- Unpack the fiber optic cable and remove the protective covers from each end. Be sure to keep the protective covers for storage when not in use. Connect the cable to the clamp arm first, then to the detector. The remaining end of the fiber optic cable will be connected after completing the capillary cartridge installation.
- Connecting the fiber optic cable in the reverse order may cause damage to the fiber.

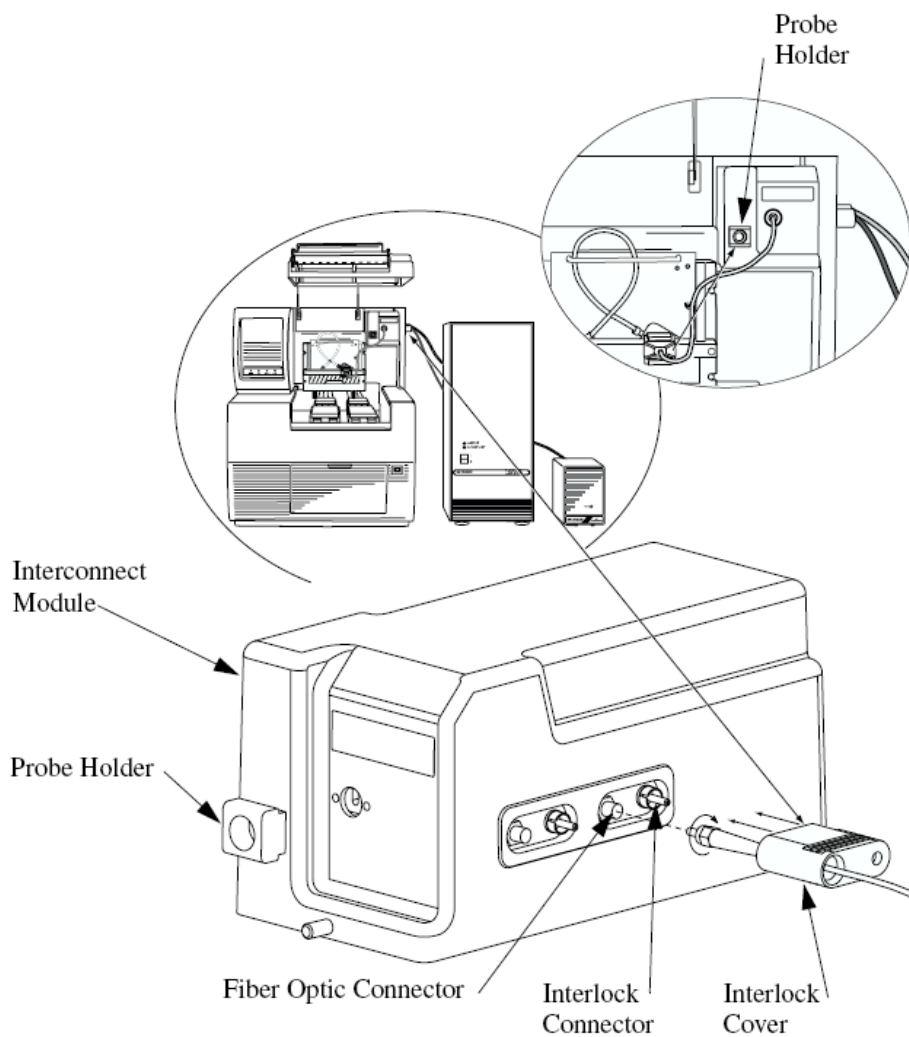
Inside the DAD detector, position 8 is for the PDA detector, which is always empty; while position 1 is for auto zero. When the capillary window is broken, clean this part and fibre head with water and wait until dry.



## LIF Detector Installation:

### 3.3 Pre-installation Requirements and overview

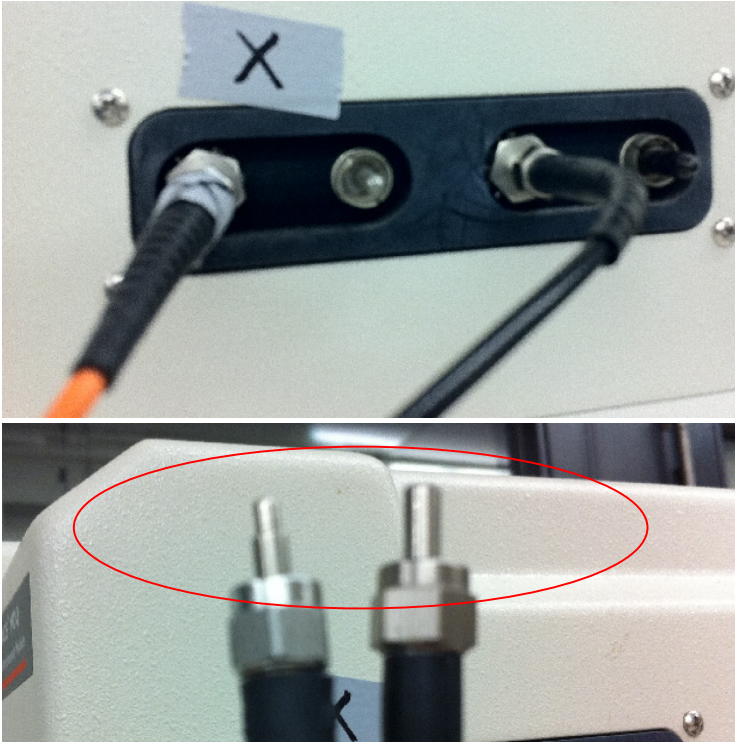
- Initial installation, which will be done by a Beckman Coulter Field Service Engineer, includes setting up the laser, connecting it to the LIF Detector System, and verifying proper system operation (including operation of the laser interlock system, which prevents the user from exposure to laser light). The LIF Detector requires software and instrument firmware version 4.0 or higher for 32 Karat Software.
- If installed, remove the UV or PDA detector from the upper-right corner of the P/ACE MDQ instrument. Install the Interconnect Module in the upper-right corner. Secure the module by finger tightening the locking screw located in the front lower middle area of this module.
- Pull back the interlock cover, hold the cable securely, and screw the fastener into the Interconnect Module. Do not allow either cable to become twisted during installation to avoid damaging the fiber optic line inside the cable. Finally, install the interlock cover.



NOTE: The black cables are optical cables. Therefore, you have to be careful with these cables because they break very easily.

We have two laser generators, lacer A is from Beckmann (left side), which has 488 nm excitation wave length and 520 nm emission wave length. Lacer B is from another company (right side). The connection tip of Beckmann's lacer fibre is smaller than lacer B's (as shown below), while lacer B's connection tip is too big to connect to the laser detector. If we want to use lacer B, the first step is to use a needle to enlarge the lacer module's connection hole.



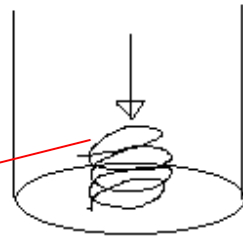
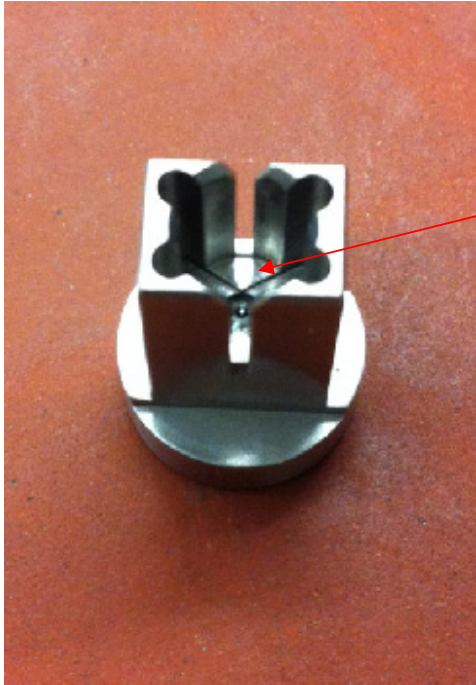


The laser detector in our lab only has channel one, which means we only have one laser channel.





When people install the laser cartridge, they should check the spring. It can be pressed up and down:

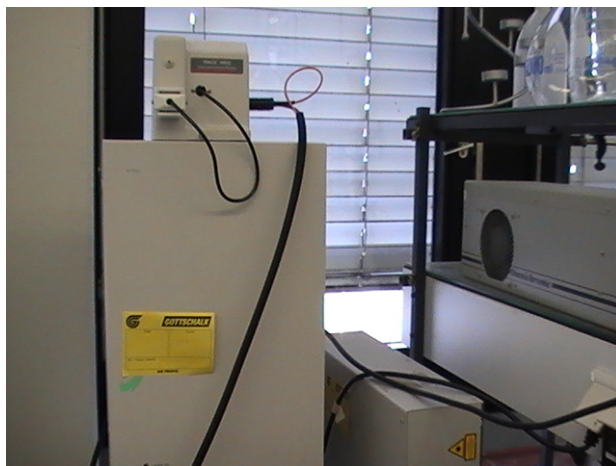


Settings for software:

- Only channel 1, no channel 2
- Normal: 16-25
- Excitation 488 nm
- Emission 520 nm
- 4Hz

Laser 1

Insert the Laser Interconnect Module into CE instrument. The laser is connected to instrument by two cables



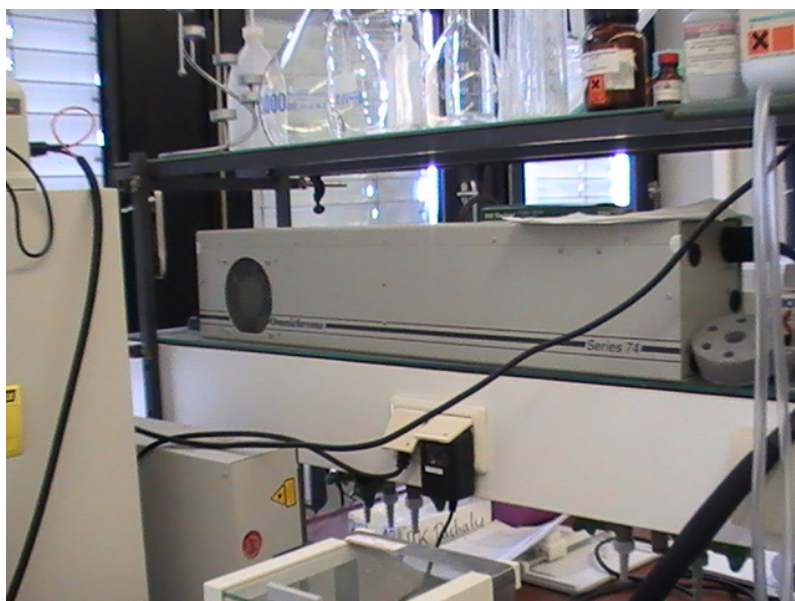
Laser 1



Laser Interconnect Module

## Laser 2

The laser has to be connected via a Remote Box to CE instrument. There have to be one cable between remote box and laser and one between remote box and CE instrument. The laser can not be switched off at the CE instrument, and it has to be done at the laser directly.



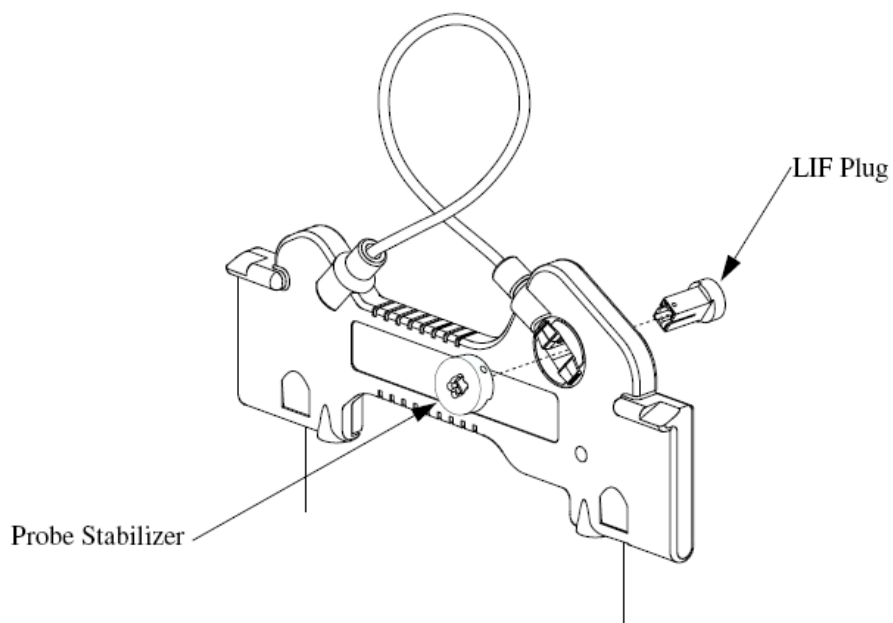
Laser 2



Remote Box

### 3.5 Preparing the Cartridge for LIF Usage

The LIF Detector uses a special plug, which is not interchangeable with those used on the UV/PDA system.



#### 6.2.4 Solutions for some problems

##### 1. Coolant low

Usually there is a leakage somewhere from the cartridge:

- The connections ->reconnect it, or change new connection
- The tube -> when you change a new tube, make sure the O ring is inside and you seal it well
- The cartridge ->change cartridge, but it is expensive

## 2. PDA light low

If the light is OK, then the detection window has problems:

- The window is dirty ->preparing the capillary window carefully without contamination. But if it is dirty already, you have to prepare a new one.
- Forgot calibration ->calibrate it after changing a new capillary
- The aperture is not fit. ->usually the 800 aperture is right size. Otherwise you have to enlarge the window a little bit. The 200 aperture is for UV detector.

## 3. No current

- Current too high -> decrease the voltage or decrease the concentration of separation buffer.
- Bubble inside ->If it comes from the sample, add additional 10psi pressure with the voltage during the separation. Or lower the current, maybe too hot.

## 4. Current leakage

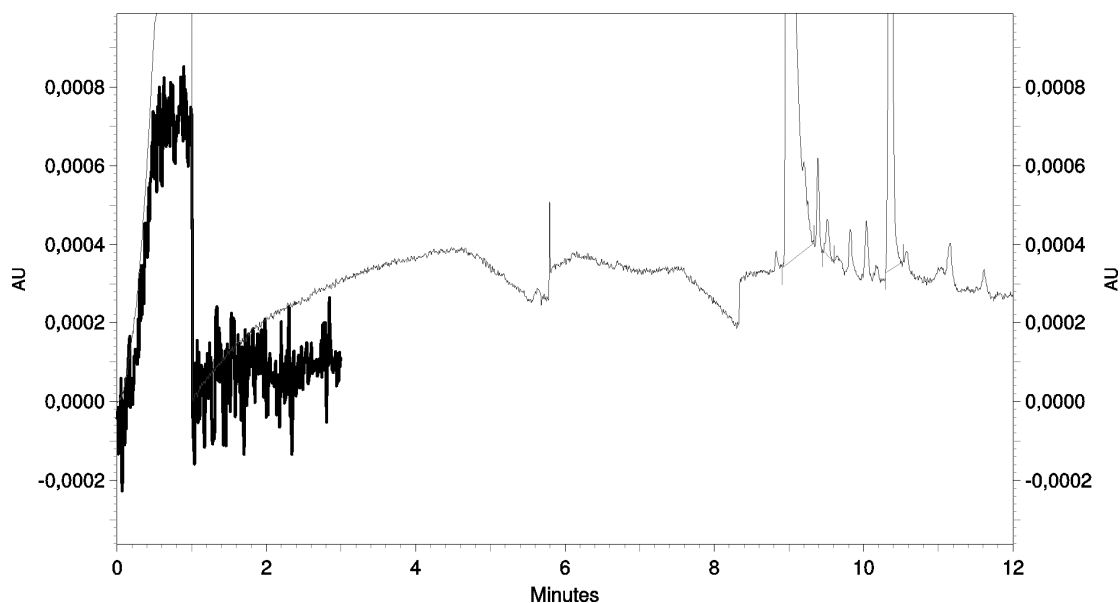
- The capillary is broken, usually the window part -> change new capillary
- The insides of CE are too wet or dirty -> clean the inside of CE and dry it.

## 5. No peak

- Maybe injection failure -> adjust the injection type, magnitude and lasting time
- Maybe the electron nodes are dirty or damaged -> if it is dirty, clean them with ethanol and water; if it is bend, make it straight again carefully
- Maybe the capillary inner wall is damaged -> change a new capillary

## 6. Broken light

When the light is broken, the baseline will be not flat, as shown below:



### 7. Contaminated buffer bottles

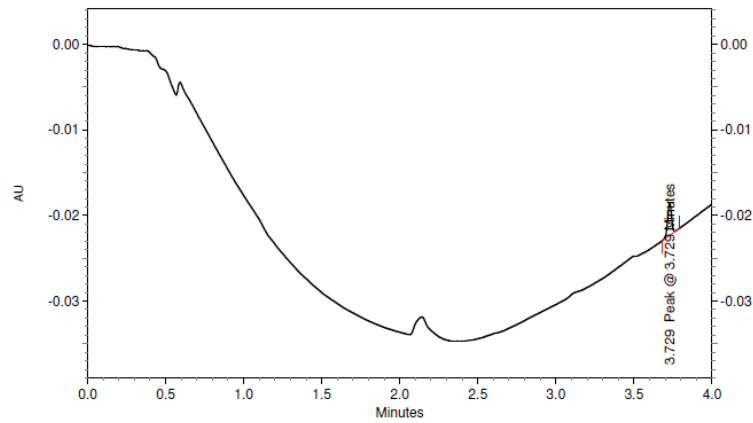
We encountered a migration time delay problem, which caused by dirty running buffer bottles and caps. The contamination was caused by Polybrene, which was used in dynamic coating method. In this case, by using dirty buffer bottles in the normal CZE mode, an extra coating effect was induced. To avoid this trouble occurs in future, we can separate the buffer bottles and caps according to different methods, and we need to use ethanol for additional cleaning step in order to remove polybrene.

The basic but most important aspects of separation buffers of CE are pure reagents and clean Millipore water. Moreover, the separation buffer bottles should be clean and buffer should be degassed before use.

### 8. Broken capillary detection window

In the very beginning the detection window was broken, so the buffer contaminated the inside of CE (including optical fibre, part of the surface of the modular, aperture and O-ring)

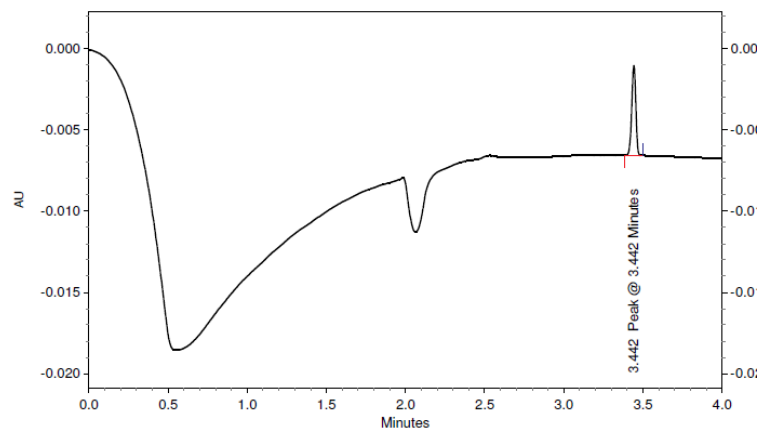
Before cleaning the electropherogram has baseline with curve shape, shown as below (this is sample with 5NT reaction mixture 100  $\mu$ L and Uridine 100  $\mu$ L):



PDA - 260nm  
Results

Nr.	Name	Zeit	Fläche	Fläche %	Korr. Fläche	K
1	Peak @ 3.729	3.729	6502	100.00	1453	

After cleaning the optical fibre (first water, then ethanol), the baseline looked better as below:

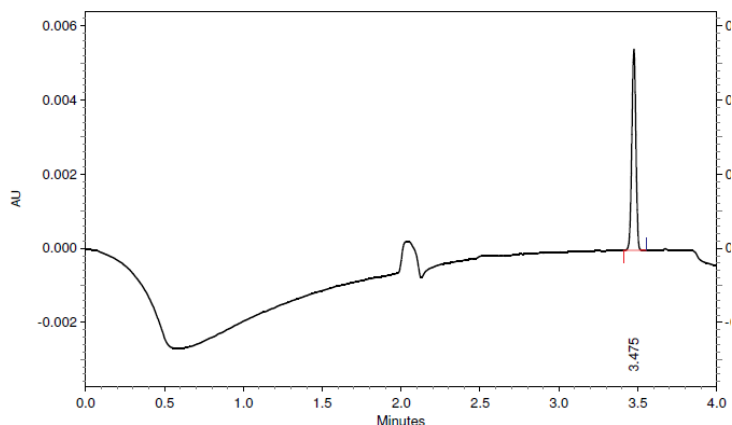


PDA - 260nm  
Results

6.

Nr.	Name	Zeit	Fläche	Fläche %	Korr. Fläche
1	Peak @ 3.442	3.442	9970	100.00	2414

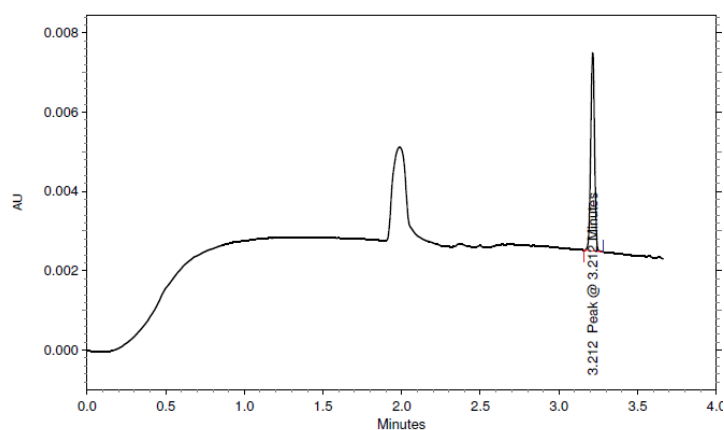
After the second cleaning of the optical fibre (first water, then ethanol) and part of the surface of the modular which attached to the detection window (only water), the detection has been improved as below:



PDA - 260nm  
Results

Nr.	Name	Zeit	Fläche	Fläche %	Korr. Fläche
1		3.475	9769	100.00	2343

After the third cleaning of the optical fibre and change clean aperture and O-ring, the baseline totally recovered:



PDA - 260nm  
Results

Nr.	Name	Zeit	Fläche	Fläche %	Korr. Fläche
1	Peak @	3.212	8438	100.00	2189

## 6.2.5 Important practical aspects

### 1. Capillary

To prepare for the CE, the capillary should be cut to the appropriate length with a ceramic knife, so that the ends of capillary is flat and square. This is especially important for the inlet end of the capillary, because it can influence the sample injection. A window is created closer to the outlet end, which ideally be approximately 0.3 cm in length. The normal FS capillary window can be prepared by burning with a flame and then wiping with an tissue with ethanol. The coated capillary window can be prepared by placing a drop of strong acid on it and then touching the



acid drop with a hot soldering iron. Before placing the capillary into a cartridge, clean it overall with a tissue with ethanol. When using a new capillary or change to a new buffer, the first step is conditioning, which is important for stable migration time, good baseline, and acceptable reproducibility.

## 2. Buffer

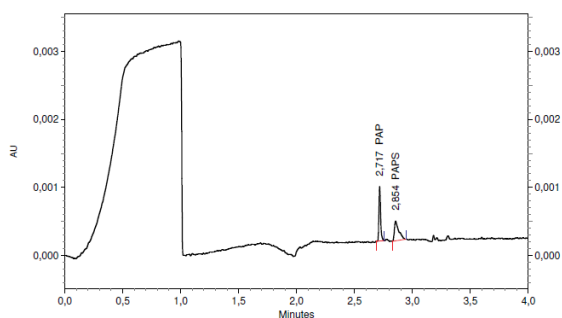
The basic but most important aspects of separation buffers of CE are pure reagents and clean Millipore water. Moreover, the separation buffer bottles should be clean and ice cold buffer should be degassed before use. Borax buffer has two advantages: It forms complex with *cis*-diols, which imparts an additional negative charge to the analyte. It generates less Joule heat than phosphate buffer.

## 3. Joule heat

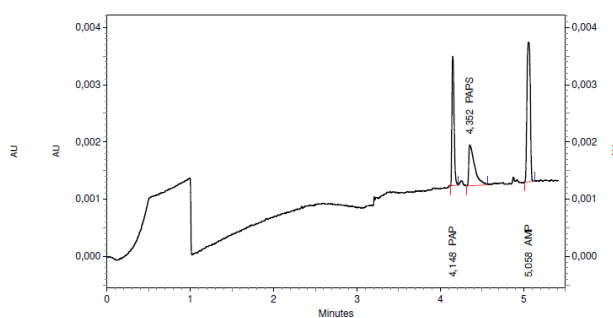
To increase the voltage or buffer concentration may increase the sharpness of the peaks and improve resolution. However, the Joule heat is also be increased, which results in bad resolution and analyte stability or even detection window damage.

## 4. Conditioning

Pre-conditioning of the new capillary is quite important for this method. The graph below shows the baseline differences: A. after 100 minutes pre-conditioning, the baseline is flat; B. after 20 minutes pre-conditioning, the baseline is not so flat.



A: After 100 min pre-conditioning



B: After 20 min pre-conditioning

## 6.3 Investigation of ecto-5'-nucleotidase as anti-cancer drug target

### 6.3.1 Capillary electrophoresis set up

All experiments were carried out by using a P/ACE MDQ capillary electrophoresis system (Beckman Instruments, Fullerton, CA, USA) equipped with a DAD detection system. Data collection and corrected peak area analysis were performed by 32 Karat software obtained from Beckman coulter (Fullerton, CA, USA). The capillary temperature was kept constant at 25°C. The electrophoretic separations were carried out by using uncoated fused-silica capillaries of 40 cm total length (30 cm effective length) × 75.5 μm (id) × 363.7 μm (od) obtained from Polymicro Technologies (Kehl, Germany). The following conditions were applied:  $\lambda_{\max}$  = 260 nm, acquisition rate 4 Hz, separation voltage = 20 kV, running buffer 40 mM borax buffer, pH 9.1, hydrodynamic injection (0.5 psi, 5 sec). The capillary was washed with 0.1 N NaOH aq. for 2 min (20 psi) and with running buffer 2 min (20 psi) before each injection. The test mixture was prepared with 100 μl sample and 100 μl internal standard (I.S.). The internal standard was 12.5 μM uridine dissolved in autoclaved Millipore water. 100 μl test mixture was pipetted to the sample vial and subsequently measured by CE. Further data analysis were carried out by software Graph Pad Prism 4 (Graph Pad Software, Inc. California) and Excel.

Time (min)	Event	Capillary conditioning method				Summary
		Value	Duration	Inlet vial	Outlet vial	
	Rinse – pressure	20 psi	10:00 min	BI:B1	BO:B1	Forward
	Rinse – pressure	20 psi	10:00 min	BI:C1	BO:B1	Forward
0:00	Separate – voltage	15 kV	30:00 min	BI:A1	BO:A1	0.5 min ramp
30:00	End					
Time (min)	Event	Sample analyzing method				Summary
		Value	Duration	Inlet vial	Outlet vial	
	Rinse – pressure	20 psi	2:00 min	BI:B1	BO:B1	Forward
	Rinse – pressure	20 psi	2:00 min	BI:C1	BO:B1	Forward
	Inject – pressure	0.5 psi	5 sec	SI:A1	BO:A1	override, forward

0:00 Separate – voltage 20 kV 5:00 min BI:A1 BO:A1 0.5 min ramp  
 5:00 End

BI: A1 – Separation buffer (Separation); BI: B1 – NaOH (Rinse); BI: C1 – Separation buffer (Rinse); BO: A1 – Separation buffer (Separation); BO: B1 – Waste

### 6.3.2 Assay description

#### 6.3.2.1 Buffer preparation

Running buffer (40 mM borax, pH 9.1) was prepared as below:

Put 3.051g borax ( $\text{Na}_2\text{B}_4\text{O}_7 \cdot 10\text{H}_2\text{O}$ ) and 200 ml Millipore water in 400ml beaker, add 16.7 ml 400 mM boric acid to adjust the pH value from 9.30 to 9.10, then to use ultrasonic bath for 5 min.

The current of CE should be around 150  $\mu\text{A}$  by using this buffer (with separate voltage 20 kV).

The components of enzyme reaction buffer were investigated, in order to figure out in which buffer can enzyme eN display maximum activity ( $V_{\max}$ ) (Table 6.1). The enzyme reaction buffer contained 20 mM HEPES, 140 mM NaCl, 1 mM  $\text{MgCl}_2$ , and 1 mM  $\text{CaCl}_2$  has been chosen. Buffer pH values were pH 7.4, pH 5.6, and pH 4.9, which were adjusted at 37°C with NaOH.

Table 6.1. Comparison of  $V_{\max}$  value of eN in different reaction buffers

	buffer	$K_m$ ( $\mu\text{M}$ )	$V_{\max}$ ( $\mu\text{mol}/\text{min}/\text{mg}$ protein)	date
1	Hepes 20 mM, NaCl 140 mM, $\text{CaCl}_2$ 1 mM, $\text{MgCl}_2$ 1 mM, pH 5.6	$155 \pm 23$	$0.917 \pm 0.116$	March 2010
2	Hepes 20 mM, NaCl 140 mM, $\text{CaCl}_2$ 1 mM, $\text{MgCl}_2$ 1 mM, pH 7.4	$110 \pm 21$	$1.5 \pm 0.3$	March 2010
3	Hepes 20 mM, NaCl 140 mM, KCl 5 mM, $\text{CaCl}_2$ 1 mM, $\text{MgCl}_2$ 1 mM, pH 7.4, with 1% DMSO	$63.6 \pm 3.5$	$0.942 \pm 0.053$	January 2010
4	Hepes 20 mM, NaCl 140 mM, KCl 5 mM, $\text{CaCl}_2$ 1 mM, $\text{MgCl}_2$ 1 mM, pH 7.4	70.38	0.9735	January 2010
5	Hepes 20 mM, $\text{CaCl}_2$ 1 mM, $\text{MgCl}_2$ 1 mM, pH 7.4, with 1%DMSO	$65.6 \pm 17.1$	$0.726 \pm 0.120$	January 2010

### 6.3.2.2 Calibration and validation

The linearity of the quantitative determination and the limits of detection (LOD) and quantification (LOQ) of the enzymatic product adenosine were determined by processing five-point calibration curves (triplicate samples with duplicate measurements) in the presence of 6.25  $\mu\text{M}$  uridine as I.S. The precision and accuracy values were determined at the following concentrations (triplicate samples with duplicate measurements): 5, 10, 20 and 40  $\mu\text{M}$ . Accuracy was determined by calculating the ratios of the predicted concentrations and the spiked values, and relative standard deviations were calculated.

If the adenosine concentration is lower than LOQ, the calculation will be not accurate. For example, if the LDQ for adenosine is 19  $\mu\text{M}$ , so the final concentration of adenosine in the reaction vial should be higher than 19  $\mu\text{M}$ . Especially for the  $K_m$  value detection: if the concentration of substrate AMP is lower than 20  $\mu\text{M}$ , the result will be not trustable, which indicates that the requiremnt of LOQ depends on the testing target: LOQ should be at least 10 folds lower than your target's  $K_m$  value.

The method for calibration is described as below:

Choose 5 or more concentrations of adenosine, and the lowest concentration should be as low as possible. Prepare the right concentrations of adenosine in a 100  $\mu\text{l}$  final volume, than add 100  $\mu\text{l}$  I.S. to it. After measurement, divide the adenosine's corrected area by I.S. corrected area then multiply with 100. Create a scatter plot with relative corrected peak area as y axis and substrate concentration as x axis. Use the linear regression to generate slope,  $y_{x=0}$ , and  $S_{y,x}$ .

Partial validation is necessary when some parameters in the system are changed (e.g. when the batch of capillary is changed). For partial validation of the bioanalytical method, accuracy should be determined using a minimum of five determinations per concentration level. The mean value should be within  $\pm 15\%$  of the theoretical value. At minimum, three concentrations representing the entire range of the standard curve should be studied: one with 3 times of LOQ, one near the centre, and one near the upper boundary of the standard curve.

### 6.3.2.3 Enzyme catalytic reaction

Reactions were initiated by the addition of *eN*.  $3.8 \times 10^{-12}$  mol *eN* per vial was consumed for pH 7.4 reaction buffer assay, and  $14 \times 10^{-12}$  mol *eN* per vial was consumed for pH 5.6 and pH 4.9 reaction buffer assay. The reaction vials were incubated at 37°C for 15 min. All enzymatic reactions were quenched by heating (5 min, 99°C).

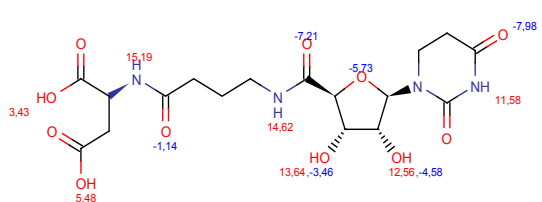
Determination of kinetic parameters for *eN*. To determine the kinetic parameters ( $K_m$  and  $V_{max}$ ), 8 different substrate concentrations were chosen. Each analysis was repeated three times in independent experiments.

Investigation of *eN* inhibitors. A group of selected compounds were initially screened at high concentrations of 100  $\mu\text{M}$ . Subsequently, full concentration-inhibition curves were determined for the most potent inhibitors, and  $\text{IC}_{50}$  values were calculated. The substrate (AMP) concentration for *eN* inhibition testing was 500  $\mu\text{M}$ , and substrate conversion was strictly controlled to be below 10%. The  $\text{IC}_{50}$  values of inhibitors were obtained by testing a suitable range of inhibitor concentrations (8 data points). The incubation time was 15 min. Negative controls were performed in the presence of heat-inactivated enzyme (5 min, 99°C). Each analysis was repeated three times in independent experiments. For the determination of the inhibition mechanism, 8 different substrate concentrations and 3 different inhibitor concentrations were used, and each analysis was carried out with duplicate measurements.

### 6.3.3 Compound preparation and selection

Table 6.2. The predicted  $\text{p}K_a$  values of pH-dependent inhibitors by the software MarvinSketch.

No.	code	Microspecies distribution % (ion charge) pH5.6	Microspecies distribution % (ion charge) pH7.4
1	AMB 193	56,56(-2) 43,15(-1)	98,80(-2)

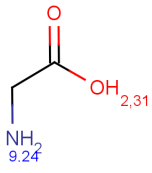
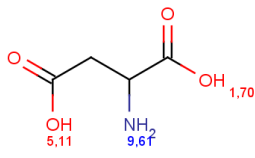
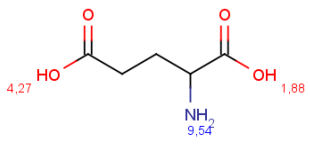


2	AMB 547		99,99(0)	99,50(0)
3	AMB 547H		98,77(-1)	99,48(-1)
4	AMB 548		99,99(0)	99,50(0)
5	AMB 548H		99,12(-1)	99,49(-1)
6	AMB 563.1		99,99(0)	99,50(0)

7	AMB 563.1H		78,53(-2) 21,40(-1)	99,08(-2)
8	AMB 565.1		78,53(-2) 21,40(-1)	99,56(-2)
9	AMB 564		99,99(0)	99,50(0)
10	AMB 564.1H		56,56(-2) 43,15(-1)	98,32(-2)
11	AMB 566.1		56,56(-2) 43,15(-1)	98,80(-2)

12	AMB 553.1		99,99(0)	99,37(0)
13	AMB 560.1 final		99,50(-1)	99,27(-1)
14	AMB 552.3a		99,87(-2)	2,30(-3) 97,69(-2)
15	ATP		73.38(-3) 24.25(-2)	66.53(-4) 33.30(-3)
16	AOPCP		73.91(-2) 25.55(-1)	15.30(-3) 84.24(-2) 0.46(-1)
17	AMP		25,73(-2) 57,52(-1) 16,73(0)	96,56(-2) 3,42 (-1) 0,02 (0)



18	Gly		99,93 (0)	98,57 (0)
19	Asp		24,59 (0) 75,38(-1)	0,51 (0) 98,88(-1)
20	Glu		95,51(-1)	99,20(-1)

Firstly I prepared 10 mM stock solution in pure DMSO for every AMB compound. Afterwards in order to achieve a higher concentration in my assay, I prepared 10 mM stock solution in water for AMB563H, AMB565, AMB566, and AMB193. Actually, it is better to prepare all compounds in water when possible. By adding a few drops of NaOH can improve the AMB compound's solubility.

Table 6.3. POMs

Compound code	Molecular formula	Molecular weight [g/mol]	Inhibitor screening* inhi% at 100 $\mu$ M
NaPW <sub>12</sub>	Na <sub>3</sub> [PW <sub>12</sub> O <sub>40</sub> ] x 7 H <sub>2</sub> O	3074	-1.86%
NaP <sub>5</sub> W <sub>30</sub>	Na <sub>15</sub> [P <sub>5</sub> W <sub>30</sub> O <sub>110</sub> ] x 30 H <sub>2</sub> O	8320	11.1%
NaP <sub>6</sub> W <sub>18</sub>	Na <sub>20</sub> [P <sub>6</sub> W <sub>18</sub> O <sub>79</sub> ] x 37 H <sub>2</sub> O	5888	-17.5%
NaP <sub>8</sub> W <sub>48</sub>	Na <sub>33</sub> H <sub>7</sub> [P <sub>8</sub> W <sub>48</sub> O <sub>184</sub> ] x 92 H <sub>2</sub> O	14446	47.6%
NaOP <sub>8</sub> W <sub>12</sub>	Na <sub>16</sub> [(O <sub>3</sub> POPO <sub>3</sub> ) <sub>4</sub> W <sub>12</sub> O <sub>36</sub> ] x 38 H <sub>2</sub> O	4532	-23.1%
NaCP <sub>8</sub> W <sub>12</sub>	Na <sub>16</sub> [(O <sub>3</sub> PCH <sub>2</sub> PO <sub>3</sub> ) <sub>4</sub> W <sub>12</sub> O <sub>36</sub> ] x 16 H <sub>2</sub> O	4128	-59.4%
KB 1	K <sub>4</sub> [(Re <sub>6</sub> S <sub>8</sub> )(OH) <sub>6</sub> ]	1632	74.5%
KB 2	K <sub>4</sub> [(Re <sub>6</sub> Se <sub>8</sub> )(OH) <sub>6</sub> ]	2007	67.8%
KB 3	K <sub>4</sub> [Re <sub>6</sub> S <sub>8</sub> (CH <sub>3</sub> COO) <sub>6</sub> ]	1938	19.7%
KB 4	K <sub>4</sub> [(Re <sub>6</sub> S <sub>8</sub> )(HCOO) <sub>6</sub> ]	1854	89.2%

\*concentration of substrate AMP: 500  $\mu$ M,  $K_m$ : 45  $\mu$ M

## 6.4 Investigation of cerebroside sulfotransferase as therapy target for metachromatic leukodystrophy

### 6.4.1 Capillary electrophoresis set up

All experiments were carried out by using a P/ACE MDQ capillary electrophoresis system (Beckman Instruments, Fullerton, CA, USA) equipped with a DAD detection system. The capillary temperature was kept constant at 15 °C. The electrophoretic separations were carried out by using fused-silica capillary of 60 cm total length (50 cm effective length)  $\times$  75.5  $\mu$ m (id)  $\times$  363.7  $\mu$ m (od) obtained from Optronis GmbH. The following conditions were applied:  $\lambda_{max}$  =

260 nm, voltage = -15 kV, running buffer 75 mM phosphate buffer, 0.002% polybrene, pH 5.6 (adjusted by phosphoric acid), electrokinetic injection (-10 kV, 30 sec). The capillary was washed with 0.2 M NaOH for 2 min, and running buffer for 2 min before each injection. Data collection and corrected peak area analysis were performed by 32 Karat software obtained from Beckman coulter (Fullerton, CA, USA). Further data analysis were carried out by software Graph Pad Prism 4 (Graph Pad Software, Inc. California) and Excel.

Capillary conditioning method						
Time (min)	Event	Value	Duration	Inlet vial	Outlet vial	Summary
	Rinse – pressure	20 psi	15:00 min	BI:B1	BO:B1	Forward
	Rinse – pressure	20 psi	15:00 min	BI:C1	BO:B1	Forward
0:00	Separate – voltage	15 kV	60:00 min	BI:A1	BO:A1	0.5 min ramp Reverse polarity
60:00	End					
Sample analyzing method						
Time (min)	Event	Value	Duration	Inlet vial	Outlet vial	Summary
	Rinse – pressure	20 psi	2:00 min	BI:B1	BO:B1	Forward
	Rinse – pressure	20 psi	2:00 min	BI:C1	BO:B1	Forward
	Inject – voltage	10 kV	30 sec	SI:A1	BO:A1	override, Reverse polarity
0:00	Separate – voltage	15 kV	12:00 min	BI:A1	BO:A1	0.5 min ramp Reverse polarity
1:00	Auto zero					
12:00	End					

BI: A1 – Separation buffer (Separation); BI: B1 – NaOH (Rinse); BI: C1 – Separation buffer (Rinse); BO: A1 – Separation buffer (Separation); BO: B1 – Waste

## 6.4.2 Assay description

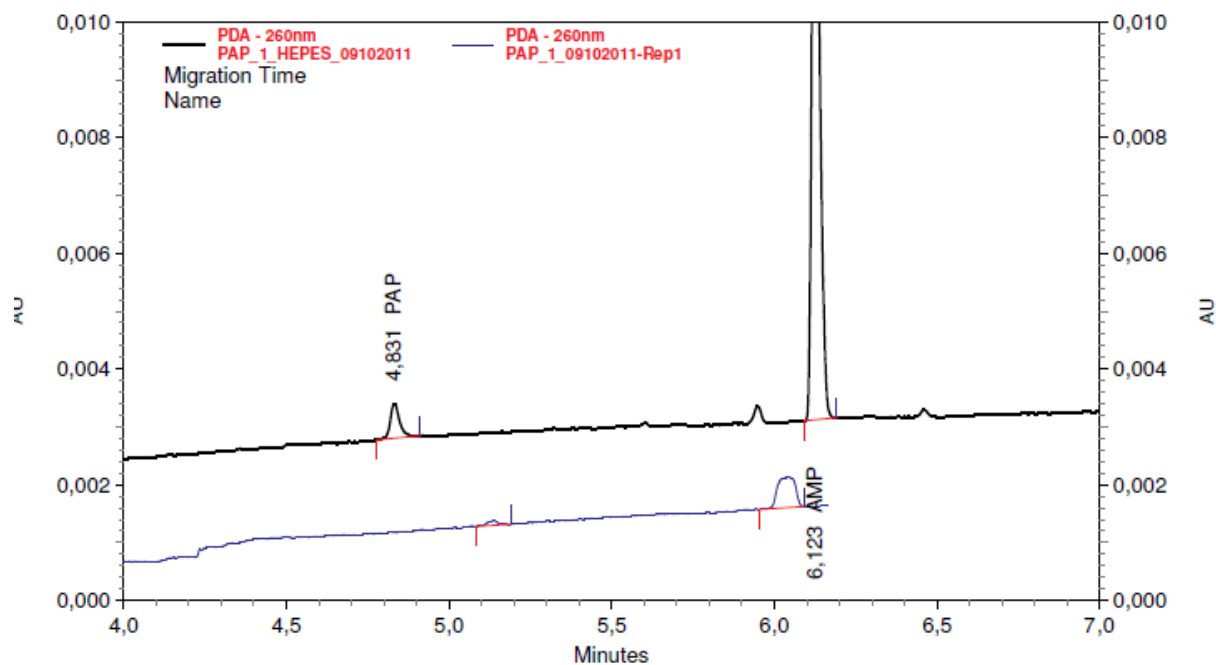
### 6.4.2.1 Buffer preparation

Running buffer (75 mM phosphate buffer, 0.002% polybrene, pH 5.6) was prepared as below:

3.34 g  $\text{Na}_2\text{HPO}_4 \cdot 2\text{H}_2\text{O}$  (177.99 g/mol) and 500  $\mu\text{l}$  1% polybrene (30 mg polybrene + 3 ml water) were added to 250 ml water, pH value was adjusted by phosphoric acid from pH 9.2 to pH 5.6, then to use ultrasonic bath for 5 min. The CE current should be around  $-80 \mu\text{A}$  by using this buffer (with separate voltage  $-15\text{kV}$ ).

BGE buffer is 5 mM phosphate buffer, 0.0001% polybrene, pH 7.4. 3.34 g  $\text{Na}_2\text{HPO}_4 \cdot 2\text{H}_2\text{O}$  (177.99 g/mol) and 500  $\mu\text{l}$  1% polybrene (30 mg polybrene + 3 ml water) were added to 250 ml water, pH value was adjusted by phosphoric acid from pH 9.2 to pH 7.4, then further 1 to 15 dilute with water.

The enzyme reaction buffer contained 10 mM HEPES, 16 mM  $\text{MgCl}_2$ . Buffer pH values was pH 7.1, which was adjusted at  $37^\circ\text{C}$  with NaOH. We found out that the detection is much better when we used HEPES buffer instead of Tris buffer. The detection difference is shown below (The analytes are: PAP 1  $\mu\text{M}$ , AMP 5  $\mu\text{M}$ ):



### 6.4.2.2 Pipetting scheme

Inhibitor screening	Substrate screening	Kinetic testing	Inhibition testing
10 µl Triton X-100 1%	10 µl Triton X-100 1%	10 µl Triton X-100 1%	10 µl Triton X-100 1%
10 µl substrate 500 µM	10 µl substrate 500 µM	10 µl substrate (different concentrations)	10 µl substrate 500 µM
10 µl inhibitor 500 µM (lipid)			Required amount of inhibitor (lipid)
Evaporate methanol/chloroform from above mixture	Evaporate methanol/chloroform from above mixture	Evaporate methanol/chloroform from above mixture	Evaporate methanol/chloroform from above mixture
25 µl PAPS (60 µM)	25 µl PAPS (60 µM)	25 µl PAPS	25 µl PAPS (60 µM)
5 µl water or inhibitor (non-lipid)	5 µl water	5 µl water	5 µl water or inhibitor (non-lipid)
20 µl CST in buffer (25 mM HEPES, 40 mM MgCl <sub>2</sub> ) 37°C, 30 min 60°C, 10 min	20 µl CST in buffer (25 mM HEPES, 40 mM MgCl <sub>2</sub> ) 37°C, 30 min 60°C, 10 min	20 µl CST in buffer (25 mM HEPES, 40 mM MgCl <sub>2</sub> ) 37°C, 30 min 60°C, 10 min	20 µl CST in buffer (25 mM HEPES, 40 mM MgCl <sub>2</sub> ) 37°C, 30 min 60°C, 10 min

#### Dilution scheme for substrate and PAPS

substrate curve (f.c. µM)	con.* volume	solvent = 1:1 methanol/chloroform	
400	2000 µM * 10 µl		
300	1500 µM * 10 µl	1500 µM =	30 µl 2000 µM + solvent 10 µl
200	1000 µM * 10 µl	1000 µM =	20 µl 1500 µM + solvent 10 µl
100	500 µM * 10 µl	500 µM =	15 µl 1000 µM + solvent 15 µl
50	250 µM * 10 µl	250 µM =	15 µl 500 µM + solvent 15 µl
25	125 µM * 10 µl	125 µM =	15 µl 250 µM + solvent 15 µl
12.5	62.5 µM * 10 µl	62.5 µM =	15 µl 125 µM + solvent 15 µl
6.25	36.25 µM * 10 µl	36.25 µM =	15 µl 62.5 µM + solvent 15 µl
PAPS in substrate curve for (f.c. µM)	need con (µM)		
400	800	800 µM =	80 µl 850 µM + water 5 µl
300	600	600 µM =	60 µl 800 µM + water 20 µl
200	400	400 µM =	40 µl 600 µM + water 20 µl
100	200	200 µM =	30 µl 400 µM + water 30 µl
50	100	100 µM =	30 µl 200 µM + water 30 µl
25	50	50 µM =	30 µl 100 µM + water 30 µl
12.5	25	25 µM =	30 µl 50 µM + water 30 µl
6.25	12.5	12.5 µM =	30 µl 25 µM + water 30 µl

inhibition curve (f.c. $\mu\text{M}$ )	con.* volume	solvent = 1:1 methanol/chloroform
2000	2 mM * 50 $\mu\text{l}$	
1000	2 mM * 25 $\mu\text{l}$	
500	2 mM * 12.5 $\mu\text{l}$	
250	1250 $\mu\text{M}$ * 10 $\mu\text{l}$	1250 $\mu\text{M}$ = 25 $\mu\text{l}$ 2 mM + solvent 15 $\mu\text{l}$
100	500 $\mu\text{M}$ * 10 $\mu\text{l}$	500 $\mu\text{M}$ = 10 $\mu\text{l}$ 1250 $\mu\text{M}$ + solvent 15 $\mu\text{l}$
30	150 $\mu\text{M}$ * 10 $\mu\text{l}$	150 $\mu\text{M}$ = 10 $\mu\text{l}$ 500 $\mu\text{M}$ + solvent 23 $\mu\text{l}$
10	50 $\mu\text{M}$ * 10 $\mu\text{l}$	50 $\mu\text{M}$ = 10 $\mu\text{l}$ 150 $\mu\text{M}$ + solvent 20 $\mu\text{l}$

#### 6.4.2.3 Calibration and validation

The test mixture was prepared with 50  $\mu\text{l}$  CST reaction sample and 50  $\mu\text{l}$  internal standard (I.S.) GDP 20  $\mu\text{M}$ . This mixture was further 1:4 diluted in buffer 5 mM phosphate with 0.0001% polybrene at pH 7.4. Then 90  $\mu\text{l}$  diluted mixture was pipetted to the CE sample vial and subsequently measured by CE. The linearity of the quantitative determination, the limits of detection (LOD) and the limits of quantification (LOQ) of the enzymatic product adenosine-3',5'-diphosphate (PAP) were determined by processing five-point calibration curves (triplicate samples with duplicate measurements) in the presence of 2.5  $\mu\text{M}$  GDP as I.S. The precision and accuracy values were determined at the following concentrations (triplicate samples with duplicate measurements): 1.25, 0.625, 0.25, 0.125 and 0.0625  $\mu\text{M}$ , in the presence of 2.5  $\mu\text{M}$  GDP as I.S. Accuracy was determined by calculating the ratios of the predicted concentrations and the spiked values, and relative standard deviations were calculated.

#### 6.4.2.4 Enzyme catalytic reaction

We carried out the CST catalytic reaction in a total volume of 50  $\mu\text{l}$ , containing 3'-phosphoadenosine-5'-phosphosulfate and cerebroside (concentrations of 3'-phosphoadenosine-5'-phosphosulfate and cerebroside varied according to assay type) in 10 mM HEPES, 16 mM  $\text{MgCl}_2$ , 0.2% (v/v) Triton X-100, pH 7.1 reaction buffer. All Lipids and Triton X-100 were prepared in chloroform/methanol (1:1), we pipetted lipids and Triton X-100 to reaction vials, and let chloroform/methanol dry before adding reaction buffer. Reactions were initiated by the addition of 938 ng human cerebroside sulfotransferase (CST), and then incubated at 37  $^\circ\text{C}$  for 30 min. All enzymatic reactions were stopped by heating (10 min, 60  $^\circ\text{C}$ ).

Reactions were initiated by the addition of CST. The reaction vials were incubated at 37°C for 30 min. All enzymatic reactions were quenched by heating (10 min, 60°C).

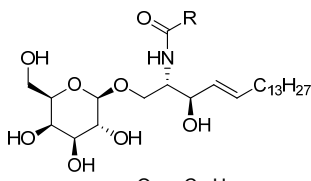
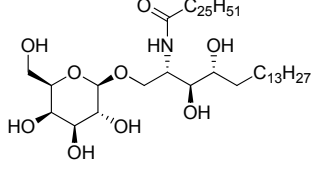
Determination of kinetic parameters for CST. For the determination of the kinetic parameters ( $K_m$  and  $V_{max}$ ), 8 different substrate concentrations were chosen. Negative controls were performed in the presence of heat-inactivated enzyme (10 min, 60 °C). Each analysis was repeated three times in independent experiments.

Investigation of CST inhibitors. For CST inhibitor characterization, full concentration-inhibition curves were determined by testing a suitable range of inhibitor concentrations, and then  $IC_{50}$  value was calculated. The substrate (cerebrosides) concentration was 100  $\mu$ M, and substrate conversion was strictly controlled to be below 15%. Negative controls were performed in the presence of heat-inactivated enzyme (10 min, 60 °C). Each analysis was repeated three times in independent experiments. For the determination of inhibition mechanism, 8 different substrate concentrations and 3 different inhibitor concentrations were used, and each analysis was carried out with duplicate measurements.

### 6.4.3 Compound preparation and selection

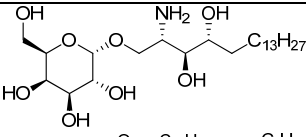
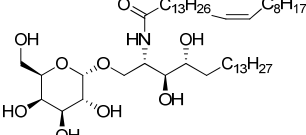
A group of analogs of cerebrosides were selected for substrate and inhibitor screening.

Table 6.4. Screening test with cerebroside analogs

Name	Structure $\beta$ lipids $\alpha$ lipids	Stock conc. (mM)	Substrate screening (activity% at 100 $\mu$ M)	Inhibitor screening on cerebrosides * (inhi% at 100 $\mu$ M)	Inhibitor screening on KRN7000 (inhi% at 100 $\mu$ M)
1 $\beta$ lipids glucocere brosides		2	19%	<b>9%</b>	-5%
2 $\beta$ - KRN7000  $\alpha$ lipids		0.25	<b>42%</b>	<b>38%</b>	-42%

3	JG185 (C2)		10	<b>40%</b>	-12%	-1%
4	JG186 (C5)		10	<b>30%</b>	-18%	-4%
5	PBS25 (C8)		2	<b>22%</b>	-	-
6	JG189 (C11)		8	<b>32%</b>	-43%	1%
7	JG195 (C14)		1	21%	-38%	-24%
8	C16		2	9%	<b>12%</b>	<b>14%</b>
9	JG187 (C19)		1	<b>25%</b>	-50%	4%
10	JG190 (C26)		1	<b>51%</b>	3%	-
11	JG188		8	<b>32%</b>	-26%	5%
12	NP230		1	15%	4%	1%



13	JG198		6	16%	4%	-30%
14	JG201		1	19%	-7%	1%

\*Cerebroside was obtained from Matreya LLC (Pleasant Gap, PA, USA); according to the supplier it consists of a mixture of saturated or unsaturated alkyls (C16:0, C18:0, C20:0, C22:0, C23:0, C24:0-C27, C24:1-C27:1) or hydroxyalkyls (C18:0(2-OH), C20:0(2-OH), C22:0(2-OH), C23:0(2-OH), C24:0(2-OH), C24:1(2-OH), C25:1(2-OH)).

## 6.5 Analysis of the *staphylococcus aureus* capsule biosynthesis pathway

### 6.5.1 Capillary electrophoresis set up

All experiments were carried out by using a P/ACE MDQ capillary electrophoresis system (Beckman Instruments, Fullerton, CA, USA) equipped with a DAD detection system. Data collection and corrected peak area analysis were performed by 32 Karat software obtained from Beckman coulter (Fullerton, CA, USA). The capillary temperature was kept constant at 15°C. The electrophoretic separations were carried out by using fused-silica capillary of 60 cm total length (50 cm effective length) × 75.5 μm (id) × 363.7 μm (od) obtained from Polymicro Technologies (Kehl, Germany) obtained from Optronis GmbH]. The following conditions were applied:  $\lambda_{\max}$  = 260 nm, separation voltage = -15 kV, running buffer 68 mM CAPS buffer containing polybrene 0.002%, pH 12.4 (adjusted by NaOH), electrokinetic injection (-1 kV, 20sec). The capillary was washed with 0.2 N NaOH aq. for 2 min (20 psi) and with running buffer 3 min (20 psi) before each injection. The test mixture was prepared with 50 μl sample dilution and 50 μl internal standard (I.S.). Sample dilution was 1:40 diluted enzyme reaction mixture in autoclaved Millipore water. The internal standard was 6.25 μM PAP dissolved in autoclaved Millipore water. 90 μl test mixture was pipetted to the sample vial and subsequently measured by CE. Further data analysis were carried out by software Graph Pad Prism 4 (Graph Pad Software, Inc. California) and Excel.

Time (min)	Event	Capillary conditioning method				Summary
		Value	Duration	Inlet vial	Outlet vial	
	Rinse – pressure	20 psi	10:00 min	BI:B1	BO:B1	Forward
	Rinse – pressure	20 psi	10:00 min	BI:C1	BO:B1	Forward
0:00	Separate – voltage	5 kV	60:00 min	BI:A1	BO:A1	0.5 min ramp Reverse polarity
60:00	End					
Time (min)	Event	Sample analyzing method				Summary
		Value	Duration	Inlet vial	Outlet vial	
	Rinse – pressure	20 psi	2:00 min	BI:B1	BO:B1	Forward
	Rinse – pressure	20 psi	3:00 min	BI:C1	BO:B1	Forward
	Inject – voltage	1 kV	20 sec	SI:A1	BO:A1	override, Reverse polarity
0:00	Separate – voltage	15 kV	10:00 min	BI:A1	BO:A1	0.5 min ramp Reverse polarity
1:00	Auto zero					
10:00	End					

BI: A1 – Separation buffer (Separation); BI: B1 – NaOH (Rinse); BI: C1 – Separation buffer (Rinse); BO: A1 – Separation buffer (Separation); BO: B1 – Waste

## 6.5.2 Assay description

### 6.5.2.1 Buffer preparation

Running buffer (68 mM CAPS buffer, 0.002% polybrene, pH 12.4) was prepared as below:

3.32g CAPS and 440  $\mu$ L polybrene 1% were added to 200 ml Millipore water, pH value was adjusted by NaOH (20 ml NaOH 1 M) from pH 6.14 to pH 12.4, then to use ultrasonic bath for 5 min.. The CE current should be around -85  $\mu$ A by using this buffer (with separate voltage -15kV).

The enzyme reaction buffer contained 10 mM KPi, 10 mM MgCl<sub>2</sub>, pH 7.5. Assays for the synthesis of UDP-2-acetamido-2,6-dideoxy- $\alpha$ -D-xylo-hex-4-ulose, additionally included 0.8% (v/v) Triton x-100. For CapD assays, cofactors NADP was added in a concentration of 3 mM for kinetic testing and 600  $\mu$ M for inhibition testing.

#### 6.5.2.2 Pipetting scheme

The pipetting works were carried out by Hannah Ulm and Marvin Rausch.

CapD kinetic	CapE kinetic
15 $\mu$ l UDP-GlcNAc (different concentrations)/H <sub>2</sub> O (control)	15 $\mu$ l UPD-GlcNAc (different concentrations)/H <sub>2</sub> O (control)
10 $\mu$ l CapD preparation	5 $\mu$ l CapE preparation
10 $\mu$ l TritonX-100 (4% (w/v))	0.5 $\mu$ l MgCl <sub>2</sub> (1 M)
10 $\mu$ l NADP (10 mM)	
5 $\mu$ l KPi (100 mM)	4.5 $\mu$ l KPi (100 mM)
ad 50 $\mu$ l H <sub>2</sub> O	ad 50 $\mu$ l H <sub>2</sub> O
CapD inhibition	CapE inhibition
5 $\mu$ l UDP-GlcNAc (10 mM)	5 $\mu$ l UDP-GlcNAc (10 mM)
5 $\mu$ l CapD preparation	5 $\mu$ l CapE preparation
10 $\mu$ l TritonX-100 (4% (w/v))	0,5 $\mu$ l MgCl <sub>2</sub> (1M)
3 $\mu$ l NADP (10 mM)	
5 $\mu$ l KPi (100 mM)	5 $\mu$ l KPi (100 mM)
+ 5 $\mu$ l inhibitor (different concentrations/DMSO (10% (w/v)))	+ 5 $\mu$ l inhibitor (different concentrations/DMSO (10% (w/v)))
ad 50 $\mu$ l H <sub>2</sub> O	ad 50 $\mu$ l H <sub>2</sub> O
CapD + CapA/B	CapE + CapA/B

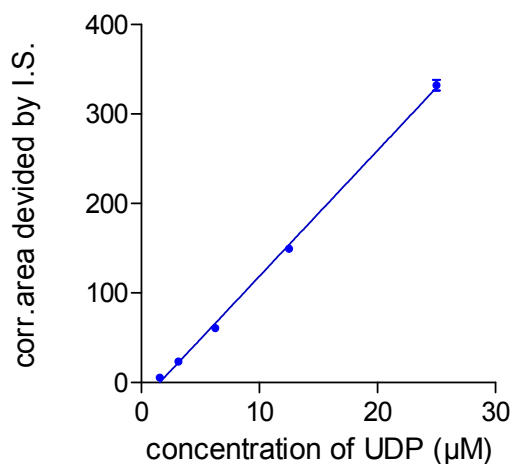
30 $\mu$ l UPD-GlcNAc (10 mM)	30 $\mu$ l UPD-GlcNAc (10 mM)
10 $\mu$ l CapD preparation	1 $\mu$ l MgCl <sub>2</sub> (1 M)
1 $\mu$ l MgCl <sub>2</sub> (1 M)	5 $\mu$ l CapE preparation
2 $\mu$ l DTT (500 mM)	2 $\mu$ l DTT (50 mM)
1 $\mu$ l ATP (100 mM)	1 $\mu$ l ATP (100 mM)
8.8 $\mu$ l KPi buffer (100 mM)	8.8 $\mu$ l KPi buffer (100 mM)
20 $\mu$ l NADP (10 mM)	
4 $\mu$ l TritonX100 (20 %)	
6 $\mu$ l CapA + 6.5 $\mu$ l CapB	6 $\mu$ l CapA + 6.5 $\mu$ l CapB
ad 100 $\mu$ l H <sub>2</sub> O	ad 100 $\mu$ l H <sub>2</sub> O

---

### 6.5.2.3 Calibration and validation

The CapD and CapE reaction products are UDP-2-acetamido-2,6-dideoxy- $\alpha$ -D-xylo-hex-4-ulose and UDP-2-acetamido-2,6-dideoxy- $\beta$ -L-arabino-hex-4-ulose, respectively. Since both compounds are not commercially available, we utilized enzymatic products for CE calibration. Recombinant CapE and PglF are both capable of catalyzing 100% conversion of the substrate UDP-D-GlcNAc. However, the final product concentrations in the reaction mixtures are lower than the initial substrate concentrations, due to simultaneous hydrolysis of substrate and products yielding UDP. To determine the actual product concentrations in the samples, we quantified the degradation product UDP, subtracted the respective values from the initial substrate amount and considered the difference to represent the amount of UDP-2-acetamido-2,6-dideoxy- $\alpha$ -D-xylo-hex-4-ulose and UDP-2-acetamido-2,6-dideoxy- $\beta$ -L-arabino-hex-4-ulose, respectively. The amount of UDP was determined as follows: UDP was diluted with water to different concentrations; then 50  $\mu$ l aliquots of the different UDP dilutions were mixed with 50  $\mu$ l of the I.S. PAP, which was prepared in biological matrix (PglF reaction mixture diluted 1:40 with water). Since UDP is also formed during *in vitro* PglF assays, UDP calibration was performed

using biological matrix as a blank value. The calibration and validation of UDP is shown as below:  $Y = 14.04 x - 21.74$



The UDP peaks in Pg1F product (1 to 80 dilution from the reaction mixture) and CapE product (1 to 320 dilution from the reaction mixture) have been chosen and calculated. According to the calculation, the concentration of UDP-2-acetamido-2,6-dideoxy- $\alpha$ -D-xylo-hex-4-ulose and UDP-2-acetamido-2,6-dideoxy- $\beta$ -L-arabino-hex-4-ulose in the 100% substrate converted samples were 2.438 mM and 1.702 mM, respectively:

UDP concentration in Pg1F reaction mixture 1 to 320 dilution: $x = (y + 21.74) / 14.04 = (10.294 + 21.74) / 14.4 = 2.282 \mu\text{M}$ Pg1F pro. con. in reaction mixture: Pg1F pro. con. in vial *320 = 2.270 mM				
I.S.	UDP	Avg. UDP/IS	Avg.UDP con. in vial	Avg. Pg1F pro. con. in vial (37.5-UDP con.)
5353	624			
3008	362			
5635	409	10.294	2.282 $\mu\text{M}$	7.093 $\mu\text{M}$
2820	197			
5424	646			
2677	319			
UDP in CapE reaction mixture 1 to 320 dilution: $x = (y + 21.74) / 14.04 = (34.817 + 21.74) / 14.4 = 4.028 \mu\text{M}$ CapE pro. con. in reaction mixture: CapE pro. con. in vial *320 = 1.711 mM				
I.S.	UDP	Avg. UDP/IS	Avg UDP con. in vial	Avg. CapE pro. con. in vial (9.375-UDP con.)

2726,0	994,			
1784,0	617,			
1849,0	635,	34.817	4.028 $\mu\text{M}$	5.347 $\mu\text{M}$
800,0	271,			
1109,0	435,			
596,0	247,			

The linearity of the quantitative determination and the limits of detection (LOD) and quantification (LOQ) of the enzymatic products UDP-2-acetamido-2,6-dideoxy- $\alpha$ -D-xylo-hex-4-ulose and UDP-2-acetamido-2,6-dideoxy- $\beta$ -L-arabino-hex-4-ulose were determined by processing six-point calibration curves (triplicate samples with duplicate measurements) in the presence of 3.125  $\mu\text{M}$  PAP as I.S. The precision and accuracy values were determined at the following concentrations (triplicate samples with duplicate measurements): 0.44, 0.89, 3.55 and 7.09  $\mu\text{M}$  for UDP-2-acetamido-2,6-dideoxy- $\alpha$ -D-xylo-4-hexulose; 0.67, 1.34, 2.67 and 5.35  $\mu\text{M}$  for UDP-2-acetamido-2,6-dideoxy- $\beta$ -L-arabino-hex-4-ulose in the presence of 3.125  $\mu\text{M}$  PAP as I.S. Accuracy was determined by calculating the ratios of the predicted concentrations and the spiked values, and relative standard deviations were calculated.

#### 6.5.2.4 Enzyme catalytic reaction

Reactions were initiated by the addition of 3  $\mu\text{g}$  CapD-His6 or 8.5  $\mu\text{g}$  CapE-His6. The reaction vials were incubated at 30°C. All enzymatic reactions were quenched by heating (5 min, 90°C). Determination of kinetic parameters for CapD and CapE. To determine the linear range of the enzymatic reactions, formation of CapD and CapE enzymatic products was monitored over time (6 time points, 10 min to 6 h) at 30°C with a substrate (UDP-D-GlcNAc) concentration of 1 mM. For the determination of the kinetic parameters ( $K_m$  and  $V_{max}$ ), 8 different substrate concentrations were chosen. For CapD assays, the cofactor NADP was added at a concentration of 2 mM. Each analysis was repeated three times in independent experiments.

Investigation of CapD and CapE inhibitors. A library of selected compounds (73 compounds for CapD; 46 compounds for CapE) (see Table 6.5 and Table 6.6) was initially screened at high concentrations of 100  $\mu\text{M}$  (for highly water-soluble compounds) or at 10  $\mu\text{M}$ , respectively. Subsequently, full concentration-inhibition curves were determined for the most potent inhibitors, and  $\text{IC}_{50}$  values were calculated. The substrate (UDP-D-GlcNAc) concentration for CapD and

CapE inhibition testing was 1 mM, and substrate conversion was strictly controlled to be below 10%. For CapD assays, the cofactor NADP was added at a concentration of 600  $\mu$ M. The IC<sub>50</sub> values of inhibitors were obtained by testing a suitable range of inhibitor concentrations (8 data points spanning three orders of magnitude). The incubation time was chosen to be within the linear range (30 min to 1 h). Negative controls were performed in the presence of heat-inactivated enzyme (10 min, 100°C). Each analysis was repeated three times in independent experiments. For the determination of the inhibition mechanism, 8 different substrate concentrations and 3 different inhibitor concentrations were used, and each analysis was carried out with duplicate measurements.

In vitro synthesis of the soluble capsule precursor UDP-D-FucNAc—The PglF-His<sub>6</sub> enzymatic product was used as substrate for reconstitution of CapN catalytic activity. For this purpose, PglF reactions were carried out overnight and quenched by heating (5 min, 95°C). CapN catalyzed synthesis of UDP-D-FucNAc was carried out in a total volume of 40  $\mu$ l. CapN-His<sub>6</sub> (12  $\mu$ g) was incubated in the presence of ~3mM UDP-2-acetamido-2,6-dideoxy-D-xylo-4-hexulose, 0.8% (v/v) Triton X-100 and 10 mM KPi, pH 7.5, for 2 h at 30°C. Alternatively, synthesis of UDP-D-FucNAc was performed in a one-pot-assay containing 3.5  $\mu$ g PglF, 12  $\mu$ g CapN, 3 mM UDP-GlcNAc, 0.8% (v/v) Triton X-100 and 10 mM KPi, in a total volume of 60  $\mu$ l. Cofactors NADH or NADPH were added in a concentration of 1.875 mM if indicated. All enzymatic reactions were quenched by heating (5 min, 90°C).

#### 6.5.2.5 The vivo study

All in vivo assays were carried out by Xue Li.

Quantitation of CP5 produced by cultures in the absence and presence of CapD inhibitor – An enzyme-linked immunosorbent inhibition assay (ELISA) method <sup>144</sup> was used to quantitate CP5 expression by *S. aureus* cultivated in vitro. The assay is based on the ability of encapsulated bacteria (trypsinized to remove protein A) or purified CP5 to absorb capsular antibodies from immune serum. The method is sensitive to ~1 ng/ml CP5 and is useful for quantitating capsule production by different *S. aureus* strains or by the same strain grown under different conditions. Briefly, wells of a microtiter plate were coated with purified CP5 (4  $\mu$ g/ml) coupled to poly-L-

lysine by the cyanuric acid chloride method <sup>145</sup>. After 18 h at 4°C, the microtiter plate was washed and blocked at 4°C overnight with 0.05% skimmed milk. The CP5+ *S. aureus* Reynolds strain <sup>146</sup> was cultivated overnight with aeration in 5 ml of Columbia broth containing ampicillin (0 – 270 µM). The bacteria were harvested, washed once in phosphate buffer, and then trypsinized (1 mg trypsin/ml of 0.1 M phosphate buffer, pH 8) for 60 min at 37°C. After washing, the bacterial suspensions were serially diluted threefold from  $\sim 3 \times 10^8$  to  $\sim 3 \times 10^5$  CFU/ml. The bacterial concentrations were verified by plating dilutions of the suspensions on tryptic soy agar plates. Polyclonal CP5-specific antiserum was diluted 1:20,000 and incubated overnight at 4°C with serial dilutions of the bacteria. Samples were centrifuged, and the absorbed serum samples (supernatants) were added to the coated and blocked microtiter plate. Following a 2 h incubation with absorbed or nonabsorbed serum samples, the plates were washed with PBS/Tween, and alkaline phosphatase-conjugated protein A/G (Thermo Scientific; 1:3000) was added to each well. After 2 hours at ambient temperature, the plate was again washed, and the substrate *p*-nitrophenyl phosphate was added. When the wells containing unabsorbed serum samples reached an OD<sub>405 nm</sub> of  $\sim 2.0$ , the plate was read on a Bio-TEK Power Wave HT ELISA reader. The concentration of each sample (CFU/ml) that resulted in 50% inhibition of antibody binding (IC<sub>50</sub>) was determined, and the IC<sub>50</sub> of cultures containing ampicillin were compared to that of cultures without ampicillin.

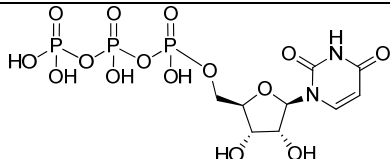
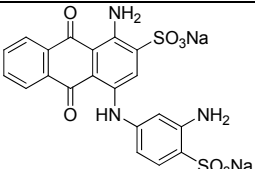
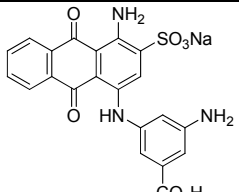
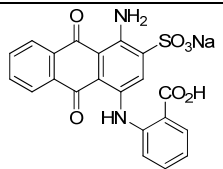
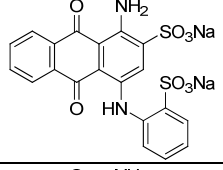
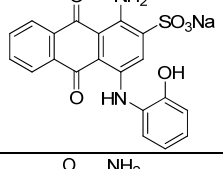
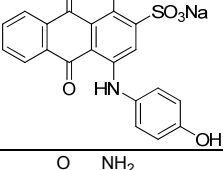
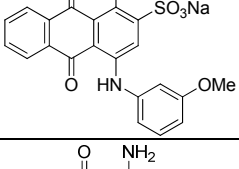
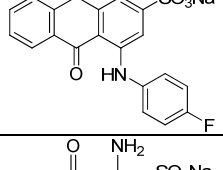
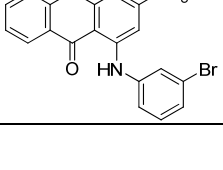
### **6.5.3 Compound preparation and selection**

A library of selected compounds (73 compounds for CapD; 46 compounds for CapE) was initially screened. The structures and screening results were shown in Table 6.5 and Table 6.6.



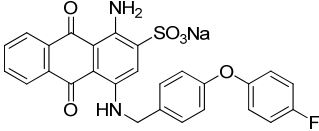
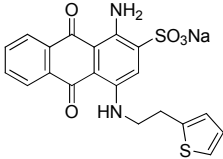
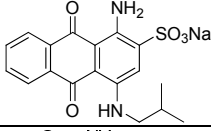
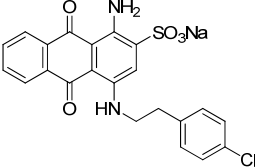
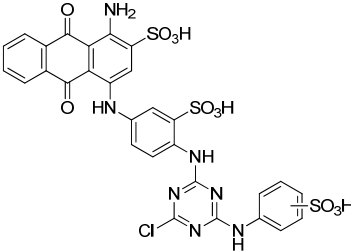
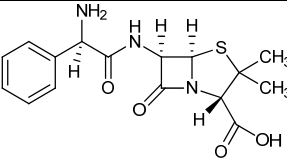
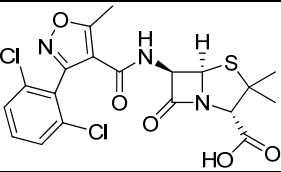
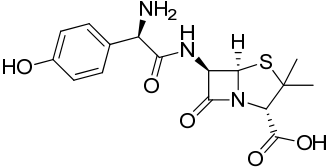
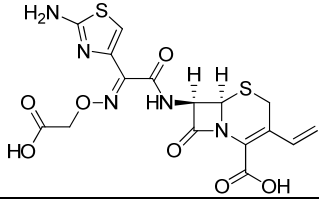
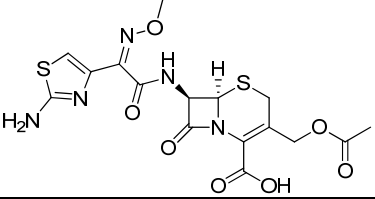
Table 6.5. CapD screening results\*

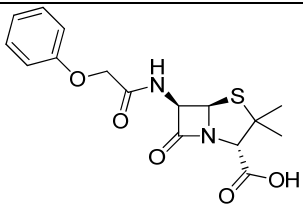
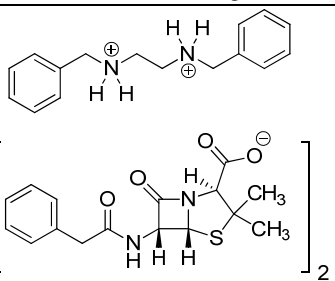
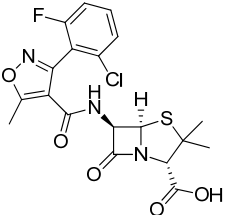
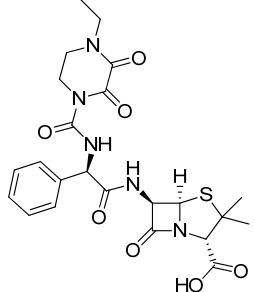
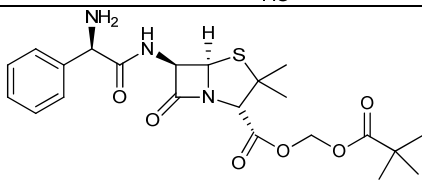
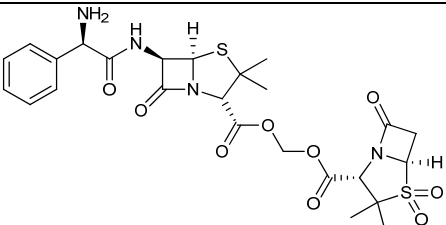
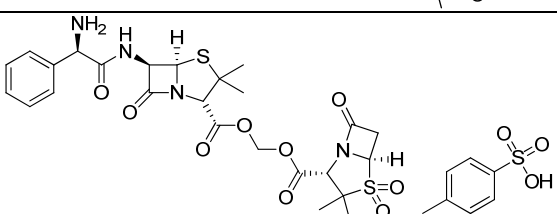
Compound (code) name	Structure	% inhibition of enzyme activity at test concentration given in brackets
UDP/UTP derivatives		
1 Ali 179 <sup>a</sup>		1% (100 μM)
2 Ali 412C <sup>a</sup>		6% (100 μM)
3 Ali 404B <sup>a</sup>		7% (100 μM)
4 Ali 411A <sup>a</sup>		15% (100 μM)
5 Ali 409A <sup>a</sup>		4% (100 μM)
6 Ali 149 <sup>a</sup>		-18% (100 μM)
7 Ali 452 <sup>a</sup>		-4% (100 μM)
46 UDP-glucose <sup>a</sup>		13% (100 μM)
9 UDP <sup>a</sup>		15% (100 μM)

10	UTP <sup>a</sup>		-4% (100 μM)
anthraquinone derivatives			
11	YB001 <sup>a</sup>		10% (10 μM)
12	YB003 <sup>a</sup>		2% (10 μM)
13	YB005 <sup>a</sup>		0% (10 μM)
14	YB009 <sup>a</sup>		25% (10 μM)
15	YB010 <sup>b</sup>		17% (10 μM)
16	YB011 <sup>a</sup>		25% (10 μM)
17	YB012 <sup>a</sup>		26% (10 μM)
18	YB013 <sup>a</sup>		24% (10 μM)
19	YB014 <sup>a</sup>		21% (10 μM)

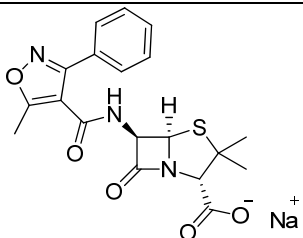
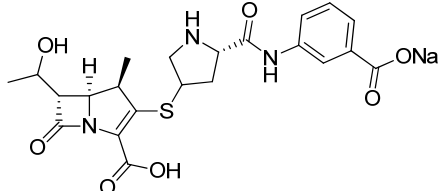
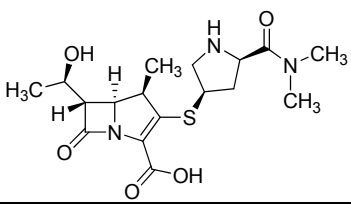
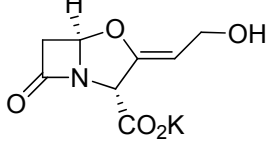
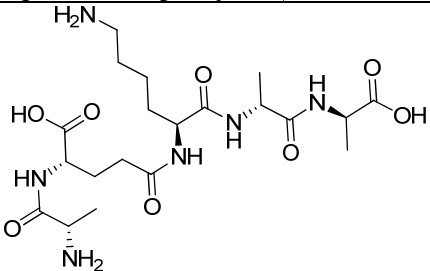
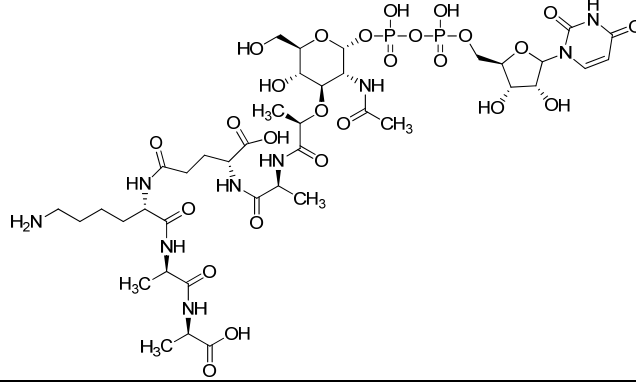
20	YB015 <sup>a</sup>		10% (10 μM)
21	YB016 <sup>b</sup>		-1% (10 μM)
22	YB017 <sup>b</sup>		14% (10 μM)
23	YB019 <sup>a</sup>		11% (10 μM)
24	YB020 <sup>b</sup>		34% (10 μM)
25	YB024 <sup>a</sup>		13% (10 μM)
26	YB028 <sup>b</sup>		29% (10 μM)
27	YB029 <sup>a</sup>		13% (10 μM)
28	YB031 <sup>a</sup>		-4% (10 μM)
29	YB032 <sup>b</sup>		25% (10 μM)

30	YB035 <sup>b</sup>		32% (10 μM)
31	YB038 <sup>a</sup>		23% (10 μM)
32	YB042 <sup>b</sup>		0% (10 μM)
33	YB047 <sup>a</sup>		20% (10 μM)
34	YB053 <sup>b</sup>		33% (10 μM)
35	YB055 <sup>a</sup>		-10% (10 μM)
36	YB056 <sup>b</sup>		27% (10 μM)
37	YB057 <sup>b</sup>		32% (10 μM)
38	YB058 <sup>b</sup>		25% (10 μM)

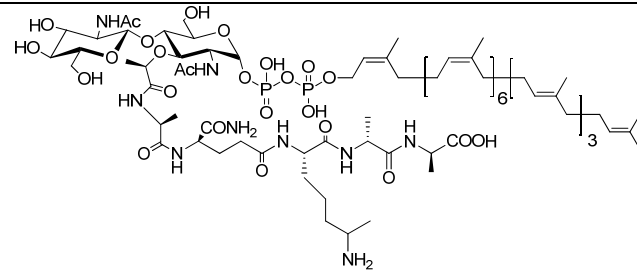
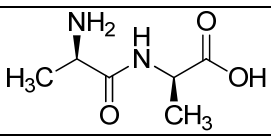
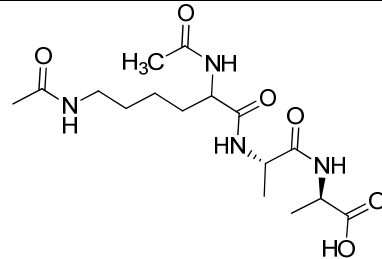
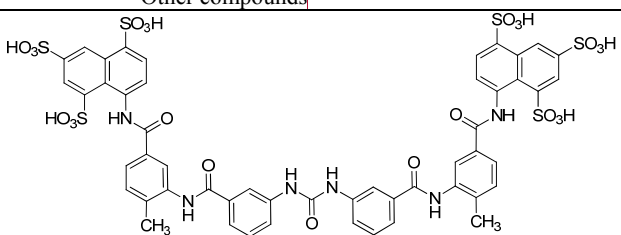
39	YB068 <sup>b</sup>		17% (10 μM)
40	YB083 <sup>b</sup>		35% (10 μM)
41	YB086 <sup>b</sup>		25% (10 μM)
42	YB087 <sup>b</sup>		32% (10 μM)
43	RB2 <sup>a</sup>		17% (10 μM)
antibiotics			
44	ampicillin <sup>b</sup>		41% (10 μM)
45	dicloxacillin <sup>b</sup>		44% (10 μM)
47	amoxicillin <sup>b</sup>		-3% (10 μM)
48	cefixime <sup>b</sup>		3% (10 μM)
49	cefotaxime sodium <sup>b</sup>		5% (10 μM)

50	phenoxymethylpenicillinic acid <sup>b</sup>		-8% (10 μM)
51	benzathine benzylpenicillin <sup>b</sup>		-3% (10 μM)
52	flucloxacillin sodium <sup>b</sup>		-5% (10 μM)
53	piperacillin <sup>b</sup>		-4% (10 μM)
54	pivampicillin <sup>b</sup> (prodrug)		-1% (10 μM)
55	sultamicillin <sup>b</sup> (prodrug)		-6% (10 μM)
56	sultamicillin tosylate <sup>b</sup> (prodrug)		1% (10 μM)

57	ticarcillin monosodium <sup>b</sup>		-8% (10 μM)
58	bacampicillin hydrochloride <sup>b</sup> (prodrug)		4% (10 μM)
59	cloxacillin sodium <sup>b</sup>		0% (10 μM)
60	penicillin G sodium salt <sup>b</sup>		-33% (10 μM)
61	mecillinam <sup>b</sup>		-6% (10 μM)
63	aztreonam <sup>b</sup>		-11% (10 μM)
64	cefuroxim sodium salt <sup>b</sup>		-12% (10 μM)
65	ceftaroline fosamil <sup>b</sup>		9% (10 μM)

68	oxacillin sodium <sup>b</sup>		16% (10 μM)
69	ertapenem sodium salt <sup>b</sup>		1% (10 μM)
70	meropenem trihydrate <sup>b</sup>		-26% (10 μM)
73	potassium clavulanate <sup>b</sup>		-23% (100 μM)
<u>biological interesting compounds</u>			
62	pentapeptide <sup>a</sup> (L-Ala-D-Glu-gamma-L-Lys-D-Ala-D-Ala)		51% (100 μM)
66	UDP-D-MurNAc-pentapeptide <sup>a</sup>		14% (100 μM)



67	lipid II <sup>a</sup>		67% (100 μM)
71	D-Ala-D-Ala <sup>a</sup>		26% (100 μM)
72	N-, N-ε-Diacetyl-Lys-D-Ala-D-Ala <sup>a</sup>		28% (100 μM)
Other compounds			
8	suramin <sup>b</sup>		-14% (10 μM)

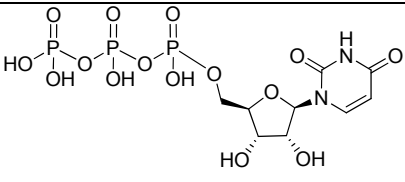
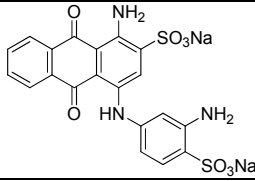
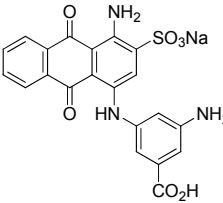
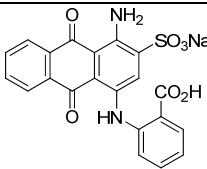
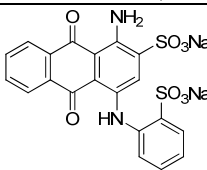
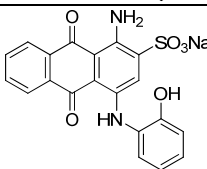
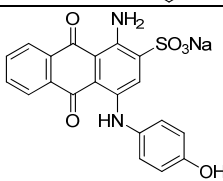
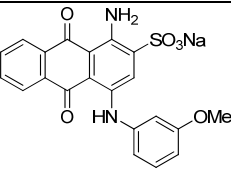
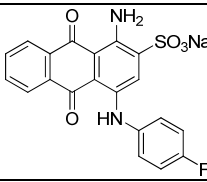
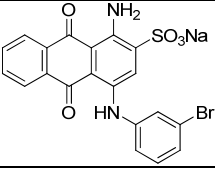
\*Compounds were screened at 10 μM or 100 μM depending on their water-solubility. Percent inhibition at the screening concentration is provided. In case of negative values the compounds activated enzymatic activity. For potent inhibitors, full concentration-inhibition curves were recorded and IC<sub>50</sub> values were determined. Final concentration of the substrate UDP-D-GlcNAc was 1 mM in all screening tests.

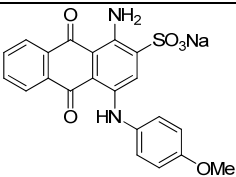
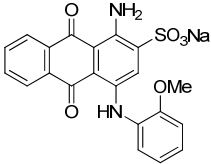
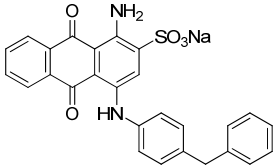
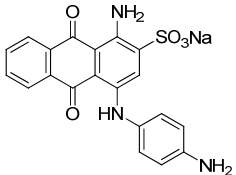
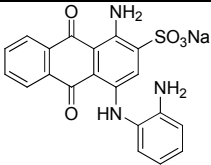
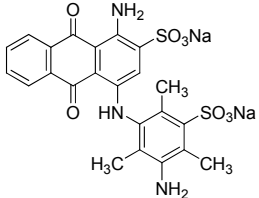
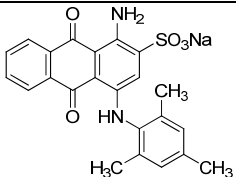
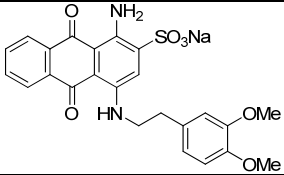
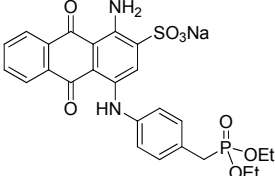
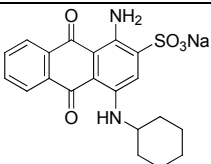
<sup>a</sup>Compounds were screened in buffer without DMSO.

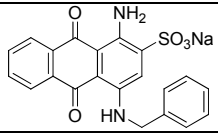
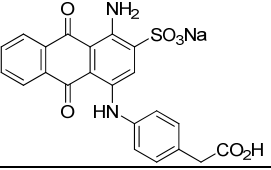
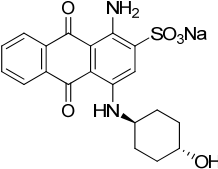
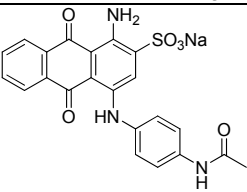
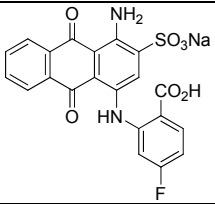
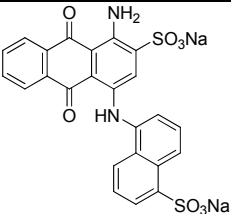
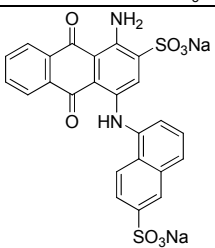
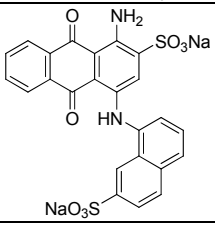
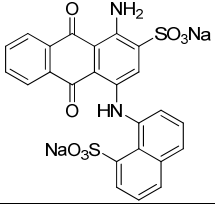
<sup>b</sup>Compounds were screened in buffer with 1% DMSO.

Table 6.6. CapE screening results\*

Compound (code) name	Structure	% inhibition of enzyme activity at test concentration given in brackets
UDP/UTP derivatives		
1 Ali 179 <sup>a</sup>		33% (100 μM)
2 Ali 412C <sup>a</sup>		27% (100 μM)
3 Ali 404B <sup>a</sup>		33% (100 μM)
4 Ali 411A <sup>a</sup>		35% (100 μM)
5 Ali 409A <sup>a</sup>		22% (100 μM)
6 Ali 149 <sup>a</sup>		18% (100 μM)
7 Ali 452 <sup>a</sup>		25% (100 μM)
46 UDP-glucose <sup>a</sup>		17% (100 μM)
9 UDP <sup>a</sup>		22% (100 μM)

10	UTP <sup>a</sup>		20% (100 μM)
anthraquinone compounds			
11	YB001 <sup>a</sup>		17% (10 μM)
12	YB003 <sup>a</sup>		18% (10 μM)
13	YB005 <sup>a</sup>		21% (10 μM)
14	YB009 <sup>a</sup>		15% (10 μM)
15	YB010 <sup>b</sup>		21% (10 μM)
16	YB011 <sup>a</sup>		7% (10 μM)
17	YB012 <sup>a</sup>		12% (10 μM)
18	YB013 <sup>a</sup>		9% (10 μM)
19	YB014 <sup>a</sup>		5% (10 μM)

20	YB015 <sup>a</sup>		7% (10 μM)
21	YB016 <sup>b</sup>		7% (10 μM)
22	YB017 <sup>b</sup>		-1% (10 μM)
23	YB019 <sup>a</sup>		9% (10 μM)
24	YB020 <sup>b</sup>		15% (10 μM)
25	YB024 <sup>a</sup>		9% (10 μM)
26	YB028 <sup>b</sup>		19% (10 μM)
27	YB029 <sup>a</sup>		13% (10 μM)
28	YB031 <sup>a</sup>		5% (10 μM)
29	YB032 <sup>b</sup>		18% (10 μM)

30	YB035 <sup>b</sup>		18% (10 μM)
31	YB038 <sup>a</sup>		15% (10 μM)
32	YB042 <sup>b</sup>		12% (10 μM)
33	YB047 <sup>a</sup>		8% (10 μM)
34	YB053 <sup>b</sup>		7% (10 μM)
35	YB055 <sup>a</sup>		-1% (10 μM)
36	YB056 <sup>b</sup>		4% (10 μM)
37	YB057 <sup>b</sup>		13% (10 μM)
38	YB058 <sup>b</sup>		0% (10 μM)

39	YB068 <sup>b</sup>		12% (10 μM)
40	YB083 <sup>b</sup>		6% (10 μM)
41	YB086 <sup>b</sup>		9% (10 μM)
42	YB087 <sup>b</sup>		17% (10 μM)
43	RB2 <sup>a</sup>		15% (10 μM)
antibiotics			
44	ampicillin <sup>b</sup>		5% (10 μM)
45	dicloxacillin <sup>b</sup>		6% (10 μM)
Other compounds			
8	suramin <sup>b</sup>		75% (10 μM)

\*Compounds were screened at 10 μM or 100 μM depending on their water-solubility. Percent inhibition at the screening concentration is provided. In case of negative values the compounds activated enzymatic activity. For potent inhibitors, full concentration-inhibition curves were recorded and IC<sub>50</sub> values were determined. Final concentration of the substrate UDP-D-GlcNAc was 1 mM in all screening tests.

<sup>a</sup>Compounds were screened in buffer without DMSO.

<sup>b</sup>Compounds were screened in buffer with 1% DMSO.

## 7 Abbreviations

ad	up to (Latin)
Ado	adenosine
ADP	adenosine-5'-diphosphate
AP	alkaline phosphatases
ATP	adenosine-5'-triphosphate
AU	absorbance units
BGE	background electrolyte
BSA	bovine serum albumin
<i>C. jejuni</i>	<i>Campylobacter jejuni</i>
C <sub>55</sub> P	bactoprenol
CAPS	3-(cyclohexylamino)-1-propanesulfonic acid
CE	capillary electrophoresis
CFU	colony forming units
CHO	Chinese hamster ovary
Ci	Curie
CNS	central nervous system
con	concentration
conc.	concentration
CP	capsular polysaccharide
CP5	serotype 5 capsular polysaccharide
CP8	serotype 8 capsular polysaccharide
cpm	counts per minute
CST	cerebroside sulfotransferase
Da	Dalton
DAD	diode array detector
DDM	<i>n</i> -dodecyl- $\beta$ -D-maltoside
D-FucNac	D-N-acetylfucosamine
D-ManNAcA	D-N-acetylmannosaminuronic acid
DMSO	dimethyl sulfoxide
<i>E. coli</i>	<i>Escherichia coli</i>
e.g.	exempli gratia (for example)
eN	ecto-5'-nucleotidase

E-NPP	ectonucleotide pyrophosphatase/phosphodiesterase family
E-NTPDase	ectonucleoside triphosphate diphosphohydrolase
EOF	electroosmotic flow
et al.	et alii (and others)
f.c.	final concentration
FASS	field amplifying sample stacking
FDA	US Food and Drug Administration
FS	fused-silica
g	gram
GPI	glycosylphosphatidylinositol
h	hour(s)
His <sub>6</sub> -tag	hexahistidine-tag
HTS	high throughput screening
I.S.	internal standard
IC <sub>50</sub>	half maximal inhibitory concentration
ICH	International Conference on Harmonisation (of Technical Requirements for Registration of Pharmaceuticals for Human Use)
IMAC	IMAC, immobilized metal ion affinity chromatography
Ino	inosine
IPTG	isopropyl- $\beta$ -D-1-thiogalactopyranoside
KD	equilibrium dissociation constant
K <sub>i</sub>	equilibrium inhibition constant
K <sub>pi</sub>	potassium phosphate buffer
l	liter
LB	lysogeny broth
L-FucNac	L-N-acetylfucosamine
LIF	laser-induced fluorescence
lipid II	undecaprenyl-pyrophosphoryl-N-acetylmuramyl-(pentapeptide)-N-acetylglucosamine
LOD	limit of detection
LOQ	limit of quantification
m	meter
M	Molar



MEKC	micellar electrokinetic chromatography
MeOH	methanol
min	minute(s)
MLD	metachromatic leukodystrophy
MRSA	Methicillin-resistant <i>Staphylococcus aureus</i>
MS	mass spectroscopy
MurNAc	D-N-acetylmuraminic acid
n	number of experiments
n/a	not available
NAD	nicotinamide adenine dicucleotide
NADH	nicotinamide adenine dicucleotide
NADP	nicotinamide adenine dicucleotide phosphate
NADPH	nicotinamide adenine dicucleotide phosphate
NaPi	sodium phosphate buffer
nd	no data
NEB	New England Biolabs
Ni-NTA	nickel-nitrilotriacetic acid
PAP	adenosine-3',5'-diphosphate sodium salt
PAPS	3'-phosphoadenosine-5'-phosphosulfate
PB	polybrene (hexadimethrine bromide)
PBP	Penicillin-binding protein
PG	peptidoglycan
POMs	polyoxometalates
rpm	rounds per minute
RSD	relative standard deviation
rt	room temperature
s	second(s)
<i>S. aureus</i>	<i>Staphylococcus aureus</i>
<i>S. pneumoniae</i>	<i>Streptococcus pneumoniae</i>
SDR	short-chain dehydrogenase/reductase
SEM	standard error of the mean
Tris	tris(hydroxymethyl)aminomethane
U	units

UDP-D-FucNAc	UDP-D-N-acetylfucosamine
UDP-D-GlcNAc	UDP-D-N-acetylglucosamine
UDP-D-ManNAcA	UDP-D-N-acetylmannosaminuronic acid
UDP-D-MurNAc-pentapeptide	UDP-D-N-acetylmuramyl-pentapeptide
UDP-L-FucNAc	UDP-L-N-acetylfucosamine
UV	ultraviolet
V	volume
VDW	the van der Waals force
vs.	versus
wt	wild-type
WTA	wall teichoic acid

## 8 Curriculum Vitae

CV Wenjin Li

---

Email: [aglaialiwenjin@msn.com](mailto:aglaialiwenjin@msn.com); [wenjinli@uni-bonn.de](mailto:wenjinli@uni-bonn.de)

### Education

Dates	Starting from 07/2009 to 11/2014
Name of organization	Bonn University Pharmazeutisches Institut, Pharmazeutische Chemie I
Title of qualification	Doctor
Principal subjects	Pharmacy Characterization of therapeutically important enzymes with polar substrates or products and identification of inhibitors by capillary electrophoresis

Dates	Starting from 12/2008 to 06/2009
Name of organization	Bonn University Pharmazeutisches Institut, Pharmazeutische Chemie I
Title of qualification	Internship
Principal subjects	Pharmacy Investigation of agonist and antagonist for GPCR receptors (P1)

Dates	10/2005-10/2008
Name of organization	Bonn University, Bonn-Aachen International Center for Information Technology

Title of qualification	Master
Principal subjects	Life Science Informatics
Master Thesis	Structure-Activity Relationships and Pharmacophore Modeling of Purine Receptor Antagonists

Dates	09/2001-09/2005
Name of organization	Southeast University, China
Title of qualification	Bachelor
Principal subjects	Biomedical Engineering

#### Scholarship, working position, working experience

- ❖ Present employment (12-2009 to 11.2014)

Scientific Assistant in Pharmazeutisches Institut. Rheinische Friedrichs-Wilhelm Universität Bonn, Germany.

- ❖ Scholarship (2010 to 2012)

Deutscher Akademischer Austauschdienst (DAAD, research assistantship stipend)

- ❖ Local organizer of conference Purines 2014 (23-27 July, 2014)

#### Publications

- ❖ Li, W.; Ulm, H.; Rausch, M.; Li, X.; O’Riordan, K.; Lee, J. C.; Schneider, T. and Müller, C. E. Analysis of the Staphylococcus aureus capsule biosynthesis pathway in vitro: characterization of the UDP-GlcNAc C6 dehydratases CapD and CapE and identification of enzyme inhibitors, *Int. J. Med. Microbiol.* **2014**. *in Press* (2012 IF 4.5)
- ❖ Ulm, H.; Rausch, M.; Li, W.; Hardt, P.; Sylvester, M.; Josten, M.; Sahl, H-G.; Müller, C. E.; Lee, J. C. and Schneider, T. Analysis of the Staphylococcus aureus capsule biosynthesis pathway *in vitro* – role of the CapAB kinase complex in pathway regulation, *Plos Pathogens*, *under revision*. (2012 IF 8.1)

- ❖ Li, W.; Zech, I; Gieselmann, V.; Müller, C.E. A dynamic pH junction method for monitoring the catalytic activity of cerebroside sulfotransferase. *Manuscript for Chromatography A*
- ❖ Borrmann, T.; Hinz, S.; Bertarelli, D.; Li, W.; Florin, N. C.; Scheiff, A. B. and Müller, C. E. 1-Alkyl-8-(piperazine-1-sulfonyl)phenylxanthenes: development and characterization of adenosine A<sub>2B</sub> receptor antagonists and a new radioligand with subnanomolar affinity and subtype specificity. *J. Med. Chem.* 2009, 52, 3994-4006. **(2012 IF 5.6)**
- ❖ Scheiff, A. B.; Yerande, S. G.; El-Tayeb, A.; Li, W.; Inamdar, G. S.; Vasu, K. K.; Sudarsanam, V. and Müller, C. E. 2-Amino-5-benzoyl-4-phenylthiazoles: development of potent and selective adenosine A<sub>1</sub> receptor antagonists. *Bioorg. Med. Chem.* 2010, 18, 2195-2203. **(2012 IF 3.2)**

#### Conference

- ❖ Li, W.; Zech, I; Gieselmann, V.; Müller, C.E. A dynamic pH junction method for monitoring the catalytic activity of cerebroside sulfotransferase. *DPhG Jahrestagung 2014, Frankfurt, Germany, 24.-26. September, 2014. (short lecture)*
- ❖ Li, W.; Zech, I; Gieselmann, V.; Müller, C.E. A new FASS method combined with dynamic pH junction for monitoring catalytic activities of cerebroside sulfotransferase. *CE-Forum Jena, Germany, 16-17 September, 2013. (oral presentation)*
- ❖ Li, W.; Brunschweiler, A.; Zimmermann, H.; Müller, C.E. Peptidonucleosides as inhibitors of ecto-5'-nucleotidase – a promising target for anti-cancer-drugs. *Purines 2014, Bonn, Germany, 23-27 July, 2014.*
- ❖ Li, W.; Ulm, H.; Schneider, T.; Sahl, H-G.; Müller, C.E. A new sensitive capillary electrophoresis method for the monitoring of enzymes involved in capsule formation of *Staphylococcus aureus*. *Frontiers in Medicinal Chemistry Joint German-Swiss Meeting on Medicinal Chemistry, Munich, Germany, 17-20 March, 2013.*
- ❖ Li, W.; Brunschweiler, A.; El-Tayeb, A.; Bhattarai, S.; Zimmermann, H.; Müller, C.E. pH dependent modulators for ecto-5'-nucleotidase – promising candidates for

anti-cancer-drugs. *Trends in Enzymology 2012: Going beyond Frontiers, Göttingen, Germany*, 03-06 June, 2012.

- ❖ Li, W.; Brunschweiler, A.; Zimmermann, H.; Müller, C.E. Peptidonucleosides as inhibitors of ecto-5'-nucleotidase – a promising target for anti-cancer-drugs. *Forth Joint German-Italian Purine Club Meeting, Bonn, Germany*, 01-15 July, 2011.

#### Notable Professional Abilities

- ❖ GPCR antagonist and agonist investigation by radiometric method and cAMP accumulation assays
- ❖ CHO cell culture and recombinant protein preparation
- ❖ Capillary electrophoresis (CE) method development
- ❖ Enzyme kinetic and enzyme inhibitor investigation

#### Background Courses

- ❖ 09/20/2010-09/24/2010: Electrophysiology of ion channels in excitable membranes
- ❖ 12/2009: Database search strategies in molecular biology and 3D models
- ❖ 09/21/2009-09/25/2009: training course for radiation protection (Strahlenschutzkurs S 4.2)
- ❖ 09/14/2009-09/16/2009: Ligand/receptor-interactions: parameters, computer-assisted data analysis and presentation

#### Personal skills

- ❖ Languages

Mother Tongue: **Chinese**

Other Languages:

	Listening	Reading	Spoken	Writing
<b>English</b>	excellent	excellent	very good	very good

---

<b>German</b>	good	good	good	good
---------------	------	------	------	------

---

❖ Computer skills:

Programming: Java, Shell language in Linux, C++, Assembly language

Database: Microsoft Access

Statistics: R

Software: Microsoft Office, FlexS, SYBYL, MOE, 32 Karat 5.0, Prism 5, ISIS Draw

❖ Driving licence: Chinese driving licence C

Personal

Date of birth: 04/05/1983

Place of birth: Shanxi

Nationality: Chinese

Marital status: Single

Gender: Female

Hobbies: fitness, dancing, travelling, music, cooking





## 9 References

- (1) Copeland, R. A. *Evaluation of Enzyme Inhibitors in Drug Discovery: A Guide for Medicinal Chemists and Pharmacologists*; John Wiley & Sons: Hoboken, 2005; pp. 1–140.
- (2) Thomas, G. *Fundamentals of Medicinal Chemistry*; WILEY: Chichester, 2007; pp. 252–254.
- (3) Changeux, J.-P.; Edelstein, S. J. Allosteric Mechanisms of Signal Transduction. *Science* **2005**, *308*, 1424–1428.
- (4) Knapp, K.; Zebisch, M.; Pippel, J.; El-Tayeb, A.; Müller, C. E.; Sträter, N. Crystal Structure of the Human Ecto-5'-Nucleotidase (CD73): Insights into the Regulation of Purinergic Signaling. *Structure* **2012**, *20*, 2161–2173.
- (5) Bisswanger, H. *Enzyme Kinetics Principles and Methods*; WILEY-VCH: Weinheim, 2002; pp. 51–58.
- (6) Copeland, R. A. *Enzymes: A Practical Introduction to Structure, Mechanism, and Data Analysis*; 2nd ed.; WILEY-VCH: New York, 2000; pp. 266–304.
- (7) Dixon, M. The Determination of Enzyme Inhibitor Constants. *Biochem. J.* **1953**, *55*, 170–171.
- (8) Dixon, B. M. The Graphical Determination of. **1972**, *129*, 197–202.
- (9) Landers, J. P. *Handbook of Capillary and Microchip Electrophoresis and Associated Microtechniques*; third ed.; CRS Press: Florida, 2008; pp. 3–74.
- (10) ICH. ICH Harmonised Tripartite Guideline, Validation of Analytical Procedures: Text and Methodology. **2005**.
- (11) FDA. Guidance for Industry Bioanalytical Method Validation. **2001**.
- (12) Simpson, S. L.; Quirino, J. P.; Terabe, S. On-Line Sample Preconcentration in Capillary Electrophoresis. Fundamentals and Applications. *J. Chromatogr. A* **2008**, *1184*, 504–541.
- (13) Kim, J. B.; Quirino, J. P.; Otsuka, K.; Terabe, S. On-Line Sample Concentration in Micellar Electrokinetic Chromatography Using Cationic Surfactants. *J. Chromatogr. A* **2001**, *916*, 123–130.
- (14) Olivares, M. L.; Vera-Candioti, L.; Berli, C. L. a. The EOF of Polymer Solutions. *Electrophoresis* **2009**, *30*, 921–929.

- (15) Zimmermann, H.; Zebisch, M.; Sträter, N. Cellular Function and Molecular Structure of Ecto-Nucleotidases. *Purinergic Signal*. **2012**, *8*, 437–502.
- (16) Fredholm, B. B.; Ijzerman, A. P.; Jacobson, K. A.; Linden, J.; Mu, C. E. International Union of Basic and Clinical Pharmacology . LXXXI . Nomenclature and Classification of Adenosine Receptors — An Update. **2011**, *63*, 1–34.
- (17) Honke, K.; Tsuda, M.; Koyota, S.; Wada, Y.; Iida-Tanaka, N.; Ishizuka, I.; Nakayama, J.; Taniguchi, N. Molecular Cloning and Characterization of a Human Beta-Gal-3'-Sulfotransferase That Acts on Both Type 1 and Type 2 (Gal Beta 1-3/1-4GlcNAc-R) Oligosaccharides. *J. Biol. Chem.* **2001**, *276*, 267–274.
- (18) Sowa, N. A.; Voss, M. K.; Zylka, M. J. Recombinant Ecto-5'-Nucleotidase (CD73) Has Long Lasting Antinociceptive Effects That Are Dependent on Adenosine A1 Receptor Activation. *Mol. Pain* **2010**, *6*, 20.
- (19) Thompson, L. F.; Eltzschig, H. K.; Ibla, J. C.; Van De Wiele, C. J.; Resta, R.; Morote-Garcia, J. C.; Colgan, S. P. Crucial Role for Ecto-5'-Nucleotidase (CD73) in Vascular Leakage during Hypoxia. *J. Exp. Med.* **2004**, *200*, 1395–1405.
- (20) Stagg, J.; Divisekera, U.; McLaughlin, N.; Sharkey, J.; Pommey, S.; Denoyer, D.; Dwyer, K. M.; Smyth, M. J. Anti-CD73 Antibody Therapy Inhibits Breast Tumor Growth and Metastasis. *Proc. Natl. Acad. Sci. U. S. A.* **2010**, *107*, 1547–1552.
- (21) Baqi, Y.; Lee, S.-Y.; Iqbal, J.; Ripphausen, P.; Lehr, A.; Scheiff, A. B.; Zimmermann, H.; Bajorath, J.; Müller, C. E. Development of Potent and Selective Inhibitors of Ecto-5'-Nucleotidase Based on an Anthraquinone Scaffold. *J. Med. Chem.* **2010**, *53*, 2076–2086.
- (22) Antonioli, L.; Blandizzi, C.; Pacher, P.; Haskó, G. Immunity, Inflammation and Cancer: A Leading Role for Adenosine. *Nat. Rev. Cancer* **2013**, *13*, 842–857.
- (23) Braun, H. Z. N.; Heine, B. K. P. New Insights into Molecular Structure and Function of Ecto-5'- Nucleotidases in the Nervous System. 310–314.
- (24) Zimmermann, H. Biochemistry, Localization and Functional Roles of Ecto-Nucleotidases in the Nervous System. *Prog. Neurobiol.* **1996**, *49*, 589–618.
- (25) Peng, Z.; Fernandez, P.; Wilder, T.; Yee, H.; Chiriboga, L.; Chan, E. S. L.; Cronstein, B. N. Ecto-5'-Nucleotidase (CD73) -Mediated Extracellular Adenosine Production Plays a Critical Role in Hepatic Fibrosis. *FASEB J.* **2008**, *22*, 2263–2272.
- (26) Kumar, V. Adenosine as an Endogenous Immunoregulator in Cancer Pathogenesis: Where to Go? *Purinergic Signal*. **2013**, *9*, 145–165.
- (27) Flögel, U.; Burghoff, S.; van Lent, P. L. E. M.; Temme, S.; Galbarz, L.; Ding, Z.; El-Tayeb, A.; Huels, S.; Bönner, F.; Borg, N.; Jacoby, C.; Müller, C. E.; van den Berg, W.

- B.; Schrader, J. Selective Activation of Adenosine A2A Receptors on Immune Cells by a CD73-Dependent Prodrug Suppresses Joint Inflammation in Experimental Rheumatoid Arthritis. *Sci. Transl. Med.* **2012**, *4*, 146ra108.
- (28) Wang, L.; Fan, J.; Thompson, L. F.; Zhang, Y.; Shin, T.; Curiel, T. J.; Zhang, B. CD73 Has Distinct Roles in Nonhematopoietic and Hematopoietic Cells to Promote Tumor Growth in Mice. **2011**, *121*, 2371–2382.
- (29) Jin, D.; Fan, J.; Wang, L.; Thompson, L. F.; Liu, A.; Daniel, B. J.; Shin, T.; Curiel, T. J.; Zhang, B. CD73 on Tumor Cells Impairs Antitumor T-Cell Responses: A Novel Mechanism of Tumor-Induced Immune Suppression. *Cancer Res.* **2010**, *70*, 2245–2255.
- (30) Resta, R.; Thompson, L. F. T Cell Signalling through CD73. *Cell. Signal.* **1997**, *9*, 131–139.
- (31) Zimmermann, H. Ectonucleotidases: Some Recent Developments and a Note on Nomenclature. *Drug Dev. Res.* **2001**, *52*, 44–56.
- (32) Zimmermann, H. Extracellular Metabolism of ATP and Other Nucleotides. *Naunyn-Schmiedeberg's Arch. Pharmacol.* **2000**, *362*, 299–309.
- (33) Colgan, S. P.; Eltzschig, H. K.; Eckle, T.; Thompson, L. F. Physiological Roles for Ecto-5'-Nucleotidase (CD73). *Purinergic Signal.* **2006**, *2*, 351–360.
- (34) Zimmermann, H. 5'-Nucleotidase: Molecular Structure and Functional Aspects. *Biochem. J.* **1992**, *285* (Pt 2), 345–365.
- (35) Sträter, N. Ecto-5'-Nucleotidase: Structure Function Relationships. *Purinergic Signal.* **2006**, *2*, 343–350.
- (36) Zimmermann, H. 5'-Nucleotidase : Molecular Structure and Functional Aspects. **1992**, *285*, 345–365.
- (37) Knöfel, T.; Sträter, N. E. Coli 5'-Nucleotidase Undergoes a Hinge-Bending Domain Rotation Resembling a Ball-and-Socket Motion. *J. Mol. Biol.* **2001**, *309*, 255–266.
- (38) Knöfel, T.; Sträter, N. Mechanism of Hydrolysis of Phosphate Esters by the Dimetal Center of 5'-Nucleotidase Based on Crystal Structures. *J. Mol. Biol.* **2001**, *309*, 239–254.
- (39) Jordheim, L. P.; Durantel, D.; Zoulim, F.; Dumontet, C. Advances in the Development of Nucleoside and Nucleotide Analogues for Cancer and Viral Diseases. *Nat. Rev. Drug Discov.* **2013**, *12*, 447–464.
- (40) Iqbal, J.; Jirovsky, D.; Lee, S.-Y.; Zimmermann, H.; Müller, C. E. Capillary Electrophoresis-Based Nanoscale Assays for Monitoring Ecto-5'-Nucleotidase Activity

- and Inhibition in Preparations of Recombinant Enzyme and Melanoma Cell Membranes. *Anal. Biochem.* **2008**, *373*, 129–140.
- (41) Izumi, H.; Torigoe, T.; Ishiguchi, H.; Uramoto, H.; Yoshida, Y.; Tanabe, M.; Ise, T.; Murakami, T.; Yoshida, T.; Nomoto, M.; Kohno, K. Cellular pH Regulators: Potentially Promising Molecular Targets for Cancer Chemotherapy. *Cancer Treat. Rev.* **2003**, *29*, 541–549.
- (42) Webb, B. a; Chimenti, M.; Jacobson, M. P.; Barber, D. L. Dysregulated pH: A Perfect Storm for Cancer Progression. *Nat. Rev. Cancer* **2011**, *11*, 671–677.
- (43) Parks, S. K.; Chiche, J.; Pouysségur, J. Disrupting Proton Dynamics and Energy Metabolism for Cancer Therapy. *Nat. Rev. Cancer* **2013**, *13*, 611–623.
- (44) Neri, D.; Supuran, C. T. Interfering with pH Regulation in Tumours as a Therapeutic Strategy. *Nat. Rev. Drug Discov.* **2011**, *10*, 767–777.
- (45) Wike-Hooley, J. L.; Haveman, J.; Reinhold, H. S. The Relevance of Tumour pH to the Treatment of Malignant Disease. *Radiother. Oncol.* **1984**, *2*, 343–366.
- (46) Sakaguchi, T.; Sawa, Y.; Kitakaze, M.; Suzuki, K.; Nishimura, M.; Kaneda, Y.; Matsuda, H. Ecto-5'-Nucleotidase Plays a Role in the Cardioprotective Effects of Heat Shock Protein 72 in Ischemia-Reperfusion Injury in Rat Hearts. *Cardiovasc. Res.* **2000**, *47*, 74–80.
- (47) Taverniers, I.; De Loose, M.; Van Bockstaele, E. Trends in Quality in the Analytical Laboratory. II. Analytical Method Validation and Quality Assurance. *TrAC Trends Anal. Chem.* **2004**, *23*, 535–552.
- (48) Servos, J.; Reiländer, H.; Zimmermann, H. Catalytically Active Soluble Ecto-5'-Nucleotidase Purified after Heterologous Expression as a Tool for Drug Screening. *Drug Dev. Res.* **1998**, *45*, 269–276.
- (49) Rücker, B.; Almeida, M. E.; Libermann, T. a; Zerbini, L. F.; Wink, M. R.; Sarkis, J. J. F. E-NTPDases and Ecto-5'-Nucleotidase Expression Profile in Rat Heart Left Ventricle and the Extracellular Nucleotide Hydrolysis by Their Nerve Terminal Endings. *Life Sci.* **2008**, *82*, 477–486.
- (50) Jamal, Z.; Afkham-Ebrahimi, A.; Saggerson, E. D. A Novel Assay for 5'-Nucleotidase Using 1,N<sup>6</sup>-Etheno-AMP as Substrate, and Comments on the Properties of the Reaction Product, Ethenoadenosine. *Biochem. J.* **1988**, *250*, 369–373.
- (51) Newby, A. C.; Luzio, J. P.; Hales, C. N. The Properties and Extracellular Location of 5'-Nucleotidase of the Rat Fat-Cell Plasma Membrane. *Biochem. J.* **1975**, *146*, 625–633.

- (52) Rhule, J. T.; Hill, C. L.; Judd, D. a.; Schinazi, R. F. Polyoxometalates in Medicine. *Chem. Rev.* **1998**, *98*, 327–358.
- (53) Brylev, K. A.; Mironov, Y. V; Kozlova, S. G.; Fedorov, V. E.; Kim, S.-J.; Pietzsch, H.-J.; Stephan, H.; Ito, A.; Ishizaka, S.; Kitamura, N. The First Octahedral Cluster Complexes with Terminal Formate Ligands: Synthesis, Structure, and Properties of K<sub>4</sub>[Re<sub>6</sub>S<sub>8</sub>(HCOO)<sub>6</sub>] and Cs<sub>4</sub>[Re<sub>6</sub>S<sub>8</sub>(HCOO)<sub>6</sub>]. *Inorg. Chem.* **2009**, *48*, 2309–2315.
- (54) Müller, C. E.; Iqbal, J.; Baqi, Y.; Zimmermann, H.; Röllich, A.; Stephan, H. Polyoxometalates--a New Class of Potent Ecto-Nucleoside Triphosphate Diphosphohydrolase (NTPDase) Inhibitors. *Bioorg. Med. Chem. Lett.* **2006**, *16*, 5943–5947.
- (55) Node, K.; Kitakaze, M.; Minamino, T.; Tada, M.; Inoue, M.; Hori, M.; Kamada, T. Activation of Ecto-5'-Nucleotidase by Protein Kinase C and Its Role in Ischaemic Tolerance in the Canine Heart. *Br. J. Pharmacol.* **1997**, *120*, 273–281.
- (56) Wink, M. .; Tamajusuku, a. S. .; Braganhol, E.; Casali, E. .; Barreto-Chaves, M. L. .; Sarkis, J. J. .; Battastini, a. M. . Thyroid Hormone Upregulates Ecto-5'-nucleotidase/CD73 in C6 Rat Glioma Cells. *Mol. Cell. Endocrinol.* **2003**, *205*, 107–114.
- (57) Sato, T.; Obata, T.; Yamanaka, Y.; Arita, M. Effects of Lysophosphatidylcholine on the Production of Interstitial Adenosine via Protein Kinase C-Mediated Activation of Ecto-5'-Nucleotidase. *Br. J. Pharmacol.* **1998**, *125*, 493–498.
- (58) Robson, S. C. Role of CD73 and Extracellular Adenosine in Disease : Presented by Maria P. Abbracchio. *Purinergic Signal.* **2011**, *7*, 367–372.
- (59) Eckhardt, M. The Role and Metabolism of Sulfatide in the Nervous System. *Mol. Neurobiol.* **2008**, *37*, 93–103.
- (60) Gieselmann, V.; Krägeloh-Mann, I. Metachromatic Leukodystrophy--an Update. *Neuropediatrics* **2010**, *41*, 1–6.
- (61) Deconinck, N.; Messaaoui, A.; Ziereisen, F.; Kadhim, H.; Sznajder, Y.; Pelc, K.; Nassogne, M. C.; Vanier, M. T.; Dan, B. Metachromatic Leukodystrophy without Arylsulfatase A Deficiency: A New Case of Saposin-B Deficiency. *Eur. J. Paediatr. Neurol.* **2008**, *12*, 46–50.
- (62) Kehrer, C.; Groeschel, S.; Kustermann-Kuhn, B.; Bürger, F.; Köhler, W.; Kohlschütter, A.; Bley, A.; Steinfeld, R.; Gieselmann, V.; Krägeloh-Mann, I. Language and Cognition in Children with Metachromatic Leukodystrophy: Onset and Natural Course in a Nationwide Cohort. *Orphanet J. Rare Dis.* **2014**, *9*, 18.

- (63) Eckhardt, M. Pathology and Current Treatment of Neurodegenerative Sphingolipidoses. *Neuromolecular Med.* **2010**, *12*, 362–382.
- (64) Honke, K.; Yamane, M.; Ishii, A.; Kobayashi, T.; Makita, A. Purification and Characterization of 3'-Phosphoadenosine-5'-phosphosulfate:GalCer Sulfotransferase from Human Renal Cancer Cells. *J. Biochem.* **1996**, *119*, 421–427.
- (65) Zaruba, M.; Hilt, D.; Tennekoon, G. Inhibition of Rat Brain Galactocerebroside Sulfotransferase by Triazine Aromatic Dyes: Interaction with the 3'-Phosphoadenosine 5'-Phosphosulfate Binding Site. *Biochem. Biophys. Res. Commun.* **1985**, *129*, 522–529.
- (66) Tennekoon, G.; Aitchison, S.; Zaruba, M. Purification and Characterization of Galactocerebroside Sulfotransferase from Rat Kidney. *Arch. Biochem. Biophys.* **1985**, *240*, 932–944.
- (67) Farrer, R. G.; Warden, M. P.; Quarles, R. H. Effects of Brefeldin A on Galactosphingolipid Synthesis in an Immortalized Schwann Cell Line: Evidence for Different Intracellular Locations of Galactosylceramide Sulfotransferase and Ceramide Galactosyltransferase Activities. *J. Neurochem.* **1995**, *65*, 1865–1873.
- (68) Kamio, K.; Honke, K.; Makita, A. Pyridoxal 5'-Phosphate Binds to a Lysine Residue in the Adenosine 3'-Phosphate 5'-Phosphosulfate Recognition Site of Glycolipid Sulfotransferase from Human Renal Cancer Cells. *Glycoconj. J.* **1995**, *12*, 762–766.
- (69) Sundaram, K. S.; Lev, M. Purification and Activation of Brain Sulfotransferase. *J. Biol. Chem.* **1992**, *267*, 24041–24044.
- (70) Sarlieve, L. L.; Neskovic, N. M.; Rebel, G.; Mandel, P. PAPS-Cerebroside Sulphotransferase Activity in Developing Brain of a Neurological Mutant of Mouse (MSD). *Exp. brain Res.* **1974**, *19*, 158–165.
- (71) Gasa, S.; Makita, A.; HIRAMA, M.; Kawabata, M. Cerebroside Sulfotransferase Activity in Human Lung Tissues. An Elevated Level in Lung Adenocarcinoma. *J. Biochem.* **1979**, *86*, 265–267.
- (72) Eckhardt, M.; Fewou, S. N.; Ackermann, I.; Gieselmann, V. N-Glycosylation Is Required for Full Enzymic Activity of the Murine Galactosylceramide Sulphotransferase. *Biochem. J.* **2002**, *368*, 317–324.
- (73) Barcenas, M.; Suhr, T. R.; Scott, C. R.; Turecek, F.; Gelb, M. H. Quantification of Sulfatides in Dried Blood and Urine Spots from Metachromatic Leukodystrophy Patients by Liquid Chromatography/electrospray Tandem Mass Spectrometry. *Clin. Chim. Acta.* **2014**, *433*, 39–43.

- (74) Ramakrishnan, H.; Hedayati, K. K.; Lüllmann-Rauch, R.; Wessig, C.; Fewou, S. N.; Maier, H.; Goebel, H.-H.; Gieselmann, V.; Eckhardt, M. Increasing Sulfatide Synthesis in Myelin-Forming Cells of Arylsulfatase A-Deficient Mice Causes Demyelination and Neurological Symptoms Reminiscent of Human Metachromatic Leukodystrophy. *J. Neurosci.* **2007**, *27*, 9482–9490.
- (75) Chen, Y.; Liu, Y.; Sullards, M. C.; Merrill, A. H. An Introduction to Sphingolipid Metabolism and Analysis by New Technologies. *Neuromolecular Med.* **2010**, *12*, 306–319.
- (76) Jungalwala, F. B.; Natowicz, M. R.; Chaturvedi, P.; Newburg, D. S. Analysis of Sulfatide and Enzymes of Sulfatide Metabolism. *Methods Enzymol.* **2000**, *311*, 94–105.
- (77) Burkart, M. D.; Wong, C. H. A Continuous Assay for the Spectrophotometric Analysis of Sulfotransferases Using Aryl Sulfotransferase IV. *Anal. Biochem.* **1999**, *274*, 131–137.
- (78) Yoshinari, K.; Petrotchenko, E. V.; Pedersen, L. C.; Negishi, M. Crystal Structure-Based Studies of Cytosolic Sulfotransferase. *J. Biochem. Mol. Toxicol.* **2001**, *15*, 67–75.
- (79) Negishi, M.; Pedersen, L. G.; Petrotchenko, E.; Shevtsov, S.; Gorokhov, a; Kakuta, Y.; Pedersen, L. C. Structure and Function of Sulfotransferases. *Arch. Biochem. Biophys.* **2001**, *390*, 149–157.
- (80) Superti-Furga, a. A Defect in the Metabolic Activation of Sulfate in a Patient with Achondrogenesis Type IB. *Am. J. Hum. Genet.* **1994**, *55*, 1137–1145.
- (81) Ebel, P.; Vom Dorp, K.; Petrasch-Parwez, E.; Zlomuzica, A.; Kinugawa, K.; Mariani, J.; Minich, D.; Ginkel, C.; Welcker, J.; Degen, J.; Eckhardt, M.; Dere, E.; Dörmann, P.; Willecke, K. Inactivation of Ceramide Synthase 6 in Mice Results in an Altered Sphingolipid Metabolism and Behavioral Abnormalities. *J. Biol. Chem.* **2013**, *288*, 21433–21447.
- (82) Rath, V. L.; Verdugo, D.; Hemmerich, S. Sulfotransferase Structural Biology and Inhibitor Discovery. *Drug Discov. Today* **2004**, *9*, 1003–1011.
- (83) Pedersen, L. C.; Petrotchenko, E.; Shevtsov, S.; Negishi, M. Crystal Structure of the Human Estrogen Sulfotransferase-PAPS Complex: Evidence for Catalytic Role of Ser137 in the Sulfuryl Transfer Reaction. *J. Biol. Chem.* **2002**, *277*, 17928–17932.
- (84) Edavettal, S. C.; Lee, K. a; Negishi, M.; Linhardt, R. J.; Liu, J.; Pedersen, L. C. Crystal Structure and Mutational Analysis of Heparan Sulfate 3-O-Sulfotransferase Isoform 1. *J. Biol. Chem.* **2004**, *279*, 25789–25797.

- (85) Pedersen, L. C.; Darden, T. a; Negishi, M. Crystal Structure of Beta 1,3-Glucuronyltransferase I in Complex with Active Donor Substrate UDP-GlcUA. *J. Biol. Chem.* **2002**, *277*, 21869–21873.
- (86) Qurishi, R.; Kaulich, M.; Müller, C. E. Fast, Efficient Capillary Electrophoresis Method for Measuring Nucleotide Degradation and Metabolism. *J. Chromatogr. A* **2002**, *952*, 275–281.
- (87) Lee, S.-Y.; Lévesque, S. A.; Sévigny, J.; Müller, C. E. A Highly Sensitive Capillary Electrophoresis Method Using P-Nitrophenyl 5'-Thymidine Monophosphate as a Substrate for the Monitoring of Nucleotide Pyrophosphatase/phosphodiesterase Activities. *J. Chromatogr. B. Analyt. Technol. Biomed. Life Sci.* **2012**, *911*, 162–169.
- (88) Lee, S.-Y.; Müller, C. E. Large-Volume Sample Stacking with Polarity Switching for Monitoring of Nucleotide Pyrophosphatase/phosphodiesterase 1 (NPP1) Reactions by Capillary Electrophoresis. *Electrophoresis* **2014**, *35*, 855–863.
- (89) Iqbal, J.; Müller, C. E. High-Sensitivity Capillary Electrophoresis Method for Monitoring Purine Nucleoside Phosphorylase and Adenosine Deaminase Reactions by a Reversed Electrode Polarity Switching Mode. *J. Chromatogr. A* **2011**, *1218*, 4764–4771.
- (90) Iqbal, J.; Lévesque, S. a; Sévigny, J.; Müller, C. E. A Highly Sensitive CE-UV Method with Dynamic Coating of Silica-Fused Capillaries for Monitoring of Nucleotide Pyrophosphatase/phosphodiesterase Reactions. *Electrophoresis* **2008**, *29*, 3685–3693.
- (91) Iqbal, J.; Scapozza, L.; Folkers, G.; Müller, C. E. Development and Validation of a Capillary Electrophoresis Method for the Characterization of Herpes Simplex Virus Type 1 (HSV-1) Thymidine Kinase Substrates and Inhibitors. *J. Chromatogr. B. Analyt. Technol. Biomed. Life Sci.* **2007**, *846*, 281–290.
- (92) El-Tayeb, A.; Iqbal, J.; Behrenswerth, A.; Romio, M.; Schneider, M.; Zimmermann, H.; Schrader, J.; Müller, C. E. Nucleoside-5'-Monophosphates as Prodrugs of Adenosine A2A Receptor Agonists Activated by Ecto-5'-Nucleotidase. *J. Med. Chem.* **2009**, *52*, 7669–7677.
- (93) Li, W.; Ulm, H.; Rausch, M.; Li, X.; O’Riordan, K.; Lee, J. C.; Schneider, T.; Müller, C. E. Analysis of the Staphylococcus Aureus Capsule Biosynthesis Pathway in Vitro: Characterization of the UDP-GlcNAc C6 Dehydratases CapD and CapE and Identification of Enzyme Inhibitors. *Int. J. Med. Microbiol.* **2014**.
- (94) Quirino, J. P.; Terabe, S. Electrokinetic Chromatography. *J. Chromatogr. A* **1999**, *856*, 465–482.
- (95) Silva, M. Micellar Electrokinetic Chromatography: A Practical Overview of Current Methodological and Instrumental Advances. *Electrophoresis* **2011**, *32*, 149–165.



- (96) El Deeb, S.; Iriban, M. A.; Gust, R. MEKC as a Powerful Growing Analytical Technique. *Electrophoresis* **2011**, *32*, 166–183.
- (97) Kim, J.-B.; Terabe, S. On-Line Sample Preconcentration Techniques in Micellar Electrokinetic Chromatography. *J. Pharm. Biomed. Anal.* **2003**, *30*, 1625–1643.
- (98) Sartori, J.; Potthast, A.; Ecker, A.; Sixta, H.; Rosenau, T.; Kosma, P. Alkaline Degradation Kinetics and CE-Separation of Cello- and Xylooligomers. Part I. *Carbohydr. Res.* **2003**, *338*, 1209–1216.
- (99) Hernández-Borges, J.; García-Montelongo, F. J.; Cifuentes, A.; Rodríguez-Delgado, M. A. Analysis of Triazolopyrimidine Herbicides in Soils Using Field-Enhanced Sample Injection-Coelectroosmotic Capillary Electrophoresis Combined with Solid-Phase Extraction. *J. Chromatogr. A* **2005**, *1100*, 236–242.
- (100) Reilly, J.; Sanchez-Felix, M.; Smith, N. W. Link between Biological Signaling and Increased Enantioseparations of Acids Using Glycopeptide Antibiotics. *Chirality* **2003**, *15*, 731–742.
- (101) Wang, T.; Kang, J. Hexokinase Inhibitor Screening Based on Adenosine 5'-Diphosphate Determination by Electrophoretically Mediated Microanalysis. *Electrophoresis* **2009**, *30*, 1349–1354.
- (102) Catai, J. R.; Somsen, G. W.; de Jong, G. J. Efficient and Reproducible Analysis of Peptides by Capillary Electrophoresis Using Noncovalently Bilayer-Coated Capillaries. *Electrophoresis* **2004**, *25*, 817–824.
- (103) Jiang, T.-F.; Lv, Z.-H.; Wang, Y.-H.; Yue, M.-E. Separation of Plant Hormones from Biofertilizer by Capillary Electrophoresis Using a Capillary Coated Dynamically with Polycationic Polymers. *Anal. Sci.* **2006**, *22*, 811–814.
- (104) Kim, J.-B.; Okamoto, Y.; Terabe, S. On-Line Sample Preconcentration of Cationic Analytes by Dynamic pH Junction in Capillary Electrophoresis. *J. Chromatogr. A* **2003**, *1018*, 251–256.
- (105) Yu, L.; Li, S. F. Y. Dynamic pH Junction-Sweeping Capillary Electrophoresis for Online Preconcentration of Toxic Pyrrolizidine Alkaloids in Chinese Herbal Medicine. *Electrophoresis* **2005**, *26*, 4360–4367.
- (106) Shihabi, Z. K. Stacking in Capillary Zone Electrophoresis. *J. Chromatogr. A* **2000**, *902*, 107–117.
- (107) Britz-McKibbin, P.; Bebault, G. M.; Chen, D. D. Velocity-Difference Induced Focusing of Nucleotides in Capillary Electrophoresis with a Dynamic pH Junction. *Anal. Chem.* **2000**, *72*, 1729–1735.

- (108) Britz-McKibbin, P.; Markuszewski, M. J.; Iyanagi, T.; Matsuda, K.; Nishioka, T.; Terabe, S. Picomolar Analysis of Flavins in Biological Samples by Dynamic pH Junction-Sweeping Capillary Electrophoresis with Laser-Induced Fluorescence Detection. *Anal. Biochem.* **2003**, *313*, 89–96.
- (109) Kim, J.-B.; Britz-McKibbin, P.; Hirokawa, T.; Terabe, S. Mechanistic Study on Analyte Focusing by Dynamic pH Junction in Capillary Electrophoresis Using Computer Simulation. *Anal. Chem.* **2003**, *75*, 3986–3993.
- (110) Britz-McKibbin, P.; Terabe, S. On-Line Preconcentration Strategies for Trace Analysis of Metabolites by Capillary Electrophoresis. *J. Chromatogr. A* **2003**, *1000*, 917–934.
- (111) Monton, M. R. N.; Imami, K.; Nakanishi, M.; Kim, J.-B.; Terabe, S. Dynamic pH Junction Technique for on-Line Preconcentration of Peptides in Capillary Electrophoresis. *J. Chromatogr. A* **2005**, *1079*, 266–273.
- (112) Britz-McKibbin, P.; Terabe, S. High-Sensitivity Analyses of Metabolites in Biological Samples by Capillary Electrophoresis Using Dynamic pH Junction-Sweeping. *Chem. Rec.* **2002**, *2*, 397–404.
- (113) Dziomba, S.; Kowalski, P.; Bączek, T. Field-Amplified Sample Stacking-Sweeping of Vitamins B Determination in Capillary Electrophoresis. *J. Chromatogr. A* **2012**, *1267*, 224–230.
- (114) Michalke, D.; Kolb, S.; Welsch, T. Influence of Buffer Zone Concentrations on Efficiency in Partial Filling Micellar Electrokinetic Chromatography. *J. Chromatogr. A* **2001**, *916*, 113–122.
- (115) Sarlieve, L. L.; Neskovic, N. M.; Rebel, G.; Mandel, P. Solubilization and Partial Purification of 3'-Phosphoadenosine-5'-Phosphosulphate: Galactocerebroside Sulphotransferase from Rat Brain. *J. Neurochem.* **1976**, *26*, 211–215.
- (116) Honke, K.; Tsuda, M.; Hirahara, Y.; Ishii, a; Makita, a; Wada, Y. Molecular Cloning and Expression of cDNA Encoding Human 3'-Phosphoadenylylsulfate:galactosylceramide 3'-Sulfotransferase. *J. Biol. Chem.* **1997**, *272*, 4864–4868.
- (117) Kalan, L.; Wright, G. D. Antibiotic Adjuvants: Multicomponent Anti-Infective Strategies. *Expert Rev. Mol. Med.* **2011**, *13*, e5.
- (118) Worthington, R. J.; Melander, C. Combination Approaches to Combat Multidrug-Resistant Bacteria. *Trends Biotechnol.* **2013**, *31*, 177–184.
- (119) O'Riordan, K.; Lee, J. C. Staphylococcus Aureus Capsular Polysaccharides. *Clin. Microbiol. Rev.* **2004**, *17*, 218–234.

- (120) Kneidinger, B.; O’Riordan, K.; Li, J.; Brisson, J.-R.; Lee, J. C.; Lam, J. S. Three Highly Conserved Proteins Catalyze the Conversion of UDP-N-Acetyl-D-Glucosamine to Precursors for the Biosynthesis of O Antigen in *Pseudomonas Aeruginosa* O11 and Capsule in *Staphylococcus Aureus* Type 5. Implications for the UDP-N-Acetyl-L-Fucosamine. *J. Biol. Chem.* **2003**, *278*, 3615–3627.
- (121) O’Riordan, K.; Lee, J. C. *Staphylococcus Aureus* Capsular Polysaccharides. *Clin. Microbiol. Rev.* **2004**, *17*, 218–234.
- (122) Schoenhofen, I. C.; McNally, D. J.; Vinogradov, E.; Whitfield, D.; Young, N. M.; Dick, S.; Wakarchuk, W. W.; Brisson, J.-R.; Logan, S. M. Functional Characterization of Dehydratase/aminotransferase Pairs from *Helicobacter* and *Campylobacter*: Enzymes Distinguishing the Pseudaminic Acid and Bacillosamine Biosynthetic Pathways. *J. Biol. Chem.* **2006**, *281*, 723–732.
- (123) Quirino, J. P.; Terabe, S. Exceeding 5000-Fold Concentration of Dilute Analytes in Micellar Electrokinetic Chromatography. *Science* **1998**, *282*, 465–468.
- (124) El-Tayeb, A.; Qi, A.; Müller, C. E. Synthesis and Structure-Activity Relationships of Uracil Nucleotide Derivatives and Analogues as Agonists at Human P2Y2, P2Y4, and P2Y6 Receptors. *J. Med. Chem.* **2006**, *49*, 7076–7087.
- (125) Baqi, Y.; Müller, C. E. Rapid and Efficient Microwave-Assisted copper(0)-Catalyzed Ullmann Coupling Reaction: General Access to Anilinoanthraquinone Derivatives. *Org. Lett.* **2007**, *9*, 1271–1274.
- (126) Voogd, T. E.; Vansterkenburg, E. L.; Wilting, J.; Janssen, L. H. Recent Research on the Biological Activity of Suramin. *Pharmacol. Rev.* **1993**, *45*, 177–203.
- (127) Schneider, T.; Sahl, H.-G. An Oldie but a Goodie - Cell Wall Biosynthesis as Antibiotic Target Pathway. *Int. J. Med. Microbiol.* **2010**, *300*, 161–169.
- (128) Barza, M.; Bruschi, J.; Bergeron, M. G.; Weinstein, L. Penetration of Antibiotics into Fibrin Loci in Vivo. 3. Intermittent vs. Continuous Infusion and the Effect of Probenecid. *J. Infect. Dis.* **1974**, *129*, 73–78.
- (129) Kiser, K. B.; Bhasin, N.; Deng, L.; Lee, J. C. *Staphylococcus Aureus* cap5P Encodes a UDP-N-Acetylglucosamine 2-Epimerase with Functional Redundancy. *J. Bacteriol.* **1999**, *181*, 4818–4824.
- (130) Portolés, M.; Kiser, K. B.; Bhasin, N.; Chan, K. H.; Lee, J. C. *Staphylococcus Aureus* Cap5O Has UDP-ManNAc Dehydrogenase Activity and Is Essential for Capsule Expression. *Infect. Immun.* **2001**, *69*, 917–923.

- (131) Talbot, G. H.; Bradley, J.; Edwards, J. E.; Gilbert, D.; Scheld, M.; Bartlett, J. G. Bad Bugs Need Drugs: An Update on the Development Pipeline from the Antimicrobial Availability Task Force of the Infectious Diseases Society of America. *Clin. Infect. Dis.* **2006**, *42*, 657–668.
- (132) Scott, D. E.; Coyne, A. G.; Hudson, S. A.; Abell, C. Fragment-Based Approaches in Drug Discovery and Chemical Biology. *Biochemistry* **2012**, *51*, 4990–5003.
- (133) Vu, H.; Roullier, C.; Campitelli, M.; Trenholme, K. R.; Gardiner, D. L.; Andrews, K. T.; Skinner-Adams, T.; Crowther, G. J.; Van Voorhis, W. C.; Quinn, R. J. Plasmodium Gametocyte Inhibition Identified from a Natural-Product-Based Fragment Library. *ACS Chem. Biol.* **2013**.
- (134) Brunschweiler, A.; Müller, C. E. P2 Receptors Activated by Uracil Nucleotides--an Update. *Curr. Med. Chem.* **2006**, *13*, 289–312.
- (135) Freissmuth, M.; Boehm, S.; Beindl, W.; Nickel, P.; Ijzerman, A. P.; Hohenegger, M.; Nanoff, C. Suramin Analogues as Subtype-Selective G Protein Inhibitors. *Mol. Pharmacol.* **1996**, *49*, 602–611.
- (136) Brigotti, M.; Alfieri, R. R.; Petronini, P. G.; Carnicelli, D. Inhibition by Suramin of Protein Synthesis in Vitro. Ribosomes as the Target of the Drug. *Biochimie* **2006**, *88*, 497–503.
- (137) Sanderson, L.; Khan, A.; Thomas, S. Distribution of Suramin, an Antitrypanosomal Drug, across the Blood-Brain and Blood-Cerebrospinal Fluid Interfaces in Wild-Type and P-Glycoprotein Transporter-Deficient Mice. *Antimicrob. Agents Chemother.* **2007**, *51*, 3136–3146.
- (138) Villalona-Calero, M. A.; Otterson, G. A.; Wientjes, M. G.; Weber, F.; Bekaii-Saab, T.; Young, D.; Murgo, A. J.; Jensen, R.; Yeh, T.-K.; Wei, Y.; Zhang, Y.; Eng, C.; Grever, M.; Au, J. L.-S. Noncytotoxic Suramin as a Chemosensitizer in Patients with Advanced Non-Small-Cell Lung Cancer: A Phase II Study. *Ann. Oncol.* **2008**, *19*, 1903–1909.
- (139) Tan, J. S.; Salstrom, S. J. Bacampicillin, Ampicillin, Cephalothin, and Cephapirin Levels in Human Blood and Interstitial Fluid. *Antimicrob. Agents Chemother.* **1979**, *15*, 510–512.
- (140) Cunnion, K. M.; Lee, J. C.; Frank, M. M. Capsule Production and Growth Phase Influence Binding of Complement to Staphylococcus Aureus. *Infect. Immun.* **2001**, *69*, 6796–6803.
- (141) Soulat, D.; Jault, J.-M.; Duclos, B.; Geourjon, C.; Cozzone, A. J.; Grangeasse, C. Staphylococcus Aureus Operates Protein-Tyrosine Phosphorylation through a Specific Mechanism. *J. Biol. Chem.* **2006**, *281*, 14048–14056.

- (142) Soulat, D.; Grangeasse, C.; Vaganay, E.; Cozzone, A. J.; Duclos, B. UDP-Acetyl-Mannosamine Dehydrogenase Is an Endogenous Protein Substrate of Staphylococcus Aureus Protein-Tyrosine Kinase Activity. *J. Mol. Microbiol. Biotechnol.* **2007**, *13*, 45–54.
- (143) Miroux, B.; Walker, J. E. Over-Production of Proteins in Escherichia Coli: Mutant Hosts That Allow Synthesis of Some Membrane Proteins and Globular Proteins at High Levels. *J. Mol. Biol.* **1996**, *260*, 289–298.
- (144) Thakker, M.; Park, J. S.; Carey, V.; Lee, J. C. Staphylococcus Aureus Serotype 5 Capsular Polysaccharide Is Antiphagocytic and Enhances Bacterial Virulence in a Murine Bacteremia Model. *Infect. Immun.* **1998**, *66*, 5183–5189.
- (145) Gray, B. M. ELISA Methodology for Polysaccharide Antigens: Protein Coupling of Polysaccharides for Adsorption to Plastic Tubes. *J. Immunol. Methods* **1979**, *28*, 187–192.
- (146) Watts, A.; Ke, D.; Wang, Q.; Pillay, A.; Nicholson-Weller, A.; Lee, J. C. Staphylococcus Aureus Strains That Express Serotype 5 or Serotype 8 Capsular Polysaccharides Differ in Virulence. *Infect. Immun.* **2005**, *73*, 3502–3511.



## 10 Acknowledgements

Heartfelt thanks to my parents, who created me and support me in all my life.

Sincere and deepest thanks to Prof. Dr. Christa E. Müller, who supervised me and helped me to find my dreaming way.

I would like to deeply thank Dr. Anke Schiedel, Prof. Dr. Ulrich Jaehde and Prof. Dr. Volkmar Gieselmann for acceptance to be my examiner.

I wish to express my sincere gratitude to my friends, who helped me to survive from my early stage of PhD study, these are: Dr. Younis Baqi, Dr. Mario Funke, Dr. Sonja Hinz, Dr. Ralf Mayer, Dr. Viktor Rempel, Dr. Benjamin Seibt, Dr. Matthias Weigt, Beate Ponatowski, Sangyong Lee, Amelie Fiene, Nicole Florin, Karen Schmeling, Carlos, Lopez, Xiaojing Yin and Cai Wang.

I am grateful to my friends, who gave me a comfortable atmosphere during my work and writing, these are: Dr. Meryerm Köse, Dr. Pillaiyar Thanigaimalai, Dr. Sabrina Gollos, Dr. Aliaa Abdelrahman, Inge Renner, Wessam Alnouri, Sanjay Bhattarai, Enas Mustafa Malik and Muhammad Rafahi.

I would like to thank all my cooperators, who worked with me and realized our research ideas together, these are: Hannah Ulm, Marvin Rausch, Dr. Tanja Schneider, Dr. Isabell Zech and Joren Guillaume.

Last but not least, I would like to thank all members in Prof. Müller's group and all assistants in the 7<sup>th</sup> semester for their generous support and sincere help.

And my dearest CE Pace-MDQ 3062282!

**Wenjin Li**

Bonn August 2014